Structural studies on kinetochore linker complexes

Daniel P Maskell

University College London

and

Cancer Research UK London Research Institute

PhD Supervisor: Dr Martin Singleton

A thesis submitted for the degree of

Doctor of Philosophy

University College London

September 2010

Declaration

I Daniel P Maskell confirm that the work presented in this thesis is my own. Where information has been derived from other sources, I confirm that this has been indicated in the thesis.

Publications arising from this Thesis

Maskell DP, Hu XW, Singleton MR. **Molecular architecture and assembly of the yeast kinetochore MIND complex.** J Cell Biol. 2010 Sep 6;190(5):823-34

Abstract

The MIND/Mis12 complex is an essential kinetochore component that is conserved throughout eukaryotes. This study has characterised both structurally and biochemically the recombinant MIND multiprotein complex from *Saccharomyces cerevisiae*. Hydrodynamic analysis identified that this complex is elongated in structure and comprises Dsn1p, Mtw1p, Nsl1p and Nnf1p in a stoichiometry of 1:1:1:1. Low-resolution structures obtained from electron microscopy (EM) and reconstructions from small angle X-ray scattering (SAXS) experiments are in agreement that the MIND/Mis12 complex in budding yeast exists as a 22 nm long structure, divided into 'head' and 'tail' regions. The head region is 8 nm in diameter and contains domains of all four subunits and is seen as a hook shape with a large cavity. The tail region appears as an elongated structure that is resistant to protease treatment. A model is proposed in this thesis for the overall structure and subunit orientation of the MIND complex.

The MIND/Mis12 complex along with the Ndc80 complex and KNL-1/Spc105p are components of the KMN network that directly attaches the kinetochore to the mitotic spindle. This study has shown that the KMN network in *Saccharomyces cerevisiae* is conserved and formed by high affinity hydrophobic interactions between MIND and the C-terminal of Spc105p and MIND and the globular Spc24p/Spc25p domain of the Ndc80 complex. Spc105p and the Ndc80 complex bind MIND with comparable affinity, indicating tight associations of the KMN network with a 1:1:1 ratio that is also observed in higher eukaryotes The interaction between the MIND and Ndc80 complexes is proposed to point the tail of the MIND complex towards the centromere.

The role of the Ipl1/Aurora B kinase was investigated for the MIND complex, with a single phosphorylation site found at serine 250 of Dsn1p. Phosphorylation did not affect either interactions between subunits of the MIND complex, nor binding between components of the KMN network, implying another role for this phosphorylation in kinetochore regulation.

Acknowledgement

I would first and foremost like to thank Dr Martin Singleton for the opportunity to carry out research in the Macromolecular Structure & Function Laboratory. I would also like to thank Dr Xiao Hu-Wen for the excellent images she has generated. This thesis would have been nowhere near as good without the help, guidance and support from Dr Isabel “Jaffa cake” Kingston, Dr Alan “Custard cream” Purvis and the rest of the MSF lab. I would like to thank Viduth, Andrea, Diego, Fabiola and Sunkler for joining me on this experience.

Finally I would like to thank my Mum, Sis and Jo for their love, support and belief throughout this PhD.

Table of Contents

Table of figures

List of tables

Abbreviations

Δ	Deletion
μl	Microlitre
μM	Micromolar
βME	β mercaptoethanol
°C	Temperature in degrees Celsius
APC	Anaphase promoting complex
ATP	Adenosine tri phosphate
AUC	Analytical ultracentrifugation
bp	base pair
CCP4	Collaborative Computer Project, Number 4
ChIP	Chromatin immunoprecipitation
c.v.	Column volumes
DLS	Dynamic light scattering
DNA	Deoxyribonucleic acid
DTT	Dithiothreitol
ECL	Enhanced chemiluminescence
EM	Electron microscopy
FPLC	Fast protein liquid chromatography
GFP	Green fluorescent protein
Hepes	4-(2 hydroxyethyl)-1-piperazineethanesulfonic acid

His	Hexahistidine
HPLC	High-performance liquid chromatography
HRP	Horse radish peroxidase
IPTG	Isopropyl-β-D-thiogalactoside
ITC	Isothermal titration calorimetry
kDa	Kilodaltons
kJ	Kilojoule
kV	Kilovolt
LB	Luria-Bertani media
M	Molar/moles per litre
mAU	Milliabsorbance unit
mg	Milligrams
ml	Millilitre
MT	Microtubule
mw	Molecular weight
NIH	National institute of health
Ni-NTA	Nickel nitrotriacetic acid
nm	Nanometer
NMR	Nuclear magnetic resonance
OD	Optical density

O/N	Overnight
PCR	Polymerase chain reaction
PDB	Protein data bank
pI	Isoelectric point
PMSF	Phenylmethylsulphonylfluoride
PVDF	polyvinylidene fluoride
rmsd	root mean square deviation
SAC	Spindle assembly checkpoint
SAXS	Small angle X-ray scattering
SDS-PAGE	Sodium dodecyl sulphate – polyacrylamide gel electrophoresis
SPB	Spindle pole body
TCEP	Tris(2-carboxyethyl) phosphine hydrochloride
TEMED	Tetramethylethylenediamine
TEV	Tobacco etch virus
Tris	Tris(hydroxymethyl)aminomethane
t.s.	Temperature sensitive
UV	Ultra violet
V	Volt

Introduction

1.1 Mitosis

The segregation of copies of DNA molecules to daughter cells (mitosis) has been a long studied field of biology. This process was first observed during the middle to late 19th Century, when scientists were able to detect the movement of DNA in cells. One of the first scientists to document this process was Walther Flemming, a German professor who published *Zellsubstanz, Kern und Zelltheilung*, a collection of work in which detailed illustrations of cells at various stages of division were shown (Flemming, 1882). Flemming termed the changes in the thread like structures he could observe as "Karyomitosis" and created the basis of research in the field of mitosis.

Genetic information in eukaryotes is contained in the form of discrete units known as chromosomes. These chromosomes must first be replicated accurately, and then the two copies must be separated with a single copy sent to each cell. The whole process requires a vast array of essential components, making sure an exact copy of genetic material is passed onto each daughter cell. Errors in chromosome segregation can result in missing or additional copies of chromosomes (termed aneuploidy). Cancerous tumours have these defects, which can lead to further mis-segregation of chromosomes in a phenomenon referred to as chromosomal instability (CIN) (reviewed in (Thompson et al., 2010)).

1.1.1 Chromosomes

De-condensed chromosomes are duplicated in S phase of the cell cycle. The two identical chromosomes (sister chromatids) are then held together by cohesin molecules, which are positioned along the whole length of the sister chromatid, physically linking them together (Nasmyth et al., 2000). As observed by Flemming in the late 19th Century cells entering M phase begin to condense their chromosomes, which become visible threadlike structures, a process known as chromosome condensation. Condensation is important as it untangles sister chromatids enabling separation and also reduces the

dimensions of the chromosome making translocation easier for a dividing cell (reviewed in (Koshland and Strunnikov, 1996)). Condensation of DNA happens at several levels to generate mitotic chromosomes. DNA is initially wrapped around nucleosome complexes consisting of histone proteins (Luger et al., 1997), which lead to the generation of chromatin fibres of DNA (reviewed in (Robinson and Rhodes, 2006)). Further compaction is created by both DNA topoisomerase II and condensin (reviewed in (Porter and Farr, 2004) and (Hudson et al., 2009)). With DNA compacted into mitotic chromosomes, the two sister chromatids align along a central axis ready for segregation.

1.1.2 Centromeric DNA

Specialised regions of DNA known as centromeric DNA (CEN) are the locus of the formation of a protein complex known as the kinetochore (see section 1.2), enabling attachment to the mitotic spindle. One of the simplest known centromeres is found within the budding yeast *Saccharomyces cerevisiae*. The centromere of chromosome III was cloned into a plasmid, allowing the plasmid to be replicated in a similar manner to the yeast chromosome (Clarke and Carbon, 1980). The centromeric boundary for chromosomes III and XI were further refined to ~125 bp, comprising an AT rich core of 87-88 bp known as CDEII (conserved DNA element) flanked by short conserved sequences of regions known as CDEI and CDEIII (Fitzgerald-Hayes et al., 1982). A CCG motif in CDEIII was shown to be conserved within all 16 chromosomes and the whole CEN region was found to be essential for correct chromosome segregation (McGrew et al., 1986). In the fission yeast *Schizosaccharomyces pombe* the centromere is larger at 40-100 kb of DNA arranged with a non-conserved core flanked by inverted repeats (reviewed in (Clarke, 1998)). In humans the centromere can range from 0.3-5 Mbp with thousands of copies of a repeating 171bp sequence known as α satellite DNA (reviewed in (Cleveland et al., 2003)).

1.1.3 The mitotic spindle

To separate the two sister chromatids protein filaments known as microtubules (MTs) are formed from the tight interaction of a heterodimer of α-tubulin and β-tubulin, that form long chains with a polarity of α-tubulin and β-tubulin (Nogales et al., 1998). 13 of these horizontal chains then associate laterally to generate a hollow cylindrical structure. The lateral interactions occur between the same monomer of tubulin (α to α, β to β), creating a helical twist to the filament (Nogales et al., 1999). The protofilaments in the microtubule all have the same polarity, creating a plus end of β-tubulin molecules and minus end of α-tubulin molecules.

The role of GTP hydrolysis is also important to the growth and reduction of the microtubule filament. If GTP is bound to β-tubulin, then protofilaments are aligned in straight lines, creating strong longitudinal and lateral binding to other tubulin subunits. After GTP hydrolysis, the protofilaments begin to curve due to changes in the structural conformation of the GDP β-tubulin (Wang and Nogales, 2005). This reduces the binding affinities and packing arrangement of the microtubule, reducing stability. Microtubules are therefore in a constant state of growth and shrinkage, depending on the GTP and GDP forms of tubulin, referred to as “dynamic instability” (Mitchison and Kirschner, 1984). Growing microtubules have a GTP tubulin cap and will continue to grow as long as the GTP tubulin molecules are available. When hydrolysis occurs, the GTP form is changed to GDP, reducing the size of the cap leading to a decrease in the microtubule stability. The microtubule begins to shrink, known as “catastrophe”. If the cap is replaced by GTP tubulin, the microtubule can re-grow in a process known as “rescue”.

The centrosome, also known as the spindle pole body (SPB) in *Saccharomyces cerevisiae* (reviewed by (Winey and O'Toole, 2001)), is the specific site of nucleation for microtubules required to segregate sister chromatids. This complex consists of the centrosome matrix and contains γ-tubulin, which is responsible for nucleating microtubules from their minus end. Within the centrosome are structures known as centrioles, which are responsible for maintenance and replication of the centrosome.

When mitosis begins the duplicated SPB's move to separate poles of the nucleus forming the basis of the mitotic spindle.

1.2 The kinetochore

Chromosomes and the mitotic spindle cannot interact with each other directly, therefore a multi-protein complex known as the kinetochore is formed to link these two components together and is the simplest role of the kinetochore in chromosome segregation. However, the successful segregation of sister chromatids is in fact a highly regulated process that requires a large number of proteins. Even in one of the simplest model organisms, *Saccharomyces cerevisiae* where a single MT binds to a single kinetochore (Peterson and Ris, 1976, O'Toole et al., 1999) a large number of proteins are recruited to form a functional kinetochore with many of these components found to be essential. This introduction will focus primarily on the budding yeast kinetochore as it has been one of the most characterised with over 70 proteins found to form at least 14 discrete complexes (reviewed by (McAinsh et al., 2003) and (Westermann et al., 2007)). A brief introduction of higher eukaryote protein complexes will highlight the conservation in structure and function of the kinetochore throughout eukaryotes.

1.3 Proteins of the *Saccharomyces cerevisiae* kinetochore

Over the past decade, proteins found to comprise the *Saccharomyces cerevisiae* kinetochore have been classified into complexes based on their interactions with other proteins and DNA. These complexes have been further assigned into one of three kinetochore regions, DNA binding, MT binding and the linker region, in which they function (figure 1.1). Regulatory components have also been investigated for their role in the fidelity of chromosome segregation.

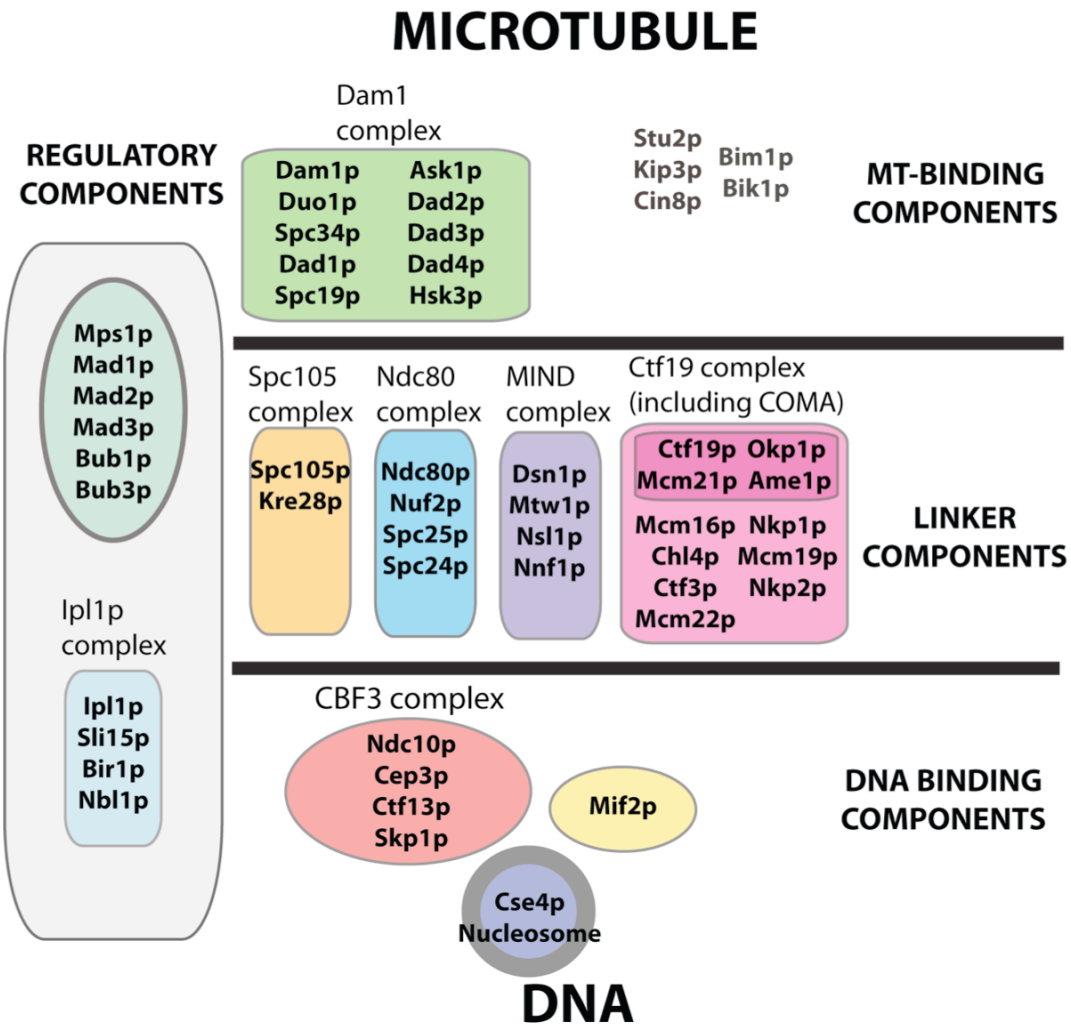

Figure 1.1 Proteins of the *Saccharomyces cerevisiae* kinetochore
Overview of the *Saccharomyces cerevisiae* proteins, known to be found at the kinetochore (some proteins have been omitted for clarity). These proteins are separated into three regions, DNA binding, MT binding and linker region as shown by thick black lines. Regulatory components that are not classified into a functional region are shown on the left hand side in the grey box. The proteins are further divided into complexes, shown by coloured spheres or boxes containing all known components, with complexes named above.

1.4 Regulatory components of the kinetochore

In order to maintain correct attachments, two regulatory components are utilised in the kinetochore. The interactions between these components have been investigated.

1.4.1 The Ipl1p complex

Ipl1p mutations had been found to lead to an increase in ploidy and create defects in chromosome behaviour (Chan and Botstein, 1993, Biggins et al., 1999). Orthologs of this protein are found in higher eukaryotes and are known as Aurora B kinase (Terada et al., 1998). In *Saccharomyces cerevisiae*, a comparison between wild type and *ipl1*-321 mutant cells showed that after release from G1, wild type cells began to separate sister chromatids after 80 minutes. In the *ipl1*-321 mutants, separation occurred at a time similar to wild type cells, yet sister chromatid segregation happened in only half of the cells (Biggins et al., 1999). To understand if the defect was either failure of separation or normal separation, with abnormal segregation, *ipl1*-321 mutants were analysed for sister chromatid separation without the spindle and the spindle checkpoint (see section 1.4.2). The *ipl1*-321 Δmad2 double mutant treated in nocodazole to de-polymerise MT, showed that sister chromatids could separate, indicating a role for Ipl1p in accurate segregation. To identify where Ipl1p was functioning, the mitotic spindle was analysed. Normal SPB´s were observed in *ipl1*-321 mutants, however spindle lengths were elongated suggesting a defect in the interactions between MTs and the kinetochore. Interactions of Ipl1p were observed with the Ndc10p component of the CBF3 complex (see section 1.5.1) and Ndc10p was found to be a phosphorylation target for Ipl1p (Biggins et al., 1999).

Ipl1p was shown to associate with a novel and essential protein known as Sli15p, which also localized to the mitotic spindle. Sli15p mutants could not segregate their chromosomes to separate poles as had also been observed in Ipl1p mutants (Kim et al., 1999). The C-terminus of Sli15p was shown to bind and increase the kinase activity of Ipl1p *in vitro* (Kang et al., 2001). This region was shown to have homology to the

human INCENP protein, which binds Aurora B, showing that the interaction is also conserved in higher eukaryotes (Adams et al., 2000, Kaitna et al., 2000). The middle region of Sli15p could bind MTs and was also found to be a phosphorylation site for Ipl1p (Kang et al., 2001). The role of the Ipl1p-Sli15p complex in bi-orientation was examined as mutants of these proteins were found to connect sister chromatids to a single SPB (Tanaka et al., 2002). The *ipl1*-321 mutant was shown to be mono-orientated and was connected primarily to the old SPB, which is present from the previous cell cycle (Tanaka et al., 2002). Mutants arrested at metaphase could not switch from mono-orientation (syntelic) to bi-orientation (amphitelic) showing that Ipl1p is required for this switch. The role of tension sensing was proposed, with the Ipl1p-Sli15p complex acting as a correction mechanism by detaching MT from kinetochores that have not generated tension (Tanaka et al., 2002).

Phosphorylation targets of Ipl1p are found in all three regions of the kinetochore, with most kinetochore complexes containing at least one subunit that can be phosphorylated by Ipl1p (Cheeseman et al., 2002, Westermann et al., 2003). Some components such as Dam1p and Ndc80p have multiple sites, with phosphorylation found to have an essential role in kinetochore function (see sections 1.6.1 and 1.7.2.2 for details). A consensus sequence for Ipl1p phosphorylation was identified as [RK]x[TS][ILV] (Cheeseman et al., 2002). In addition another protein was found to associate with the Ipl1p-Sli15p complex, known as Bir1p (Cheeseman et al., 2002). Bir1p and Sli15p were shown to form a complex that linked the CBF3 complex to MTs in an *in vitro* reconstituted system (Sandall et al., 2006). This link was required for Ipl1p kinase activity to correct syntelic attachments, leading to the proposal that Bir1p-Sli15p relays the tension state of the kinetochore to the activity of Ipl1p. In the absence of tension, Bir1p, Sli15p and Ipl1p could form a complex that can phosphorylate various targets, leading to detachment of the kinetochore from the MTs. This allows the MTs from opposite poles to re-attach in a correct manner leading to bi-orientation. With correct attachments, tension is created, which is proposed to either inactivate Ipl1p or move substrates from Ipl1p activity, leading to a stable MT-kinetochore interaction (Sandall et al., 2006).

1.4.2 The spindle assembly checkpoint (SAC)

Kinetochore-MT interactions are also regulated by the spindle assembly checkpoint (SAC) which is a negative regulator of a ubiquitin ligase complex known as the anaphase promoting complex (APC) (King et al., 1995) (reviewed in (Peters, 2006)). The APC targets the degradation of Securin/Pds1p leading to anaphase and chromosome segregation (Cohen-Fix et al., 1996).

Proteins of the spindle assembly checkpoint (figure 1.1) were first identified by screening mutants that could still undergo mitosis even with the addition of MT poisons (Hoyt et al., 1991, Li and Murray, 1991). An additional component, Mps1p, was also identified as over-expression of this protein inhibited mitosis in normal cells (Hardwick et al., 1996). The signal that these components generate are amplified as a single unattached kinetochore was shown to prevent anaphase (Rieder et al., 1995), highlighting the importance of kinetochore attachment to the progression of the cell cycle. In *Xenopus* and humans, Mad2 was found to localise to unattached kinetochores (Chen et al., 1996, Li and Benezra, 1996), with Mad2 turnover observed to be the mechanism in which the SAC signal is first generated (Howell et al., 2000). Structural studies observed a conformational activation for Mad2, finding that the C-terminal could undergo a structural re-arrangement. When bound to Mad1, Mad2 is found in a closed state with its C-terminal wrapped around Mad1 in a seatbelt like mechanism (Luo et al., 2002, Sironi et al., 2002). This Mad1-Mad2 dimer can bind to a Mad2 molecule in an open state, creating a dimerisation between and open and closed Mad2 molecule (Mapelli et al., 2007, Yang et al., 2008). Mad1 is required to link Mad2 to the kinetochore and it is also necessary for the interaction between Mad2 and Cdc20 a known activator of the APC (Hwang et al., 1998). Mad1 and Cdc20 both bind using a similar domain, indicating that both Mad1 and Cdc20 compete for Mad2 binding (Sironi et al., 2002, De Antoni et al., 2005). Two other proteins, Mad3/BubR1 and Bub3 interact with the Mad2-Cdc20 dimer, generating the mitotic checkpoint complex (MCC) (Hardwick et al., 2000, Sudakin et al., 2001). This complex along with other components of the SAC are found at unattached kinetochores, supporting the notion that this state is a catalyst for the formation of the “wait anaphase” signal that inhibits the APC (Howell et al., 2004).

Ipl1p was required for the activation of the SAC by Mps1p expression (Biggins and Murray, 2001). Protein levels of Pds1p cycle in wild type cells due to degradation by the APC and can be used to determine if cells are undergoing anaphase (Cohen-Fix et al., 1996). Pds1p levels were stabilized by overexpression of Mps1p indicating that the checkpoint is activated to prevent anaphase. However in the *ipl1*-321 mutants with Mps1p overexpression, levels of Pds1p cycled similar to wild type cells, indicating a role of Ipl1p in a functional spindle assembly checkpoint signal (Biggins and Murray, 2001). To identify if tension defects could activate the SAC, various t.s. mutants that are found in each region of the kinetochore were investigated in the presence and absence of Ipl1p. Each mutant tested showed that levels of Pds1p were stabilised leading to a metaphase arrest. In double mutants with the loss of Ipl1p function, levels of Pds1p cycled like wild type cells, indicating a role for Ipl1p in spindle checkpoint activation (Pinsky et al., 2006).

1.5 The DNA binding components of the kinetochore

To link DNA to the kinetochore requires proteins that can associate specifically with CEN DNA, forming a platform to bind to other kinetochore proteins.

1.5.1 The CBF3 complex

The CBF3 complex is specific to organisms with point centromeres such as *Saccharomyces cerevisiae* (Meraldi et al., 2006). This complex binds to the CDEIII region within the CEN DNA (Lechner and Carbon, 1991) and consists of four proteins, Ndc10p, Cep3p, Ctf13p and Skp1p (Doheny et al., 1993, Goh and Kilmartin, 1993, Jiang et al., 1993, Lechner, 1994, Connelly and Hieter, 1996), which all are required for the stable interaction between CEN DNA and MTs at the kinetochore (Goh and Kilmartin, 1993, Sorger et al., 1994). Biochemical and structural analysis of the CBF3 complex has indicated the stoichiometry of the complex as 2:2:1:1 Ndc10p:Cep3p:Ctf13p:Skp1, giving the complex an overall molecular mass of ~450

kDa (Espelin et al., 1997, Pietrasanta et al., 1999). A zinc finger domain in the N-terminal of Cep3p was identified (Lechner, 1994) with DNA binding found to occur between Cep3p and the conserved CCG motif within CDEIII (Espelin et al., 1997). Crystal structures of the Cep3p protein without the zinc finger have lead to the proposal of two different models on how DNA is bound by this complex (Purvis and Singleton, 2008, Bellizzi et al., 2007). Ndc10p has also been shown to bind CDEII, suggesting that this binding along with the CBF3 complex binding to CDEIII may initiate the recruitment of further kinetochore proteins (Espelin et al., 2003).

1.5.2 The Cse4p/CENP-A nucleosome

A feature of all kinetochores is the incorporation of a centromere specific nucleosome. In *Saccharomyces cerevisiae* this was discovered by analysis of a *cse*4-1 mutant, which caused an increase in chromosome nondisjunction and cells to arrest with large buds and short bipolar spindles (Stoler et al., 1995). Cse4p was shown to share sequence identity to histone H3, suggesting that it formed a specialised nucleosome involved in chromosome segregation similar to the human CENP-A (centromere protein). Cse4p interacts specifically with CEN DNA *in vivo* as seen by cross-linking chromatin immunoprecipitation (ChIP) assays and immunofluorescence inspection (Meluh et al., 1998). The Cse4p containing nucleosome was proposed to wrap CEN DNA, bringing CDEI and CDEIII regions into close proximity and creating an interaction with the CBF3 complex and the non-essential Cbf1p protein that has a role in DNA bending (Niedenthal et al., 1993). However, the CBF3 complex was found to be required for Cse4p binding (Ortiz et al., 1999), whereas the Cse4p nucleosome was not required for Ndc10p to associate with CEN DNA (Measday et al., 2002), indicating that CBF3 is first recruited to the CEN DNA followed by the incorporation of the Cse4p nucleosome.

1.5.3 Mif2p/CENP-C

Mif2p (mitotic fidelity) in budding yeast was found to be another CEN DNA interacting protein, with identified sequence conservation to the human ortholog CENP-C (Meluh and Koshland, 1995). Mif2p requires both the CBF3 complex and the Cse4p nucleosome in order to bind to CEN DNA (Westermann et al., 2003, Meluh and Koshland, 1997) A DNA binding motif known as an 'A-T Hook' is also found in Mif2p (Meluh and Koshland, 1995) with DNA binding proposed to occur at the CDEIII region of CEN DNA, along with the CBF3 complex (Cohen et al., 2008). Interactions with the MIND complex (see section 1.7.4.1) (Westermann et al., 2003) and Ctf19 complex (see section 1.7.1)(Ortiz et al., 1999) have been observed, with Mif2p required for their recruitment to the kinetochore (Cohen et al., 2008). Mif2p has also been found to be phosphorylated by the Ipl1p kinase, with *mif*2 phosphorylation mutant cells showing metaphase arrest (Westermann et al., 2003).

1.6 The microtubule binding components of the kinetochore

The other important function of the kinetochore is to bind to MTs in order to segregate chromosomes by utilising the dynamic properties of MTs.

1.6.1 The Dam1 complex

The Dam1 complex comprises 10 essential proteins (figure 1.1) and binds to MTs *in vitro* (Cheeseman et al., 2001a), with *dam*1 and *duo*1 mutants showing spindle defects (Cheeseman et al., 2001b). Ipl1p/Aurora B phosphorylation sites for multiple components of the dam1p complex were identified (Cheeseman et al., 2002). Mutations at single sites showed no defects, yet mutations of all the identified Dam1p phosphorylation sites resulted in lethality, indicating a role of phosphorylation in regulating MT-kinetochore interactions (Cheeseman et al., 2002). Two separate studies found that recombinantly expressed Dam1 complexes forms rings around MTs *in vitro* (Westermann et al., 2005, Miranda et al., 2005). The binding between Dam1 complexes

and MTs were found to occur via electrostatic interactions between the C-termini of Dam1p and α/β tubulin, forming a Dam1 ring complex that acts as collar around the MT (Westermann et al., 2005). A conformational change was observed in the Dam1p C-terminus between un-bound and MT bound states of the complex providing further evidence of an electrostatic interaction between Dam1 complexes and α/β tubulin (Wang et al., 2007).

1.6.2 Other MAPS and motors

Microtubule associated proteins (MAPS)/plus-end tracking proteins (+TIPs), such as Stu2p, Bim1p and Bik1p associate together at the plus ends of MTs and are involved in controlling the dynamics in this region of the MT (Wolyniak et al., 2006). Of these proteins only Stu2p is found to be essential (He et al., 2001) and can bind to both free tubulin heterodimers and MTs via its TOG domains suggesting a role in MT plus end stability (Al-Bassam et al., 2006). Kinesin motors such as Kip3p and Cin8p, although non-essential, have roles in assembly and elongation of bipolar spindles (reviewed in (Hildebrandt and Hoyt, 2000)) and have been shown to be recruited to the kinetochore (Tytell and Sorger, 2006).

1.7 The linker components of the kinetochore

Connecting the DNA and MT binding components of the kinetochore is the linker region. To date four complexes have been assigned to this area.

1.7.1 The Ctf19 complex

Ctf19p was first discovered in 1999, with mutants showing severe missegregation defects (Hyland et al., 1999). Cross-linking and immunoprecipitation techniques suggested that this protein both interacts with CEN DNA and locates to the nuclear face

of the spindle pole, suggesting a role in the linker region of the kinetochore. Affinity tagged Ctf19p isolated 12 different proteins from yeast cell lysate, named the Ctf19 complex (Cheeseman et al., 2002) (see figure 1.1 for all proteins identified). One of these proteins Mtw1p, is found to be part of another complex (see section 1.7.4.1). Various interactions between proteins of the Ctf19 complex had already been observed (Ortiz et al., 1999) (Measday et al., 2002) (Pot et al., 2003), indicating that this complex may exist in various subunit conformations. A stable association between Ctf19p, Okp1p, Mcm21p and Ame1p (referred to as the COMA complex) was found (De Wulf et al., 2003). The role of the Ctf19 complex including the COMA complex is poorly understood, as only Okp1p and Ame1p are essential for viability, which is unlike most kinetochore complexes where every subunit is essential.

1.7.2 The Ndc80 complex

In 1997, yeast-two hybrid screens of cDNA libraries identified a 1.8-kb cDNA that interacted with the expressed retinoblastoma susceptibility gene (Rb), a known tumour suppressor. Northern blotting using a fragment of this cDNA identified a 2.3 kb mRNA product found in all cell types that were tested (Chen et al., 1997). The expression levels observed in tumour cell lines were higher than in normal cells and the transcript was named *highly expressed in cancer* (HEC/Hec1). The levels of expression during the cell cycle also varied, indicating a role in cell division. The cDNA of Hec1 was sequenced, identifying an open reading frame encoding a 642 amino acid, 72 kDa protein, with heptad repeats spanning almost two-thirds of the sequence. Western blots in various cell types, using anti-Hec1 antibodies, found that Hec1 could only be detected in dividing cells with high mitotic indices. Hec1 was shown to associate with the centromere and when anti-Hec1 antibodies were injected into cultured cells, chromosomes could still condense but failed to segregate and spindles failed to orientate properly resulting in daughter cells with abnormal amounts of DNA.

Characterisation of proteins in the SPB's of *Saccharomyces cerevisiae* identified a protein Ndc80p (nuclear division cycle) that shared sequence conservation to the heptad repeats found in Hec1 (Wigge et al., 1998). Inactivation of Ndc80p expression was

shown to be lethal, and a *ndc*80-1 t.s. mutant was shown to be anaphase defective, with DNA remaining associated to one spindle pole. Interestingly Hec1 expression could rescue the lethal phenotype in *Saccharomyces cerevisiae* cells with inactivated Ndc80p expression, showing functional conservation between these proteins (Zheng et al., 1999).

In addition to Ndc80p, other proteins were found in SPB spindle preparations. Similarities in immuno-EM staining patterns highlighted two other proteins, Spc25p and Spc24p (spindle pole body components), suggesting possible associations with Ndc80p (Wigge et al., 1998). To confirm this two separate studies tagged Ndc80p with protein A in order to extract other interacting proteins from yeast cell lysate (Wigge and Kilmartin, 2001, Janke et al., 2001). Spc25p and Spc24p were both identified as had been suggested and another protein, Nuf2p (nuclear filament-related) was also identified by immunoprecipitation with Ndc80p protein A and Ndc80p-6HA (haemagglutinin) (Janke et al., 2001, Wigge and Kilmartin, 2001). Nuf2p had been previously identified as an essential 451 amino acid, 53 kDa protein with coiled-coil regions (Osborne et al., 1994). A *nuf*2-61 t.s. mutant showed cell cycle arrest with partially divided nuclei and short bipolar spindles. *spc*25-1, *spc*25-7 *spc*24-1 and *spc*24-2 t.s. mutants had comparable phenotypes to the *ndc*80-1 mutant, with cells that could segregate their SPB's but with DNA found at a single SPB. Further evidence of an complex consisting of Ndc80p, Nuf2p, Spc25p and Spc24p was provided by identification of genetic interactions between all 4 proteins (Wigge and Kilmartin, 2001, Janke et al., 2001). ChIP assays identified an interaction between the Ndc80p complex and CEN DNA, which was found to require Ndc10p for this association (see section 1.5.1) (Janke et al., 2001, He et al., 2001). The interaction with CEN DNA in an Ndc10p dependent manner and the observation that GFP tagged Ndc80p components localise to the same position of known kinetochore proteins, identified the Ndc80 complex as a kinetochore component (Janke et al., 2001, He et al., 2001).

1.7.2.1 The conservation and function of the Ndc80 complex

Orthologs of Nuf2p have been found in humans, *Schizosaccharomyces pombe, Xenopus* and *Caenorhabditis elegans* (Wigge and Kilmartin, 2001, Nabetani et al., 2001, Howe et al., 2001, McCleland et al., 2003). In *Xenopus*, a physical interaction between Ndc80p and Nuf2p was also observed along with orthologs of Spc25p and Spc24p (McCleland et al., 2003, McCleland et al., 2004). Human orthologs of Spc25p and Spc24p have also been found by immunoprecipitation (Bharadwaj et al., 2004) and sequence searches (McCleland et al., 2004).

Studies in model organisms have helped elucidate the role of the Ndc80 complex in the kinetochore. In *Saccharomyces cerevisiae*, the t.s mutant *spc*24-2 was found to be checkpoint deficient, as they had a similar anaphase defect behaviour to *Δmad2* cells when analysed by flow cytometry (Janke et al., 2001). *spc*25-7 mutants identified that Bub1p and Mad2p were not found to localise to the kinetochore, whereas *ndc*80-1 mutants showed localisation of Bub1p and Mad2p, indicating that different regions of the Ndc80 complex are involved in different functions (Gillett et al., 2004). RNAi of components of the Ndc80 complex in humans, identified chromosome alignment and spindle defects as well as loss of Mad1 and Mad2 from unattached kinetochores (Martin-Lluesma et al., 2002, DeLuca et al., 2002, DeLuca et al., 2003, McCleland et al., 2003, DeLuca et al., 2005).

1.7.2.2 The *structure of the Ndc80 complex*

In 2005, recombinantly expressed Ndc80 complex was shown to comprise a hetero-tetramer with a stoichiometry of 1:1:1:1 (Wei et al., 2005). Stable sub-complexes of Spc25p/Spc24p and Ndc80p/Nuf2p were identified that could re-constitute the complete complex. This recombinant complex was analysed using low angle rotary shadowing electron microscopy, which showed the complex to be ‘rod-like’ in structure with globular ends, with a total length of 57 nm (figure 1.2 A). The lengths of the coiled-coil regions were predicted to be ~ 30-40 nm for Ndc80p and Nuf2p and ~ 15 nm for Spc24p and Spc25p, based on the predicted coiled-coil domains. Combining these

lengths with the dimensions observed in the EM images proposed that the sub-complexes associate via the N-termini coiled-coil regions of Spc24p/Spc25p and the C-termini coiled coil regions of Ndc80p and Nuf2p. This model was confirmed by both limited proteolysis and antibody labelling, showing that a stable interaction between all four coiled-coil domains was observed even with the removal of the globular domains (Wei et al., 2005). Wei *et al* (2005) further proposed an orientation of the Ndc80 complex with the globular N-termini of Ndc80p and Nuf2p facing towards the MT and the globular C-termini of Spc24p and Spc25p facing towards the centromere (figure 1.2 A). At the same time another study of recombinantly expressed human Ndc80 complex was observed by scanning force microscopy to also have an elongated structure (Ciferri et al., 2005). The human Ndc80 complex was shown to have similar associations of the four subunits to those of the *Saccharomyces cerevisiae* Ndc80 complex, suggesting a conserved structural organisation of the Ndc80 complex throughout eukaryotes.

Crystallographic and NMR studies were used to show high-resolution structures of the Spc24p/Spc25p globular domains (figure 1.2 C) (Wei et al., 2006). Both globular domains contain an anti-parallel β sheet sandwiched between α helices. A pseudo-2-fold symmetry was observed, creating a 'butterfly' shape, with the interaction between the two domains occurring via hydrophobic residues. Sequence conservation for these domains is seen throughout eukaryotes, with helix 2 of Spc24p found to contain highly conserved hydrophobic residues (figure 1.2 C). This helix faces away from the coiled-coil rod and is implicated as a binding interface for other kinetochore proteins.

A pivotal structural finding was the identification that the globular region of human Ndc80p/Hec1 folds as a calponin-homology (CH) domain (figure 1.2 B) (Wei et al., 2007). This domain is also present in a known microtubule binding protein EB1 (end binding) (the *Saccharomyces cerevisiae* ortholog is Bim1p (see section 1.6.2)) (Hayashi and Ikura, 2003). The CH domain in Hec1 shares only 11% sequence identity with the CH domain of EB1, yet both fold into a similar shape, with hydrophobic residues found in the loop between helix 4 and 5 and within helix 6, creating a hydrophobic core, which in EB1 had been shown to bind MTs (Hayashi and Ikura, 2003). However, the CH domain of Hec1 does not bind MTs independently, therefore the intact globular N-terminals domains of both Ndc80p and Nuf2p from *Saccharomyces cerevisiae* were

used to characterise MT binding (Wei et al., 2007). Additionally, an unstructured N-terminal tail, with a large number of positively charged residues, was proposed to interact with the MT. When this tail was removed from the Ndc80p and Nuf2p globular heterodimer, MT binding affinity was reduced ~ 10 fold (Wei et al., 2007).

At the same time other studies also confirmed that the N-terminal tail of Ndc80 is important for MT binding both *in vitro* and *in vivo*. The Ndc80p protein had been previously detected as a substrate for the Ipl1p/Aurora B kinase (Cheeseman et al., 2002) (see section 1.4.1). The N-terminal tail region was found to have multiple Ipl1p/Aurora B phosphorylation sites and when the tail was phosphorylated, the MT binding affinity was shown to decrease (Cheeseman et al., 2006). Phosphonull mutants of the N-terminal tail of *Caenorhabditis elegans* Ndc80p were shown to bind MTs *in vitro* with comparable affinities to the wild type Ndc80 complex even in presence of Ipl1p/Aurora B and ATP. However, *in vivo* phosphonull mutants within the N-terminal tail of Hec1 showed hyperstretched kinetochores in Ptk1 cells (DeLuca et al., 2006). Truncated Hec1 with the N-terminal tail removed, could not rescue MT interactions within both HeLa and PtK1 cells that had been depleted of endogenous Hec1 (Miller et al., 2008, Guimaraes et al., 2008).

The structure of the coiled-coil region of the Ndc80 complex was characterised by cross-linking studies followed by mass spectrometry analysis (Maiolica et al., 2007). This confirmed a tetramerisation domain between the coiled coil regions of all subunits, as had been previously proposed (Wei et al., 2005, Ciferri et al., 2005). It also identified a gap within the Hec1-Nuf2 coiled-coil domain forming a 50 amino acid stretch of the Hec1 subunit, which was proposed to create a loop. Using this information, a construct was engineered in which the coiled-coil regions were removed from the sequence to create a complex with the globular N-terminal domain of Hec1 fused to the globular C-terminal domain of Spc25, creating a single polypeptide chain. This was also done for the N-terminal of Nuf2 and the C-terminal of Spc24, combing these fusions to create an engineered hetero-dimer, known as Ndc80 ‘bonsai’. This was crystallised and the structure solved (figure 1.2 D), identifying a second CH domain in the Nuf2 globular head (Ciferri et al., 2008). The Spc24/Spc25 globular domain from the human Ndc80 complex was also observed to have a similar structure to the budding yeast

Spc24/Spc25 domains, confirming structural conservation that had been previously suggested (figure 1.2 E) (Wei et al., 2006). The Hec1/Nuf2 head binding to MTs was analysed, and positively charged lysine residues were found to form patches on the surface of the Hec1/Nuf2 head separated by a negatively charged ridge. Multiple lysine residues in both Hec1 and Nuf2 mutated to either alanine or glutamate showed reductions in the binding affinity to MTs, indicating that both Hec1 and Nuf2 are necessary for MT binding. Removal of the acidic tails of tubulin by protease treatment reduced the affinity of Ndc80 bonsai-MT interactions, providing further indication of an electrostatic interaction between the heads of Hec1/Nuf2 and MTs (Ciferri et al., 2008). Visualisation of the *Caenorhabditis elegans* Ndc80 complex bound to a MT lattice was observed by negative stained EM (Cheeseman et al., 2006). These studies suggested that 1-2 Ndc80 complexes bind per α and β tubulin dimer, with all complexes binding at a similar angle and orientation relative to the MT (figure 1.2 F).

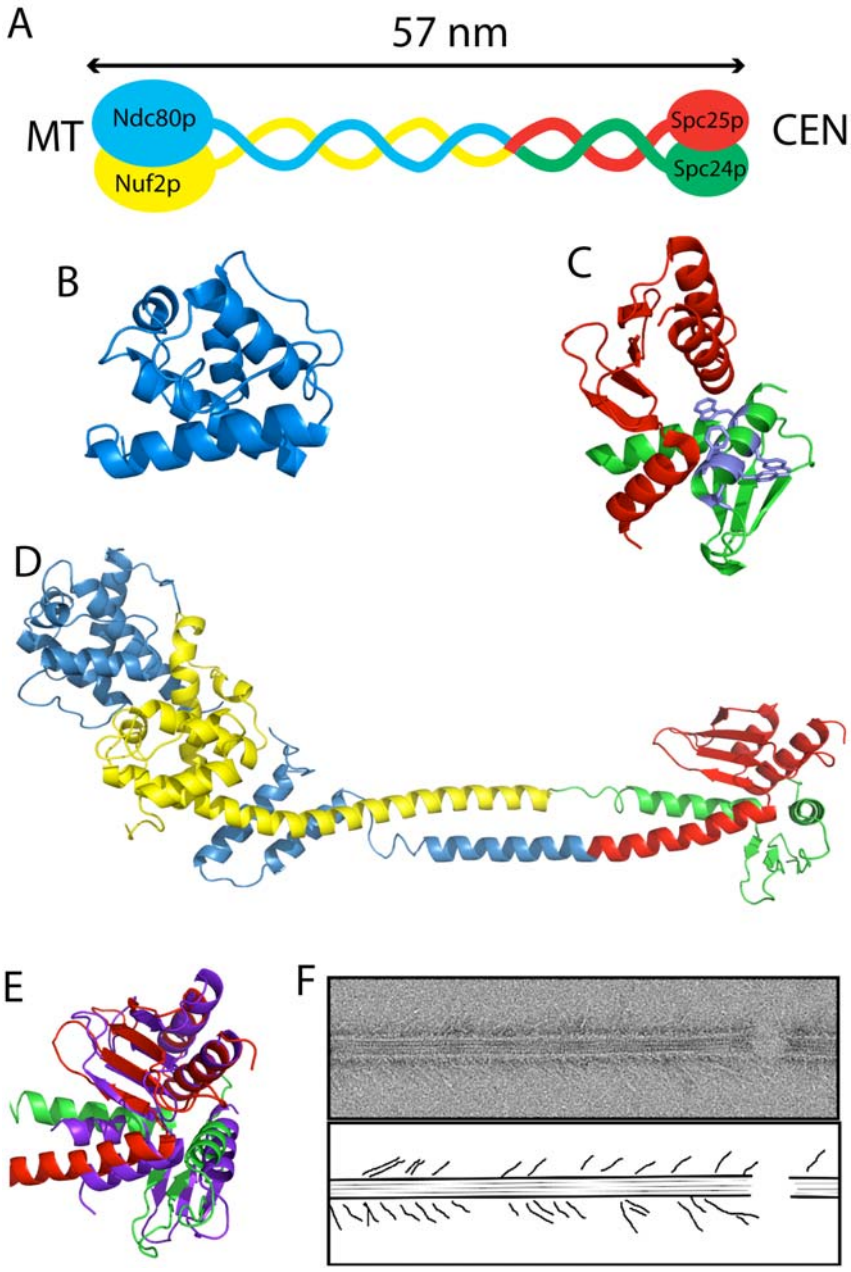

Figure 1.2 Structure of the Ndc80 complex

A) Adapted from(Wei et al., 2005). Schematic representation of the Ndc80 complex with subunits, Ndc80p (blue), Nuf2p (yellow), Spc24p (green) and Spc25p (red), with the length and orientation towards the MT or CEN also shown. B) CH domain of Hec1 this domain has structural homology to EB1 a known MT binding protein. C) Crystal structure of the Spc24 (green) /Spc25 (red) globular domains. Hydrophobic residues that were identified as a potential interaction surface are shown in blue. D) Crystal structure of the Ndc80 `bonsai` complex, complete globular heads with truncated coiled-coil region. CH domains are seen in the Ndc80 and Nuf2p heads. E) Structural alignment of the human SpcG domains from Ndc80 `bonsai´ (red and green) against the SpcG domains from *Saccharomyces cerevisiae* (purple), highlighting the conservation of this domain. F) Taken from (Cheeseman et al., 2006), the top panel is a negatively stained image of Ndc80 complex bound to a MT, showing a specific orientation of the protein on the MT and it's angle of binding. The bottom panel is a trace of the image

1.7.3 Spc105p/KNL-1/blinkin

The Spc105p protein was discovered in the same SPB analysis study that identified Ndc80p, Spc25p and Spc24p (Wigge et al., 1998). Immunoprecipitation of a protein A tagged Spc105p, identified an association with YDR532C (also known as Kre28p), as well as components of the Ndc80 complex (see section 1.7.4.1) (Nekrasov et al., 2003), the MIND complex (see section 1.7.4.1) (Nekrasov et al., 2003, De Wulf et al., 2003) and the Mcm21p subunit of the COMA complex (see section 1.7.1) (Pagliuca et al., 2009). However, immunoprecipitation using protein-A tagged Kre28p only observed an interaction with Spc105p, suggesting these proteins form a discrete complex (Nekrasov et al., 2003). Spc105p and Kre28p were confirmed as kinetochore proteins by observation of centromere localisation by ChIP, immuno-EM and fluorescence microscopy (Nekrasov et al., 2003, De Wulf et al., 2003). Spc105p was found to be an essential protein as cell growth arrested in *spc*105 t.s. mutants (Nekrasov et al., 2003).

1.7.3.1 Conservation and function of the SPC105 complex

Studies using an RNAi-based functional genomic screen in *Caenorhabditis elegans* embryos was used to detect chromosome segregation defects by observation of trapped nuclei in the cleavage furrow of the embryo. RNAi depleted proteins generating this phenotype were described as KNL “kinetochore-null”, with a novel protein KNL-1 identified. This protein localises to the kinetochore throughout mitosis and was shown to require CENP-A (see section 1.5.2) and CENP-C (see section 1.5.3) at the kinetochore for this localisation. Immunoprecipitation using anti-KNL-1 antibodies could also pull down Ndc80 and Nuf2 proteins (see section 1.7.2), indicating an interaction with kinetochore proteins. KNL-1 was found by sequence alignments to be the ortholog of *Saccharomyces cerevisiae* Spc105p (Cheeseman et al., 2004). KNL-1 was shown to interact with another protein, KNL-3 (the ortholog of Dsn1p see section 1.7.4.3). KNL-1 on its own was found to bind directly to MTs and form a network with Ndc80 and Mis12/MIND complexes (see section 1.8) (Cheeseman et al., 2006). In

Schizosaccharomyces pombe, overexpression of Spc7, an ortholog of Spc105 and KNL-1 could suppress a mutant of Mal3, the Bim1p/EB1 ortholog (see section 1.6.2) (Kerres et al., 2004). AF15q14, the human ortholog of KNL-1, was also found by sequence alignments and confirmed as the human version when pulled out from HeLa cells using tagged hMis12 (Cheeseman et al., 2004). Direct interactions of AF15q14 with Bub1 and Mad3/BubR1 were observed by yeast two-hybrid screens, leading to AF15q14 being renamed blinkin (bub-linking kinetochore protein) (Kiyomitsu et al., 2007).

1.7.4 The Mis12/MIND complex

In 1999 a *mis12-537* (minichromosome instability) t.s. mutant identified in *Schizosaccharomyces pombe* showed a chromosome missegregation phenotype with unequal segregation of chromosomes (Goshima et al., 1999). The *mis*12^{+} gene was isolated and Mis12 was identified as a 259 amino acid, 30 kDa protein. It was shown to be essential as spores lacking this gene were not viable. GFP-tagged Mis12 was observed to localise to centromeres throughout the cell cycle and ChIP assays showed that Mis12 interacts with CEN DNA and is important for structural maintenance of the centromere. Sequence searches identified the *Saccharomyces cerevisiae* ortholog Mtw1p (mis twelve-like). Mis12 and Mtw1p were shown to share sequence identity in the N-terminal and coiled-coil regions in the central part of the protein. The role of Mtw1p in chromosome segregation was also studied (Goshima and Yanagida, 2000) which characterised a conserved function for this protein. ChIP assays showed that Mtw1p interacts with CEN DNA during interphase and mitosis and this interaction is dependent on Ndc10p (see section 1.5.1). Mtw1p was also found to be an essential protein, with a *mtw*1-1 t.s. mutant showing a missegregation phenotype with long spindles and unequal segregation of sister chromatids, similar to the *mis12-537* mutant in *Schizosaccharomyces pombe* (Goshima et al., 1999).

1.7.4.1 The MIND complex in Saccharomyces cerevisiae

The MTW1 gene encoding Mtw1p protein was found to be a dosage suppressor of a t.s. mutant *nnf*1-17 (necessary for nuclear function) (Euskirchen, 2002). Previous studies had identified that the gene NNF1 was essential for cell viability (Shan et al., 1997). The Nnf1p protein was shown to be located in the nuclear envelope and depletion of this protein lead to defects in nuclear migration with an increase in large buds, abnormal numbers of nuclei in cells and elongated microtubules. In addition to MTW1, another dosage suppressor gene DSN1 (dosage suppressor of NNF1) was found to rescue the *nnf*1-17 t.s. mutant at the restrictive temperature (Euskirchen, 2002). DSN1 was shown to encode for a 576 amino acid, 66 kDa protein. A synthetic lethal screen found another set of genes that interact with NNF1, NSL (NNF1 synthetic lethal), which identified NSL1, encoding a 216 amino acid, 25 kDa protein. All 4 genes were shown to be essential and the proteins Dsn1p, Mtw1p, Nsl1p and Nnf1p, co-localised near the SPB and were suggested to exist as a complex (Euskirchen, 2002).

In 2003, 5 papers were published within one month of each other describing the interaction of these proteins in *Saccharomyces cerevisiae* (Nekrasov et al., 2003, Westermann et al., 2003, Pinsky et al., 2003, Scharfenberger et al., 2003, De Wulf et al., 2003). Immunoprecipitation assays found that Dsn1p, Mtw1p, Nsl1p and Nnf1p were interacting together and ChIP assays determined that all these proteins interact via other kinetochore proteins to CEN DNA and localise to the kinetochore (Scharfenberger et al., 2003, De Wulf et al., 2003, Nekrasov et al., 2003). The four proteins associating together were referred to as either the Mtw1 or MIND complex (Mtw1p including Nnf1p Nsl1p Dsn1p). These four proteins were also observed in pull-down assays to interact with other kinetochore proteins including components of the Ndc80 complex (see section 1.7.2) (Nekrasov et al., 2003, Westermann et al., 2003, De Wulf et al., 2003), Spc105p (see section 1.7.3) (De Wulf et al., 2003, Nekrasov et al., 2003), components of the Ctf19p complex (see section 1.7.1) (Westermann et al., 2003, Pinsky et al., 2003, De Wulf et al., 2003) and Mif2p (see section 1.5.3) (Westermann et al., 2003, Pinsky et al., 2003).

Mtw1p (Wigge and Kilmartin, 2001) and the Mtw1/MIND complex (Nekrasov et al., 2003) were isolated and identified from SPB extracts, indicating that the Mtw1/MIND complex associated with the MT binding face of the kinetochore. The Mtw1/MIND complex was also shown to interact with both the Ctf19 complex (Westermann et al., 2003, Pinsky et al., 2003, De Wulf et al., 2003) and Mif2p (Westermann et al., 2003, Pinsky et al., 2003), indicating an interaction with known kinetochore proteins that are localised to the centromere (Meluh and Koshland, 1995, Ortiz et al., 1999, Measday et al., 2002, Cheeseman et al., 2002). These interactions placed the Mis12/MIND complex in an overlapping region, suggesting it might provide a "bridge" between the DNA and MT binding sites of the kinetochore (Nekrasov et al., 2003). Hydrodynamic analysis of the Mis12/MIND complex indicated that the complex was extended in structure and various intermediates in the formation of the complete complex were observed (De Wulf et al., 2003). The complex stoichiometry was also proposed to be equimolar between all subunits by densitometric analysis by SDS-PAGE (Westermann et al., 2003).

1.7.4.2 The Role of Mtw1/MIND complex in chromosome segregation in Saccharomyces cerevisiae

The role of the Mtw1/MIND complex in the fidelity of chromosome segregation was also examined. *nsl*1-5 and *dsn*1-7 t.s. mutants each showed observable phenotypes (Nekrasov et al., 2003) similar to the *nnf*1-17 (Euskirchen, 2002) and *mtw*1-1 (Goshima and Yanagida, 2000) mutants. In the *nnf*1-17 and *mtw*1-1 mutants shifted to the non-permissive temperature, protein levels of the other subunits of the Mtw1/MIND complex were substantially reduced and their association with CEN DNA was abolished (De Wulf et al., 2003). A possible role in tension sensing was also suggested for Mtw1p, as unequal separation of sister chromatids was seen in the *mtw*1-1 mutants (Goshima and Yanagida, 2000). The role of sensing and monitoring tension between chromosomes and kinetochores had been identified for Ipl1/Aurora B kinase (see section 1.4.1) (Biggins and Murray, 2001). The protein levels of a known anaphase inhibitor Securin/Pds1p was used to characterise the relationship between Ipl1 and

Mtw1p. In the *mtw*1-1 mutant, levels of Pds1p were constant with no cyclic behaviour observed, however in the double mutant *mtw*1-1/*ipl*1-321, the cyclic behaviour of Pds1p protein levels was restored. This indicated that defects in Mtw1p create tension problems that are sensed by Ipl1p and lead to activation of the spindle checkpoint, preventing segregation (Pinsky et al., 2003). The *mtw*1-1 mutant was shown to have centromeres that were unattached to microtubules and in the double mutant this attachment defect was suppressed, identifying that *mtw*1-1 mutants can bind microtubules, but the attachment is incorrect and therefore released in a Ipl1p dependent manner (Pinsky et al., 2003). Nsl1p depletion was also shown to reduce levels of Pds1p in cells that have an active spindle checkpoint due to treatment with a microtubule depolymerising compound nocodazole, compared to cells with normal levels of Nsl1p (Scharfenberger et al., 2003). An *nsl*1-16 t.s. mutant was also implicated in the failure to create bi-polar attachments and Nsl1p depletion was shown to affect the levels of the Dam1 complex (see section 1.6.1). *In vitro* phosphorylation of the Mtw1/MIND complex identified that only Serine 250 on the Dsn1p subunit was a site for Ipl1p phosphorylation. However, *dsn*1 mutants (S250A and S250D) were viable and showed no observable mutant phenotype (Westermann et al., 2003).

1.7.4.3 Conservation of the Mtw1/MIND complex

Typical bioinformatics searches could not find any potential orthologs in higher eukaryotes, therefore searches were carried out by creating N-terminal ‘blocks’ of protein followed by a coiled-coil region that had been identified as conserved between Mis12 and Mtw1p. Three further fungal and two plant Mis12/Mtw1p orthologs were found and used as new block searches, which led to the identification of the human ortholog of Mis12 (Goshima et al., 2003). hMis12 was shown to localise to the centromere throughout the cell cycle and co-localised with the human equivalents of Cse4p and Mif2p (CENP-A and CENP-C), identifying hMis12 as a kinetochore protein.

A higher eukaryotic homologue of Mis12/Mtw1p was also identified using an RNAi-based functional genomic screen in *Caenorhabditis elegans* oocytes that had previously identified KNL-1 (see section 1.7.3) (Desai et al., 2003) and KNL-3 (Cheeseman et al.,

2004). Immunoprecipitation using KNL-1 and KNL-3 could pull out the Mis12/Mtw1p homologue along with other known kinetochore proteins leading to KNL-3 being identified as an ortholog of Dsn1p (Cheeseman et al., 2006). These reports into higher eukaryotes established that the function of Mis12/Mtw1p is not only conserved throughout lower to higher eukaryotes, but also conserved between kinetochores at regional, holocentric and point centromeres. With this conservation apparent, the question was whether the whole complex is conserved throughout evolution.

Schizosaccharomyces pombe orthologs of Dsn1p, Nsl1p and Nnf1p were found to rescue the t.s. *mis*12-537 mutant and localised to the centromere (Obuse et al., 2004). All three proteins also co-purified with affinity tagged Mis12 (Liu et al., 2005), indicating that the Mis12/MIND complex is conserved in *Schizosaccharomyces pombe*. Human orthologs of components of the Mis12/MIND complex were also identified by immunoprecipitation with hMis12 (Obuse et al., 2004, Kline et al., 2006). When the human Dsn1p equivalent was knocked-down by RNAi, kinetochore misalignment and elongated spindles were observed (Obuse et al., 2004). Co-expression of the human Mis12/MIND complex in bacteria, showed an association of a stable complex throughout affinity and size exclusion chromatography (Kline et al., 2006), with an elution profile suggesting that this complex consists of a hetero-tetramer with a single copy of each protein. Sequential RNAi depletion of each subunit in chicken DT40 cells indicated that all four proteins are interdependent for kinetochore localisation and stability of the complex. HeLa cells with RNAi of hDsn1, hNnf1, hNsl1 or hMis12, were shown to remain in mitosis on average for 8 hours compared to normal cells that completed mitosis in approximately 1 hour. Chromosome alignment defects were also seen with hMis12 RNAi, confirming a role for the human Mis12/MIND complex in chromosome alignment and segregation. hMis12 has been identified to function in the bi-orientated attachments of microtubules to kinetochores, similar to the role suggested for Mis12/Mtw1p proteins in *Schizosaccharomyces pombe* and *Saccharomyces cerevisiae* (Goshima et al., 1999, Goshima and Yanagida, 2000, Goshima et al., 2003, Kline et al., 2006), further highlighting the role of the Mis12/MIND complex in tension sensing and the correct attachment to microtubules. RNAi of hNnf1, in combination with depolymerisation of MTs by nocodazole prevented Mad1, Mad2, Bub1 and BubR1/Mad3p (components of the SAC) from interacting with the kinetochore,

indicating a role of the MIND complex in recruiting SAC proteins (McAinsh et al., 2006). Human Mis12/MIND complex was also found to interact with the heterochromatin binding protein HP1, suggesting that human Mis12/MIND may be linked to heterochromatin without the requirement of CENP-A (Obuse et al., 2004).

Inspection of the amino acid sequences of orthologs of the Mis12/MIND complex by PCOILS (Lupas et al., 1991) predicts coiled-coil regions in all four components (figure 1.3). Similar coiled-coil regions are also observed in other linker complexes including the Ndc80 and Spc105 complexes (see section 1.8 and figure 1.5). However, the predicted coiled-coil regions within orthologs of the MIND complex are not conserved to specific lengths or locations within sequences. This differs to orthologs of the Ndc80 complex, in which all components show conservation in both length and location of their coiled-coil motifs. This would indicate that there might be some variation in the structure of the MIND complex within eukaryotes based on this initial sequence inspection.

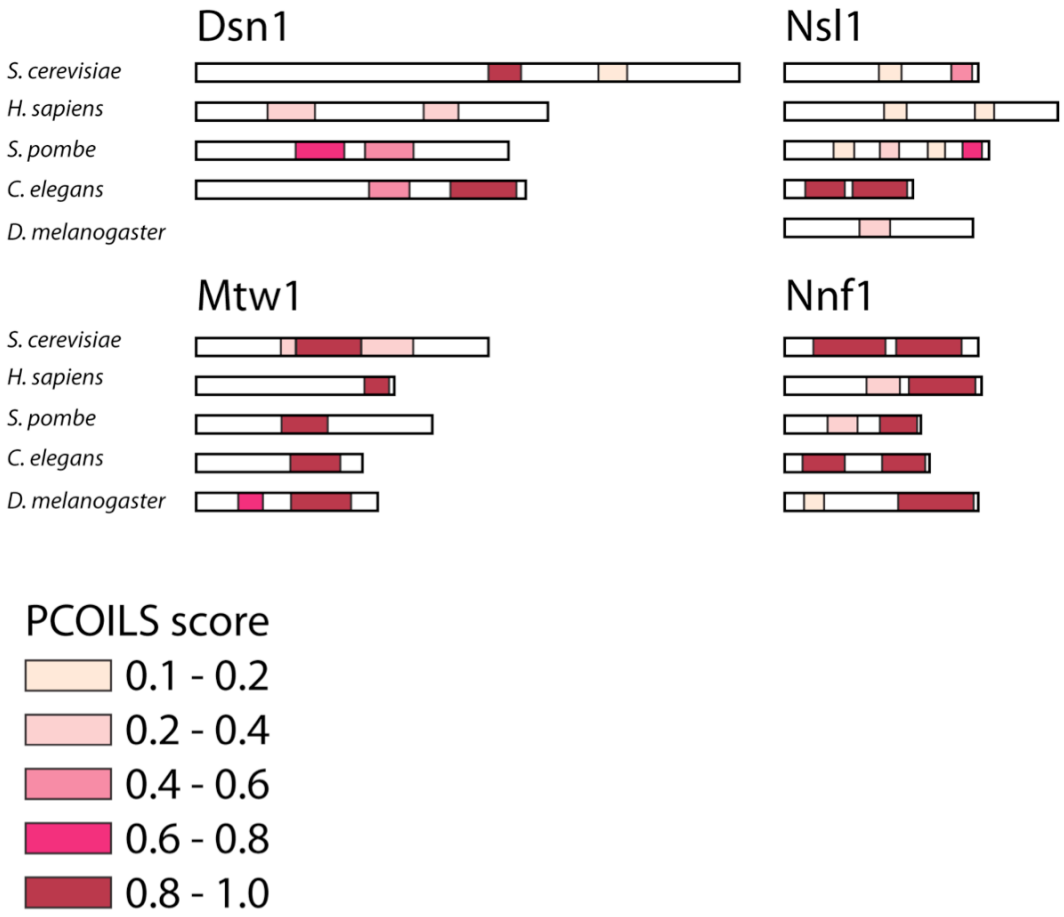

Figure 1.3 Coiled-coil predictions for the MIND complex

Schematic view of the orthologs of components of the Mis12/MIND complex. Coiled-coil regions are indicated by coloured blocks, corresponding to length and position generated by PCOILS (Lupas et al., 1991). All rectangles are to scale. Probability of each region being coiled-coil is indicated by colour intensity with reference to PCOILS score chart.

1.8 The KMN network

At the same time as each of the Ndc80, Spc105 and MIND complexes were found to exist as discrete complexes within the kinetochore, these proteins were also being implicated in the formation of a larger conserved network in all eukaryotes (Nekrasov et al., 2003, Cheeseman et al., 2004, Liu et al., 2005, Meraldi et al., 2006, Przewloka et al., 2007).

The first biochemical characterisation of this network came from an *in vitro* reconstitution of a network comprising KNL-1, Mis12 and Ndc80 complexes from *Caenorhabditis elegans* and was referred to as the KMN network (Cheeseman et al., 2006). MT binding was found in both the Ndc80/Nuf2 dimer and KNL-1, but was not observed in the third component the Mis12 complex. When the Spc24/Spc25 dimer and the Mis12 complex were added together with the Ndc80/Nuf2 dimer and KNL-1, the MT binding affinity of this network was found to be greater than the KNL-1 and Ndc80/Nuf2 complex binding affinities added together (Cheeseman et al., 2006). This suggested a role for the Mis12 complex in providing a platform for KNL-1 and the Ndc80 complex to generate a more favourable interaction with the MT and therefore producing this observed synergistic increase in binding (Cheeseman et al., 2006). Electron tomography of kinetochores from PtK1 cells observed a meshwork of fibres that connected adjacent MTs to one another and to chromatin, with this matrix proposed to be the KMN network along with other linker complexes (Dong et al., 2007).

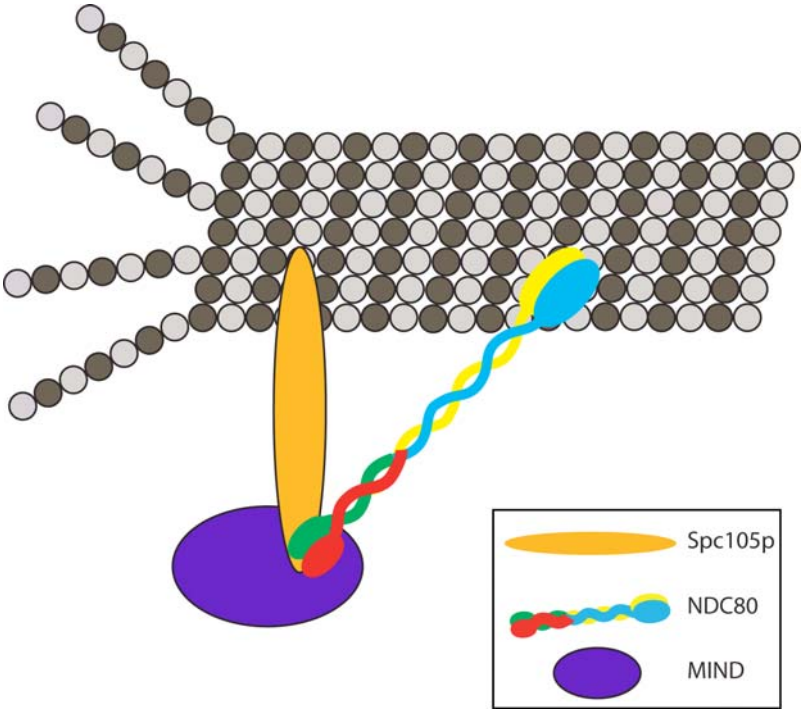

Figure 1.4 Model of the MT binding of the KMN network

Adapted from (Cheeseman et al., 2006). A Microtubule comprised as light and dark grey circles (α and β tubulin) bound to Spc105 (orange oval) and Ndc80 (blue, yellow, red and green components as shown in figure 1.2). Binding orientation is known for Ndc80 (Cheeseman et al., 2006). Two discrete MT binding sites are proposed for the KMN network. KNL1/Spc105 and Ndc80 complex are further bound by MIND complex (purple oval). The specific interaction sites between all components are unknown.

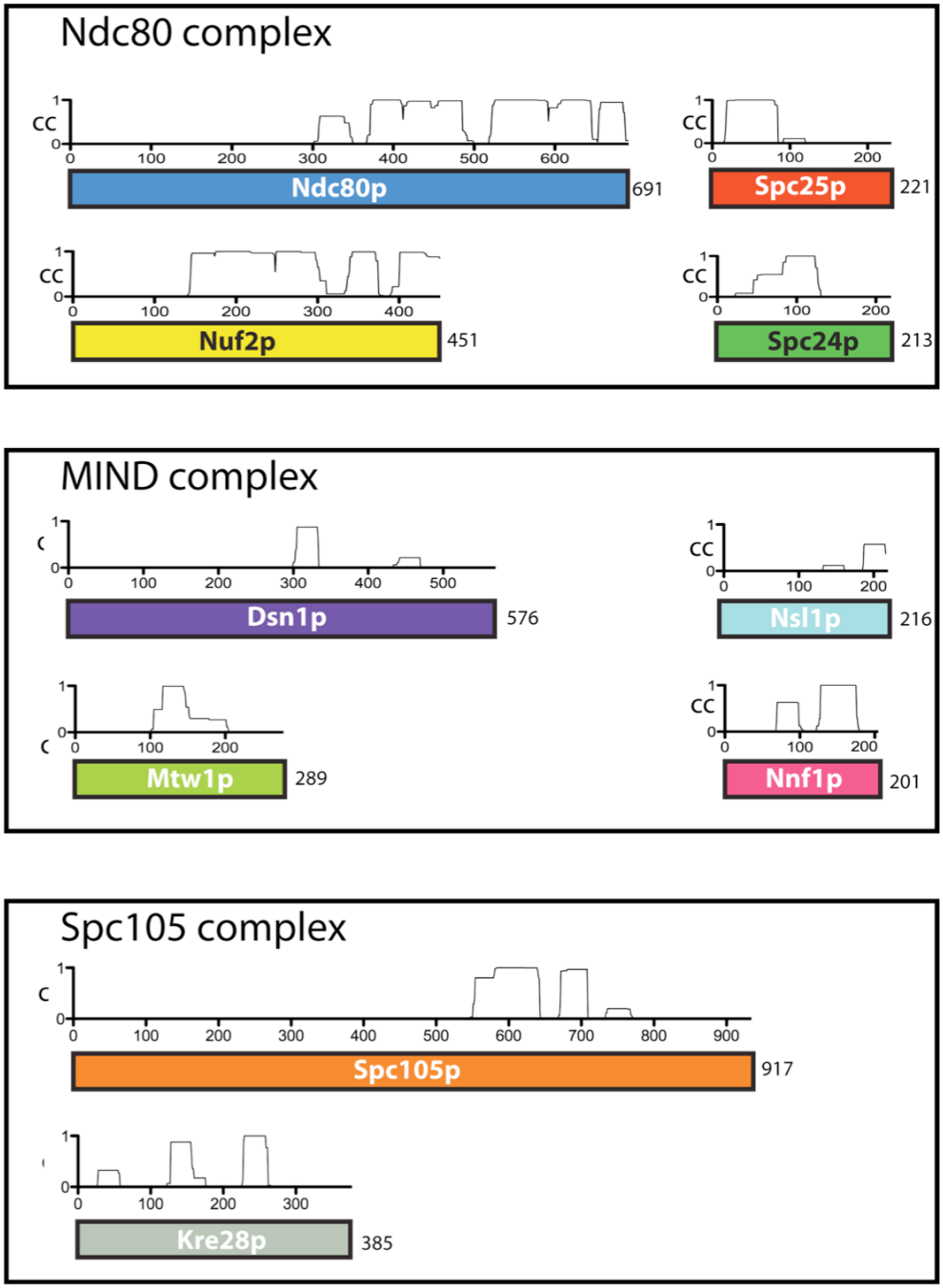

Figure 1.5 Coiled-coil predictions of components of the KMN network

Adapted from (Ciferri et al., 2008).The three KMN complexes are shown in separate boxes with their components shown as a named coloured rectangles drawn to scale. Above each rectangle is the output file from PCOILS (Lupas et al., 1991), with the coiled-coil score (cc) plotted against the amino acid in the sequence. All components of the KMN network possess predicted coiled coil regions, indicating potential flexibility in this network. Ydr532c is also referred to as Kre28p and is included in this schematic as it has been shown to bind with Spc105p (Nekrasov et al., 2003).

1.9 Structure of the *Saccharomyces cerevisiae* kinetochore

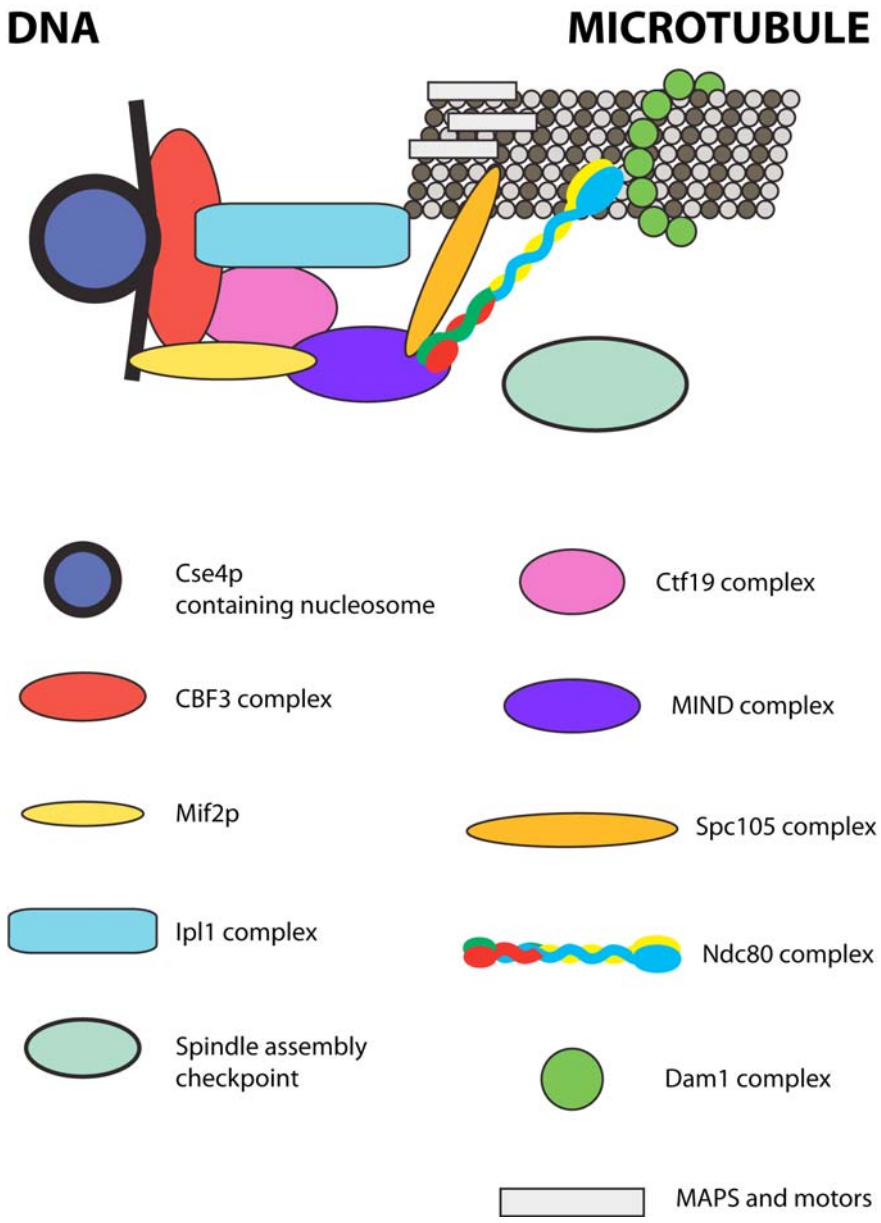

Figure 1.6 Model of the *Saccharomyces cerevisiae* kinetochore

Adapted from (Westermann et al., 2007). Schematic representation of the architecture of the *Saccharomyces cerevisiae* kinetochore. For simplicity only single complexes are shown (apart from the Dam1 ring). Components are also identified below, labelled with complex name. The spindle assembly checkpoint is included, but as its is a transient association it is shown not to be part of the structure of the kinetochore Some structural information is shown for the Ndc80 complex and Dam1 complexes creating a ring formation. The quantity of each protein complex required to form a functional kinetochore is discussed further in this section.

In vivo analysis using quantitative fluorescence microscopy indicates that one CBF3 complex, one Cse4p nucleosome (with 2 copies of Cse4p) and a dimer of Mif2p are found at the kinetochore during metaphase and may act as a platform to recruit further kinetochore proteins (Joglekar et al., 2006). 16-20 copies of the Dam1 complex are found at metaphase, which correlate to the formation of a ring around the MT (Westermann et al., 2005, Miranda et al., 2005). The linker region has each component in various amounts, 5 Spc105p, 6-7 MIND complexes and 8 Ndc80 complexes (Joglekar et al., 2006). If a KMN network is formed in *Saccharomyces cerevisiae* it may be formed from multiple copies of each complex in an undetermined ratio or some complexes such as Ndc80 might associate at the kinetochore without forming part of the KMN network. 3 Ctf19 complexes are observed which is less than the values for the other components, suggesting that they may provide a supporting role in linking complexes together.

1.10 Research objectives

The KMN network has been suggested to be the main MT binding site of the kinetochore, with all three components, Ndc80, Spc105 and MIND of this network have been found to be essential for cell viability. This network is also a substrate for Ipl1p kinase activity, identifying it as a key site for phospho-regulation of MT-kinetochore attachments. Structural and functional characterisation has focused primarily on the Ndc80 complex, which has lead to a detailed understanding of its role in MT attachment (see section 1.7.2). The other two components, the MIND complex and Spc105p are poorly understood with respect to structure.

The aim of the work described in this thesis was to characterise both the MIND complex and Spc105p from *Saccharomyces cerevisiae* using structural and biochemical techniques. Together with the previously published data of the characterised Ndc80 complex, this study would lead to a greater understanding of both the KMN network and the overall structure of the kinetochore. The role of the Ipl1p kinase

phosphorylation of the MIND complex was also investigated to identify its effects on the formation of the KMN network.

Chapter 2.

2.1 Aims

The Mis12/MIND complex is essential and conserved throughout eukaryotes (Euskirchen, 2002, Cheeseman et al., 2004, Obuse et al., 2004), however very little structural information is known about this complex. It has been shown to consist of four subunits, Dsn1p, Mtw1p, Nsl1p and Nnf1p, however the subunit stoichiometry for the complex has yet to be accurately determined. Previous studies in *Saccharomyces cerevisiae* using Coomassie stained SDS-PAGE densitometry analysis (Westermann et al., 2003) had suggested that an equimolar ratio of all the subunits of the MIND complex. Glycerol gradients and size exclusion chromatography analysis (De Wulf et al., 2003) of the MIND complex suggested various intermediates occur before the full complex is formed. The aims in this results chapter were to express, purify and characterise the MIND complex from *Saccharomyces cerevisiae* using recombinant expression systems.

2.2 Expression and purification of the MIND complex

The recombinant MIND complex was prepared by co-expression in *Escherichia coli* of the four components of this complex, Dsn1p, Mtw1p, Nnf1p and Nsl1p. Constructs containing the genes of interest were already available in the lab (see section 6.2). pDSN1, pMTW1 and pNNF1.NSL1 were co-transformed into *Escherichia coli* BL21(DE3) RIL cells. Protein expression was carried out following the standard protocol (see section 6.5).

2.2.1 Affinity purification of the MIND complex

pDSN1 contains a N-terminus His-tag and the MIND complex was initially purified by Ni-NTA affinity chromatography using a 5ml HisTrap FF column (see section 6.6.1.2). A 20-500mM imidazole gradient eluted a single peak (figure 2.1 A),

with SDS-PAGE (figure 2.1 B) showing four distinct protein bands that, by comparison to the protein marker, have similar masses to each subunit. All four bands were excised from the gel and sent to the Protein Analysis & Proteomics laboratory, Cancer Research UK for mass spectrometry analysis. Each band was confirmed to be one of the four subunits, identifying that the complex is stable during affinity purification. An additional band observed at around 62 kDa was identified to be the *Escherichia coli* protein chaperone Hsp70. Chaperone contamination is often observed when expressing recombinant proteins in *Escherichia coli* (CCP4 bulletin board). In order to facilitate the removal of this contaminant, denatured protein along with ATP was added as a wash stage during affinity chromatography. Denatured *Escherichia coli* proteins are added as a preferred substrate for the chaperone. Substrate binding and release from Hsp70 is coupled to the chaperones ATPase activity. Therefore ATP would bind to the chaperone and lead to turn over and release of the MIND complex and would allow the chaperone to bind the denatured proteins (Rial and Ceccarelli, 2002). As neither the chaperone nor the denatured protein contain a His-tag, they should elute from the column leaving only the MIND complex bound. However, this method was unsuccessful and no reduction in chaperone contamination was seen (data not shown), suggesting that MIND may posses unfolded regions that lead to tight binding with the chaperone.

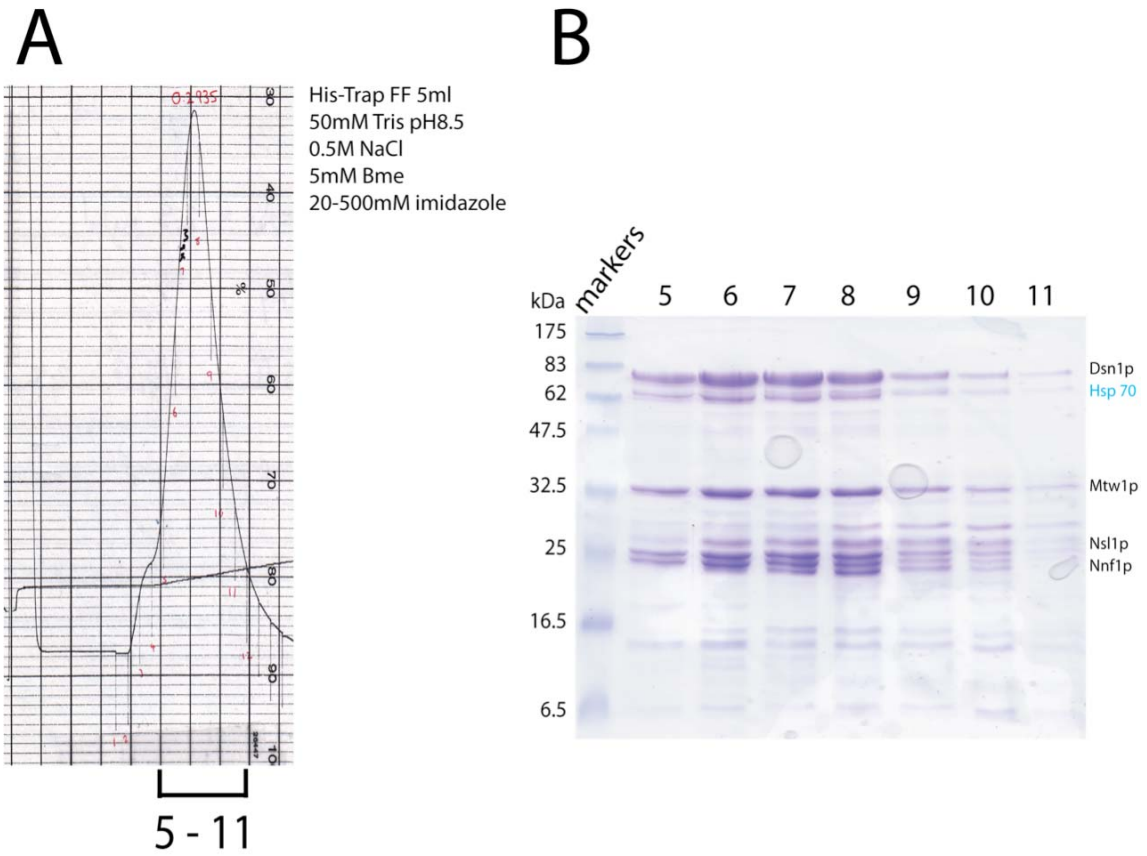

Figure 2.1 Affinity purification of the recombinant MIND complex

A) Elution profile of the MIND complex (black line), which elutes as a single peak from a 5ml HisTrap FF column. B) SDS-PAGE of fractions eluted from Figure 2.1 A. All four bands are observed in fractions 5-11 with proteins identified. The molecular weights from amino acid composition are, 66 kDa for Dsn1p, 33 kDa for Mtw1p, 25 kDa for Nsl1p, 23.6 kDa for Nnf1p.

2.2.2 Size exclusion purification of the MIND complex

Further purification was carried out by loading fractions containing the MIND complex onto a pre-equilibrated size exclusion, Superdex 200 16/60 column. From the elution profile (figure 2.2 A) a single peak was observed with a higher molecular weight shoulder eluting first. SDS-PAGE of the fractions from this elution (figure 2.2 B), showed that all subunits of the MIND complex were present in both the peak and the shoulder. The MIND complex used for subsequent experiments was taken from the main part of the peak.

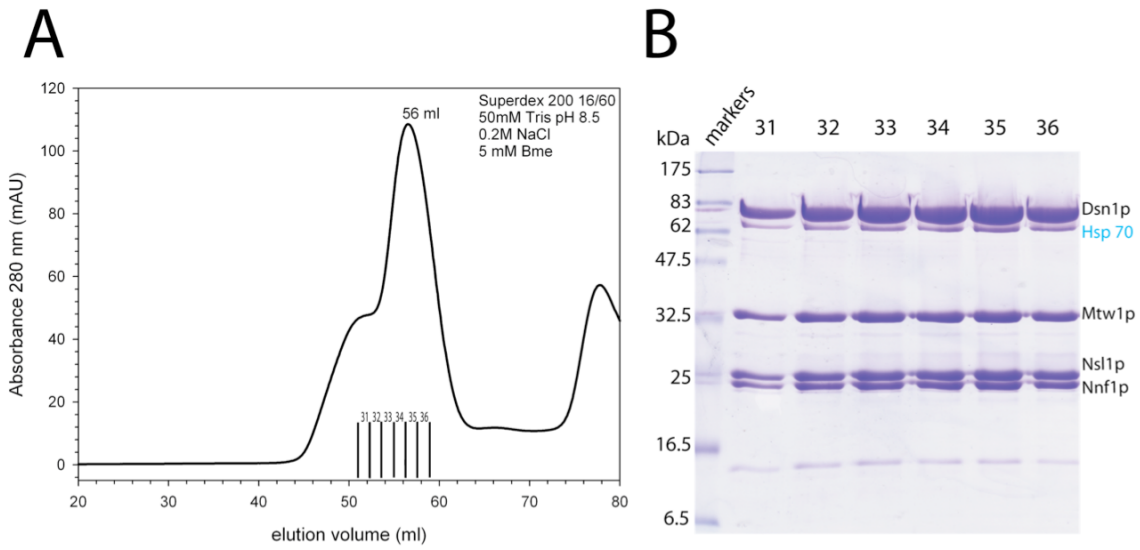

Figure 2.2 Size exclusion chromatography of the MIND complex.

A) Elution profile of MIND complex from size exclusion chromatography. Elution volume and relevant fractions of the peak have been marked. B) SDS-PAGE of fractions eluted from A). four bands corresponding to the MIND complex subunits are seen in fractions 31-36.

The elution volume from size exclusion chromatography can provide information on the molecular mass of a protein. A calibration curve (figure 6.1) was created for the superdex 16/60 column using known molecular weight standards and their elution volumes (see section 6.6.2). Using Equation 1 and Equation 2, the molecular mass of a protein can be calculated from its elution volume from the column.

$$Kav = \frac{(Vr - Vo)}{(Vc - Vo)}$$ **Equation 1**

$$Mw = e^{\frac{(2.2356 - Kav)}{0.1630}}$$ **Equation 2**

Vr = elution volume of the protein

Vo = elution volume of the void (45.8 ml) (obtained from blue dextran elution profile)

Vc = bed volume of the column (115ml)

The mass of the complex predicted from amino acid composition, with a single subunit of each of the four complexes would be 147.9 kDa. Previous studies (De Wulf et al., 2003) have suggested that the MIND complex may exist as intermediates with various molecular weights *in vivo*. During size exclusion chromatography only one peak corresponding to MIND is seen. The MIND complex eluted at 56 ml, giving a predicted molecular mass using Equations 1 and 2, of 366 kDa. This calculation is based on the assumption that the protein adopts a completely spherical shape when eluting from the column. Either the MIND complex is comprised of multimers of all subunits in an unknown ratio, or it may not be spherical, adopting a more extended shape (De Wulf et al., 2003), which would lead to an inaccurate molecular mass prediction from size exclusion chromatography.

2.2.3 Anion exchange purification of the MIND complex

Anion exchange chromatography was carried out to increase the purity of the MIND complex. The theoretical isoelectric point (pI) of the MIND complex using amino acid composition and the SCRIPPS protein calculator server (www.scripps.edu/~cdputnam/protcalc.html) was calculated to be 5.1. An anion exchange Mono Q 5/50 GL column using a 0.1 – 1 M NaCl gradient at pH 7.5 eluted the MIND complex at a conductivity of 30 mS/cm. The purity at this stage was still not sufficient (data not shown) as Hsp70 was still present in an amount that was unsuitable for further analysis.

Estimated charges for the MIND complex and the *Escherichia coli* chaperone Hsp70, were calculated at various pH values using the SCRIPPS protein calculator server. The aim was to find a pH in which the charge difference between the MIND complex and Hsp70 were sufficient to enable separation by anion exchange chromatography. Purification using a Mono Q 5/50 GL column with a buffer at pH 8.5, was found to be the most successful pH to separate the MIND complex from Hsp70. Subsequently all previous purification steps carried out at pH 7.5 were changed to a pH of 8.5. This had no effect on the initial purification steps (data not shown), but removed the need for dialysis into a suitable buffer at a pH of 8.5 for anion exchange

chromatography. The anion exchange profile showed a small initial peak of Hsp70 at a conductivity of 26 mS/cm followed by a major peak at a conductivity of 34 mS/cm (figure 2.3 A). Analysis by SDS-PAGE (figure 2.3 B) showed that the major peak contained all subunits of the MIND complex. A shoulder observed on the right side of this peak was found to be Mtw1p and Nnf1p components of the MIND complex, suggesting partial dissociation.

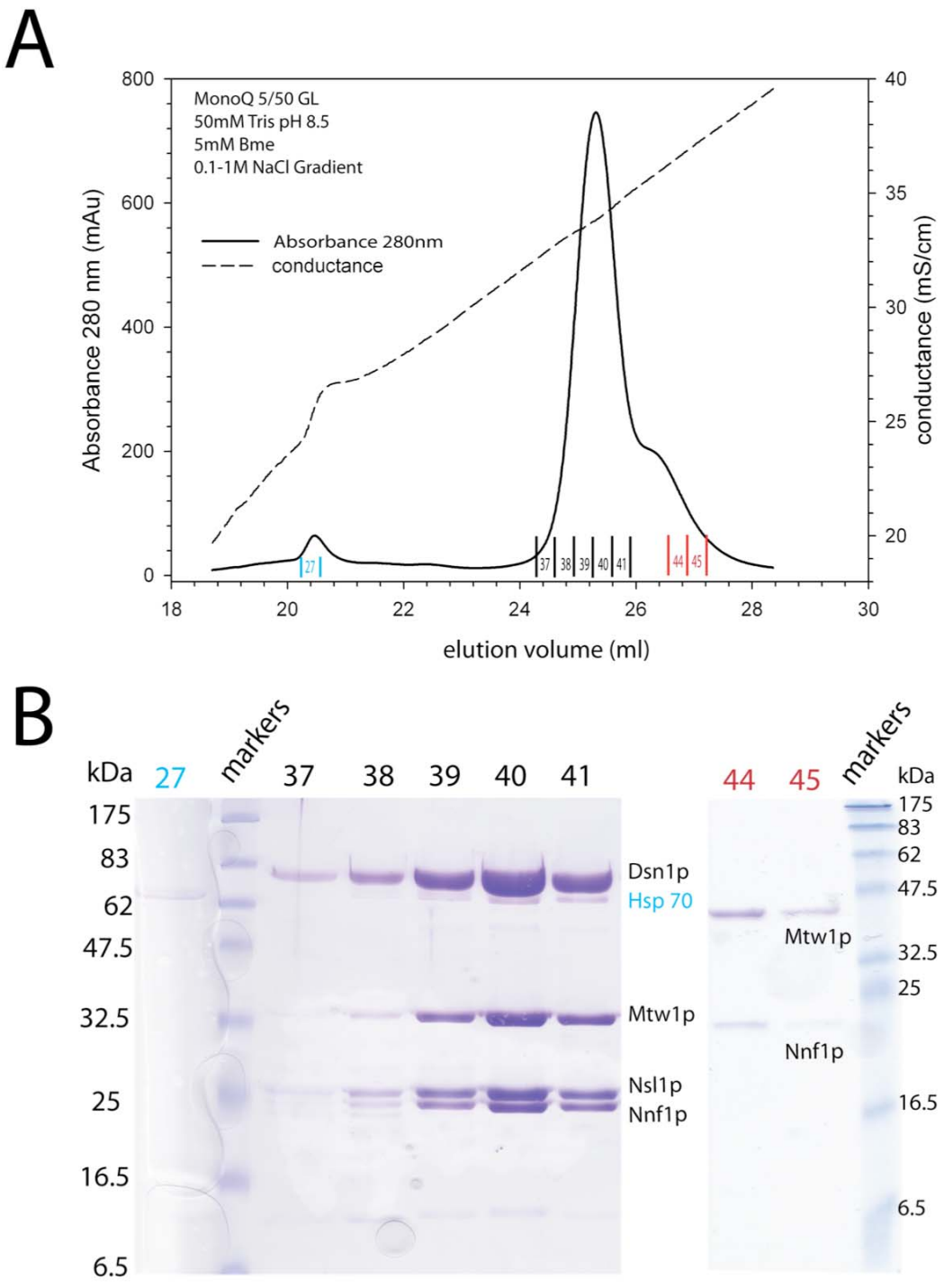

Figure 2.3 Anion exchange chromatography of the MIND complex

A) Elution profile of MIND complex from anion exchange chromatography. Absorbance reading of elution at 280 nm is the continuous line, conductance is the dashed line. Relevant fractions of the peak are marked. The fraction highlighted in blue is the *Escherichia coli* chaperone Hsp70. Fractions highlighted in red are from dissociation of the MIND complex. B) SDS-PAGE of fractions eluted from A), with the black, blue and red fractions corresponding to colours used in A).

2.3 Expression and purification of Mtw1p / Nnf1p and Dsn1p / Nsl1p sub-complexes

The observed dissociation of the MIND complex (see section 2.2.3) suggested that Mtw1p and Nnf1p could associate as an intermediate in the formation of the full complex. Neither Dsn1p or Nsl1p were observed to dissociate during purification by anion exchange chromatography. However, previous studies (De Wulf et al., 2003) had identified various species with different calculated molecular masses. One of the species corresponded to a molecular weight of 89 kDa. Although various combinations of the subunits could make up this molecular weight species, one plausible combination is the Dsn1p (66 kDa) and Nsl1p (25 kDa) proteins, associating together in a 1:1 ratio.

2.3.1 Co-expression and purification of Mtw1p and Nnf1p

The pMTW1 construct was already available (see section 6.2). The NNF1 gene was cloned into the pET28a vector using the NdeI and XhoI forward and reverse restriction sites. This vector encodes an N-terminal His-tag on Nnf1p to allow affinity purification. The two constructs were co-transformed and expressed in *Escherichia coli* BL21(DE3) RIL cells using the standard protocol (see section 6.5). The co-expressed Mtw1p and Nnf1p were initially purified using the Ni-NTA batch purification method (see section 6.6.1.1). SDS-PAGE (figure 2.4 A) identified that Mtw1p and Nnf1p proteins eluted from the Ni-NTA resin together, indicating an association. Protein containing fractions were loaded onto a pre-equilibrated size exclusion Superdex 200 16/60 column. A single peak in the elution profile was observed (figure 2.4 B), with SDS-PAGE (figure 2.4 C) observing that both Mtw1p and Nnf1p associate together, forming a stable complex during size exclusion chromatography. The gel also indicated that the ratio of this complex could be 1:1. The peak eluted at a volume of 70 ml, corresponding to a molecular weight of 105.9 kDa. The molecular masses of Mtw1p and Nnf1p are 33 kDa and 23.6 kDa respectively and a heterodimer with one copy of each protein would be 56.6 kDa. The calculated mass of 105.9 kDa suggests that either an association is occurring between the two hetero-dimers, assuming a spherical shape

is adopted during the elution or the complex is extended in solution making calculations from size exclusion inaccurate.

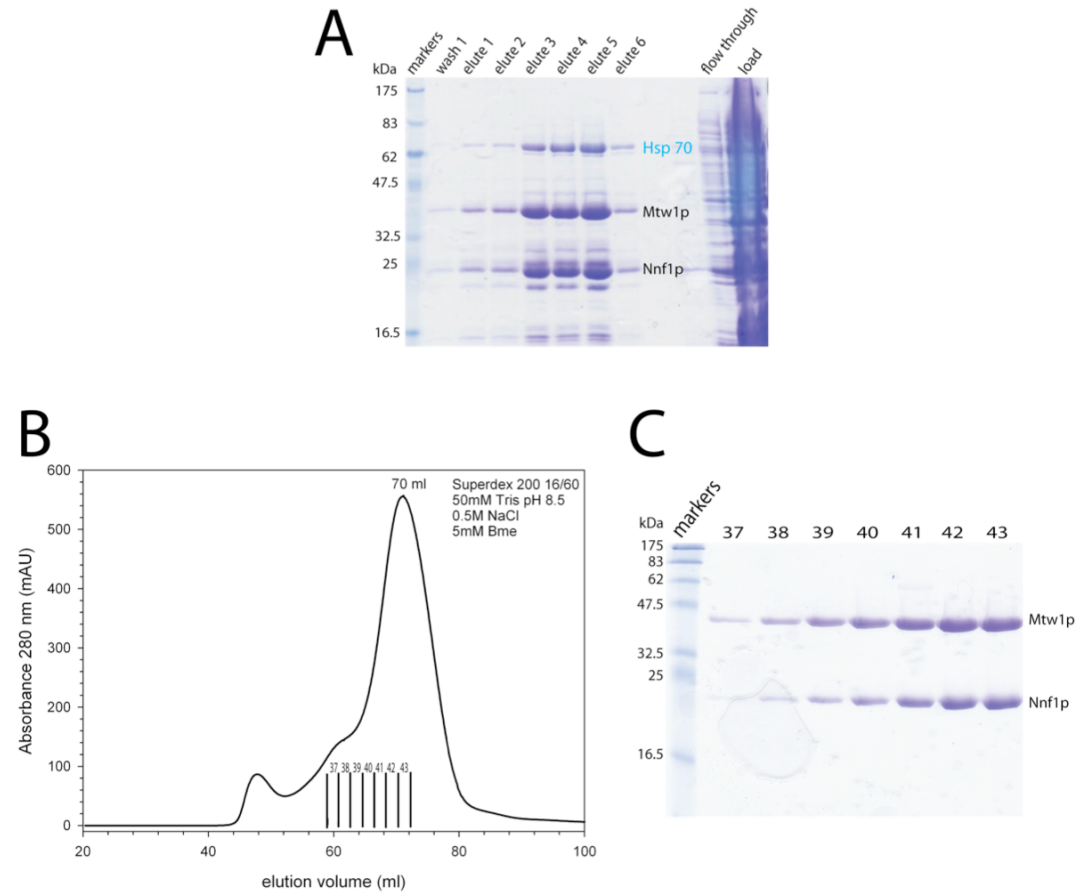

Figure 2.4 Co-expression and Purification of Mtw1p and Nnf1p

A) SDS-PAGE of the elution of Mtw1p and Nnf1p co-expression by Ni-NTA resin batch purification, relevant proteins are identified. B) Elution profile of Mtw1p and Nnf1p co-expression from size exclusion chromatography. Elution volume and relevant fractions of the peak have been marked. C) SDS-PAGE of fractions eluted from B)

2.3.2 Co-expression and purification of Dsn1p and Nsl1p

The pDSN1 construct with a N-terminal His-tag was already available (see section 6.2). The NSL1 gene was cloned into a pET22a vector the using the NdeI and XhoI forward and reverse restriction sites. The two constructs were co-transformed and expressed in *Escherichia coli* BL21(DE3) RIL cells using the standard protocol. The co-expression of Dsn1p and Nsl1p was initially purified using the Ni-NTA batch purification method. SDS-PAGE (figure 2.5A) showed that Dsn1p and Nsl1p proteins eluted from the Ni-NTA resin, indicating an association. Hsp70 contamination was also seen, along with probable proteolysis products of Dsn1p. Co-purification of Dsn1p and Nsl1p by size exclusion chromatography (figure 2.5 B) also identified a stable association. SDS-PAGE (figure 2.5 C) suggested that the proteins were associating in a 1:1 ratio. The molecular mass calculated from the gel filtration elution volume of 59 ml, giving an estimated mass of 280 kDa. The molecular mass of a hetero-dimer of Dsn1p and Nsl1p is 91 kDa, therefore this complex may comprise of more that one copy of both Dsn1p and Nsl1p. Another explanation is that the sub-complex is extended in solution leading to an inaccurate calculation of the molecular mass of this sub-complex.

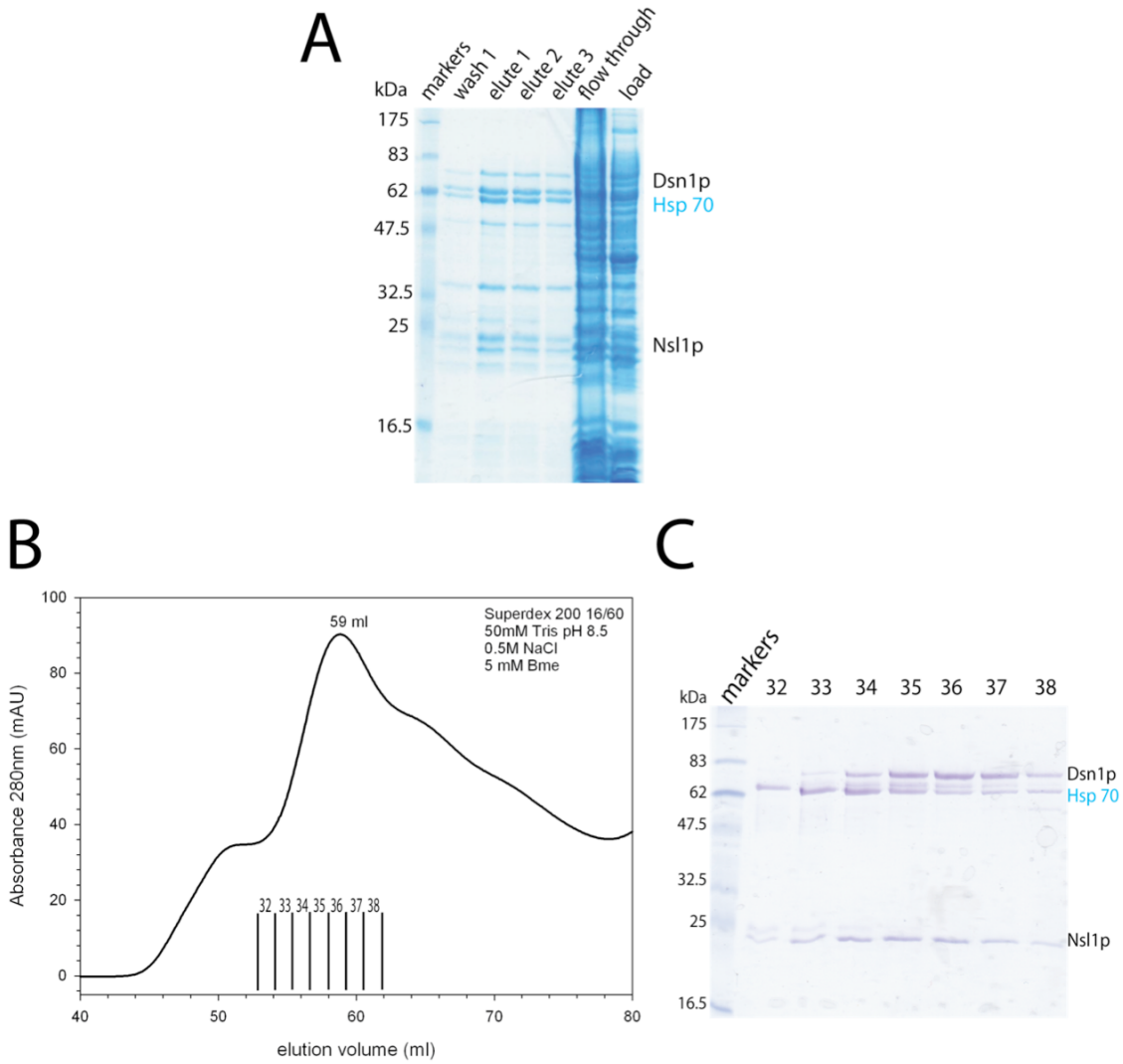

Figure 2.5 Co-expression and purification of Dsn1p and Nsl1p

A) SDS-PAGE gel of the elution of Dsn1p and Nsl1p co-expression by Ni-NTA resin batch purification, relevant proteins are identified. B) Elution profile of Dsn1p and Nsl1p co-expression from size exclusion chromatography. Elution volume and relevant fractions of the peak have been marked. C) SDS-PAGE of fractions eluted from B), a proportion of the *Escherichia coli* chaperone Hsp70 is seen to elute before Dsn1p and Nsl1p in fractions 32 and 33. Chaperone is still seen to associate with the Dsn1p and Nsl1p complex. A ladder of bands is also observed indicating proteolysis at either N or C-termini of Dsn1p

2.4 Reconstitution of the MIND complex from Dsn1p/Nsl1p and Mtw1p/Nnf1p sub-complexes

The association of the Dsn1p/Nsl1p and Mtw1p/Nnf1p sub-complexes was examined by analytical gel filtration. Equimolar amounts of each complex were mixed and incubated overnight at 4°C on a rolling platform. The sample was loaded onto a pre-equilibrated size exclusion Superdex 200 10 / 300 GL column and eluted. A single peak was observed from the elution profile (figure 2.6 A), with SDS-PAGE (figure 2.6 B) showing that all protein subunits were present in this peak. The elution profiles from the reconstituted MIND and the MIND complex purified in section 2.2.3 can be superimposed, indicating that the MIND complex can be reconstituted from Dsn1p/Nsl1p and Mtw1p/Nnf1p sub-complexes.

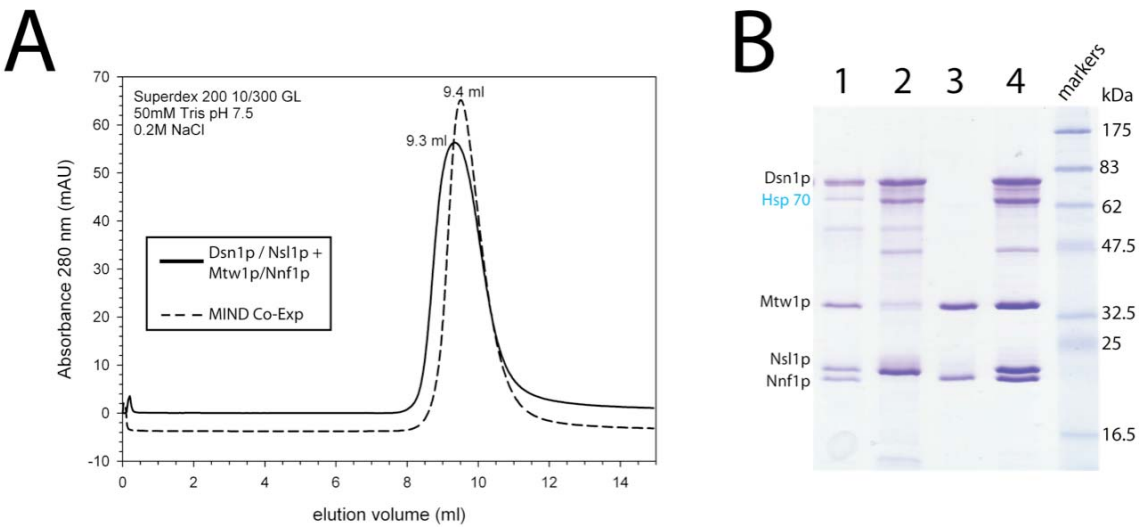

Figure 2.6 Reconstitution of the MIND complex

A) Elution profiles from analytical size exclusion chromatography of MIND reconstituted from Dsn1p/Nsl1p and Mtw1p/Nnf1p (continuous line) and co-expressed MIND complex from all 4 subunits (dashed lines). Both peaks have comparable elution volumes. B) Lanes: 1-intact complex from co-expression of all 4 proteins, 2–Dsn1p/Nsl1p sub-complex, 3–Mtw1p/Nnf1p sub-complex, 4–Complex reconstituted from Dsn1p/Nsl1p and Mtw1p/Nsl1p sub-complexes.

2.5 Hydrodynamic characterisation of the MIND complex

The MIND complex elutes as a single peak from affinity, size exclusion and anion exchange chromatography. However, the exact stoichiometry of the MIND complex could not be comprehensively identified from these studies. SDS-PAGE indicates that all proteins are present in a similar ratio, but how many copies of each subunit are present in the MIND complex is unknown. To further assess the homogeneity of the purified MIND complex and subunit composition, dynamic light scattering and analytical ultracentrifugation experiments were carried out.

For all these experiments the MIND complex (purified to the level observed in figure 2.3B), Dsn1p/Nsl1p and Mtw1p/Nnf1p were dialysed into a 50 mM Tris-HCl pH 7.5, 100mM NaCl buffer.

2.5.1 Dynamic light scattering of the MIND complex

Dynamic light scattering (DLS) was used to analyse the MIND complex. Passing a laser through particles in solution scatters the light in all directions, which is detected and can be used to calculate a hydrodynamic radius. This radius is used to calculate a molecular weight of the particle. The MIND complex was concentrated to 0.5 mg/ml, filtered and analysed at 25°C (figure 2.7). The MIND complex was observed by DLS to have a major species with diameter of 17 nm, corresponding to a molecular weight of 500 kDa, significantly larger in molecular weight than both a hetero-tetramer (147.9 kDa) or a hetero-octamer (295.8 kDa). Larger species were observed, with diameters of 855 and 4620 nm, with these large diameters indicating either protein aggregation or debris contamination. This type of analysis proved inconclusive, as calculations are based on the assumption that proteins are spherical in shape. This means that if the MIND complex has more extended shape as had been previously suggested (De Wulf et al., 2003), then the obtained values from DLS experiments would be inaccurate.

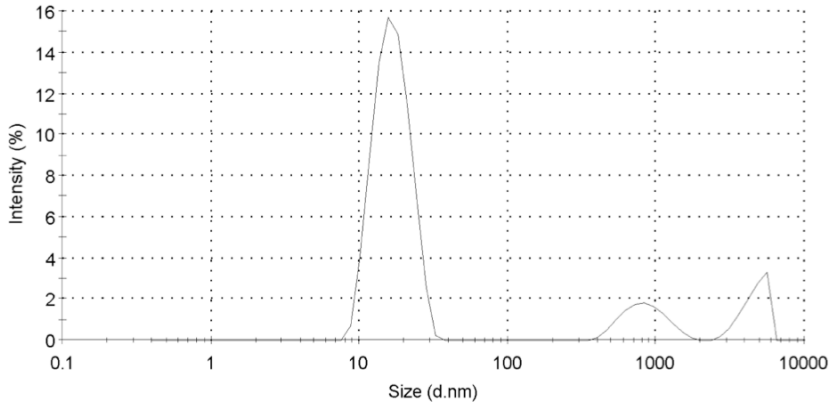

Figure 2.7 Size distribution analysis of the hydrodynamic diameter of the MIND complex

3 peaks are observed with the major species corresponding to a hydrodynamic radius of 17 nm. Other species are present but with lower intensities. The calculated diameters of 855 and 4620 nm correspond to molecular weights in the mega Dalton (MDa) range indicating some form protein aggregation or debris contamination.

2.5.2 Analytical ultracentrifugation of the MIND complex and the Dsn1p/Nsl1p and Mtw1p/Nnf1p sub-complexes

To accurately determine the molecular weight and subunit composition of the MIND complex, analytical ultracentrifugation (AUC) was used. The use of a large centrifugal force over time causes proteins in solution to move from the top of the cell/meniscus to the bottom of the cell. A concentration boundary is created and the sedimentation velocity provides information about the proteins shape and molecular weight. Sedimentation velocity (SV) experiments were carried out to determine the sedimentation coefficients (s) of the purified MIND complex and purified Dsn1p/Nsl1p and Mtw1p/Nnf1p sub-complexes. The data measured in SV experiments is the concentration profile in the radial direction as a function of time.

Fitting of the Lamm equation (see section 6.10.2) was carried out by the program Sedfit (Schuck, 2000) SV data were analysed by continuous c(s) distribution with no prior knowledge. Partial specific volume ($\bar{\nu}$) and buffer density (ρ) were calculated using the SEDNTERP program (http://www.rasmb.bbri.org/).

The c(s) analysis (figure 2.8 A, table 2.1) of the MIND complex identified a single peak with a corrected sedimentation coefficient ($S_{20,w}$) of 3.23, which gave a

calculated molecular mass of 147.7 kDa. This is consistent with the mass of a tetramer composed of a single copy each subunit. There is no observed self-association of this complex that would indicate any other higher order species occurring in solution. The frictional coefficient value of 3.09 indicates that MIND has an extended conformation. c(s) analysis of the Dsn1p/Nsl1p (figure 2.8 B, table 2.1) suggests 3 species in solution during SV experiments. The first peak corresponds to a molecular mass of 87.7 kDa, which would be a hetero-dimer of Dsn1p and Nsl1p, the second peak gave a calculated molecular mass of 167 kDa, indicating self-association of this sub-complex and the final peak would indicate multimerisation, with a molecular mass of 334 kDa. c(s) analysis of the Mtw1p/Nnf1p sub-complex (figure 2.8 C, table 2.1) identifies a single species. The calculated molecular mass of 57.7 kDa corresponds accurately to a hetero-dimer of Mtw1p and Nnf1p. Dsn1p/Nsl1p and Mtw1p/Nnf1p complexes both have frictional coefficients (table 2.1) that indicate they both adopt extended shapes in solution, with Mtw1p/Nnf1p having a larger frictional coefficient compared to the Dsn1p/Nsl1p sub-complex.

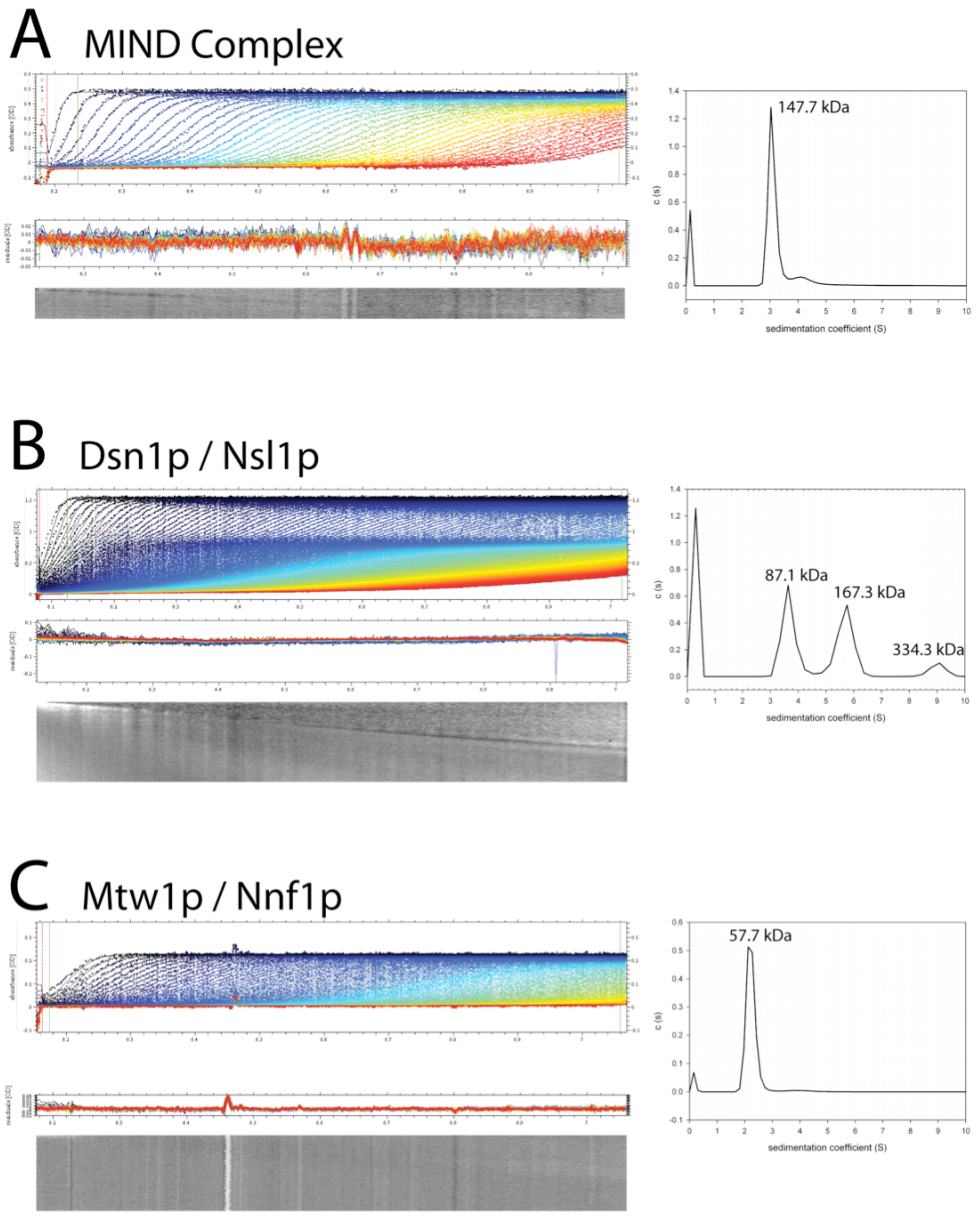

Figure 2.8 Sedimentation velocity experiments for the MIND complex and Dsn1p/Nsl1p and Mtw1p/Nnf1p sub-complexes

For all figures, the top left graph is the data scans used for the analysis with fitted curves. Residuals are plotted in the middle graph, with the bitmap of the residuals shown below. The graph on the right is the c(s) distribution with the sedimentation coefficient peaks labelled with the calculated molecular weight obtained from Sedfit marked. A) Data obtained for the MIND complex. The residual bitmap is uniformly gray indicating a good fit for the data. Whiter vertical lines in the bitmap would indicate some dirt on the outside of the sector cell window. A single peak is observed from the c(s) distribution. B) Data obtained for the Dsn1p/Nsl1p complex. The residual bitmap has a diagonal line that is seen to run from the top left to the bottom right indicating a slight mismatch between the data and fitted curves. This could be attributed to the fact that multiple sedimentation coefficient values have been calculated from the c(s) distribution, when the model chosen was for a non-interacting discrete species. C) Data obtained for the Mtw1p / Nnf1p complex. The residual bitmap is uniformly gray indicating a good fit for the data. Whiter vertical lines in the bitmap would indicate some dirt on the outside of the sector cell window. A single peak is observed from the c(s) distribution.

Sample	partial specific volume ($\bar{V}$)	hydration (g/g)	*S* *(s)*	$S_{20,w}$ *(s)*	derived molecular mass (kDa)	frictional coefficient f/f_0	stokes radius (nm)	rmsd
MIND	0.7326	0.4527	3.11	3.23	147.7	3.09	10.81	0.00759
Dsn1 / Nsl 1	0.7282	0.4527	3.35	3.49	87.1	1.85	5.23	0.00809
Mtw1 / Nnf1	0.7397	0.4528	2.26	2.32	57.7	2.32	5.76	0.00468

Table 2-1 Hydrodynamic parameters for the MIND complex, Dsn1p/Nsl1p and Mtw1p/Nnf1p sub-complexes

Buffer density, ρ was calculated by SEDNTERP to be 1.0089 g/cm^3

2.6 Crystallisation trials of the MIND complex

The fact that the MIND complex is a single species when observed by AUC experiments indicated that it would be suitable for crystallographic analysis. SDS-PAGE gels also showed a sufficient level of purity to carry out trials. The yield from 12 litres of culture was around 2 mg of MIND complex, which was enough to carry out multiple crystallisation screens. 10 different 96 well crystal screens were used (table 6.16). These screens were done at 3 different concentrations of the MIND complex and at 2 temperatures. The concentrations tried were, 5 mg/ml, 7mg/ml and 9.3 mg/ml. The different temperatures were 4°C and 16°C. Concentrations were calculated (see section 6.8) for the MIND complex before and after filtering the sample through a 0.22μM centrifuge filter. The concentration values were the same before and after filtering the MIND complex at 5 mg/ml and 7 mg/ml. For the final concentration the initial concentration was 10 mg/ml, after filtering, the concentration dropped to 9.3 mg/ml. This suggested that aggregation was occurring when concentrated to 10 mg/ml and the MIND complex was not concentrated further. In total 60 screens of the MIND complex were carried out. Analysis of the screens was done at 1 day, 3 days and then at repeating 1-week intervals after the initial inspection date.

Screens of the MIND complex at 5 mg/ml showed that approximately 20 % of the drops had precipitation ranging from fine granular precipitate to heavier brown

aggregation. Screens at 7 mg/ml showed a larger percentage of precipitation for each screen with approximately 30 % showing precipitation. Screens at 9.3 mg/ml showed over half the drops had some form of precipitation. There was no observable difference in the screens at the varying temperatures. From all the screens, none of the conditions showed any type of protein crystal growth over a 2-month period. The fact that precipitation occurred identified that the concentrations used were sufficient to for the MIND complex to reach a degree of super-saturation in which crystal growth may have been achieved (Rhodes, 2006).

2.7 Analysis of the MIND complex using electron microscopy

For this section Dr Xiao Hu-Wen captured all images

The MIND complex was further analysed using electron microscopy (EM). Although the size of the complex (147.9 kDa) is smaller than what is usually considered appropriate to visualise by EM, the information obtained from the sedimentation velocity experiments suggest that the MIND complex is extended, allowing the possibility to observe the complex using this method.

The purified sample (see section 2.2) was diluted into buffer consisting of 100mM NaCl, 50mM Tris pH 8.5 and 5mM βme. Serial dilutions of the protein were carried out, ranging from 1:10 to 1:1000, protein to buffer. The protein at various dilutions were deposited onto carbon-coated grids, negatively stained (see section 6.12) and visualised using a JEOL 1010 electron microscope operated at 80 kV. Initial images contained a large amount of background noise and interpretation of the structure of the particles was difficult. Some particles could be seen as elongated complexes approximately 30 nm in length (figure 2.9). These complexes seemed to adopt many different conformations with branched regions seen on one terminus for some particles and both termini for others.

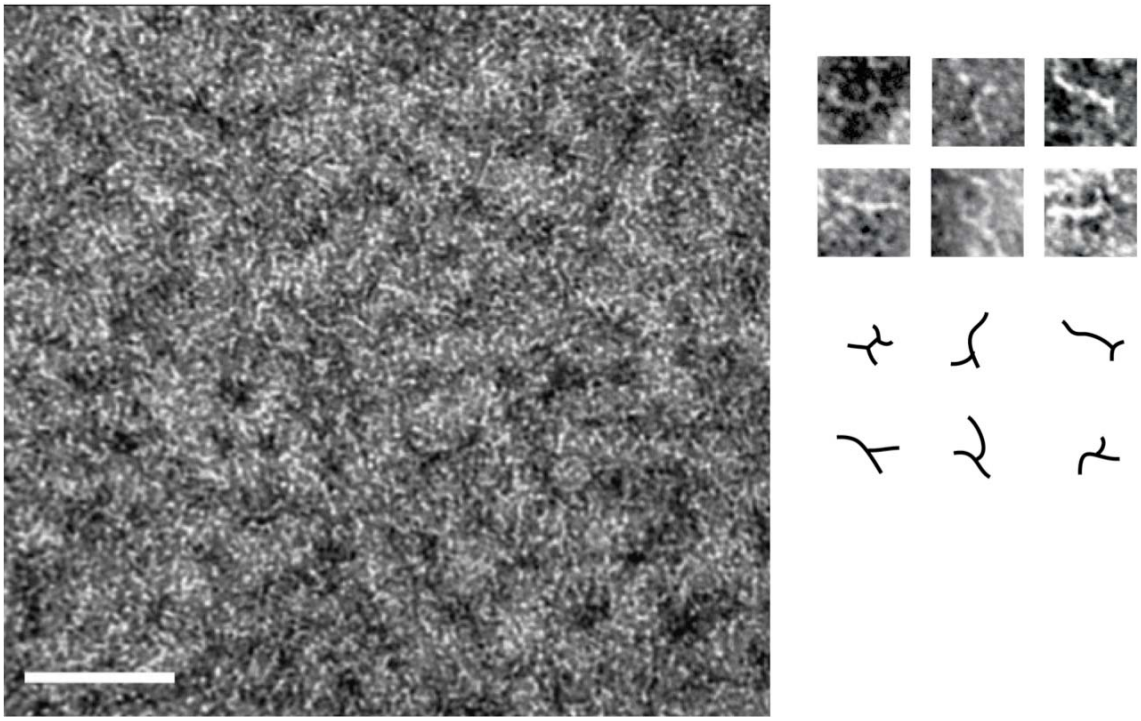

Figure 2.9 EM Images captured of the MIND complex

Samples used were taken directly from ion-exchange chromatography and diluted. Images were taken at a magnification of x20000. The large square on the left is the EM field, with the white scale bar indicating 100 nm. The top right shows six image panels magnified to indicate the various conformations the MIND complex adopts. Below these panels are schematic traces of the structures of the complexes.

The large heterogeneity of particles observed in these images and unsatisfactory background noise, lead to re-evaluation of the previous purification procedure for the MIND complex. Previous purifications of the MIND complex (see section 2.2) were done to achieve maximum amount of protein for studies such as crystallisation trials. To observe the MIND complex using electron microscopy, a sufficient dilution in protein concentration would be required to observe single particles that are not overlapping. An additional purification step of size exclusion purification (figure 2.10 A and B) was carried out after the standard purification of the MIND complex (see section 2.2). The amount of protein loaded onto the size exclusion column was less than 0.1 mg/ml. The protein was then diluted into various buffer conditions in order to reduce background and promote the observation of single particles. A dilution to approximately 0.05 mg/ml was observed to be the optimum concentration to visualise single MIND complexes. The optimal buffer was 20 mM Tris pH 7.5 and 50mM NaCl. Other factors were found to improve the data. The whole purification process and negative staining had to be

completed within 1 day or there was a significant decrease in the quality of the observed particles. Any freezing of the MIND complex, including flash freezing with liquid nitrogen lead to deterioration of the images observed.

Taking into account all these criteria, single particles of the MIND complex were observed using negative staining techniques and images collected were significantly improved. The particles observed are homogenous (figure 2.10 C) when compared to the initial images (figure 2.9). The complex has an overall structure like a comma, with distinct head and a tail region, with the only variability arising from differences in the head to tail angle. 30 images were measured using the Image J software (NIH) (table 2.3). The complex was measured to have an average length of 21.7 ± 2 nm. The globular head is has an average diameter of 8.2 ± 1 nm. The tail region has a length of 14 ± 2 nm. Selecting the most common orientation of the MIND complex, two-dimensional single particle averaging using the EMAN suite of programs (Ludtke et al., 1999), generated an overall structure of the MIND complex (figure 2.10 C). This averaging identified some other features that were present in the MIND complex. The head region from these averages shows a hook like conformation in some of the classes. The terminus of the tail is also seen to be more globular from these reconstructions.

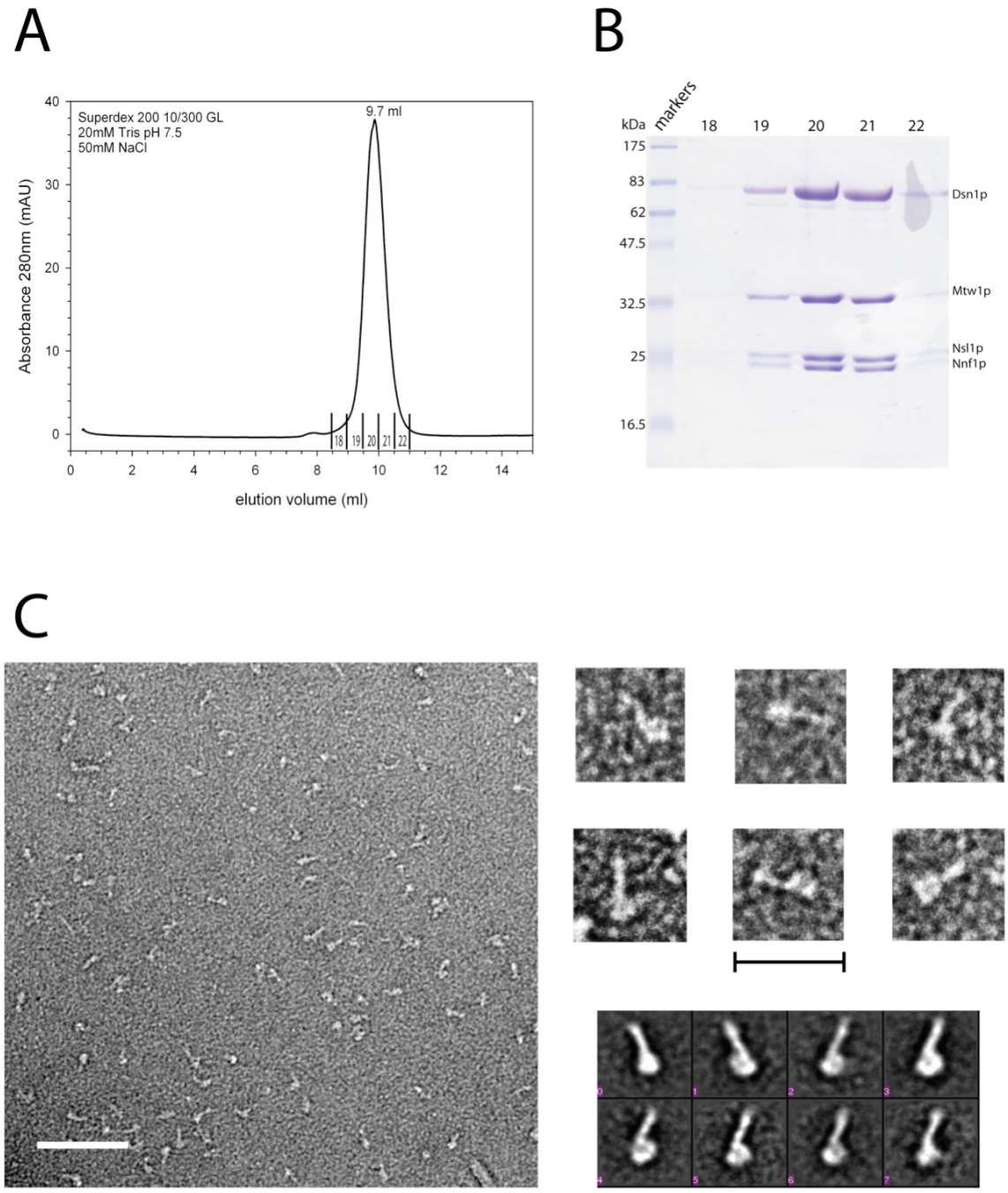

Figure 2.10 Optimization and visualisation of negatively stained MIND complex

A) Elution profile of MIND complex from a superdex 200 10 / 300 GL column. A single species is observed with relevant fractions indicated. B) SDS-PAGE of fractions from A). All four bands are observed during this purification, with proteins identified. C) Shown on the left is the EM field taken at a magnification of x20000, with the white scale bar indicating 100 nm. The top right shows 6 panels magnified indicating the conformation of the MIND complex, the scale bar is 50 nm. Below right is the two-dimensional class averaging of 336 images into eight classes.

Class	Number of images (n)
0	70
1	63
2	26
3	39
4	36
5	40
6	39
7	23

Table 2-2 Number of particles in each class used for two-dimensional class averaging

	Average (nm)	Standard deviation	Min value (nm)	Max value (nm)
Low Angle Rotary Shadowing				
Overall length	22.1	3.22	18.4	30.5
Negative stain				
Overall length	21.7	2.02	19.9	27.5
Head diameter	8.2	1.26	6.3	10.8
Tail length	14	2	11	18.8

Table 2-3 Analysis of MIND complex particles from EM images

30 images were analysed with average, standard deviation and range of particle sizes presented

The MIND complex was also analysed by electron microscopy using low angle rotary shadowing. MIND from the gel filtration purification (figures 2.10 A and B) was given to Dr Xiao Hu-Wen and Dr Martin Singleton for analysis using this method.

In brief, the MIND complex was mixed with 155mM ammonium acetate (pH 7.0) and glycerol in a 1:1:3 ratio. 20 μl was sprayed onto a freshly cleaved mica surface,

and dried under a vacuum. Specimens were rotary shadowed with a layer of 2 nm platinum-carbon at an angle of 7.5°, followed by a layer of 10 nm of carbon at an angle of 90°. The replicas were floated off onto water and picked up by a copper grid. Grids were then analysed in the JEOL 1010 electron microscope operated at 80 kV. The images obtained from this analysis showed that the MIND complex could also be visualised by this technique (figure 2.11). The images observed had an average length of 22.1 nm. This is similar to the length determined by negative stain electron microscopy. The complex appears more rod like in structure with the head and tail regions more difficult to distinguish by low angle rotary shadowing, which may be due to the way the stain is deposited on the MIND complex.

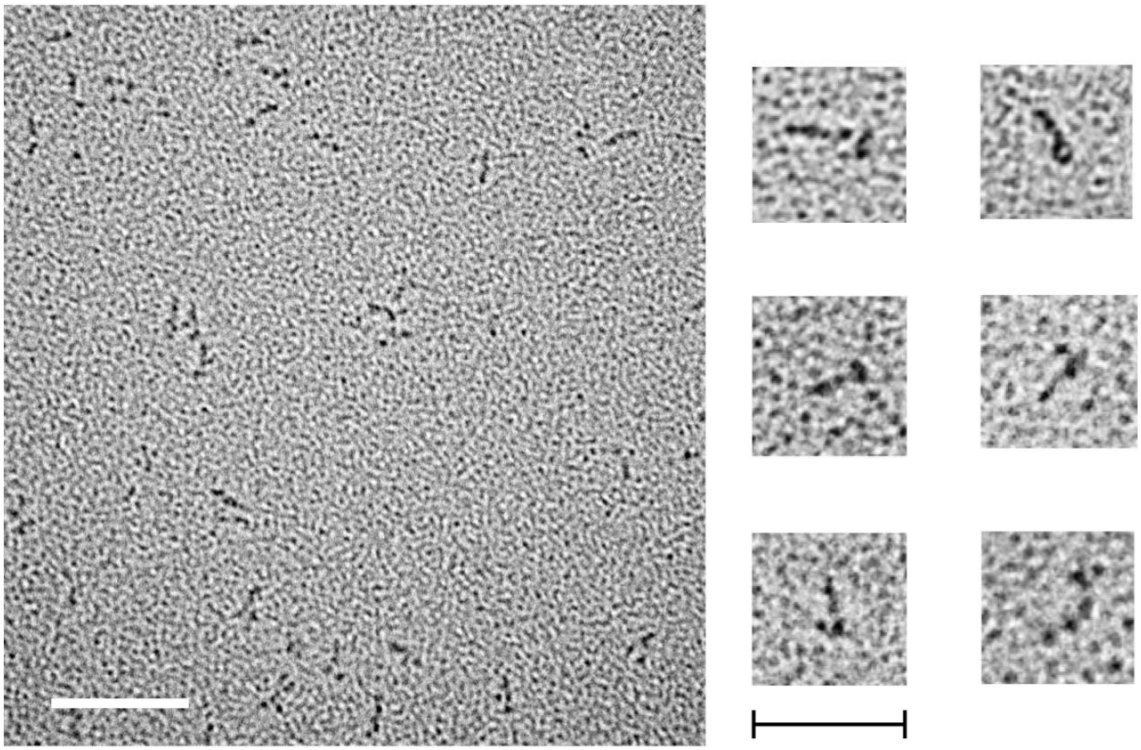

Figure 2.11 Low angle rotary shadowing EM of the MIND complex

Left is the EM field with images taken at a magnification of x20000, with the white scale bar indicating 100 nm. The right shows 6 images magnified to indicate the typical conformation, the scale bar is 60nm.

2.8 Summary

The MIND complex was expressed using a *Escherichia coli* recombinant system and purified. The molecular mass of the MIND complex was determined using analytical ultracentrifugation as 147.7 kDa, this corresponds accurately to a single species in solution, consisting of Dsn1p, Mtw1p, Nsl1p and Nnf1p in a equimolar ratio of 1:1:1:1. The formation of the complex arises from the association of hetero-dimers of the Dsn1p/Nsl1p and Mtw1p/Nnf1p proteins. Using AUC, the hetero-dimers and the full MIND complex were shown to adopt extended structures in solution.

Crystallisation trials of the MIND complex were unsuccessful even though the protein was purified to homogeneity and concentrated to a level to allow crystal formation to occur. The complex was analysed using EM and initial images were inconclusive and did not show consistent particles. Modifications to the protein purification steps, lead to EM images with consistent structures. Using negative staining, the MIND complex was seen to consist of both globular and extended domains, named the ‘head’ and ‘tail’ regions respectively. The head had an average diameter of 8 nm, and the tail had an average length of 14 nm, generating an overall length for the complex of 22 nm. Variability is seen in the angle between the head and tail regions, indicating flexibility between these regions. Two-dimensional class averaging of the MIND complex, showed that the head region adopts a hooked shape with a cavity in the centre. The tail was also suggested to have a globular region at the tip.

Chapter 3.

3.1 Aims

Although the MIND complex was purified to homogeneity (see section 2.2), crystallisation of the complete complex was unsuccessful. AUC and EM studies have shown that the MIND complex is extended in structure with multiple domains (see sections 2.5.2 and 2.7). Predicted coiled-coil regions were identified for all protein subunits of the MIND complex (figure 1.3). Although crystal structures of coiled-coil domains have been solved (O'Shea et al., 1991) the flexibility of these domains can decrease the probability of crystal formation of complete complexes (Maiolica et al., 2007). Removal of these domains can generate structures that can be crystallised (Ciferri et al., 2008). However it is not known how important these flexible/coiled-coil domains may be to the overall structure and formation of the MIND complex. Orthologs of the MIND complex in higher eukaryotes also posses coiled-coil domains, highlighting a conservation for these motifs (figure 1.3).

3.2 Truncations of the MIND complex based on bioinformatics analysis

Heptad repeats are common structural motifs forming the basis of coiled-coil regions (Hodges, 1992). Investigating the amino acid sequence for these repeats using PCOILS (Lupas et al., 1991) revealed that three of the four protein subunits of the MIND complex have high scoring (values greater than 0.6, see figure 1.3) potential coiled-coil regions. The largest subunit Dsn1p, has high scoring coiled-coil regions from residues 303 to 332 and 433 to 460. These were thought to be the major coiled-coil domain of the MIND complex and may comprise the ‘tail’ region that is observed in EM images. The unfolded or extended tail region may be a factor in preventing the MIND complex crystallising. Removal of these domains by truncating Dsn1p was the initial approach undertaken to create a complex that may crystallise.

3.2.1 Expression and purification of MIND Dsn1$_{1-290}$

A Dsn1p construct was available with the carboxyl terminus truncated to Arginine 290. This construct pDSN1$_{1-290}$, was transformed into *Escherichia coli* BL21(DE3) RIL cells along with the pMTW1 and pNSL1.NNF1 constructs. The product of this co-expression was called MIND Dsn1$_{1-290}$.

MIND Dsn1$_{1-290}$ was first purified by Ni-NTA batch purification. SDS-PAGE (figure 3.1 A) showed only two bands at 32.5 kDa and 25kDa when compared to molecular weight markers. The predicted molecular weight of Dsn1$_{1-290}$ is 32 kDa, which is close to the molecular weight of Mtw1p (33 kDa) suggesting that these proteins could not be separated during SDS-PAGE. In some cases SDS-PAGE (data not shown) cannot differentiate Nsl1p and Nnf1p. The sample was loaded onto a size exclusion Superdex 200 10/300 column for further analysis. The elution profile (figure 3.1 B) identified two peaks, SDS-PAGE (figure 3.1 C) showed that the first eluting peak was the chaperone Hsp70 associating with MIND Dsn1$_{1-290}$ and the second peak was the MIND Dsn1$_{1-290}$ complex. SDS-PAGE could now resolve four proteins in this peak, but the ratio of each protein was not 1:1:1:1. Sub-stoichiometric amounts of Nsl1p were observed, and as the peak was eluting, the amount of Nsl1p present in the complex decreased significantly, implicating that the C-terminal region (290-576) of Dsn1p was important for Nsl1p binding. This complex was deemed unsuitable for crystallisation trials, as the dissociation of the Nsl1p subunit generated a heterogeneous sample.

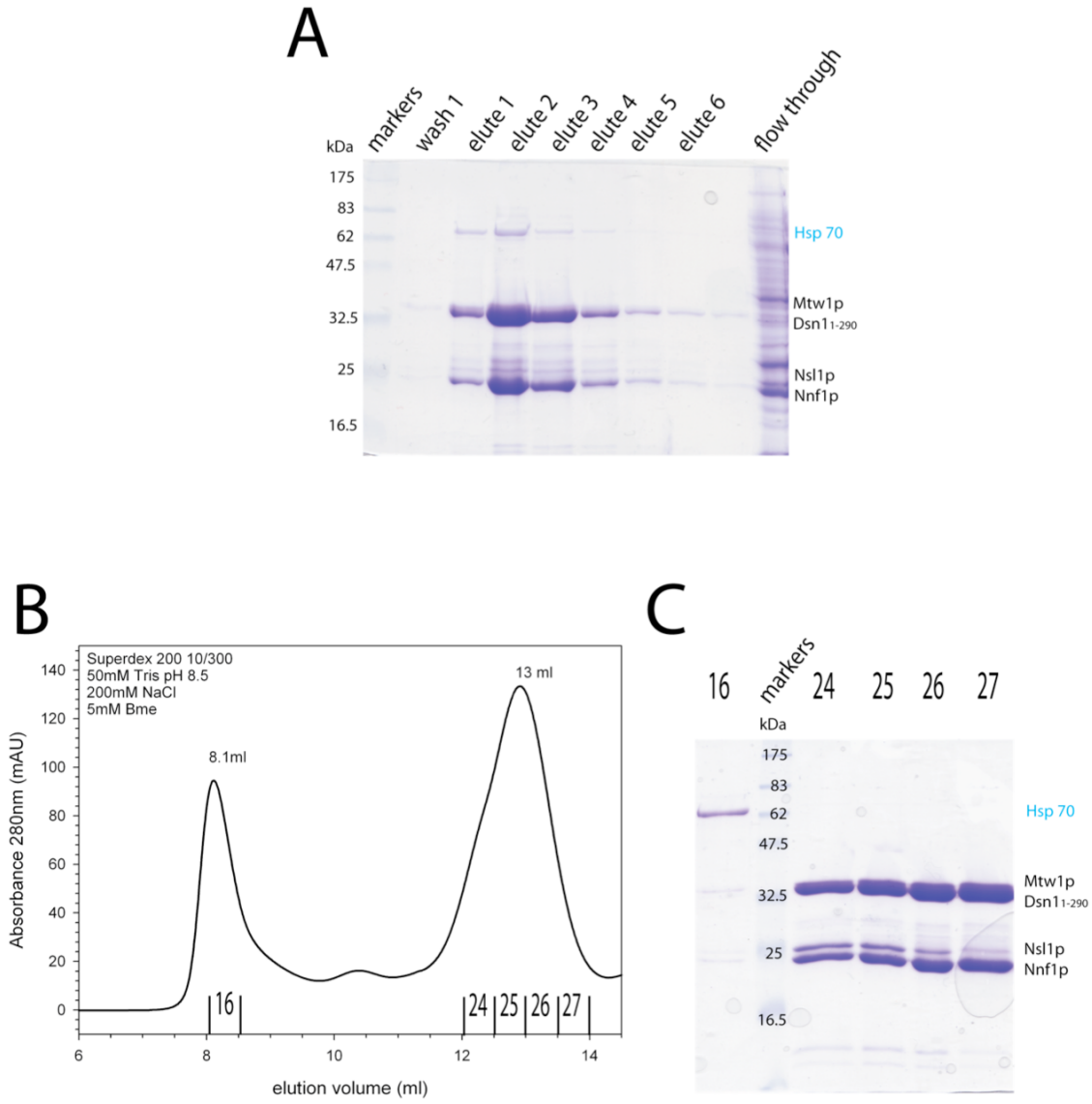

Figure 3.1 Expression and purification of MIND Dsn1$_{1\text{-}290}$

A) SDS-PAGE of Ni-NTA affinity purification of MIND DSN$_{1\text{-}290}$. 2 major bands are observed from the elution fractions with proteins identified on the right with molecular marker weights on the left. The molecular weights for the proteins are, 32 kDa for Dsn1$_{1\text{-}290}$, 33 kDa for Mtw1p, 25 kDa for Nsl1p, 23.6 kDa for Nnf1p. The small difference in molecular weights for Dsn1$_{1\text{-}290}$ and Mtw1p make it difficult to see separate bands for these proteins. B) Elution profile of MIND DSN1$_{1\text{-}290}$ from size exclusion chromatography. Elution volume and relevant fractions have been marked. C) SDS-PAGE of fractions eluted from B) with proteins identified on the right. The first peak corresponds to Hsp70 contaminant and a small amount of MIND Dsn1$_{1\text{-}290}$ seen in fraction 16. Separation of the proteins is observed, however, the Dsn1$_{1\text{-}290}$ and Mtw1p bands can be seen to overlap each other. Nsl1p is seen in sub-stoichiometric amounts and the band decreases in intensity from fractions 24-27.

3.2.2 Expression and purification of MIND Dsn1$_{1-490}$

Further bioinformatics analysis using the program HHPred (Soding et al., 2005) predicted that the C-terminus of Dsn1p shares amino acid sequence homology to the coiled-coil region of bovine fibrinogen (PDB code 1DEQ) (Brown et al., 2000). This region corresponds to amino acid residues glutamate 490 to the C-terminal lysine residue of Dsn1p. A construct was created that was truncated after glutamate 490 by insertion of an stop codon TAA into the reverse primer. The DSN1 gene was cloned from residues 1-490 into pET28a vector using the restriction sites NdeI and XhoI. This construct was transformed into *Escherichia coli* BL21(DE3) RIL cells along with the pMTW1 and pNSL1.NNF1 constructs. The product of this co-expression was called MIND Dsn1$_{1-490}$.

MIND Dsn1$_{1-490}$ was first purified by Ni-NTA batch purification. SDS-PAGE (figure 3.2 A) revealed that four bands were present indicating a stable association. The sample was then loaded onto a pre-equilibrated size exclusion Superdex 200 16 / 60 column. The elution profile (figure 3.2 B) showed a small initial peak, followed by the major peak. SDS-PAGE (figure 3.2 C) found that the initial peak contained a small amount of the MIND Dsn1$_{1-490}$ complex associating as a higher order species. The second peak contained all four subunits in an observed 1:1:1:1 ratio. The theoretical pI of the complex was calculated to be 5.10 by using the SCRIPPS protein calculator server and the complex was further purified by anion exchange chromatography. MIND Dsn1$_{1-490}$ was bound to a anion exchange Mono Q 5/50 GL column in a buffer at pH 8.5 and eluted by a NaCl gradient. The elution profile (figure 3.2 D) observed a major peak that eluted at 32 mS/cm. SDS-PAGE (figure 3.2 E) showed that all proteins of this complex were present in an equimolar ratio. A shoulder was observed on the left side of the peak and was shown to be the Mtw1p and Nnf1p proteins that have been previously seen to dissociate during anion exchange chromatography (see section 2.2.3).

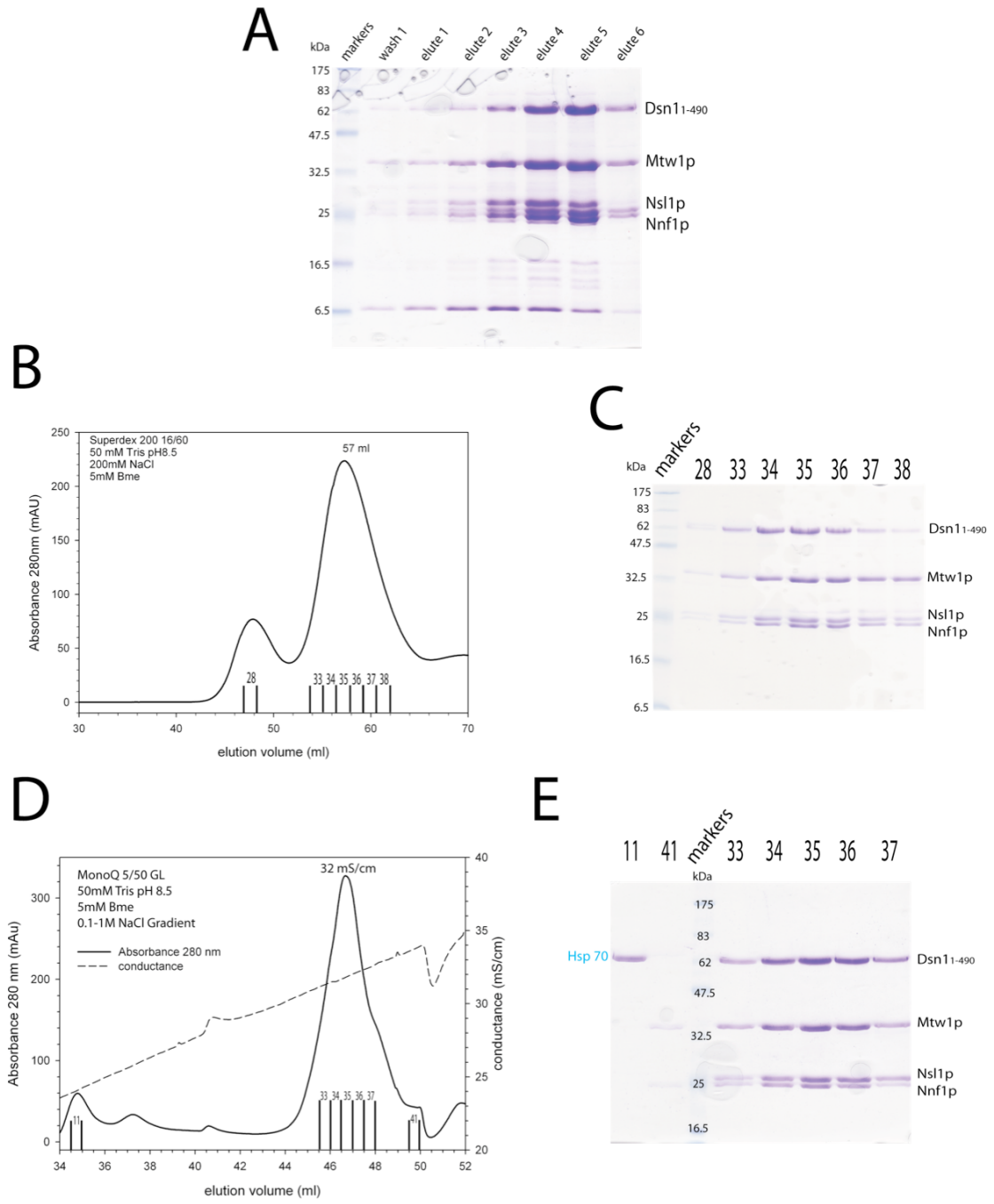

Figure 3.2 Expression and purification of the MIND Dsn1$_{1\text{-}490}$

A) SDS-PAGE of Ni-NTA affinity purification of MIND DSN$_{1\text{-}490}$. Bands are observed corresponding to each protein identified on the right. The calculated molecular weights for the proteins are, 56 kDa for Dsn1$_{1\text{-}490}$, 33 kDa for Mtw1p, 25 kDa for Nsl1p, 23.6 kDa for Nnf1p. B) Elution profile of MIND DSN1$_{1\text{-}490}$ from size exclusion chromatography. Elution volume and relevant fractions have been marked. C) SDS-PAGE of fractions eluted from B) with bands identified. All protein subunits are observed in equal intensities. D) Elution profile of MIND DSN1$_{1\text{-}490}$ from anion exchange chromatography. Absorbance at 280 nm is the continuous line and conductance is the dashed line. Relevant fractions are marked on the profile. E) SDS-PAGE of fractions eluted from D) with proteins identified. Fraction 11 is Hsp70 contamination. Fractions 33-37 show all subunits in equal ratios. Fraction 41 shows a dissociation of the complex that is also seen in Figure 2.3 B.

3.2.3 Crystallisation trials of the MIND Dsn1$_{1-490}$

The final yield and purity of the MIND Dsn1$_{1-490}$ complex was sufficient to carry out crystallisation trials. 10 different 96 well crystal screens with MIND Dsn1$_{1-490}$ at a concentration of 11 mg/ml were set up. As full-length MIND complex crystallisation screens showed no observable difference between 4°C and 16°C (see section 2.6), screens were only carried out at 16°C. Approximately 50 % of the drops contained precipitate after 1 week. No observable crystal growth was observed over a 3-month period.

3.3 Limited proteolysis of the MIND complex

As crystallisation of the full length MIND complex and the truncations based on bioinformatics approaches were unsuccessful, further techniques were considered to create suitable constructs for crystallisation studies. As observed in EM studies (see section 2.7), the MIND complex is a multi-domain structure with a globular 'head' and extended 'tail' region. It appears that the tail region is the more variable domain with a range of head to tail angles observed (see section 2.7) and it was thought to contain most of the predicted coiled-coil regions. This extended tail may increase mobility of the polypeptide chain in this area. Proteases can be used to preferentially digest flexible or unfolded regions within proteins and a correlation has been made between sites of limited proteolysis in proteins and crystallographic temperature factors (B factors), with larger B factors indicating sites that are susceptible to protease treatment (Fontana et al., 1986).

Trypsin was used at a fixed concentration over a time course (see section 6.7.1), with SDS-PAGE (figure 3.3) showing that the two largest protein subunits, Dsn1p and Mtw1p were subject to trypsin digest, while the other subunits Nsl1p and Nnf1p were resistant to this protease treatment. The bands observed from the SDS-PAGE were excised and sent to the Protein Analysis & Proteomics laboratory Cancer Research UK for analysis. Band 1 was a fragment Dsn1p, band 2 was a break down product of the

chaperone Hsp70 and band 3 corresponded to Mtw1p. Bands 1 and 3 were further analysed to define the N and C termini of these protease products.

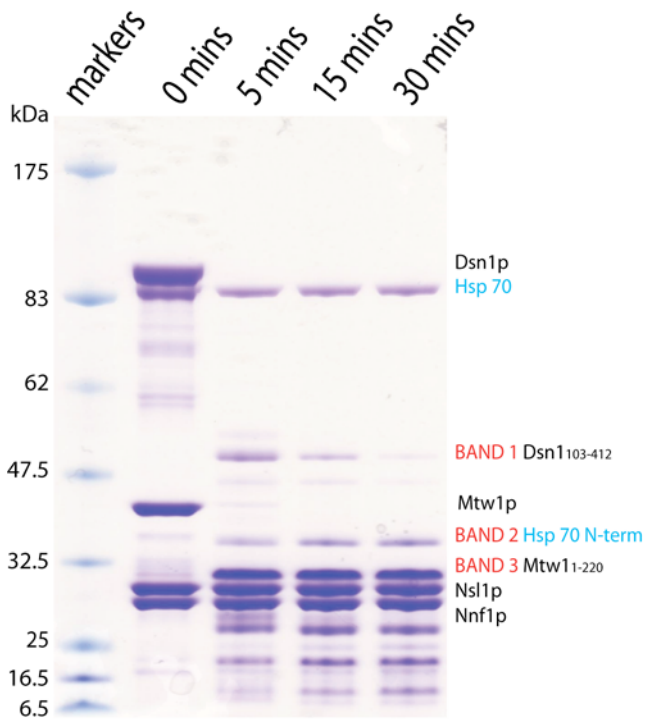

Figure 3.3 Limited proteolysis of the MIND complex

SDS-PAGE of a trypsin digestion over 30 minutes. Samples were taken at various time points as marked on the top of the gel, and the reaction was quenched by heat inactivation. Protease resistant domains are labelled as determined by mass spectrometry and Edman analysis.

To determine the N-terminus of the protease resistant cores of Dsn1p and Mtw1p, proteins bands were transferred to a PVDF membrane and sent for Edman sequencing analysis (Edman, 1960). Band 1 gave the first 5 N-terminal amino acids as [G,A,R]VENF, corresponding to residues RVENF at positions 103-107 in Dsn1p. Using intact mass data, the C-terminus was found to be the arginine residue at position 412. Edman sequencing of band 3 gave the amino acid sequence SAPTMRSTSTI, corresponding to residues 2-12 of Mtw1p, as the N-terminal Methionine is often removed during recombinant expression of proteins (Hirel et al., 1989). Using intact mass data, the C-terminus was found to be the arginine residue at position 220.

3.4 Expression and purification of ΔMIND

Expression constructs were generated for the protease resistant Dsn1p and Mtw1p domains. For the Dsn1p domain, a forward primer was created that contained the start codon ATG before the arginine residue at position 103. A reverse primer was generated that was truncated at the arginine residue 412 by addition of the stop codon TAA to the primer. This PCR product was cloned into the pET28a vector (Novagen) using the forward restriction site NdeI, and the reverse restriction site XhoI, encoding an N-terminal His-tag. For the Mtw1p domain, the normal forward primer was used. A reverse primer was created that was truncated at the arginine residue 220 by the addition of the TAA stop codon. This PCR product was cloned into the pET22a vector (Novagen) using the forward and reverse restriction sites NdeI and XhoI. The $pDSN1_{103-412}$ and $pMTW1_{1-220}$ were transformed along with the pNNF1.NSL1 construct, into *Escherichia coli* BL21(DE3) RIL cells. For simplicity the product of this co-expression was named ΔMIND.

ΔMIND was first purified by Ni-NTA batch purification. SDS-PAGE (figure 3.4 A) showed four bands that corresponded to the predicted molecular weights of the proteins. The presence of all four proteins indicated a stable association of all subunits in this complex. Hsp70 chaperone was also seen to co-elute with the ΔMIND complex, indicating flexible or unfolded regions may still be present. Further purification was carried out by loading the fractions of interest onto a pre-equilibrated size exclusion Superdex 200 16/60 column. The elution profile (figure 3.4 B) observed a minor peak at 48 ml followed by a major peak at 61 ml. SDS-PAGE (figure 3.4 C) showed that the minor peak contained all four subunits of the ΔMIND complex along with Hsp70. The minor peak elution volume would indicate that this is similar to the higher order species, which was also seen during purification of the full length MIND complex (see section 2.2.2). The main elution peak contained all subunits in an observed equimolar ratio of 1:1:1:1, indicating that these proteins associate as a stable complex during size exclusion chromatography. The calculated molecular mass based on amino acid composition is 109 kDa, the elution volume of 61 ml corresponds to a molecular mass of 293 kDa using Equations 1 and 2, suggesting an elongated structure. A theoretical pI

value of 4.79 was calculated for ΔMIND using the SCRIPPS protein calculator server and was further purified by an anion exchange chromatography. The complex was bound to a anion exchange Mono Q 5/50 GL column in a buffer at pH 8.5 and eluted by a 0.1-1M NaCl gradient. The elution profile (figure 3.4 D) could observe two main peaks, eluting at 36 mS/cm and 39 mS/cm. SDS-PAGE (figure 3.4 E) showed that the peak at 36 mS/cm comprised all four proteins in equimolar ratio and the peak at 39 mS/cm contained $Dsn1_{103-412}$ and Nsl1p in a 1:1 ratio along with sub-stoichiometric amounts of $Mtw1_{1-220}$, Nnf1p and the chaperone Hsp70.

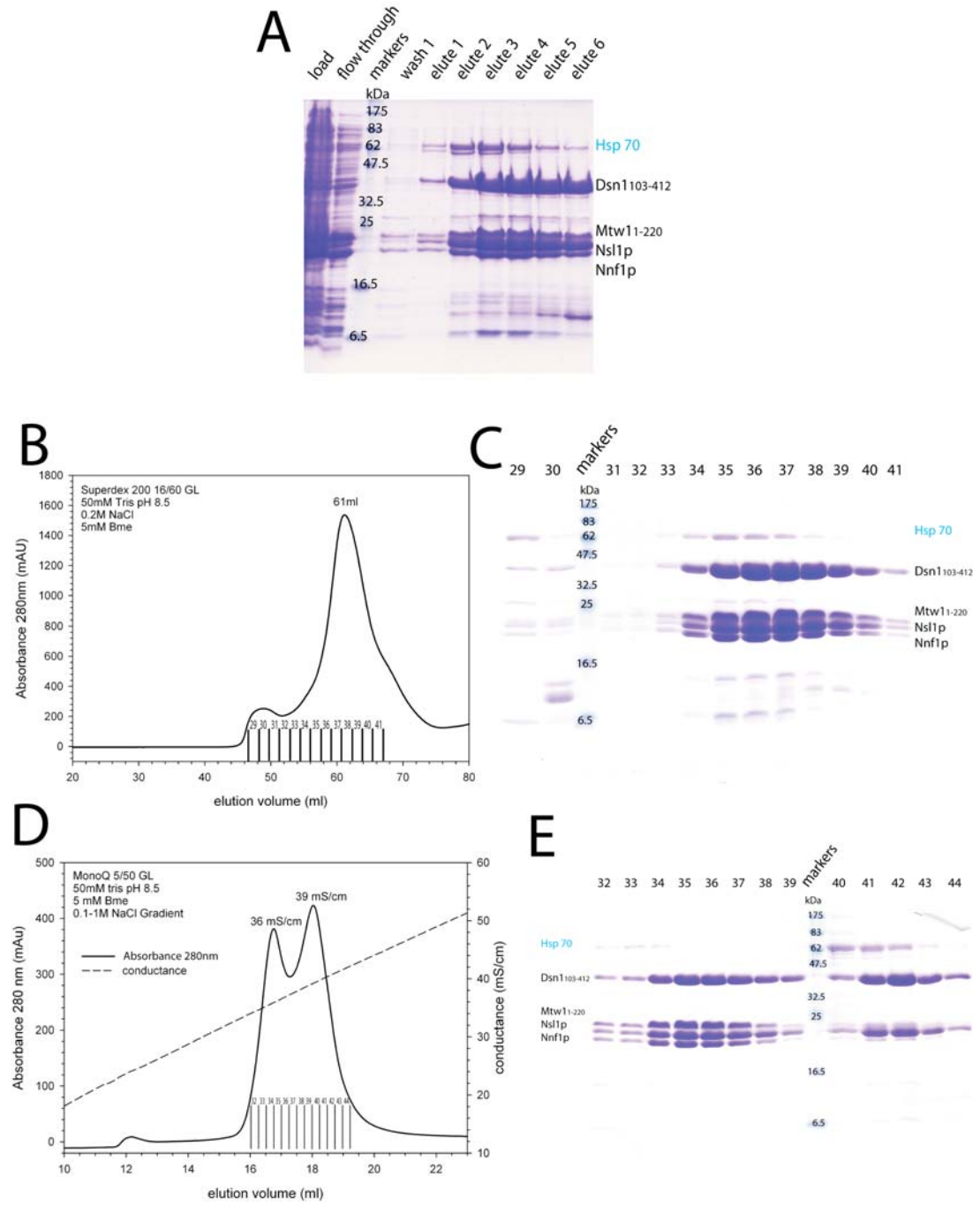

Figure 3.4 Expression and purification of ΔMIND

A) SDS-PAGE of fraction from Ni-NTA affinity purification. Bands are observed corresponding to each protein identified on the right. The molecular weights are 35.2 kDa for $Dsn1_{103-412}$, 25.4 kDa for $Mtw1_{1-220}$, 25 kDa for Nsl1p, 23.6 kDa for Nnf1p. B) Elution profile from size exclusion chromatography. Elution volume for the major peak is shown along with relevant fractions. C) SDS-PAGE of fractions from B) with proteins identified on the right. Fractions 29 and 30 indicate some multimerisation of ΔMIND along with the chaperone Hsp70 and other contaminants. Fractions 34-41 show all four bands in equal ratios. D) Elution profile from anion exchange chromatography. Absorbance readings at 280nm and conductance are marked by the black and dashed lines respectively. Two major peaks are observed with relevant fractions indicated. E) SDS-PAGE of fractions eluted from D) with proteins identified on the left. Fractions 32-39 correspond to ΔMIND with all 4 bands present in equal ratios. Fractions 40-44 are a breakdown product along with Hsp70 association. The major bands are $Dsn1_{103-412}$ and Nsl1p.

3.4.1 Crystallisation trials of ΔMIND

Purification of ΔMIND showed partial dissociation, however, a sufficient amount of the complex containing all subunits in a equimolar ratio was purified to homogeneity to carry out crystallisation trials. 10 different 96 well crystal screens at concentrations of 10.3 and 15.1 mg/ml were set up at 16°C. After 3 days, both screens showed that approximately 50% of the drops contained precipitate, ranging from fine granular to heavy aggregation. No observable crystal growth was observed over a 3-month period.

3.5 Small angle X-ray scattering

As crystallisation trials to investigate the structure of the MIND complex and truncations were unsuccessful, other types of structural characterisation were considered. The images that were seen by EM analysis identified the MIND complex was elongated with distinct domains. The different staining techniques led to some ambiguity in the structure of the 'head' and 'tail' regions. Low-angle rotary shadowing suggests that the MIND complex is more rod like in structure, with the head domain being less distinct, whereas negative stain techniques clearly show distinct head and tail regions (see section 2.7). Further structural information of the MIND complex and ΔMIND was generated by small-angle X-ray scattering (SAXS) experiments.

SAXS can analyse biological molecules such as proteins in solution and can provide low-resolution structural information. Protein in solution is exposed to a X-ray source and the scattering data is collected. The solution without protein is also exposed to the X-ray source, with this scattering subtracted from the protein sample scattering data, creating scattering data that is from the protein only. This scattering data can be used to determine parameters such as molecular mass, the radius of gyration (R_G) and the maximum particle diameter (D_{max}). The scattering data can also be transformed to allow *ab initio* modelling, generating three-dimensional reconstructions.

3.5.1 Protein purification for SAXS experiments

The MIND and ΔMIND complexes were purified as previously described (see sections 2.2 and 3.4). The proteins were then dialysed into 50 mM Tris pH7.5, 100mM NaCl, 2 mM dithiothreitol (DTT) and 4 % glycerol (v/v) buffer, DTT acts to protect from radiation damage during exposure to the X-ray source and glycerol acts as a cryo-protectant for transportation as samples needed to be flash frozen in liquid nitrogen in order to be sent to the synchrotron. The protein samples and buffer taken from the final dialysis step were flash frozen in liquid nitrogen for shipping to the EMBL-Hamburg DESY synchrotron. Data were collected on beamline X33.

3.5.2 SAXS analysis of the MIND complex

All data manipulations were carried out using the ATSAS 2.1 suite of programs (EMBL Hamburg)

Scattering data of the MIND complex was collected at a concentration range of 0.1 to 4 mg/ml. Scattering data for buffer was also collected and subtracted from the protein sample, generating scattering curves. Each curve was checked for radiation damage and aggregation effects, which can be identified by a non-linear Guinier region and then scaled and merged using the program PRIMUS. The output file was then analysed by both the automated PRIMUS program and by manual analysis using the program PRISM (figure 3.5 A).

The data were transformed by plotting the intensity of the scattering (I) against the momentum transfer of scattering (q), with ln(I) on the y-axis and q^2 on the x-axis. Using the Guinier equation (Equation 3) the radius of gyration R_G and the intensity of the scattering when q=0, I(0) were calculated.

$$\ln(I) = \ln I(0) - \frac{(q^2 R_G^2)}{3} \qquad \textbf{Equation 3}$$

The upper limits for the Guinier regions is defined as $q < 1.3/R_G$ for proteins. Using PRIMUS, the Guinier region was determined and linear regression was carried out in the PRISM program (figure 3.5 B). The line y = mx + c can be applied to the Guinier equation with the y intercept being I(0) and the R_G is the gradient of the line, m. Guinier analysis gave value for R_G and I(0) as 7.5 and 121.5 respectively.

The scattering curve was also analysed by a Kratky plot (figure 3.5 C). A plot of q^2(I) on the y-axis against q on the x-axis analyses the folded state of a protein. Globular proteins have a bell shaped curve, extended or unfolded proteins lack this bell-shape and have a maximum that ends in a plateau. The Kratky plot for MIND shows a maximum that decreases slightly into a plateau, indicating an extended structure with possible unfolded regions.

GNOM was used to carry out an indirect transformation of the one-dimensional scattering data creating the distance distribution function *P(r)*. GNOM calculates by an indirect Fourier transform of the scattering curve, a real space representation of the frequency of all inter-atomic vector lengths within a protein. This provides information about the symmetry and shape of the protein. The maximum distance of the particle is manually assigned, leading to multiple *P(r)* graphs with different D_{max} values. The best fit (highest alpha value) of the scattering data was when the value for D_{max} was found to be a value of 22 nm (figure 3.6 A). The shoulder on the right side of the *P(r)* curve indicates the MIND complex is a multi-domain complex. R_G and I(0) values of 7.23 and 112.8 obtained from *P(r)* analysis are more accurate as the whole scattering curve is used for their estimation, instead of the Guinier region used for previous calculations.

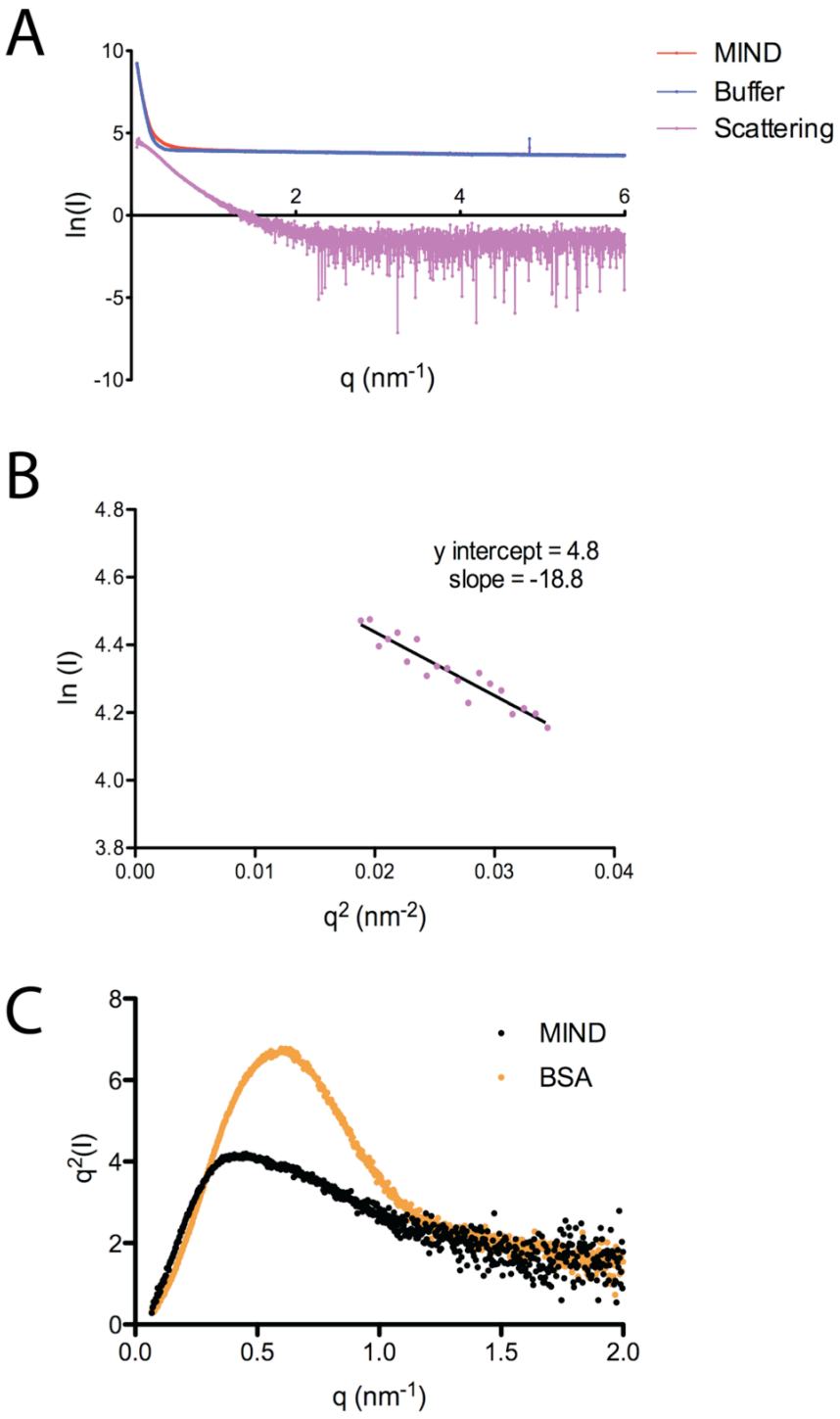

Figure 3.5 Scattering curves, Guinier analysis and Kratky plot for the MIND complex

A) Scaled and merged scattering curve from the MIND complex in buffer (Red line), buffer alone (Blue line) and the subtraction of the buffer from MIND (Pink line). The curves were generated by the program PRIMUS and plotted in PRISM. B) Guinier plot of the MIND scattering curve. Using the y-intercept and the gradient of the line, values of R_G and I(0) were calculated. C). Kratky plot of the MIND complex. A globular compact protein would have a bell shaped curve like Bovine serum albumin (BSA) (orange line). MIND (black dots) has a maximum that decreases into a plateau, indicating an extended structure with multiple domains**.**

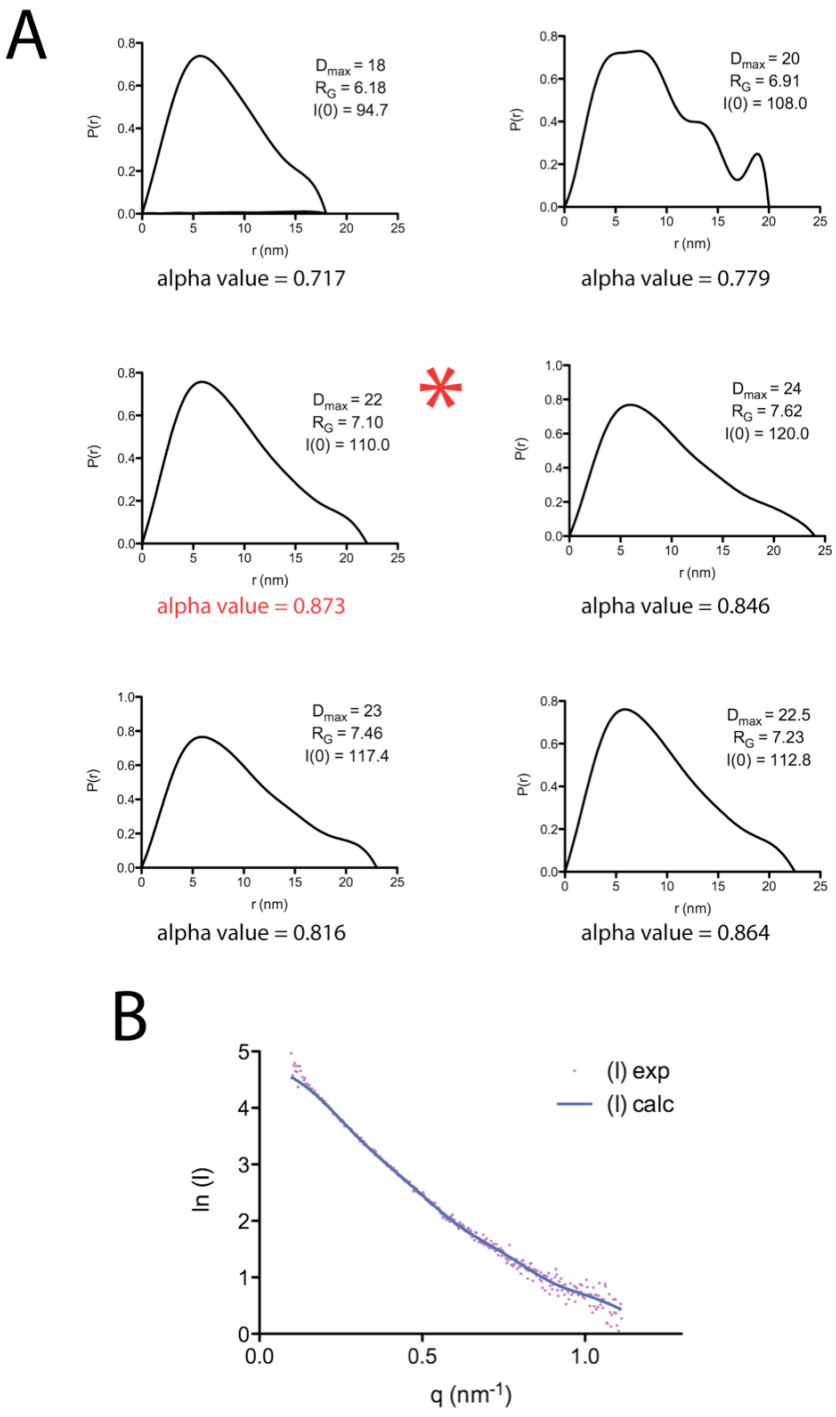

Figure 3.6 Pair distribution functions and scattering curve for modelling for MIND

A) Pair distribution functions P(r) calculated from the X-ray scattering data. Each curve uses a different D_{max} value ranging from 2.5 – 3.5 R_G. The best D_{max} value is indicated by an asterisk (middle left). The P(r) function is indicative of an extended, multi-domain structure. B) Scattering curve (Pink dots) of the MIND complex, with calculated model scattering curve (Blue line) used for *ab-initio* modelling calculated from GNOM.

Using the output file from GNOM (figure 3.6 B), *ab initio* modelling was carried out to generate a low-resolution structure of the MIND complex. Bead-type models of the protein were built using the program DAMMIN. A typical reconstruction (figure 3.7 A) was 22 nm in length and 8nm across the widest part of the head domain. Seven of the ten separate simulations identified that the head of the molecule contains a cavity in the centre (figure 3.7 B) giving the head a hook shaped conformation in these reconstructions. Variations in the head domain can be described by poor scattering data in this region leading to ambiguity of how the head is modelled during reconstructions. Another explanation could be that this region is flexible and the head can undergo structural re-arrangements. There is also an identifiable lobe region between the head and tail regions of the molecule. The tail region also seems to have a globular tip. Using the program DAMAVER all models were aligned, averaged and a filtered model generated (figure 3.7 C). This averaged model had the same dimensions as each individual reconstruction, but the cavity in the head region that is seen in some models is not observed as either the ambiguity or flexibility in this region has been averaged out.

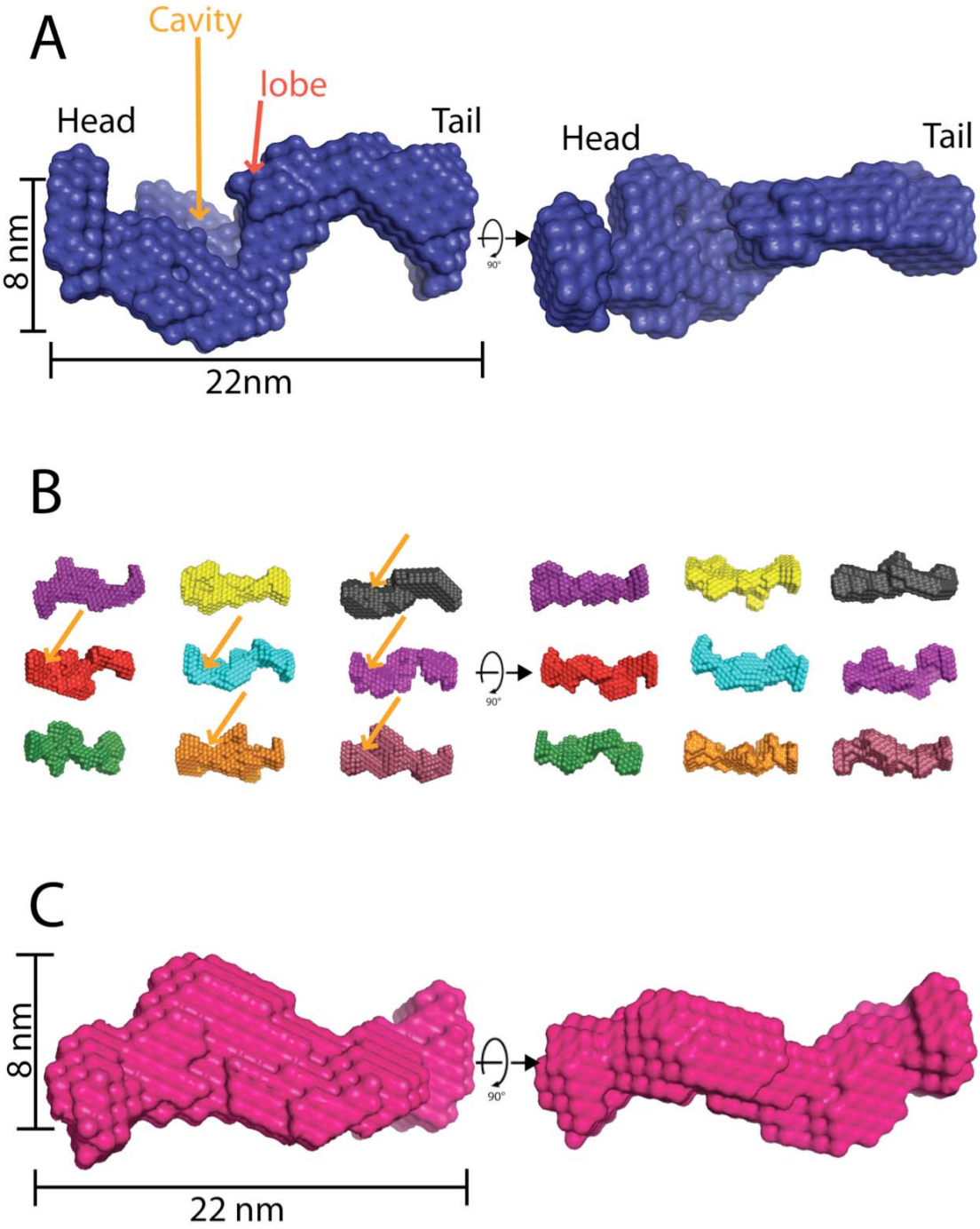

Figure 3.7 *Ab-initio* reconstruction of the MIND complex using DAMMIN

A) Three-dimensional low-resolution DAMMIN reconstruction of the MIND complex. The structure is 22 nm long at has both head and tail regions. The head has a diameter of 8nm at its largest point. A cavity is seen in the head region along with a lobe region that is joined to the tail. A 90° rotation is shown on the left. B) 9 separate reconstructions in DAMMIN using the same data set used in A). Head and tail regions can be indentified in each reconstruction, showing a similar overall shape, although there are variations observed in the head region. Cavities seen in the head regions of the models are indicated by an orange arrow. C) Averaged, filtered reconstruction derived from the 10 models from A) and B). The reconstruction is the same length of 22 nm and 8nm in diameter at its largest width. The head domain is less obvious in the averaged model, with the cavity no longer identifiable as can be seen in individual reconstructions**.**

3.5.3 SAXS analysis of ΔMIND

ΔMIND was analysed at a concentration range of 0.2–3 mg/ml, scattering curves were linear in the Guinier region indicating that no radiation damage or aggregation affects were occurring. The best curves were then scaled and merged using PRIMUS, with the output files being analysed by PRISM (figure 3.8 A). Data was transformed for Guinier analysis (figure 3.8 B). The y-intercept and gradient were calculated from PRISM as 4.48 and -9 respectively giving values for R_G as 5.2 nm and for I(0) as 88.23. The Kratky plot (figure 3.8 C) identified that ΔMIND was also extended in solution. The *P(r)* curve generated by GNOM (figure 3.9 A) found a D_{max} of 17.5 nm gave the best alpha value. The R_G and I(0) values from GNOM were 5.23 and 87.07 respectively, which are in good agreement with the value calculated from the Guinier analysis. The right side of the *P(r)* curve has a shoulder indicating a multi-domain complex. Low-resolution models of ΔMIND were generated using DAMMIN. A typical reconstruction (figure 3.10 A) was 17nm in length and 8 nm across the largest width of the particle. 10 separate models were generated (figure 3.10 B) using the same scattering curve, with some variation seen between the reconstructions. These models were averaged using DAMAVER and the filtered model (figure 3.10 C) had the same length of 17 nm and was 8nm across at the widest point.

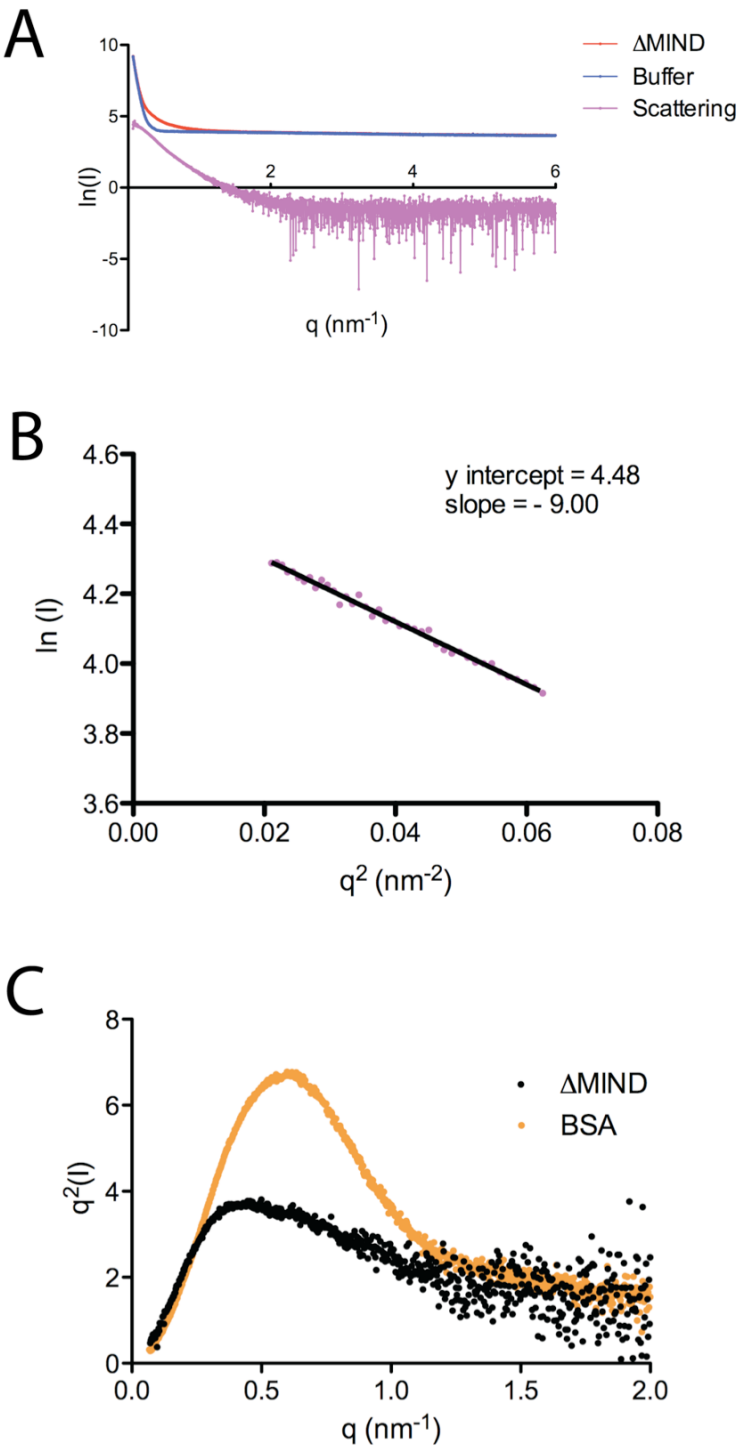

Figure 3.8 Scattering curves, Guinier analysis and Kratky plot for ΔMIND

A) Scaled and merged scattering curves for ΔMIND in buffer (Red line), buffer alone (Blue line) and the subtraction of the buffer from ΔMIND (Pink line). The curves were generated by the program PRIMUS and plotted in PRISM. B) Guinier plot of the ΔMIND scattering curve. Using the y-intercept and the gradient of the line, giving values of R_G as 5.2 nm and I(0) as 88. C) Kratky plot of the ΔMIND complex. A globular compact protein would have a bell shaped curve like Bovine serum albumin (BSA) (orange line). ΔMIND has a maximum that decreases into a plateau, indicating an extended structure with multiple domains.

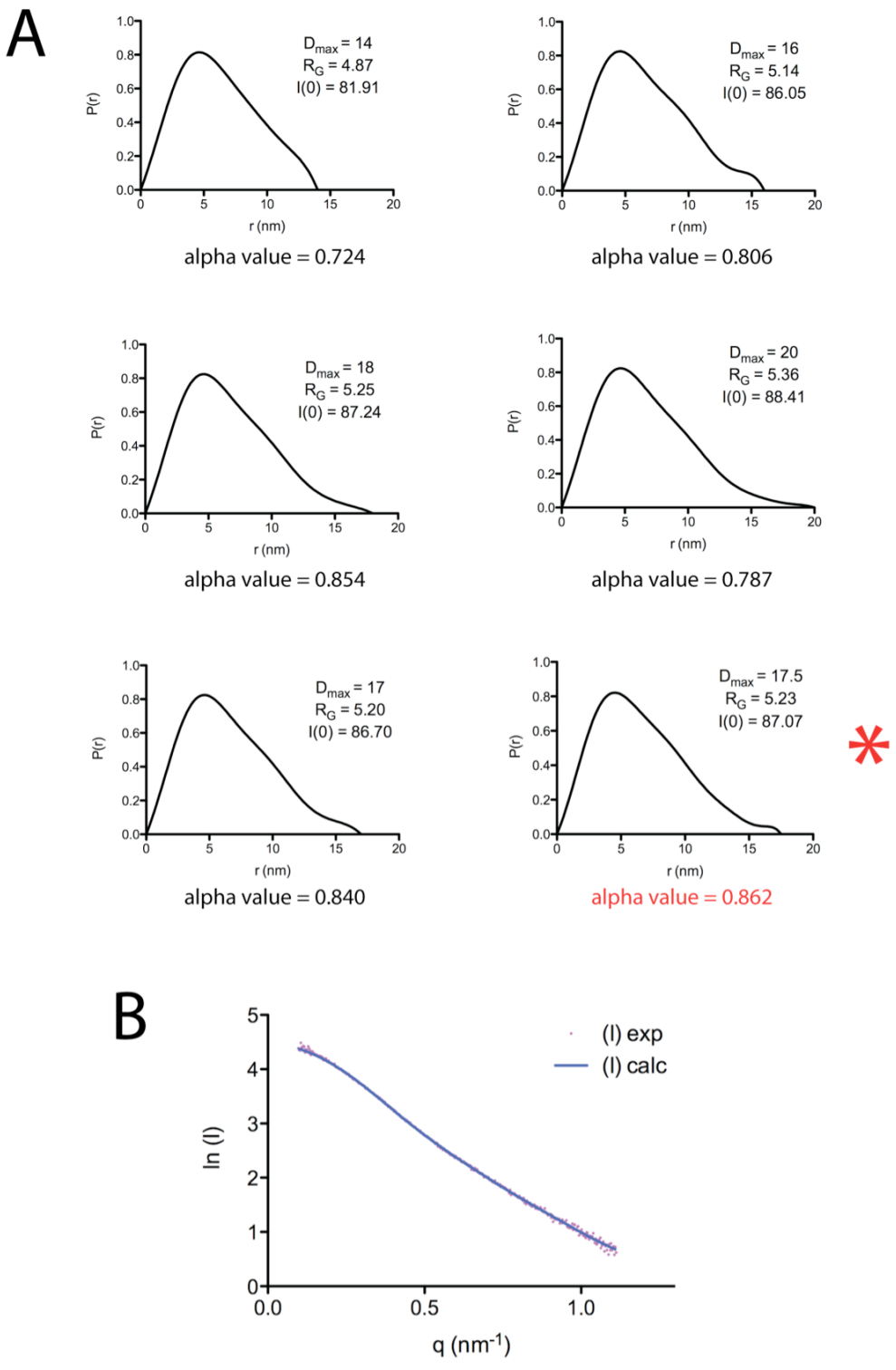

Figure 3.9 Pair distribution functions and scattering curve for modelling for ΔMIND.

A) Pair distribution functions P(r) calculated from the X-ray scattering data. Each curve uses a different D_{max} value ranging from 2.5 – 3.5 R_G. The best D_{max} value is indicated by an asterisk (bottom right). The P(r) function is indicative of an extended, multi-domain structure. B) Scattering curve (Pink dots) of the ΔMIND complex, with calculated model scattering curve (Blue line) used for *ab-initio* modelling calculated from GNOM.

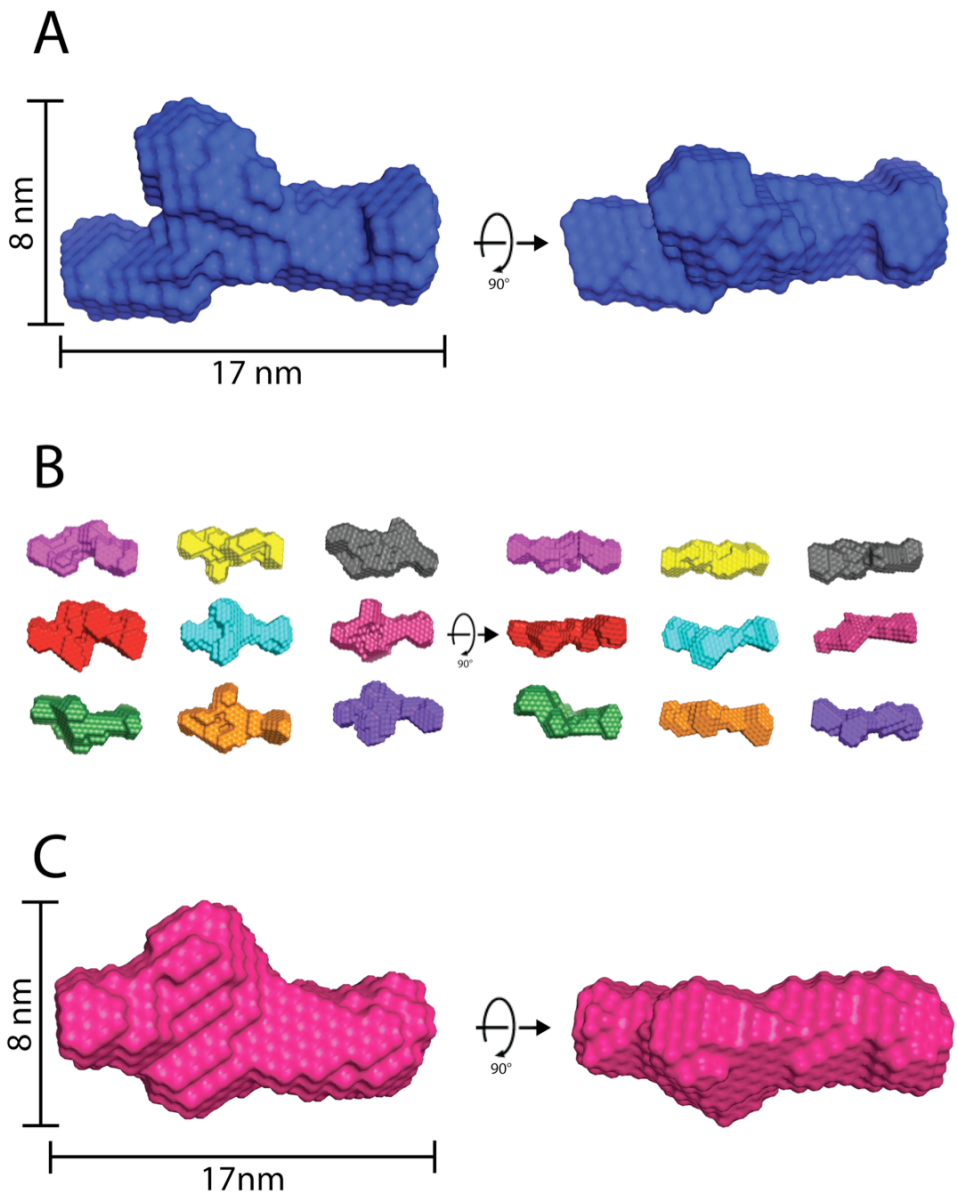

Figure 3.10 *Ab-initio* reconstruction of ΔMIND using DAMMIN

A) Three-dimensional low-resolution DAMMIN reconstruction of ΔMIND. The structure is 17 nm long. A 90° rotation is shown on the left. B) 9 separate reconstructions in DAMMIN using the same data set for A), showing a similar overall shape, although there are variations observed in the head region. C) Averaged, filtered reconstruction derived from the 10 models from A) and B). The reconstruction has the same length of 17 nm as seen in A) and B).

3.6 Expression and purification of $Dsn1_{103-412}$ / Nsl1p

During expression and purification of the ΔMIND, a sub-complex of $Dsn1_{103-412}$ and Nsl1p was observed (see section 3.4). Nsl1p has the lowest scores for predicted coiled coil regions (figure 1.3), suggesting it may be globular and removal of the N and C terminal of Dsn1p may also mean that this truncated version might also be more globular. These constructs were co-expressed to investigate whether a stable complex could be purified. $pDSN1_{103-412}$ (containing an N-terminal His-tag) and pNSL1 were co-transformed into *Escherichia coli* BL21(DE3) RIL cells. $Dsn1_{103-412}$ and Nsl1p were initially purified using Ni-NTA batch purification. SDS-PAGE (figure 3.11 A) showed bands that correspond to $Dsn1_{103-412}$ (35.2 kDa) and Nsl1p (25 kDa). Both protein bands are present in equal ratios, indicating a stable equimolar association. The relevant fractions were then loaded onto a pre-equilibrated size exclusion Superdex 200 16/60 column, with a single peak observed (figure 3.11 B), with SDS-PAGE (figure 3.11 C) showing that $Dsn1_{103-412}$ and Nsl1p were present in equimolar ratios. The sub-complex molecular weight is 60.2 kDa based on a.a. composition, the elution volume of 69 ml corresponds to a predicted molecular weight of 115 kDa, suggesting either an extended structure or a possible hetero-tetramer containing two copies of each protein**.**

3.6.1 Crystallisation trials of $Dsn1_{103-412}$/Nsl1p

10, 96 well crystal screens were tried for $Dsn1_{103-412}$/Nsl1p at a concentration of 15 mg/ml. After 3 days, screens showed that over 50% of the drops contained precipitate. No observable crystal growth was observed over a 3-month period.

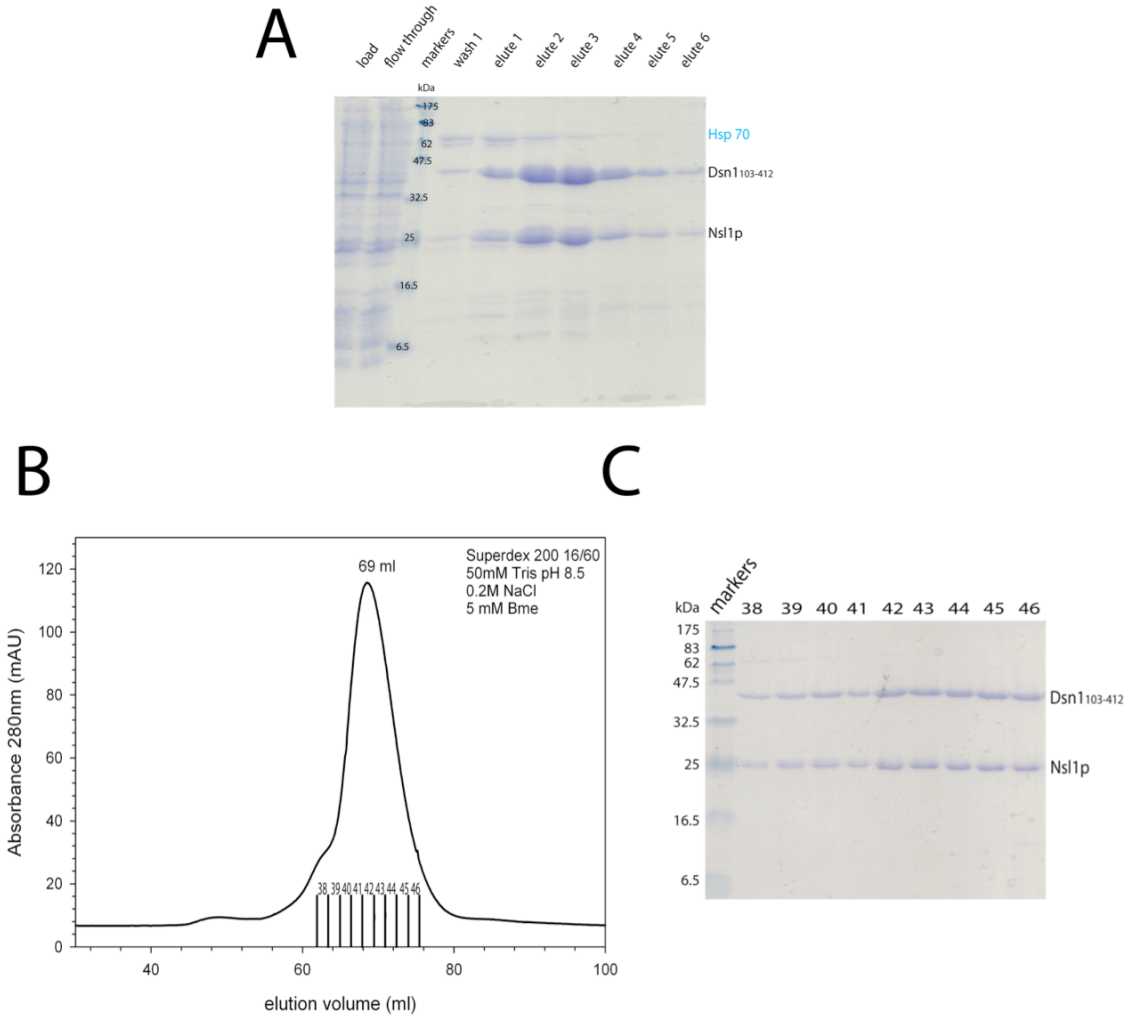

Figure 3.11 Expression and purification of Dsn1$_{103-412}$ /Nsl1p

A) SDS-PAGE of Ni-NTA affinity purification of Dsn1$_{103-412}$ / Nsl1p with bands labelled. Bands are seen corresponding to the molecular weights of Dsn1$_{103-412}$ (35.2 kDa) and Nsl1p (25 kDa). Both proteins are seen in equal ratios. B) Elution profile of Dsn1$_{103-412}$ / Nsl1p from size exclusion chromatography. A single peak is seen from the elution profile with elution volume and relevant fractions marked. C) SDS-PAGE of fractions from B), with proteins identified on the right. Fractions show that Dsn1$_{103-412}$ and Nsl1p still associate in equal amounts during the elution.

3.7 Determining the location of individual subunits in the MIND complex

This work was done in collaboration with Dr Xiao Hu-Wen and Dr Martin Singleton

One way to define the location of the individual proteins in the complex is to modify the proteins termini, so that they could be differentiated. EM would allow the mapping of individual proteins in the complex.

3.7.1 Identification of protein termini using Nanogold labelling

A Ni-NTA nanogold particle (Nanoprobes) (Hainfeld et al., 1999) is available that specifically binds a His-tag and can be observed under electron microscopy. This specific binding to the His-tag can be identified by the appearance of a dark spot when observed in the electron microscope. The MIND complex was purified following the standard EM protocol (see section 2.7) and incubated with a 10 times molar excess of the Ni-NTA nanogold solution for 1 hour at 4°C. This was then loaded onto a pre-equilibrated size exclusion Superdex 200 10/300 column and eluted. This additional elution step was included to remove unbound Ni-NTA nanogold (figure 3.12 A). The protein was then stained using uranyl acetate (see section 6.12) and particles of the MIND complex could be seen, however no nanogold labelling was observed under negative stain (data not shown). The nanogold particle is ~1.8 nm in diameter and may be too small to be detected by negative staining techniques. To overcome this problem, a solution of Goldenhance^{TM} (Nanoprobes) was used to make the overall diameter of the nanogold particle larger. After addition of Goldenhance^{TM}, nanogold particles could now be observed, interacting with the MIND complex (figure 3.12 B). Incorporation of a nanogold particle into the complex was low (~10%), yet it was possible to identify the location on the complex where it bound. The nanogold particles were all found to be associating at the head region as shown by a black dot. Nanogold labelling increased the

diameter of the head domain by 1.5–2 times and the black spot affected the contrast of the particles, reducing visibility of the tail domain. The addition of Goldenhance™ meant it was also difficult to control the size of the gold particle. However the particles showed consistent binding to the head region showing specificity. Seven further constructs, each containing a single His-tag on a different N or C termini were expressed and purified following the standard purification procedures (see section 2.2). These were nanogold labelled along with the additional goldenhance step. Of the eight constructs tried, only the original Dsn1p N-terminal His-tag complex showed any conclusive binding of the nanogold particle to a specific region of the complex.

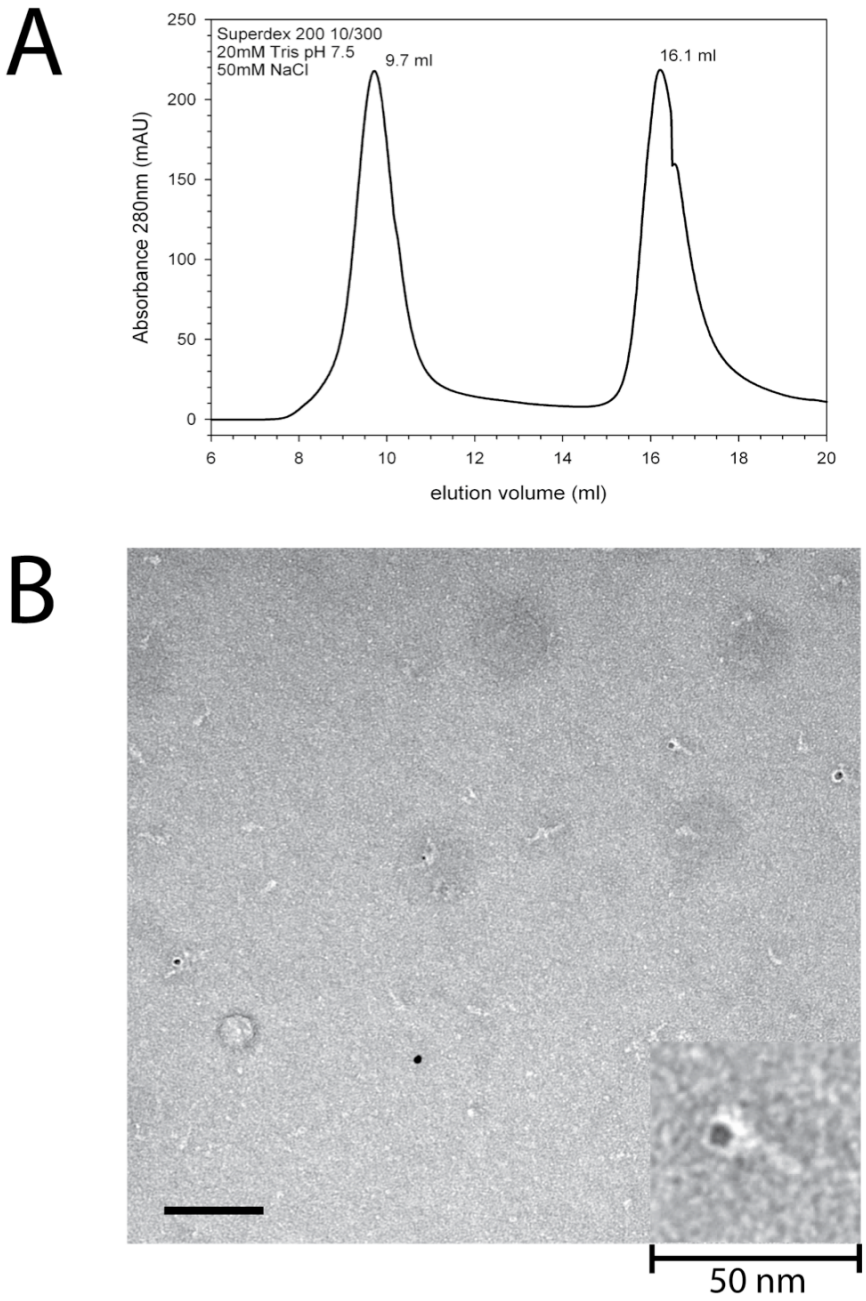

Figure 3.12 Nanogold labelling of the MIND complex

A) Elution profile of the N-terminal Dsn1p His-tagged MIND complex. The complex bound to gold elutes at 9.7ml the same elution volume as seen in figure 2.10. The peak at 16.1 ml is the unbound gold eluting at the bed volume of the size exclusion column. B) EM field of negatively stained MIND complexes. Complexes with black dots have been Nanogold labelled. Images were taken at a magnification of x20000 using a JEOL 1010 electron microscope operated at 80 kV. The scale bar in the EM field view is 100 nm. The bottom right panel is a magnified view of a single complex that has been labelled with a nanogold particle with the scale indicated.

3.7.2 Identification of protein termini using maltose-binding protein fusions

A different approach was considered to map the subunits of the MIND complex using EM. Adding extra amino acids to each termini using the maltose binding protein (MBP) would allow the opportunity to observe additional electron density in these regions. Unlike nanogold labelling, the contrast of the images would not be affected as this moiety would be of the same density of the MIND complex. A series of constructs were created encoding the 43.4 kDa MBP on either the N and C termini of each of the subunits. All constructs contained a His-tag either on the N-terminus of MBP, or the N-terminus of the specific protein subunit to which MBP was fused to the C-terminus. Purification of MIND complexes containing MBP fusions required modifications from standard protocols (see section 2.2), with MBP fused to the C-terminal of Dsn1p (C-MBP Dsn1p MIND complex) used as an example.

During protein expression (see section 6.5), 0.2% glucose (v/v) was added to LB broth during growth. The C-MBP-Dsn1p MIND complex was initially purified by Ni-NTA affinity purification with the relevant protein fractions diluted to a conductance < 15mS/cm and purified by ion exchange chromatography (figure 3.13 A). SDS-PAGE (figure 3.13 B) showed that the C-MBP fusion was being cleaved, so to remove complexes without the MBP fusion, fractions were passed through amylose affinity resin. C-MBP-Dsn1 MIND complex bind to the amylose resin, while MIND complexes that do not have the MBP fusion will flow through the column. The MBP fusions were then eluted by the addition of 10mM maltose to the buffer. A large elution volume of 20ml was required to recover all MBP fusion protein from the resin, this was concentrated and loaded onto a pre-equilibrated size exclusion Superdex 200 10/300 GL column. Two peaks were observed in the elution profile (figure 3.13 C), with the first peak eluting in the void region and the second peak deduced to be the C-MBP-Dsn1 MIND complex due to a similar elution volume from previous purifications of MIND complex (see section 2.7). For all constructs purified, the final concentration of protein obtained was already at an approximate concentration of 0.05 mg/ml, suitable for EM

analysis without further dilutions required. Of the eight constructs expressed, seven MBP fusion complexes could be purified for EM analysis. The C-terminal MBP fusion to Mtw1p was unstable and was not observed at the Ni-NTA purification stage (data not shown). Overall yields of MBP fused MIND complexes were significantly reduced compared to MIND complex purification. This was mainly due to the proteolytic cleavage between the protein and the MBP fusion that occurred for all constructs. All N-terminal MBP fusion MIND complexes contained additional density that could be identified in the head region when compared to normal MIND complex (figure 3.13 D). Of the three C-terminal constructs analysed, only C-MBP Dsn1p and C-MBP Nnf1p showed additional electron density, with both constructs observed to have extra density in the tail region giving the complex a “dumb-bell” shape.

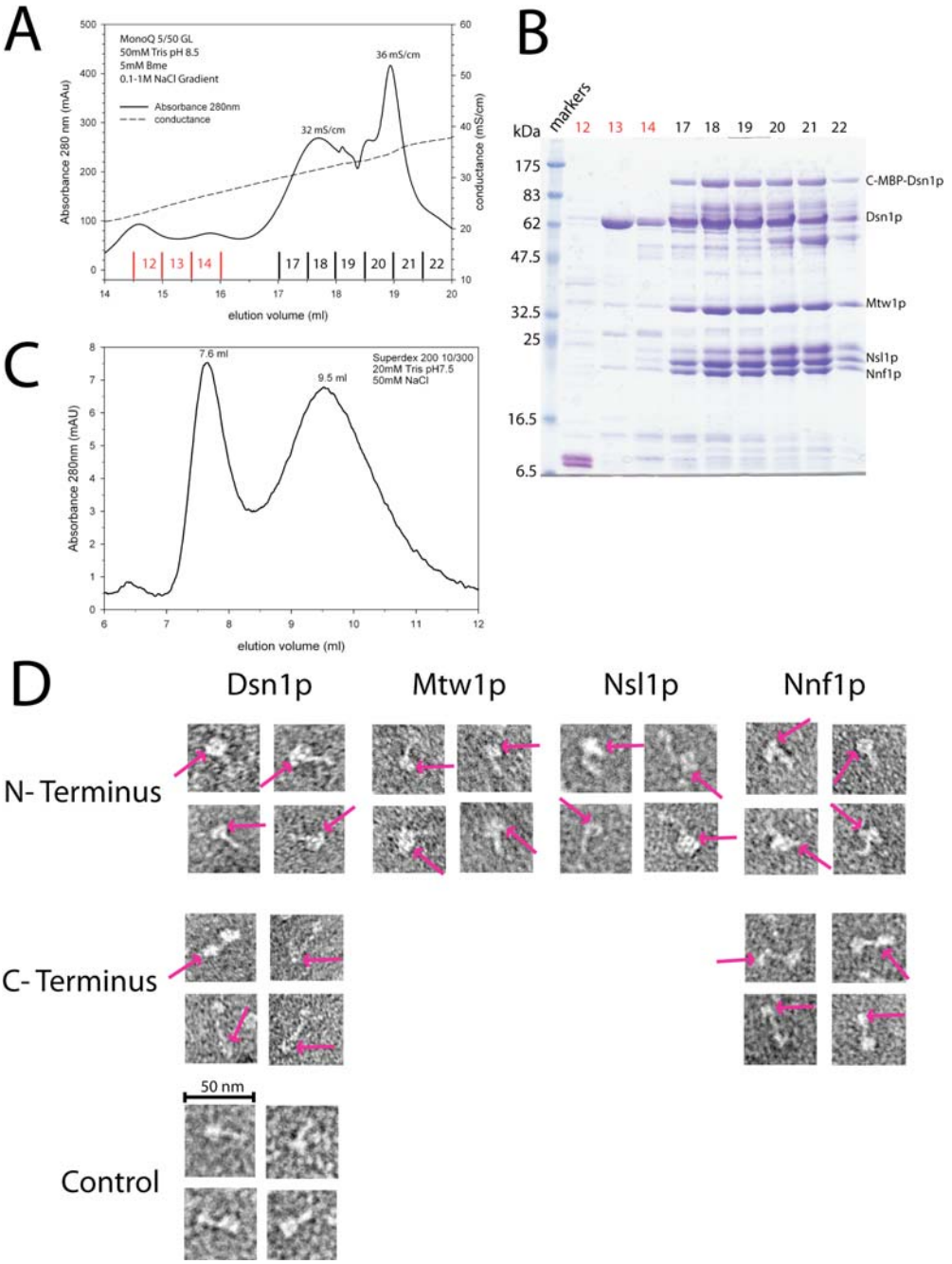

Figure 3.13 Expression, purification and visualisation of MBP fusion MIND complexes

A) Elution profile of C-MBP-Dsn1 MIND from anion exchange chromatography. Absorbance reading and conductance are continuous and dashed lines respectively. Relevant fractions and conductance values are marked. B) SDS-PAGE of fractions eluted from A), with proteins identified on the right. The molecular weight for MBP-Dsn1 is 109.3 kDa. Dsn1p (66 kDa) is also observed, indicating cleavage of the MBP-fusion. C) Elution profile of C-MBP-Dsn1 MIND from size exclusion chromatography after elution from amylose resin. Two peaks were seen from this elution. A peak was seen to elute in the void region and was discarded. The second peak had a elution volume comparable to the MIND complex (see section 2.7). D) EM images of N and C terminal MBP-MIND fusion constructs. Additional density arising from MBP fusions are indicated by pink arrows. Images of normal MIND complexes are used as a control. The scale bar is for all images.

3.8 Summary

The MIND complex was analysed using bioinformatics and limited proteolysis to identify flexible and extended domains. Some of the resulting complexes such as MIND $Dsn1_{1-290}$ were unstable with observable subunit dissociation, indicating that some of proposed extended regions are necessary for complex formation. One complex ΔMIND, was a promising candidate for crystallisation trials, as exposed and potential extended regions had been identified and removed experimentally. However this complex failed to crystallise, further supporting the idea that the subunits may associate via flexible interactions. SAXS analysis of the MIND complex, showed that that it was extended structure with multiple domains. Models generated from the scattering data by DAMMIN were in good agreement with respect to size and shape of the MIND complex as had been seen by EM analysis. The models of ΔMIND would suggest that the tail is intact, forming a stable structure, whereas the head region is susceptible to protease treatment.

By EM analysis using MBP fusions, the head region of the MIND complex was found to contain the N-termini of all four subunits indicating a possible site of interaction for all components of the complex. The C-termini of the MBP-Nnf1p and MBP-Dsn1p subunits are observed by these experiments to be in the tail region of the molecule.

Chapter 4.

4.1 Aims

A study of the *Caenorhabditis elegans* KMN complex (Cheeseman et al., 2006) provided insights into the roles of the individual sub-complexes in the formation of a dynamic microtubule-binding interface. The aims of the work presented in this result chapter were to see if the KMN network is also formed in *Saccharomyces cerevisiae*. To achieve this, all 3 components would be expressed and purified for analysis using both EM and biochemical techniques.

The Ndc80 complex has been extensively studied and the complex has been shown to be a 57 nm long rod with globular heads on either side (Wei et al., 2005.) These globular termini have been crystallised, showing that the Ndc80/Nuf2 head binds MTs and the Spc24/Spc25 head points towards the centromere (Ciferri et al., 2008). The Spc24/Spc25 globular head has been proposed to interact with the other proteins (Wei et al., 2006). To investigate possible interactions with the MIND complex, both the Ndc80 complex and Spc24/25 dimers alone would be recombinantly expressed.

The third member of the *Caenorhabditis elegans* KMN network KNL-1 (Spc105p in *Saccharomyces cerevisiae*) is a large protein that has been shown to bind microtubules *in vitro* (Cheeseman et al., 2006). KNL-1/Spc105p is poorly conserved throughout organisms, with very little structural information known. Spc105p will be cloned and expressed along with the other components of the KMN network for further characterisation.

4.2 Expression and purification of the Ndc80 complex

The recombinant Ndc80 complex was prepared by co-expression of the four subunits, Ndc80p, Nuf2p, Spc25p and Spc24p. pNDC80HT.SPC24 and pNUF2.SPC25 constructs were co-transformed into *Escherichia coli* BL21(DE3) RIL cells. Expression was carried out following standard protocol (see section 6.5). Ndc80p has an N-terminal His-tag, so the complex was initially purified by affinity chromatography, using a 5ml HisTrap FF column. A 20-500mM imidazole gradient eluted the Ndc80 complex as a single peak (figure 4.1 A) and SDS-PAGE (figure 4.1 B) showed four proteins, with similar weights to the molecular markers. These bands were sent for mass spectrometry analysis and were confirmed to be all four subunits of the Ndc80 complex. The complex was stable during affinity chromatography, however Hsp70 contamination was observed, similar to that seen for the purification of the MIND complex (see section 2.2) The denatured protein and ATP wash step (see section 6.6.1.3) was added to try and remove the chaperone, but was found to be unsuccessful.

Further purification was carried out by loading fractions containing the Ndc80 complex onto a pre-equilibrated size exclusion, Superdex 200 16/60 column. Two peaks were observed in the elution profile (figure 4.1 C), and SDS-PAGE (figure 4.1 D) showed that the first peak contained all four proteins of the Ndc80 complex. The second peak was predominantly Hsp70, showing that the two elution peaks overlap, creating cross contamination. The right side of first peak was cut to remove the chaperone contamination from the Ndc80 complex.

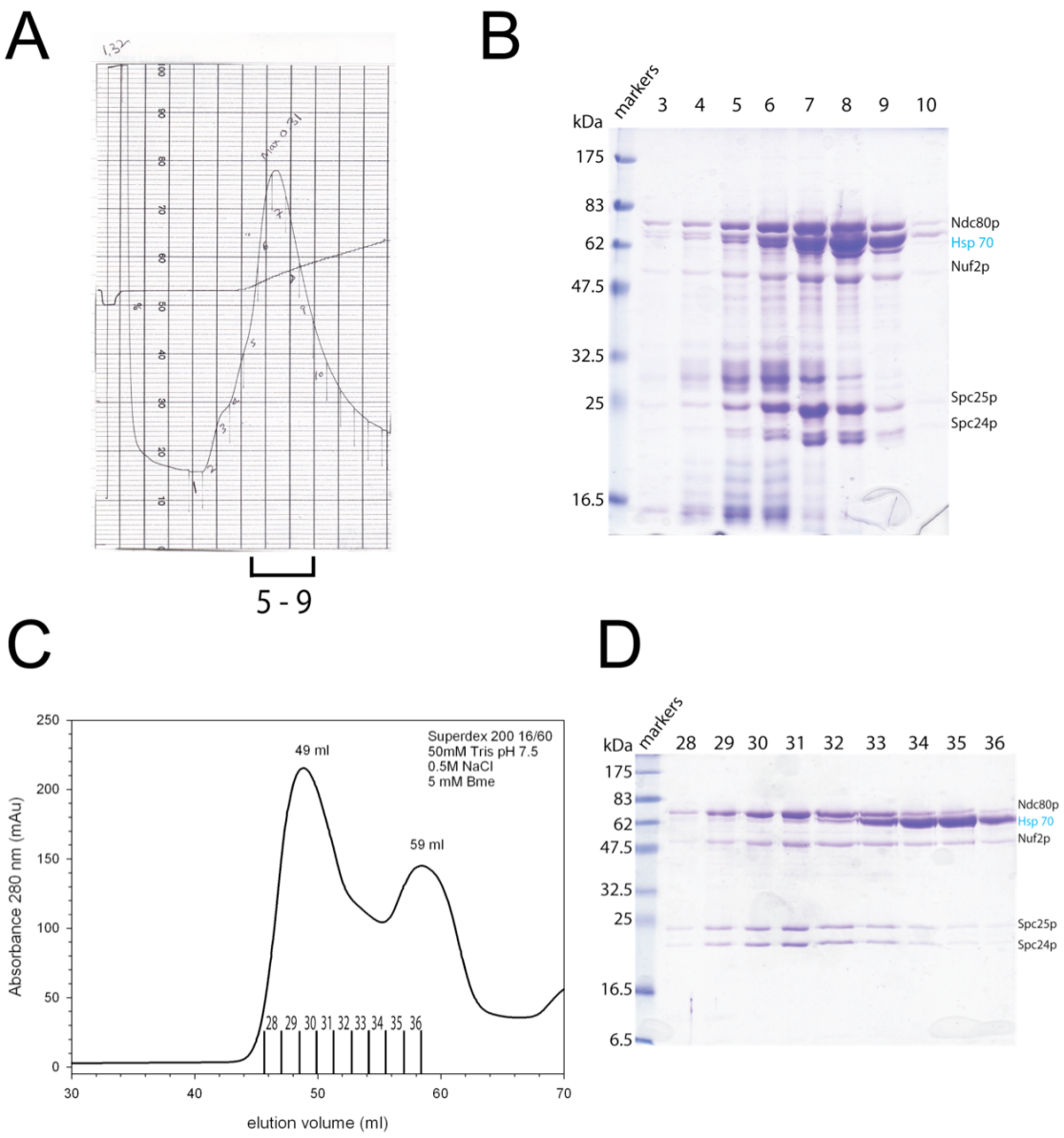

Figure 4.1 Expression and purification of the Ndc80 complex

A) The Ndc80 complex elutes as a single peak from a HisTrap FF column. B) SDS-PAGE of the fractions eluted from A). All four subunits are present in fractions 5-9 with proteins identified. Hsp70 contamination is also observable by SDS-PAGE. The molecular weights from amino acid composition are, 80.5 kDa for Ndc80p, 53kDa for Nuf2p, 25.2 kDa for Spc25p, 24.6 kDa for Spc24p. C) Elution profile of the Ndc80 complex from size exclusion chromatography with elution volume and relevant fractions marked. D) SDS-PAGE of elution profile shown in C), all four protein bands are seen in fractions 28-31. Fractions 32-36 is the elution of the Hsp70 chaperone contaminant**.**

4.3 Expression and purification of the Spc24/Spc25 and SpcG dimers

The Spc24/25 dimer was expressed by co-transformation of the pSPC24 and pSPC25 into *Escherichia coli* BL21(DE3) RIL cells. pSPC24 contained a N-terminal His-tag and the Spc24/Spc25 dimer was initially purified using Ni-NTA affinity purification, followed by size exclusion chromatography on a pre-equilibrated Superdex 75 10/300 GL column. The elution profile (figure 4.2 A) shows a small first peak followed by a major peak. SDS-PAGE (figure 4.2 B) identified that the first peak contains Spc24p and Spc25p, and may be dimers self associating via unbound coiled coil termini. The major peak also contained Spc24p and Spc25p, with each protein in an equimolar ratio and was used for subsequent experiments.

Using the pSPC24$G_{154\text{-}213}$ and pSPC25$G_{133\text{-}221}$ constructs, the identified globular domains of the Spc24p/Spc25p dimer (Wei et al., 2006) were co-transformed into *Escherichia coli* BL21(DE3) RIL cells and expressed, with the product of this expression referred to as SpcG. The His-tag on Spc24g was used to initially purify SpcG using Ni-NTA resin, followed by size exclusion chromatography on a pre-equilibrated Superdex 75 10/300. A single peak was observed in the elution profile (figure 4.2 C), with both proteins present in an equal ratio as shown by SDS-PAGE (figure 4.2 D).

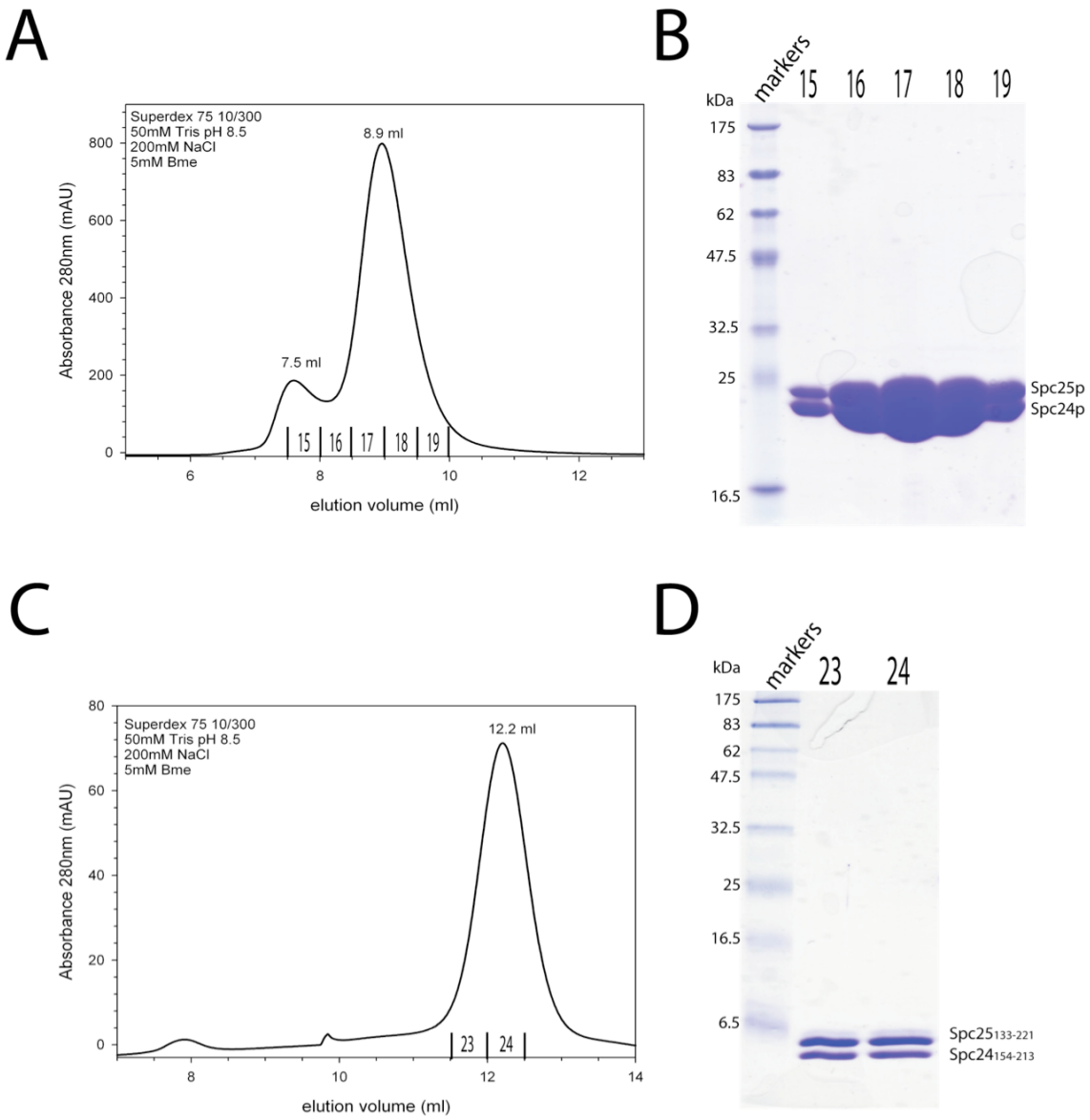

Figure 4.2 Expression and purification of Spc24/Spc25 dimers

A) Elution profile from size exclusion chromatography of Spc24/Spc25 dimers. Elution volumes and relevant fractions have been marked. B) SDS-PAGE of fractions eluted from A). Both proteins are present in equal ratios. C) Elution profile from size exclusion chromatography of SpcG. Elution volume and relevant fractions have been marked. D) SDS-PAGE of fractions in C), show that SpcG interact in a equal ratio.

4.4 Interactions of the MIND and Ndc80 complexes by analytical gel filtration

The interaction between the MIND and Ndc80 complexes was first analysed by analytical gel filtration. Equimolar amounts of MIND and Ndc80 complexes at approximately 0.1 mg/ml were mixed and left to incubate at 4°C for 1 hour on a rolling platform. The mixture was loaded onto a pre-equilibrated Superdex 200 10/300 GL column. The elution profile (figure 4.3) identified two peaks that slightly overlap making it difficult to identify if a interaction was occurring.

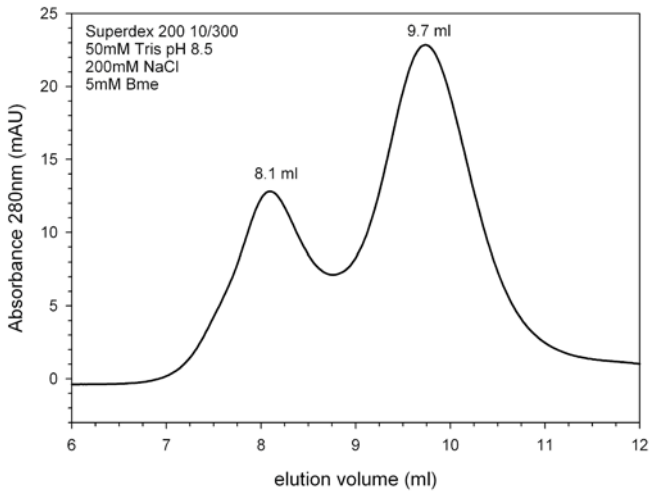

Figure 4.3 Analytical gel filtration of MIND-Ndc80 interaction

The elution profile from analytical gel filtration identifies two peaks that overlap, making it difficult to identify clear binding. No observable shifts in elution volumes is observed for both proteins as the Ndc80 complex on its alone elutes at 8.1 ml (see section 4.7) and the MIND complex elutes at 9.7 ml (see section 2.7).

4.5 Interaction studies of the MIND and Ndc80 complexes by pull down assays

As the interaction between the MIND and Ndc80 complexes could not be comprehensively determined by analytical gel filtration, the interaction was tested by pull down assays using Ni-NTA affinity resin. A His-tagged protein will bind to Ni-NTA resin, other proteins that do not have a His-tag will only remain associated to the resin by stably interacting with bound proteins. As all complexes contained a His-tag used for affinity purification, tobacco etch virus (TEV) protease was used to remove the His tag from the Dsn1p subunit. Once the His-tag was removed from Dsn1p, the MIND complex can only bind the Ni-NTA resin via an interaction with the Ndc80 complex. The MIND and Ndc80 complexes were observed to associate together and eluted as a stable species containing all eight proteins (figure 4.4 A). The equal intensities of each the protein bands suggest that this interaction is equimolar between each complex. A stable interaction is also observed between the MIND complex and the Spc24/ Spc25 dimer (figure 4.2 B) and SpcG (figure 4.4 C).

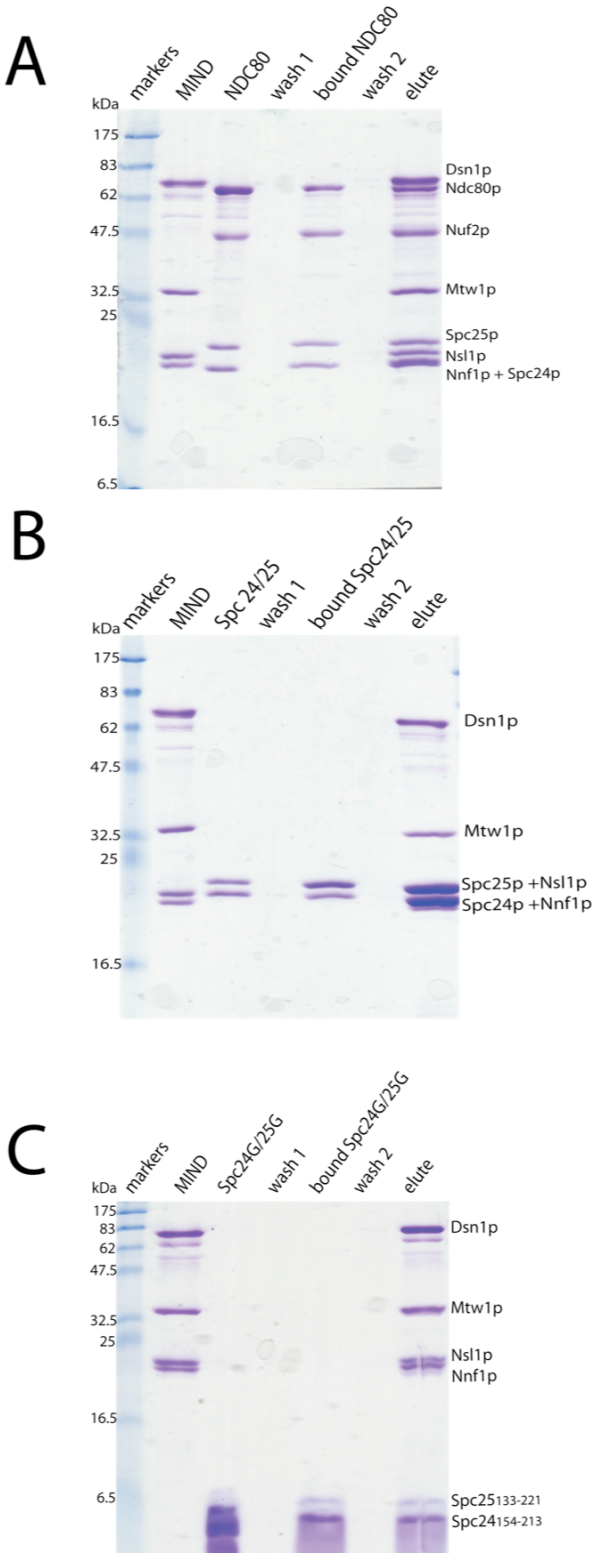

Figure 4.4 Pull down assays between MIND and Ndc80 complexes

A) His-tagged Ndc80 complex interaction with the MIND complex. Ndc80 complex was bound to the resin, washed and MIND complex was added. Resin was washed and proteins were eluted from the beads. The same experimental procedure was carried out for only the Spc24p/Spc25p proteins (B) and SpcG (C).

4.6 Studying the MIND–Ndc80 interaction by isothermal titration calorimetry

From pull down experiments (figure 4.4 A), the stoichiometry of the MIND-Ndc80 interaction appeared to be 1:1. To test this and gain more quantitative data, the interaction was analyzed by isothermal titration calorimetry (ITC). ITC provides thermodynamic characterisation by measuring directly the heats of binding to generate a binding curve. By integration of the binding curve, both enthalpy values (ΔH) and entropy values (TΔS) are calculated. Using these values, free energy (ΔG) can also be calculated giving the energy profile of binding (Ladbury and Doyle, 2004). With the molar concentrations of each protein determined, the gradient and the mid point of the binding curve give values of the binding constant (K_B) and stoichiometry of binding (N) respectively.

To prevent erroneous heat changes due to buffer mismatch, both proteins had to be buffer exchanged into identical buffers. MIND and Ndc80 complexes were dialyzed into a buffer containing the reducing agent TCEP as other reducing agents are more volatile and produce heat upon oxidation, which can affect experimental measurements. The initial buffer used contained 50mM Tris pH 7.5, 100mM NaCl, 0.5mM TCEP. Initial MIND and Ndc80 isotherms (data not shown) generated inconclusive data, as the Ndc80 complex was unstable and dissociated quickly in solution (data not shown). Concentrating the complex greater than 0.5 mg/ml lead to precipitation, and the complex could not be flash frozen, decreasing the amount of time available for purification and data collection. The purification protocol was modified so that the buffer used for size exclusion chromatography was the also the buffer used for the ITC experiments. Addition of 4 % glycerol to the buffer prevented the precipitation of the complex at concentration greater than 0.5 mg/ml and reduced dissociation of the complex.

The purification protocol for the MIND complex was also modified for ITC experiments. Protein from affinity chromatography (see section 2.2.1) was diluted with 50 mM Tris pH 8.5 until the conductance was < 15mS/cm and loaded onto a anion exchange MonoQ 5/50 GL column for anion exchange purification. The elution profile (data not shown) showed the MIND complex eluted at a similar conductance to previous purification stages (see section 2.2.3) This sample was then loaded onto a size exclusion Superdex 200 16/60 column pre-equilibrated with ITC buffer (50mM Tris pH 7.5, 100mM NaCl, 4% glycerol (v/v), 0.5mM TCEP). The elution profile (data not shown) was the same as previously seen (see section 2.2.2). For an ITC experiment, the solution in the syringe must have at least a 10 fold molar excess so that binding can be observed (Ladbury and Doyle, 2004) The MIND complex was concentrated to 9.1 mg/ml corresponding to a molar concentration of 62 μM. The Ndc80 complex was concentrated to 0.7 mg/ml, corresponding to 4 μM.

Consistent binding isotherms could be generated (figure 4.5 A), with the dissociation constant (K_D) which is equivalent to $1/K_B$ was determined as 71 nM ± 17 nM (figure 4.5 B). Modelling the data on a single-site interaction gave a 1:1 association for the interaction between MIND and Ndc80 complexes. The energy profile of the interaction (figure 4.5 B) indicated hydrophobic interactions and favourable redistribution of hydrogen bonds (Ladbury and Doyle, 2004). The interaction between the MIND complex and the Spc24/Spc25 and SpcG complexes was also examined using ITC. A reproducible binding curve could not be generated for the interaction between MIND and SpcG (data not shown). Isotherms were observed for MIND and Spc24/Spc25 interactions (figure 4.5 C), by injecting Spc24p/Spc25p at 70μM into the MIND complex in the cell at 6μM. The isotherm for this interaction never went to completion due to the heat of dilution when injecting the Spc24p/Spc25p. The K_D value obtained was still in the nanomolar range with a value 183 ± 79 nM (figure 4.5 D). The large error in this value meant it was difficult to correlate the value to the dissociation constant values obtained from the interaction between MIND and Ndc80 complexes. The association between MIND and Spc24p/Spc25p was 1:1, comparable to that seen for the interaction between the MIND and Ndc80 complexes. The energy profile of the interaction (figure 4.5 D) was also similar, with the binding suggested to occur by

hydrophobic interactions and hydrogen bond re-arrangements (Ladbury and Doyle, 2004).

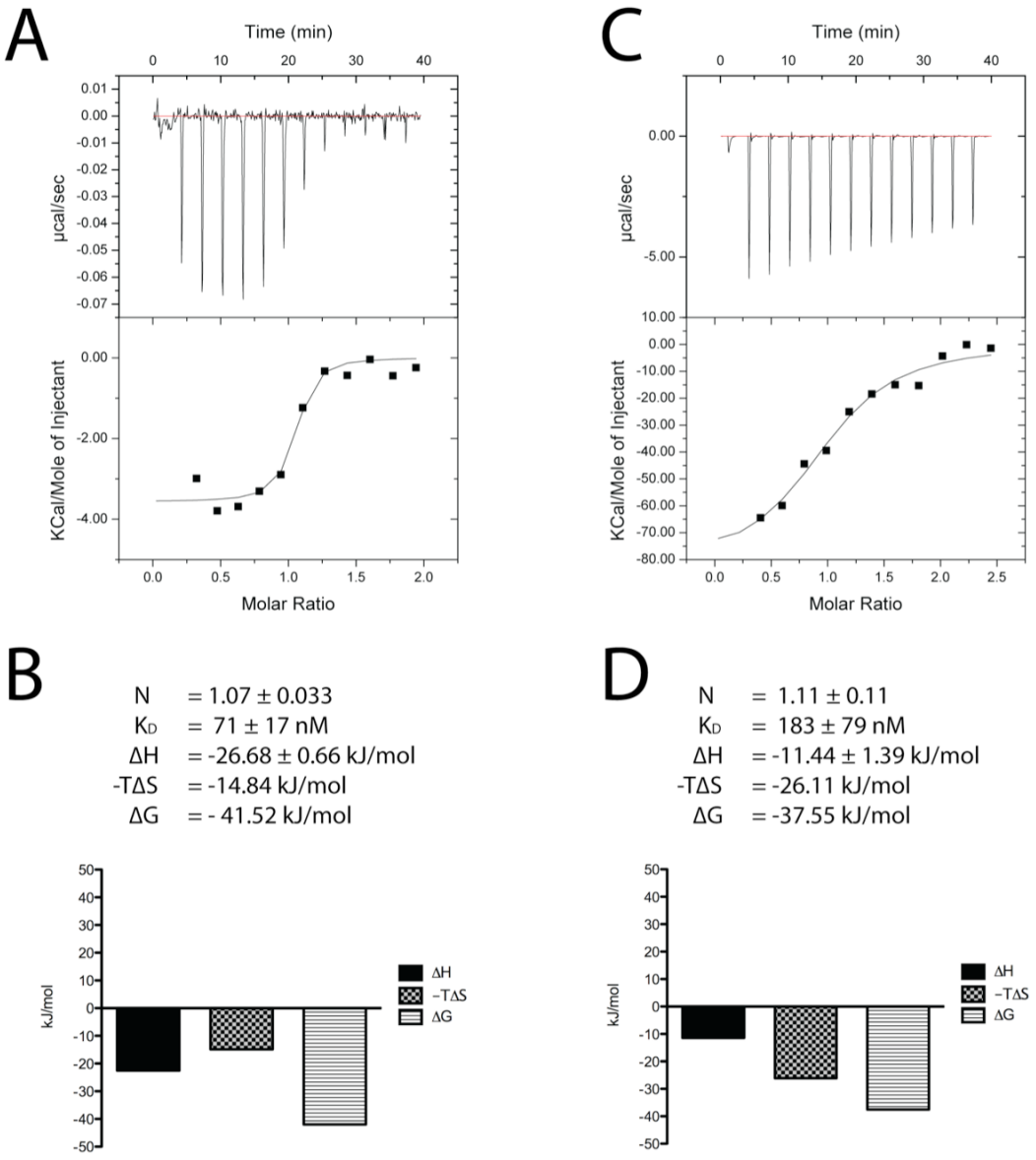

Figure 4.5 Binding of Ndc80 components to the MIND complex identified by ITC

A) Binding isotherm of the interaction between Ndc80 and MIND complexes. Top is the raw data obtained from injecting MIND (syringe) into Ndc80 complexes in the cell, indicating an exothermic binding reaction at 30°C. Bottom is the fitted curve of the raw data above. Data was fitted using single site binding and the thermodynamic parameters were obtained as shown in B). Thermodynamic data and the energy profile of the interaction between Ndc80 and MIND complexes. Values were converted from kcal/mol to kJ/mol (1kcal/mol = 4.18 kJ/mol) C) Binding isotherm obtained from injecting Spc24p Spc25p dimer (syringe) into MIND complex in the cell. D) Thermodynamic data and energy profile of the interaction.

4.7 Studies of the MIND-Ndc80 interaction by electron microscopy

For this section Dr Xiao Hu-Wen captured all images

The MIND-Ndc80 interaction was analysed by electron microscopy to see if the binary complex could be directly visualised. To achieve this, the Ndc80 complex was initially examined to see if it could be observed by EM as previous studies (Wei et al., 2005) have achieved. The purified Ndc80 complex for EM analysis was prepared as described for the MIND complex (see section 2.7). Using this preparation, the Ndc80 complex could be visualised (figure 4.6 B (ii)), with dimensions in agreement with previous studies (Wei et al., 2005). The Ndc80/Nuf2 and Spc24/25 globular termini are difficult to differentiate in these images. To determine the termini of the Ndc80 complex nanogold labelling (see section 3.7.1) was used. The MT binding head of Ndc80p has a N-terminal His-tag that had been previously used for affinity purification (see section 4.2) The Ndc80 complex was incubated with gold, eluted (figure 4.6 A) and goldenhanced. The Ndc80/Nuf2 head could be differentiated (figure 4.6 B (iii) and (iv))

Equal molar ratios of MIND and Ndc80 (with and without gold incorporation) complexes were added together and left to associate for 1 hour at 4°C on a rolling platform. Dilutions to a final concentration of approximately 0.05 mg/ml were made and the samples were negatively stained for analysis. Several images showed that the MIND complex was associating with a single terminus of the Ndc80 complex (figure 4.6 B (v) and (vi)). Using gold labelled Ndc80 complexes, the Spc24p/Spc25p terminus was observed to be interacting with the MIND complex (figure 4.6 B (vii)). The measured lengths of Ndc80 and MIND complexes were comparable to those of the individual complexes. The head domain of the MIND complex appeared to be the point of interaction with the Spc24p/Spc25p globular terminus, with the tail region of the MIND complex angled away from the coiled-coil shaft of the Ndc80 complex.

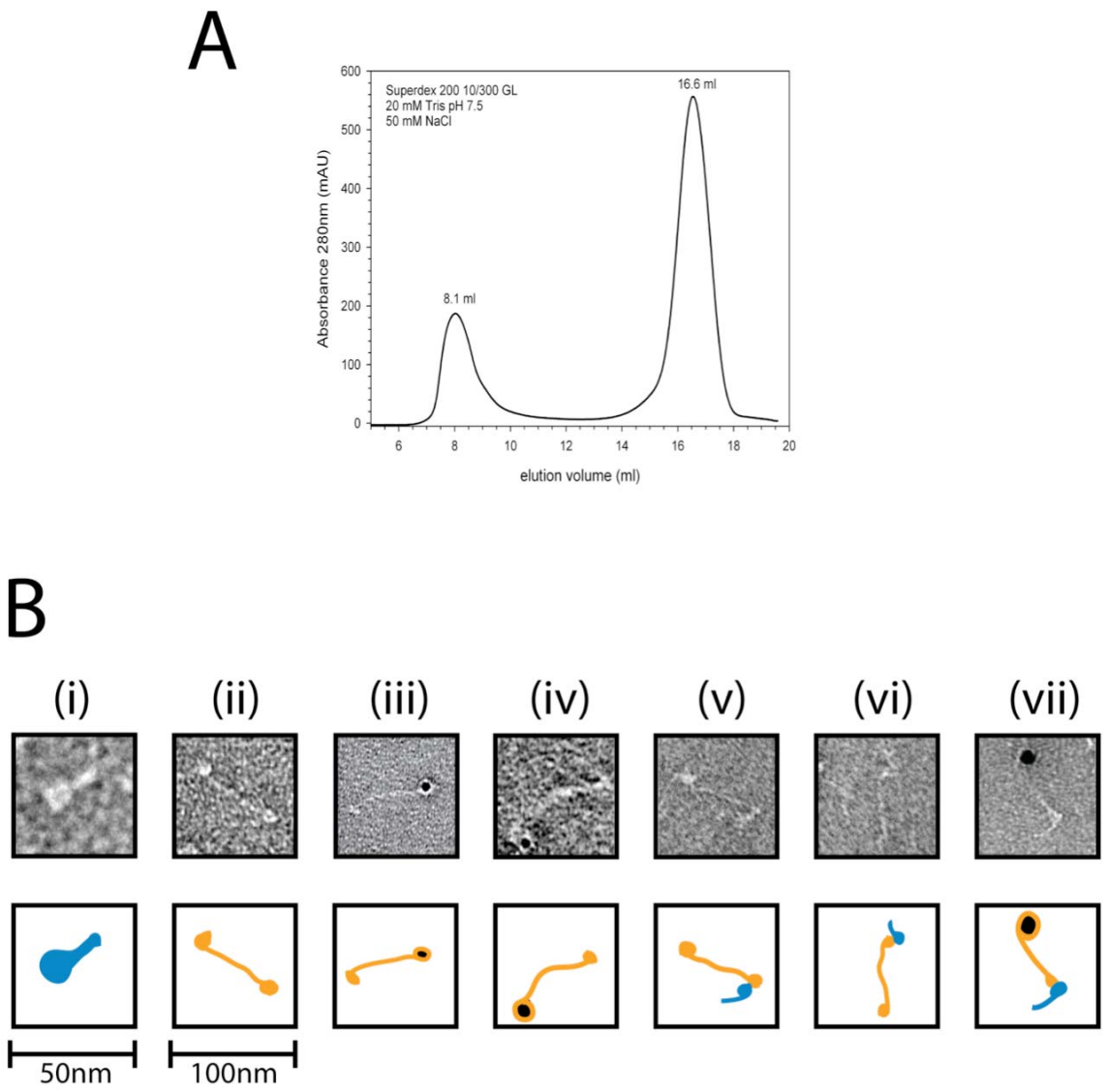

Figure 4.6 Visualisation of the NDC80–MIND interaction using EM

A) Elution profile of the NDC80 complex that had been nanogold labelled. The first peak is the NDC80 complex with the second peak being the unbound nanogold particles eluting at the bed volume of the column. B) Single particle images of the NDC80 and MIND complexes, and the binary NDC80-MIND interaction. Some NDC80 molecules are labelled with a nanogold particle at the microtubule binding termini. Schematic pictures are shown in boxes below, with MIND in blue and NDC80 in orange with black indicating the nanogold particle. (i) MIND complex (ii) Ndc80 complex (iii) and (iv) Ndc80 nanogold labelled (v) and (vi) MIND and Ndc80 interactions (vii) MIND and nanogold labelled Ndc80 interaction.

4.8 Expression and purification of Spc105p

Spc105p is a 917 amino acid, 105 kDa protein. Putting the sequence into the Foldindex server (Prilusky et al., 2005) predicted that the first half of the protein is unfolded. The approach was used to clone both the full-length protein and residues 648-917 for expression in *Escherichia coli*.

4.8.1 Molecular cloning of Spc105p using *Escherichia coli* expression systems

Genomic DNA from *Saccharomyces cerevisiae* (a gift from the Chromosome Segregation Laboratory, Cancer Research UK) was used as a template for PCR amplification of SPC105. The forward primers for full length SPC105 and $SPC105_{648-917}$ contained a BamHI restriction site. The reverse primer contained a XhoI restriction site. The SPC105 constructs were cloned into the plasmid vector pET28a, which generated an N-terminal His-tag, enabling affinity purification. The constructs were named pSPC105 and $pSPC105_{648-917}$.

4.8.2 Expression trials of Spc105p and $Spc105_{648-917}$ in *Escherichia coli*

pSPC105 and $pSPC105_{648-917}$ were separately transformed into *Escherichia coli* BL21(DE3) cells. Expression of Spc105p and $Spc105_{648-917}$ was compared between samples that were induced and non-induced with IPTG. Expression could not be observed for Spc105p (figure 4.7 A) or $Spc105_{648-917}$ (data not shown). Various concentrations of IPTG were also tested for both constructs with no observable difference detected (data not shown). The supernatant of induced samples of both proteins were then each passed through separate 50μl slurrys of Ni-NTA resin, the resin was washed and the beads directly analysed by SDS-PAGE (figure 4.7 B). No

observable protein was bound to the resin indicating no soluble protein was being expressed for either constructs.

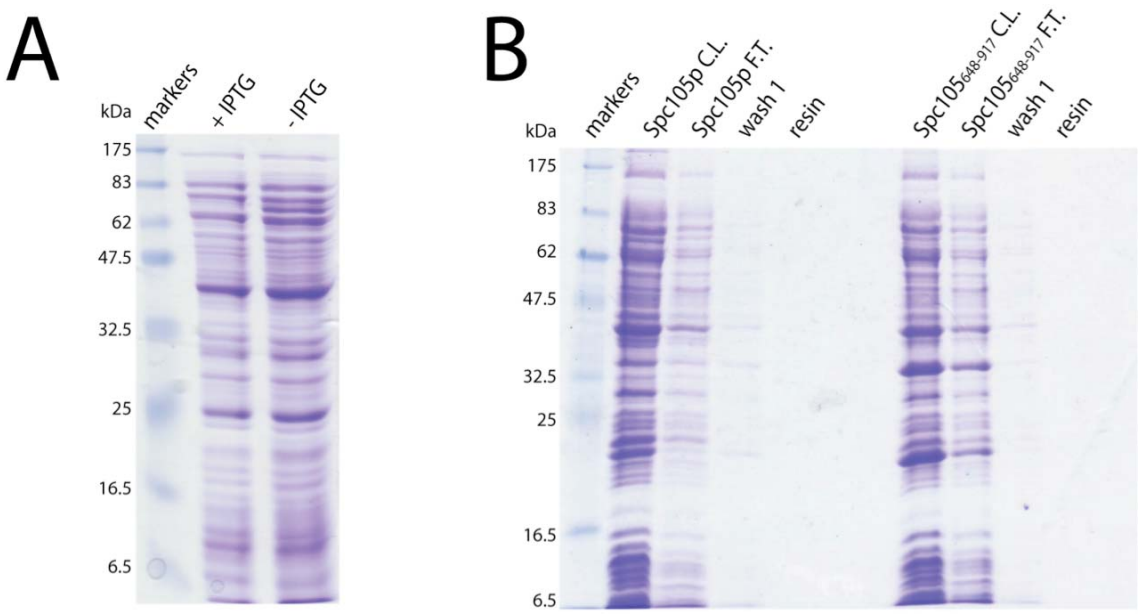

Figure 4.7 Expression tests for Spc105p

A) SDS-PAGE of Spc105p expression, comparing induced and un-induced (with IPTG) cultures. Typically additional bands of protein would be observed with the addition of IPTG. For Spc105p test expression, no obvious band was observed around the 105 kDa region by comparison to molecular weight markers. B) SDS-PAGE of test purification of Spc105p proteins. Crude lysate of test expression was passed through Ni-NTA agarose resin as Spc105p and $Spc105_{648\text{-}917}$ were cloned with a N-terminal His-tag to aid purification. Analysis of the resin identified no proteins at around 105 kDa for spc105p or 31 kDa for $Spc105_{648\text{-}917}$, compared to molecular weight markers.

4.8.3 Molecular cloning of Spc105p using baculovirus expression systems

Baculovirus expression systems were then used to see if recombinant Spc105p could be expressed. Using the same PCR insert generated in section 4.8.1, SPC105 and $SPC105_{648\text{-}917}$ were cloned separately into the pFastBac^{TM}HT vector using the restriction sites BamHI and XhoI, generating a TEV cleavable N-terminal His-tag for affinity purification. The pFastBacSPC105 and pFastBac$SPC105_{648\text{-}917}$ were then transformed into DH10Bac^{TM} cells, for transposition between the vector and the bacmid. Successful bacmid transpositions were isolated and sent to the Protein

Production Laboratory Cancer Research UK, for transfection, identification and optimization of protein expression in Sf9 cells. Expression was identified for Spc105p by a western blot using anti-His antibodies detecting the N-terminal His-Tag. No expression was observed for $Spc105_{648-917}$.

4.8.4 Expression and purification of Spc105p from baculovirus expression systems

6 litres of Sf9 cells were infected with Spc105p containing virus, and provided as a pellet the Protein Production Laboratory Cancer Research UK. The pellet was re-suspended in buffer as described in section 6.5.2. Extraction of the protein was modified from standard protocols (see section 6.5.3), by changing to 3 x 20 second sonication pulses, as Sf9 insect cells have weaker cell walls than *Escherichia coli* cells.

Spc105p was initially purified by Ni-NTA affinity purification. SDS-PAGE (figure 4.8) showed multiple bands, and Spc105p could not be differentiated as the gel was heavily contaminated with other proteins. A sample from Ni-NTA purification was loaded onto a pre-equilibrated size exclusion Superdex 200 10/300 GL column. The buffer contained 0.5M NaCl to reduce electrostatic interactions, increasing the possibility of removing contaminating proteins. Two peaks were observed in the elution profile (figure 4.8 B), with the first peak running in the void region of the column. SDS-PAGE (figure 4.8 C) showed two bands, in both the first and second peak. The top band was running at a molecular weight greater than 83 kDa based on a comparison to the marker, the second band was between 47.5 and 63 kDa. Although Spc105p expression had been previously identified by anti-His antibodies (see section 4.8.3), the protein bands were excised and sent for mass spectrometry analysis. The top band was identified to be Spc105p with full coverage of the amino acid sequence observed. The other band was identified to be α/β tubulin. The large amount of protein contamination could not be removed by either Ni-NTA affinity or size exclusion chromatography in concentrations of 1M NaCl (data not shown) indicating that further purification would not be possible for Spc105p. As truncations of Spc105p could not be expressed either in *Escherichia coli* or Sf9 cells, it was thought that generation of further truncations would

be unsuccessful. This prevented the opportunity to characterise the KMN network by EM studies, which was a major aim of this thesis.

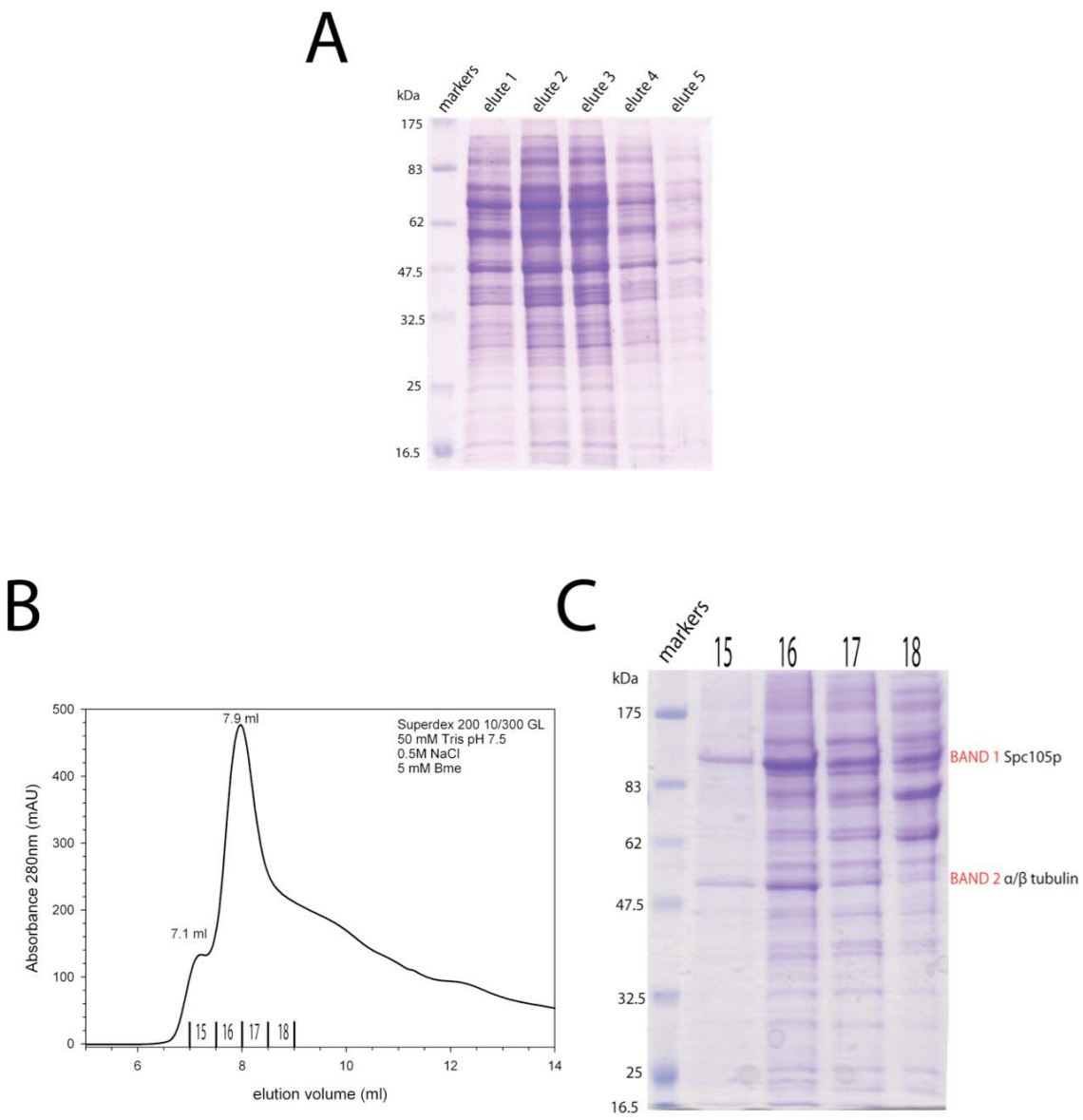

Figure 4.8 Expression and purification of Spc105p using baculovirus expression systems

A) SDS-PAGE analysis of Spc105p elution by Ni-NTA resin batch purification, with multiple bands observed. B) Elution profile of Spc105p from size exclusion chromatography, with elution volumes and relevant fractions marked. C) SDS-PAGE of fractions eluted from B), indicating Spc105p is still heavily contaminated.

4.9 Interaction studies between the MIND complex and Spc105p using peptide array assays

As Spc105p could not be expressed, peptides of the sequence would be synthesised onto a membrane and interactions with the MIND complex would be investigated. Specific interactions with peptides can be detected and related back to the structure of the Spc105p protein. A membrane was generated by the Peptide Synthesis Laboratory Cancer Research UK that was spotted with 21-residue peptides covering the whole Spc105p sequence with a two-residue increment per spot. The array was probed with the MIND complex, and bound protein detected using anti-His antibodies, that bind to the His-Tag on the N-terminal of Dsn1p. After controlling for non-specific peptide interactions using anti-His antibodies alone (figure 4.9 A), the MIND complex binding to regions of peptides were identified (figure 4.9 B). Previous studies (Kiyomitsu et al., 2007) have shown that the C-terminal of human KNL1 (blinkin) is responsible for interactions with the human Mis12/MIND complex. Therefore, C-terminal interacting peptide regions were the first to be examined. Two regions were observed in the C-terminal, both constituting hydrophobic motifs that show conservation when aligned with other fungal Spc105p proteins (figure 4.9 C).

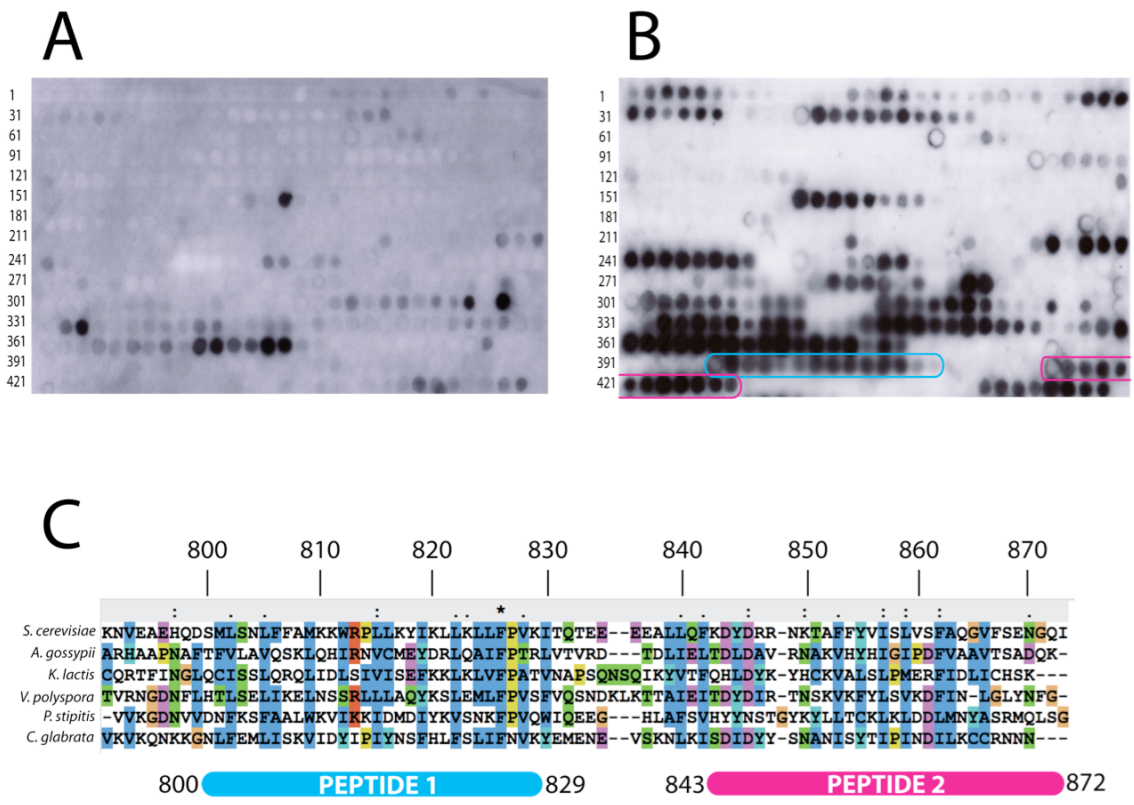

Figure 4.9 Peptide array of Spc105p probed by MIND complex

A) Peptide array control. The membrane was incubated with anti-His antibodies to identify regions that have non-specific interactions with the antibody. Spots were developed by the secondary antibodies conjugated to HRP B) the membrane was incubated with the MIND complex, washed and then incubated with anti-His antibodies to probe for the interactions between MIND and spc105p peptides. Spots were developed as discussed in A). Two regions of peptides that exhibit strong specific binding to MIND complex are highlighted in blue and pink. C) ClustalW (Thompson et al., 1994) sequence alignment of the C-terminal of 6 fungal orthologs of Spc105p. The sequences corresponding to the peptides are indicated.

4.9.1 Interaction studies between the MIND complex and Spc105p C-terminal peptides by isothermal titration calorimetry

To confirm these interactions, the peptides were synthesised by the Peptide Synthesis laboratory Cancer Research UK, for ITC experiments. Peptide 1 could be synthesised and purified by HPLC for ITC experiments. Peptide 2 could not be sufficiently purified by HPLC to yield enough product to carry out ITC experiments. Lyophilised peptide 1 was dissolved in the ITC buffer (see section 4.6) to a concentration of 100 μM. The MIND complex was concentrated to 1 mg/ml, corresponding to 7μM. Initial isotherms, at 30°C proved inconclusive with an inconsistent baseline measurements, making it difficult to determine binding (data not shown). The temperature was reduced to 16°C, which enabled consistent binding isotherms to be generated (figure 4.10 A). The dissociation constant K_D was determined to be in the nanomolar range, with a value of 111 nM ± 27 nM. Modelling the data on a single-site interaction gave a 1:1 association. Both values are comparable to the association between MIND and Ndc80 complexes, yet the energy profile differs (figure 4.10 B). The energy profile of the interaction between the MIND complex and Spc105 peptide 1 indicates a hydrophobic interaction with the positive enthalpy change relating to unfavourable hydrogen bond re-arrangements, involving solvent redistribution (Ladbury and Doyle, 2004).

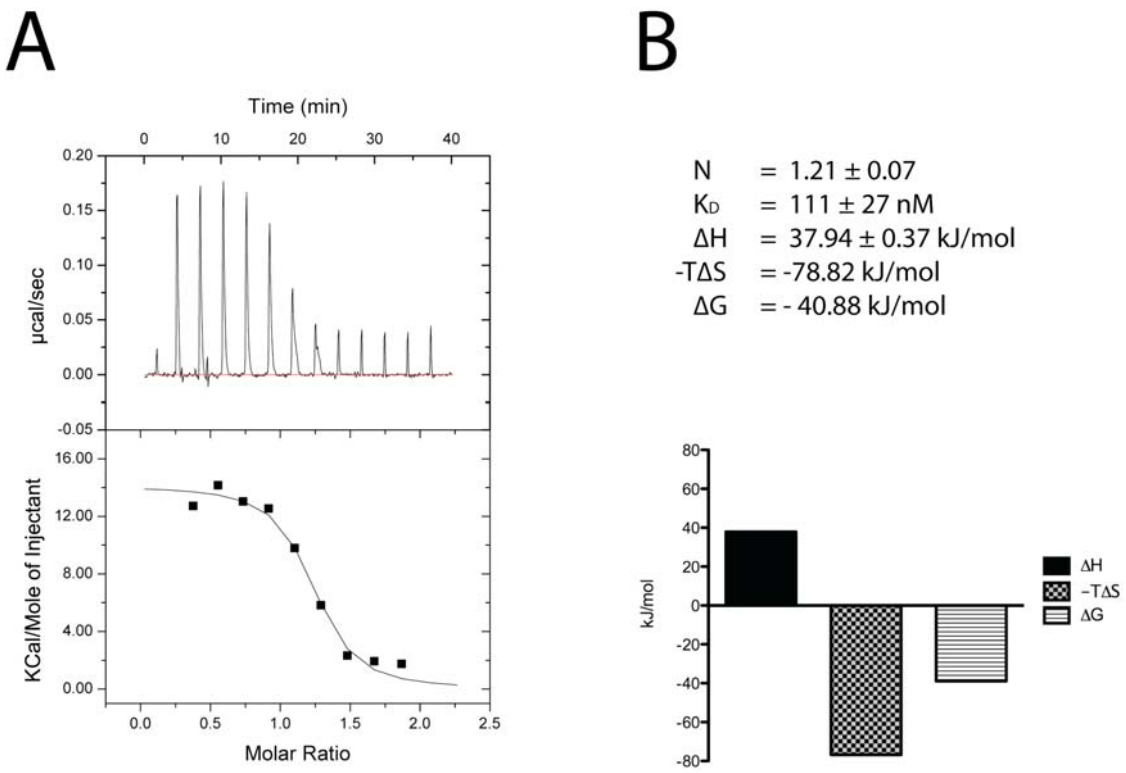

Figure 4.10 Interaction between the MIND complex and Spc105 Peptide 1

A) Binding isotherm of the interaction between MIND and Spc105 peptide 1. Top is the raw data, from injecting Spc105 peptide 1 at 100 μM (syringe) into MIND in the cell at 7μM, indicating an endothermic binding reaction at 16°C. B) Thermodynamic values and energy profile of the interaction between MIND and Spc105 peptide 1.

4.10 Phosphorylation of the MIND complex by Ipl1p

It has been observed that a large number of inner kinetochore proteins, including Dsn1p at residue serine 250 are directly phosphorylated by the budding yeast Aurora B kinase, Ipl1p (Cheeseman et al., 2002, Westermann et al., 2003). The MIND complex in this study was also tested for Ipl1 phosphorylation to see if phosphorylation affected the interactions both between the subunits and with other components of the KMN network. To achieve this, Ipl1p was recombinantly expressed using *Escherichia coli* expression systems. Two constructs were expressed, pIPL1 and pIPL1/IN, with the second construct containing the activating IN-box peptide from Sli15p (Adams et al., 2001).

4.10.1 Expression and purification of Ipl1p

Both constructs were transformed separately into *Escherichia coli* BL21(DE3) RIL cells and expressed following standard protocols. The proteins were initially purified using Ni-NTA agarose resin, followed by size exclusion chromatography on a pre-equilibrated Superdex 200 16/60 column. Single peaks were observed in both elution profiles (figures 4.11 A and C). SDS-PAGE (figure 4.11 D) showed that the IN box associates with Ipl1p during size exclusion chromatography.

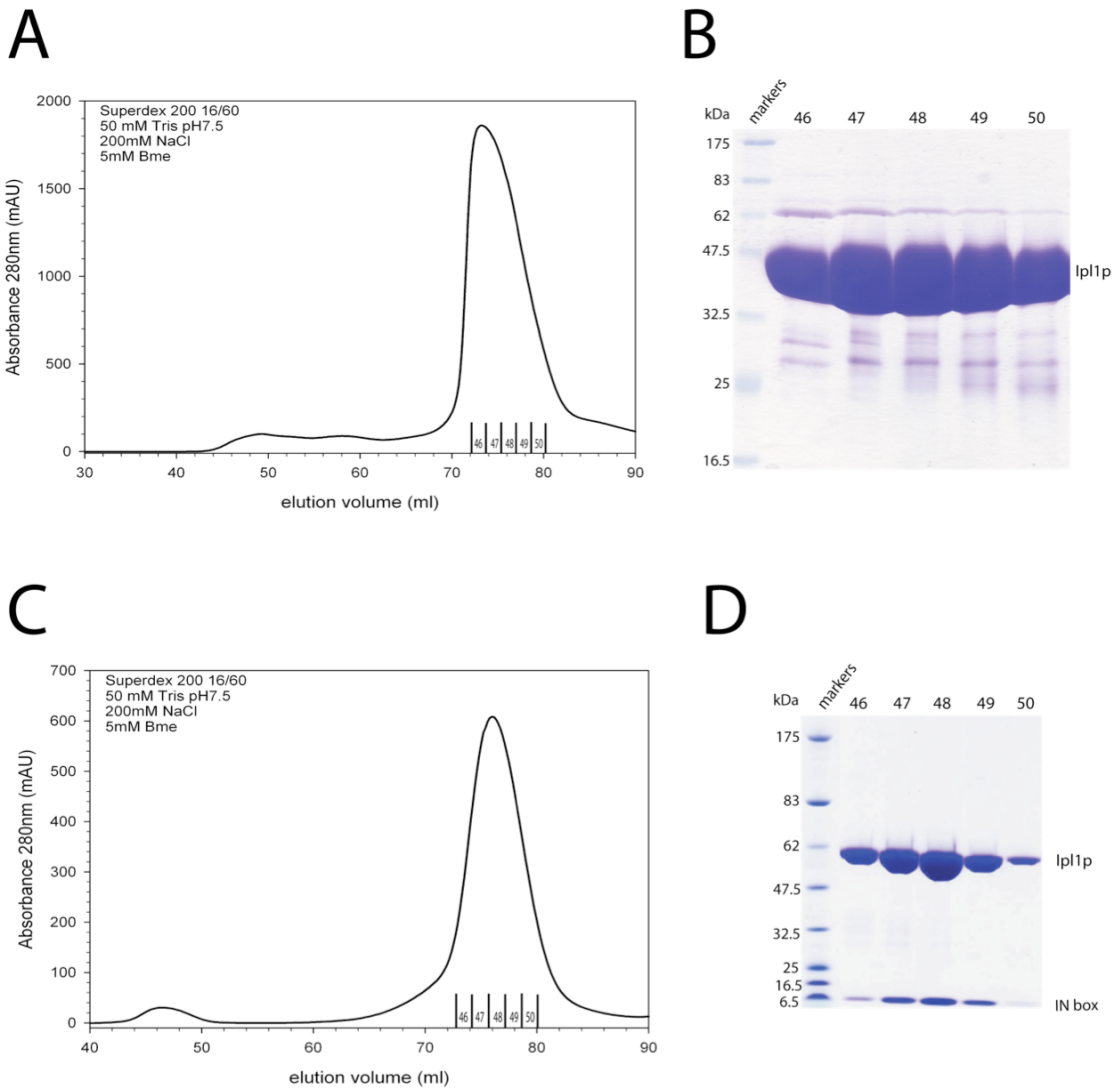

Figure 4.11 Purification of Ipl1p and Ipl1p/IN box

A) Elution profile from size exclusion chromatography of Ipl1p. Elution volumes and relevant fractions have been marked. B) SDS-PAGE of fractions eluted from A). C) Elution profile from size exclusion chromatography of Ipl1p/IN box. Elution volume and relevant fractions have been marked. D) SDS-PAGE of fractions in C), the IN box is seen to associate with Ipl1p.

4.10.2 Identification of MIND phosphorylation by SDS-PAGE

The MIND complex was dialysed into a buffer containing ATP and $MgCl_2$ for phosphorylation studies using Ipl1p and Ipl1p/IN box. A molar ratio of 1:100 Ipl1p or Ipl1p/IN box to MIND was used to see if the complex could be phosphorylated *in vitro*. The reaction was incubated for 3 hours at room temperature on a rolling platform and analysed by SDS-PAGE (figure 4.12 A). A possible small shift in the Dsn1p corresponding band could be observed for both Ipl1p and Ipl1p/IN box. However this shift was not conclusive, so further analysis was required. The addition of a PhosTag™ (Kinoshita et al., 2004) ligand to the acrylamide gel was used to increase the difference between phosphorylated and unphosphorylated proteins. This ligand binds specifically to phosphate groups and decreases the mobility of phosphorylated proteins during SDS-PAGE. A significant shift was observed for the phosphorylated Dsn1p using this ligand (figure 4.12 B). Ipl1p and Ipl1p/IN box showed phosphorylation of only the Dsn1p subunit with no observable shift for the other proteins. Complete phosphorylation was observed when MIND was incubated with Ipl1p bound to the IN box peptide indicating that the IN box bound to Ipl1p is the most active form of the protein.

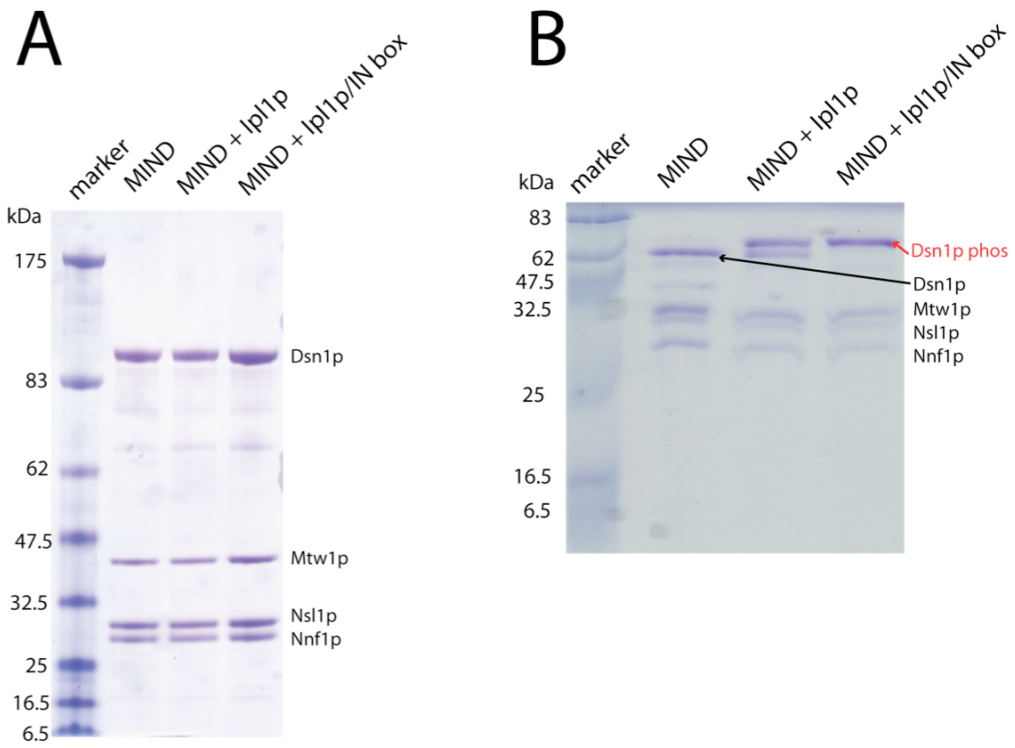

Figure 4.12 Phosphorylation assays of the MIND complex

A) 4-12% gradient SDS-PAGE showing a minimal shift in the Dsn1p band after phosphorylation by either Ipl1p or Ipl1p/IN box. B) 10% SDS-PAGE with the addition of Phos-Tag™ acrylamide, which, specifically bind to phosphate groups affecting mobility in SDS-PAGE. A shift is seen in Dsn1p when either Ipl1p or Ipl1p/IN box phosphorylated MIND. A fraction of unphosphorylated is seen in the MIND + Ipl1 lane. Complete phosphorylation is seen when MIND is incubated with Ipl1p and the activating IN box.

4.10.3 Identification of phosphorylation sites by mass spectrometry

To identify phosphorylation sites, all bands corresponding to the subunits of the MIND complex were excised and sent for mass spectrometry analysis. Only Serine 250 of Dsn1p was found to be phosphorylated (figure 4.13) consistent with previous studies (Westermann et al., 2003).

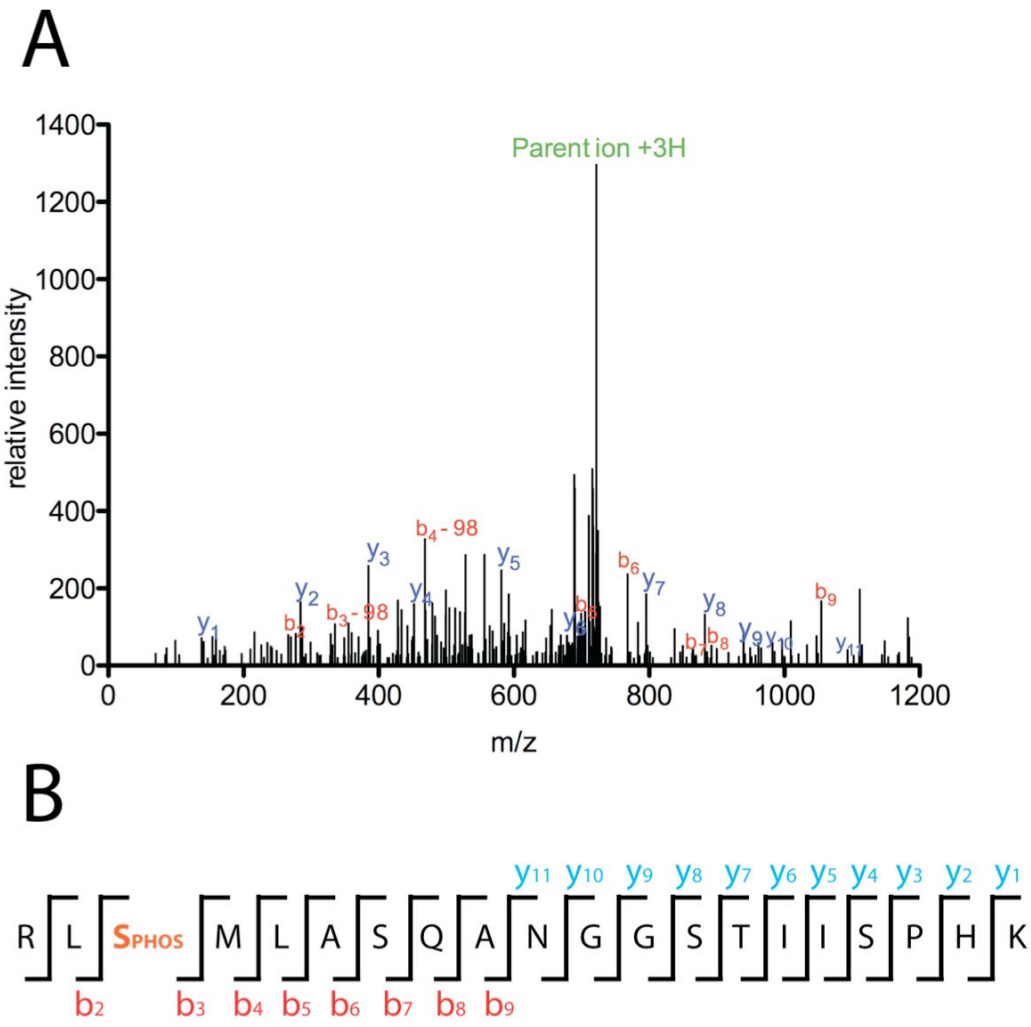

Figure 4.13 Mass spectrometric analysis of Dsn1p

A) Assignment of the b and y ions for the fragmentation spectra of the peptide shown in B). Peaks corresponding to the b fragment series with a neutral loss of 98 Da, which relates to the loss of a phosphate group from phosphoserine occurring at the first serine in the peptide only, which corresponds to serine 250 in Dsn1p.

4.11 Interactions of the phosphorylated MIND complex

After incubation of MIND with Ipl1p/IN box, the interaction between the subunits of MIND complex was examined by size exclusion chromatography. Both the elution profile and subunit ratio (figure 4.14 A and B) were similar to un-phosphorylated MIND complex (see section 2.2.2).

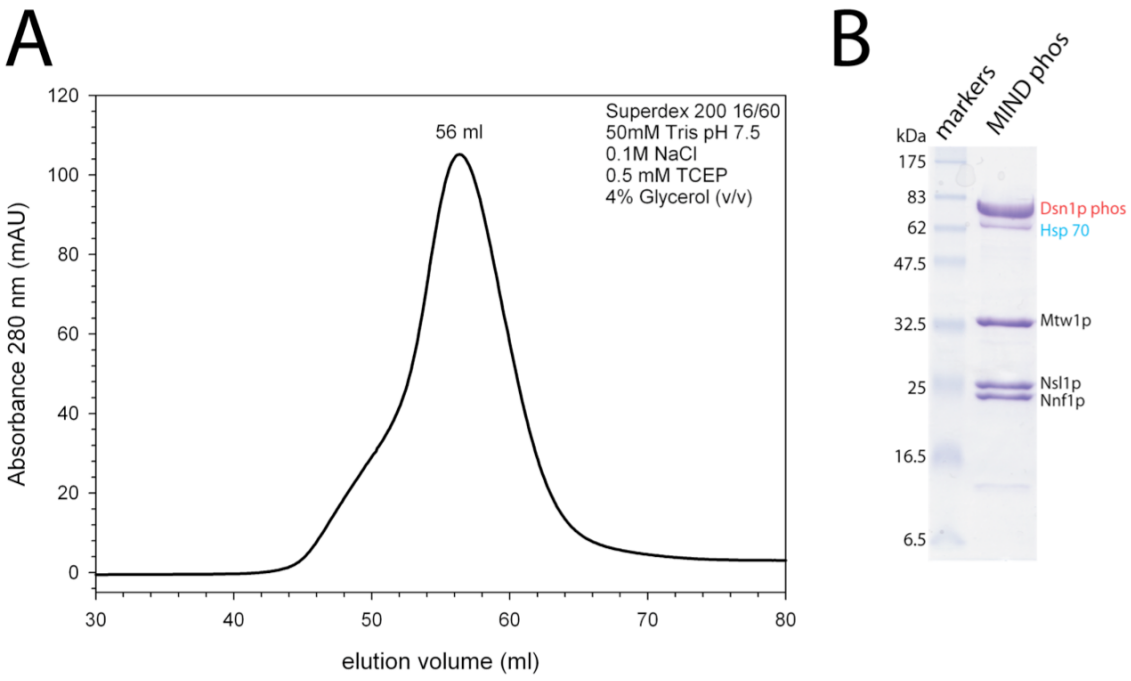

Figure 4.14 Formation of the phosphorylated MIND complex

A) Elution profile from size exclusion chromatography of phosphorylated MIND, a single peak is observed with the elution volume marked. B) SDS-PAGE of a fraction corresponding to 56ml, indicating that all four subunits are present in equal ratios.

The phosphorylated MIND complex was then used for ITC experiments with both the NDC80 complex and the Spc105p peptide 1, to see if their associations would be affected by phosphorylation. The association between phosphorylated MIND and Ndc80 complexes (figures 4.15 A and B) were comparable to normal binding with similar association constants, stoichiometry of binding and energy profiles. Association

between phosphorylated MIND and Spc105p peptide 1 (figures 4.15 C and D) was also comparable to normal binding.

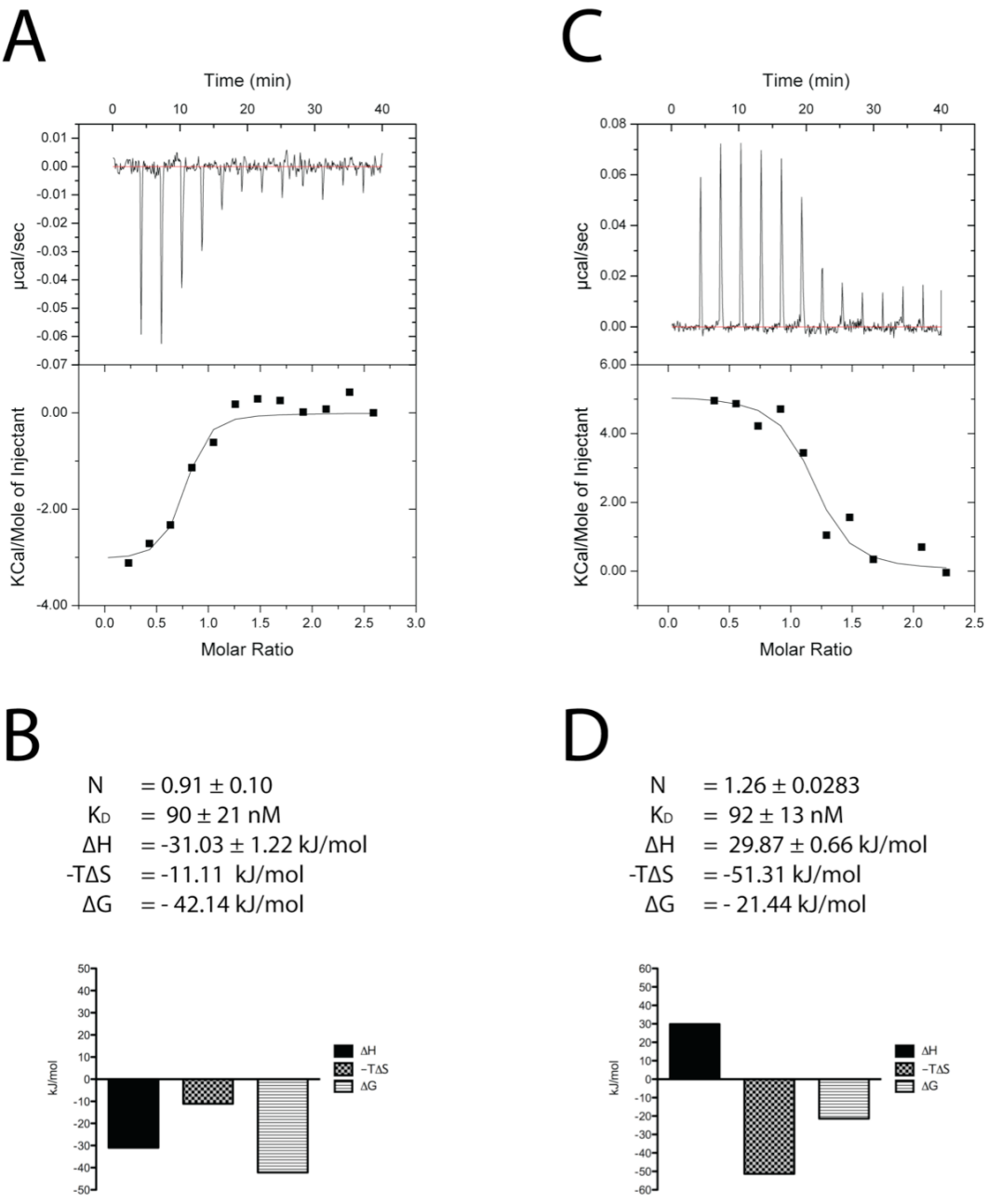

Figure 4.15 Interactions of phosphorylated MIND with Ndc80 and Spc105 peptide1

A) Binding isotherm of the interaction between Ndc80 and phosphorylated MIND complexes. Top is the raw data obtained from injecting phosphorylated MIND (syringe) into Ndc80 complexes in the cell, indicating an exothermic binding reaction at 30°C. Bottom is the fitted curve of the raw data above. B) Thermodynamic data and energy profile of the interaction between Ndc80 and phosphorylated MIND complexes. C) Binding isotherm obtained from injecting Spc105p peptide1 (syringe) into phosphorylated MIND complex in the cell. D) Thermodynamic data and energy profile of the interaction.

4.12 Summary

A stable interaction has been identified between the MIND and Ndc80 complexes using a variety of techniques. The interaction was observed to have nanomolar affinity, and a stoichiometry of 1:1. The energy profile of binding indicates both hydrophobic interactions and hydrogen bonding create the association between MIND and Ndc80 complexes. The interaction was seen by EM analysis to occur via the head region of the MIND complex and the Spc24/Spc25 globular termini of the Ndc80 complex. Spc105p could not be expressed or purified to adequate levels to reconstitute the whole KMN network for EM analysis. Interactions between the MIND complex and peptides of Spc105p could be identified by peptide array analysis. The interacting region within the C-terminal of Spc105p was shown to consist of hydrophobic residues that are conserved within fungi with point centromeres. One of the regions could be synthesised and ITC experiments identified a binding affinity that is comparable to the interaction between MIND and Ndc80 complexes, with both nanomolar affinity and 1:1 stoichiometric binding. The energy profile of this binding indicates a hydrophobic interaction, which correlates back to the hydrophobic stretch of residues.

The MIND complex could be phosphorylated *in vitro* by Ipl1p, with serine 250 of the Dsn1p subunit found to be the only site, which had been previously identified (Westermann et al., 2003). Phosphorylation was found not to affect the association of the MIND complex, as it was a stable species during size exclusion chromatography. Phosphorylation of the MIND complex was also shown not to affect the interactions between both MIND-Ndc80 and MIND-Spc105 peptide 1 with binding affinities and stoichiometry similar to un-phosphorylated MIND.

Chapter 5. Discussion

5.1 Structural and biochemical characterisation of the MIND complex

This work describes the first structural characterisation of the *Saccharomyces cerevisiae* MIND complex, an essential kinetochore component, conserved throughout eukaryotes. Sufficient purity and yields of the recombinant MIND complex, comprising Dsn1p, Mtw1p, Nnf1p and Nsl1p could be achieved for a variety of structural and functional studies.

Previous studies in *Saccharomyces cerevisiae* cell extracts (De Wulf et al., 2003) had shown by glycerol gradients and size exclusion chromatography, three species of the MIND complexes with molecular weights of 89 kDa, 153 kDa and 215 kDa. This suggested intermediate complexes such as a trimer of Mtw1p, Nsl1p and Nnf1p for the 89 kDa species, all 4 subunits in a 1:1:1:1 ratio for the 153 kDa species and all four subunits plus an unidentified subunit or multiple copies of one or more subunits in a different stoichiometry for the 215 kDa species. When the recombinant MIND complex in this study was examined by size exclusion chromatography, only one peak corresponding to the MIND complex was observed. The calculated molecular weight based on elution volume gave a value of 366 kDa, which was far greater than any species identified previously. Hydrodynamic analysis had found that the MIND complex adopts an extended shape (De Wulf et al., 2003), making molecular weight predictions based on elution volumes inaccurate as calculations are based on proteins being spherical. Sedimentation velocity experiments were used to determine the hydrodynamic parameters of the recombinantly expressed MIND complex. A single elongated species was observed with a sedimentation coefficient that gave a derived molecular weight of 147.7 kDa. This corresponded accurately to the molecular weight of a hetero-tetramer comprising Dsn1p, Mtw1p, Nsl1p and Nnf1p in a 1:1:1:1 molar ratio.

During anion exchange chromatography a small proportion of the MIND complex was seen to dissociate. Mtw1p and Nnf1p co-eluted as a shoulder from the main elution peak, indicating a possible intermediate in the formation of the complete MIND complex. An interaction between the human homologues of these proteins has been seen by yeast two-hybrid studies, as well as an interaction between human versions of Dsn1p and Nsl1p (Kiyomitsu et al., 2007). Although a complex of Dsn1p and Nsl1p was not observed during anion exchange chromatography, this did not rule out the possibility that these proteins may associate together. To test associations of sub-complexes prior to the generation of the full MIND complex, Dsn1p/Nsl1p and Mtw1p/Nnf1p were co-expressed and purified separately. A stable interaction was observed for both sub-complexes and, in addition, when these purified sub-complexes were added together in solution, they could successfully reconstitute the full MIND complex. Hydrodynamic analysis identified that both sub-complexes adopted extended structures in solution with Mtw1p/Nnf1p being more extended in shape compared to Dsn1p/Nsl1p. The interaction between Dsn1p/Nsl1p and Mtw1p/Nnf1p is stable in solution, as sedimentation velocity experiments show no dissociation of the full MIND complex. As dissociation of the MIND complex was only observed during anion exchange chromatography, an electrostatic interaction is likely to occur between the sub-complexes, which is partially responsible for generating the complete MIND complex.

As the MIND complex could be both purified to homogeneity and was observed to exist as a single species in solution, crystallisation trials were carried out. Disappointingly, despite extensive efforts, the full length MIND complex could not be crystallised. The field of mitosis research still lacks an overall understanding of kinetochore architecture and high-resolution structures of core components are vital in relating structure to function (Ciferri et al., 2008). Other methods have been devised to overcome this lack of structural information, particularly the implementation of high-resolution light microscopy to map protein positions in kinetochores (Joglekar et al., 2009, Wan et al., 2009). Although important in understanding the location of proteins during various

processes of the cell cycle, the finer details of the nature of essential protein-protein interactions cannot be determined by these methods alone.

As sedimentation velocity experiments indicated that the MIND complex existed as an extended structure, EM analysis was used to visualise a low-resolution image of the MIND complex. Initial EM images were discouraging, with heterogeneity observed in the structure of these particles and high background noise reduced image quality. Modifications to the purification protocol were successfully implemented for the purification of the MIND complex for EM analysis and single particles of the MIND complex could be clearly observed. The complex was seen to be an extended structure, consistent with previous sedimentation velocity data. The complex was shown by two complimentary staining methods to be 22 nm in length with two distinct domains. Negative staining shows that the MIND complex adopts a 'comma shape' with a globular 'head' 8 nm in diameter and a 'tail' 14 nm long. Low angle rotary shadowing showed a similar morphology but with less distinct head and tail regions. Although the particles are homogenous with respect to overall organisation, variability was observed in the angle between the head and tail regions. Using negatively stained images for two-dimensional single particle averaging, finer structural details were observed. The globular head seemed to be arranged into a hook shape with a cavity in the middle. The tail was observed to have a slightly globular tip, indicating globular domains are present at both ends of the MIND complex. The thickness of the tail region observed by EM, suggests that it is unlikely to contain a single coiled-coil pair, as it is wider than the known single coiled-coil rod of the NDC80 complex observed in EM images from this study. When comparing images of MIND and Ndc80 complexes, the rod of the Ndc80 complex is difficult to visualise in some images, whereas the tail of the MIND complex is always observed.

Structural characterisation of the Ndc80 complex was initially carried out by EM studies (Wei et al., 2005, Ciferri et al., 2005), determining a length of 57 nm for the Ndc80 complex. Sequence analysis of the four protein subunits, EM studies and limited proteolysis lead to a proposed model of assembly and orientation of this complex in the kinetochore (Wei et al., 2005, Ciferri et al., 2005), which was verified by cross linking experiments and the generation of crystal structures (Wei et al., 2006, Wei et al., 2007,

Maiolica et al., 2007, Ciferri et al., 2008). These structures have been successfully related back to the function of the Ndc80 complex in the kinetochore and additionally highlighted the structural conservation between *Saccharomyces cerevisiae* and humans (Ciferri et al., 2008). This approach was used to investigate the structure of the MIND complex, however, unlike the Ndc80 complex in which coiled-coil regions are conserved in the termini of all orthologs, the coiled-coil region in the orthologs of the MIND complex are less well conserved (figure 1.3), in length and position in the sequence. It is therefore more difficult to relate the predicted coiled-coil regions in the MIND complex to structural domains and overall shape.

Truncations of the MIND complex based on bioinformatics analysis were generated with the assumption that coiled-coil regions in the MIND complex would be the most flexible domains and may therefore prevent crystallisation. Removal of the coiled-coil regions of the Ndc80 complex allowed crystallisation of the resulting complex (Ciferri et al., 2008). The first truncation, MIND $Dsn1_{1-290}$, could not generate a stable complex and although the second truncation, MIND $Dsn1_{1-490}$, associated as a stable complex, crystallisation trials were unsuccessful. A more direct analysis of protein flexibility was carried out by limited proteolysis experiments, which determined that every predicted coiled-coil region was resistant to protease treatment. Although this went against the assumption that these regions would be susceptible to protease digestion, it is similar to results seen for the Ndc80 complex (Wei et al., 2005). The coiled-coil regions must therefore be important in generating a stable core of the MIND complex. Further evidence for this was shown by the dissociation of the Nsl1p subunit after the removal of coiled-coil domains in Dsn1p, this emphasises the importance of this coiled-coil domain in holding the complex together. Limited proteolysis was used to identify a stable core known as ΔMIND and expression and purification showed association of all subunits through both affinity and size exclusion chromatography. However during anion exchange chromatography, dissociation of a sub-complex containing the $Dsn1_{103-412}$ and Nsl1p components was clearly observed. Previously in this study, the MIND complex was shown to partially dissociate into sub-complexes during anion exchange chromatography. The dissociation was more pronounced in ΔMIND, indicating that either C or N-terminal regions of Dsn1p or the C-terminus of Mtw1p could be involved in the electrostatic interaction required for the formation of the complete MIND

complex. Crystallisation trials of ΔMIND were unsuccessful, indicating that the structure of this stable core may also be flexible and that binding between each component may involve coiled-coil interactions, similar to how the Ndc80 complex is formed (Maiolica et al., 2007).

The $Dsn1_{103-412}$/Nsl1p sub-complex was also examined by co-expression and purification, with a stable interaction observed throughout both affinity and size exclusion chromatography. Crystallisation trials of this sub-complex were carried out, with no success. The formation of the $Dsn1_{103-412}$/Nsl1p sub-complex compared to the previously expressed MIND $Dsn1_{1-290}$ construct, which showed dissociation of the Nsl1p, identified that amino acids 290-412 in the sequence of Dsn1p are important for a stable interaction with the Nsl1p protein. Within this region is a predicted coiled-coil domain from residues 303-332 and although Nsl1p has the lowest scoring predicted coiled-coil regions (figure 1.3), the interaction between these two subunits may arise from a predominantly coiled-coil association. $Mtw1_{1-220}$ still contains all predicted coiled-coil regions and Nnf1p is predicted to contain mostly coiled-coil regions and is completely protease resistant. Both coiled-coil regions in $Mtw1_{1-220}$ and Nnf1p span 100 residues and this may indicate how they associate together.

Further structural characterisation of the MIND complex was required as discrepancies were observed between EM images from negative staining and low angle rotary shadowing. Although the length of the complex was in agreement, differences in the shape of the head region were observed between each staining technique. The MIND complex was therefore further analysed using SAXS. The distance distribution function derived from the experimental data was consistent with an elongated multi-domain protein complex. The maximum length of the molecule (D_{max}) was 22 nm, which was the same length observed by EM. The DAMMIN reconstructions were also in agreement with images obtained from EM studies. Head and tail regions could be identified, with the head 8 nm in diameter and the tail 14 nm long. The tail section was seen to be thicker in the SAXS reconstructions and a clear globular domain was observed at the tip. There is also a lobe observed in the SAXS models, between the head and tail regions, indicating a large folded domain (figure 5.1). Analysis of the head region showed that it has a large central cavity, giving the head a hook like structure,

which had also been seen by two-dimensional class averaging of the negatively stained images of MIND complexes. The head region adopted multiple conformations in the SAXS reconstructions, indicating possible ambiguity in the scattering data in this region. Equally it could also suggest that there is significant flexibility within the head region, providing a possible explanation in the differences observed between EM images observed by negative staining and low angle rotary shadowing. The head could adopt certain conformations depending upon how the complex is stained. Low angle rotary shadowing may generate structures in which the head is open, whereas negative staining might favour a closed conformation, creating images with a more globular head.

ΔMIND was also examined by SAXS to identify the stable protease resistant core of the complex. It was initially predicted that the tail region might be the most flexible domain when analysing EM data, however SAXS reconstructions indicated that it is in fact the head region that is most susceptible to protease treatment. Comparing the two models of MIND and ΔMIND (figure 5.1), it is possible to see that the majority of the head domain is not present in the ΔMIND model. The tip of the tail is also slightly reduced, but the overall length of the tail is conserved. The lobe seen in the full-length MIND complex SAXS reconstructions is also seen in ΔMIND reconstructions, indicating further that it is a stable folded domain.

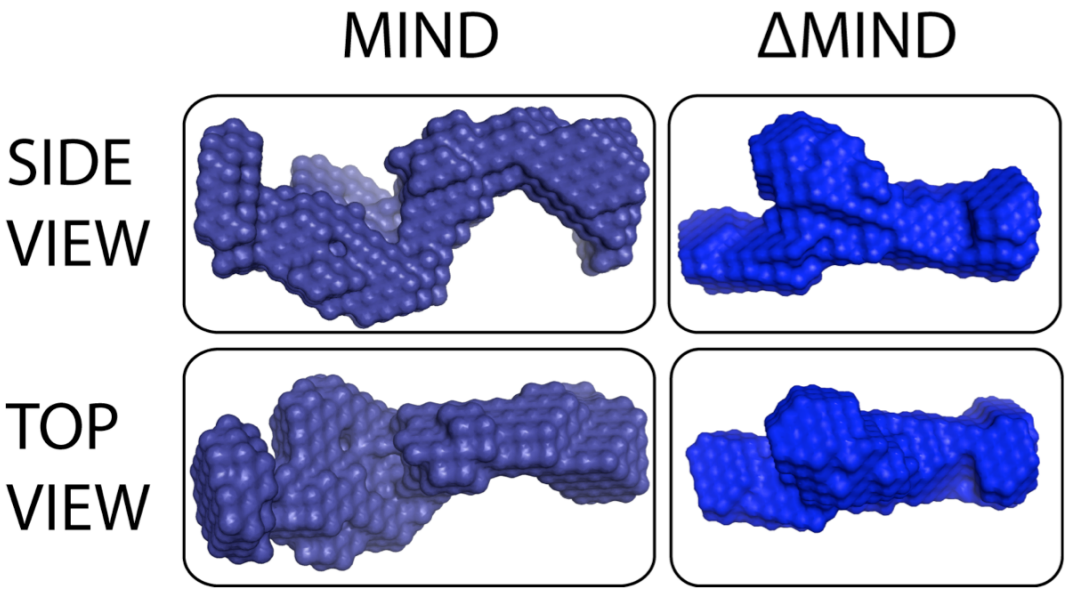

Figure 5.1 Comparison of MIND and ΔMIND SAXS reconstructions

Single reconstructions of the MIND (navy blue) and ΔMIND (royal blue) complexes, using DAMMIN for *ab-initio* modelling, shown from side and top views. The full length MIND complex image shows clear head and tail domains, whereas ΔMIND is significantly reduced in the head region. The globular tip of the tail region of ΔMIND also appears to be reduced, although the overall length of 14 nm is conserved. The lobe region is shown to be conserved between MIND and ΔMIND, suggesting that it is a stable folded domain that could be an important site of interaction for the formation of the KMN network.

A high-resolution crystal structure of the MIND complex would have provided accurate information on how each subunit is orientated. As it was not possible to crystallise full length or truncated MIND complexes in this thesis, EM studies were used to define the location of the individual proteins in the intact complex. The initial approach of nanogold labelling was promising and could place the N-terminal of His-tagged Dsn1p in the head region. Seven further constructs, expressed and analysed by nanogold labelling were unsuccessful and subunit termini locations could only be observed for the initial construct tried. Therefore a new approach was undertaken in which a series of constructs were created with a MBP moiety. The additional electron density from this fusion could be mapped for 6 of the 8 constructs by EM inspection. The head region of the MIND complex was shown to consist of the N-termini of all four subunits. The tail was observed to comprise both C-termini of Dsn1p and Nnf1p.

A structural model of the MIND complex has been generated that combines EM, SAXS and subunit orientation data generated in this thesis (figure 5.2). Data from high-resolution light microscopy of the relative positions of human Mis12/MIND complexes (Wan et al., 2009) has also been included to show consistency of this model with other studies. The hook shape of the head region and lobe are not represented in this model, as the MIND complex constituents cannot be accurately defined to these structures.

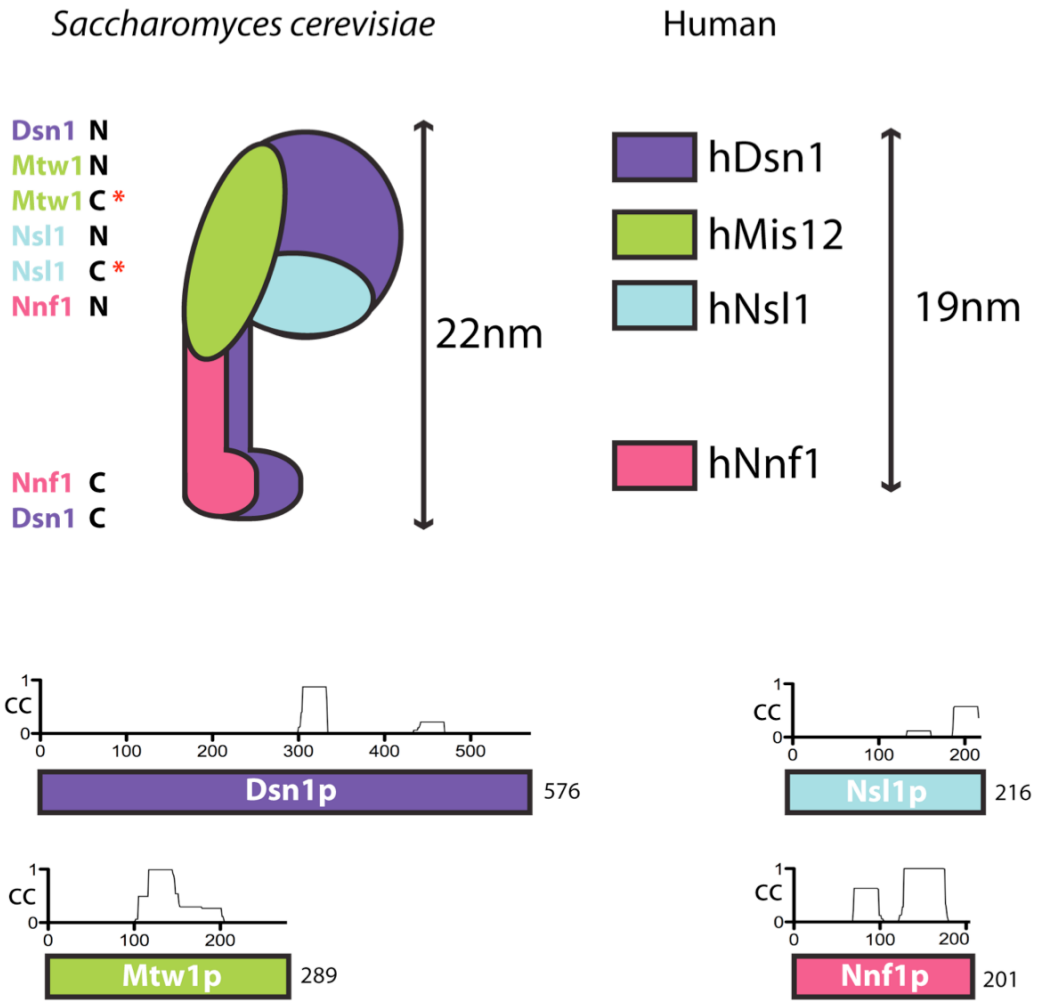

Figure 5.2 Model of the MIND complex

Top Left) Subunit orientation of the *Saccharomyces cerevisiae* MIND complex generated from the structural, hydrodynamic and biochemical data in this study. Overall structure is modelled on the comma shape observed by EM. MBP labelling shows that the head contains the N-termini of all four subunits, indicating that the head is the probable site of tetramerisation for the MIND complex. Sub-complexes of Mtw1p (green)/Nnf1p (pink) and Dsn1p (purple)/Nsl1p (light blue), which were both determined to be extended in solution, with Dsn1p shown by both MBP labelling and truncations to extend the whole length of the complex with the N-termini in the head and the C-termini in the tail. Nnf1p is also found to extend its C-terminal into the tail region with both Dsn1p and Nnf1p proposed to create the globular domain at the end of the tail. The positions of the C-termini of Mtw1p and Nsl1p could not be characterised (indicated by red asterisk) in this study, so have been assigned to the head region. Top Right) Relative positions of the human components of the MIND complex derived from light microscopy (Wan et al., 2009), showing consistency with the model generated in this study. Bottom) adapted from (Ciferri et al., 2008) Predicted coiled-coil region of subunits of the *Saccharomyces cerevisiae* MIND complex. All four proteins are shown as coloured bars, drawn to scale with PCOILS prediction (Lupas et al., 1991) of coiled-coil regions shown above.

5.2 The KMN network in *Saccharomyces cerevisiae*

Biochemical analysis in this study has shown that the MIND and Ndc80 complexes interact in a 1:1 equimolar ratio, with nanomolar affinity and with an energy profile indicating both hydrophobic interactions and hydrogen bonding occur in this association. The crystal structure of the globular domains of Spc24p/Spc25p found a hydrophobic groove on helix 2 of Spc24p that was proposed to be an interaction site (Wei et al., 2006). Studies in this thesis have shown that the interaction between the MIND and Ndc80 complexes only require the globular C-terminal domains of Spc25p and Spc24p, which includes helix 2, further supporting the notion that this may be the binding surface for the MIND complex and that the association is generated predominantly by hydrophobic interactions. EM analysis in this thesis observed that this interaction occurred between the head region of the MIND complex and the Spc24p/Spc25p globular domains. The tail region of the MIND complex points away from the NDC80 complex, suggesting that the C-termini of Nnf1p and Dsn1p are facing towards the centromere and may interact with inner kinetochore proteins.

Despite extensive efforts, Spc105p could not be purified sufficiently to allow the full KMN network to be generated for EM analysis. It would have been of great interest to directly visualise the region in which Spc105p interacted with the MIND and Ndc80 complexes. Using peptide array analysis it was possible to identify interacting regions between the full length MIND complex and Spc105p peptides. Previous studies had indicated that the C-terminal of the human homologue of Spc105p (blinkin) interacts with the human Dsn1 and Nsl1p proteins (Kiyomitsu et al., 2007). The data from the peptide array in this study also characterised regions in the C-terminal of Spc105p that interact with the MIND complex. Two Spc105p peptides close to each other in sequence showed an interaction with the MIND complex, with further inspection highlighting the conservation of these hydrophobic residues within fungi with point centromeres. One of the peptides was synthesised and was shown by ITC to bind to MIND with nanomolar affinity and recapitulated a hydrophobic interaction that was

predicted from sequence inspection. The binding was also comparable in both affinity and stoichiometry to the Ndc80-MIND interaction. Hydrophobic interactions seem to be the predominant type of interaction in the generation of the *Saccharomyces cerevisiae* KMN network. The data from this study would suggest that the MIND complex, Spc105p and Ndc80 complex form a tightly associating KMN network in a equimolar ratio. In contrast, *in vivo* analysis of the relative amounts of *Saccharomyces cerevisiae* kinetochore proteins during metaphase suggested that 6-7 MIND complexes, 8 Ndc80 complexes and 5 Spc105p proteins are present (Joglekar et al., 2006). Data from this thesis would suggest that all these proteins would be in fact forming KMN networks and would not function independently once recruited to the kinetochore, suggesting that the previously identified ratio at metaphase may need to be re-evaluated. This 1:1:1 ratio for the KMN network has also been seen in chicken DT40 cells (Johnston et al., 2010)

Analysis of the *Caenorhabditis elegans* KMN network found that although the MIND equivalent has no identifiable microtubule binding affinity, it synergistically increases MT binding for Ndc80 and KNL-1 (Cheeseman et al., 2006). Data from this thesis have shown that the MIND complex interacts with the Spc24/Spc25 termini of the NDC80 complex via its flexible head domain. A yeast 3-hybrid interaction identified that hKNL-1/blinkin interacts with both hDsn1 and hNsl1 (Kiyomitsu et al., 2007), increasing the plausibility that Spc105p may also interact with the head region of the MIND complex. High-resolution light microscopy studies identifies that human KNL-1/blinkin is more proximal to the centromere than the Ndc80 complex (Wan et al., 2009). A model of KMN network formation is proposed in this thesis (figure 5.3), suggesting that Spc105p and the Ndc80 complex bind to different domains of the MIND complex head regions. The MIND complex associates with both Spc105p and the Ndc80 complex with comparable affinity, providing a platform for these proteins to create higher affinity binding to MTs. The flexible hooked shaped head of the MIND complex may further facilitate MT binding by providing an optimal geometry for interactions with Spc105p and the NDC80 complex that increases MT binding affinity.

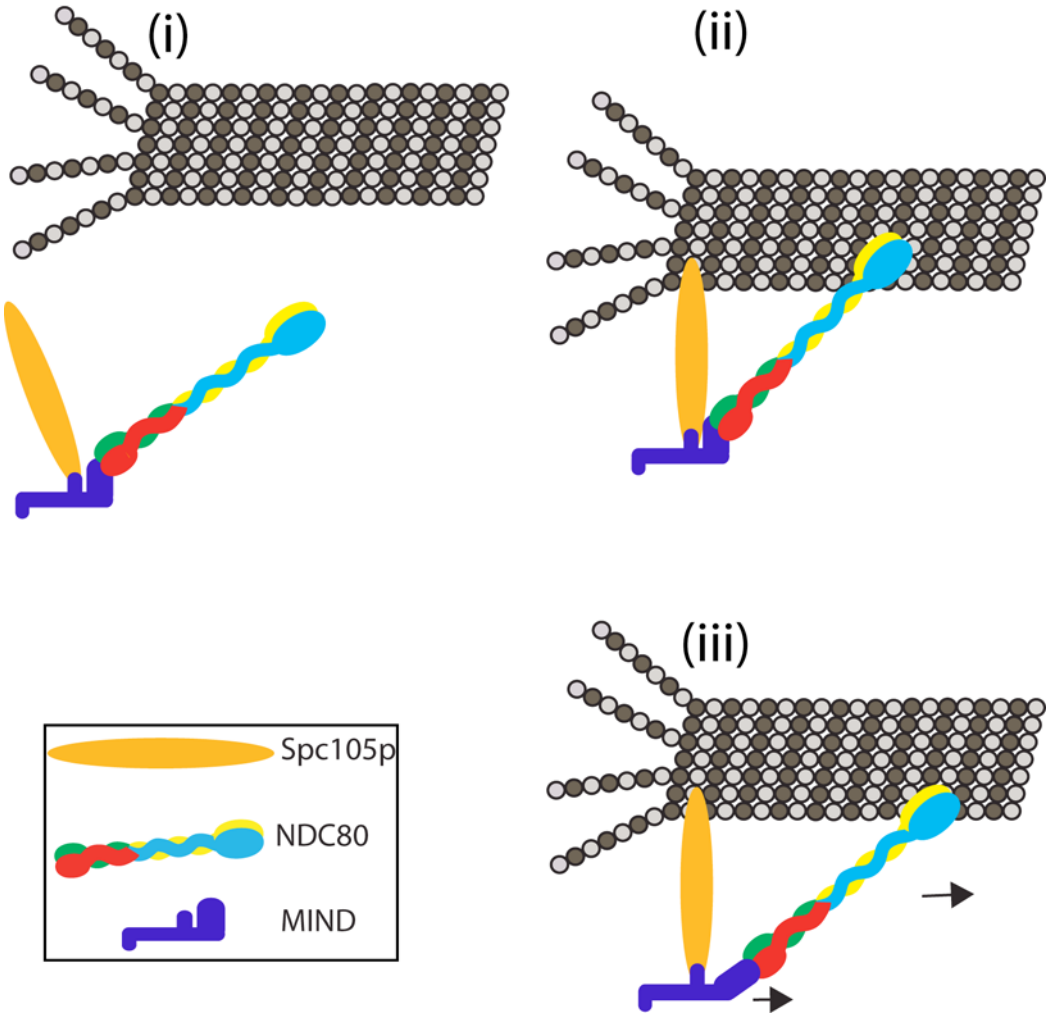

Figure 5.3 Formation of the KMN network in *Saccharomyces cerevisiae*.

Proposed generation of the KMN network on MTs, shown as light and dark grey circles. KMN components, Spc105p (orange oval), Ndc80 (yellow, blue, red and green complex), MIND (purple) are described in the box. (i) The Ndc80 and Spc105p are both proposed to bind to the head region of the MIND complex at different regions, creating two separate binding sites and therefore MT binding arms. (ii) Once the complete KMN network is formed it can then bind to the MT and the MIND complex may re-orientate both the Ndc80 complex and spc105p to create more favourable binding. (iii) The flexible head of MIND may undergo a confirmation change, further increasing the MT binding affinity of the KMN network (as observed by (Cheeseman et al., 2006)).

With the crystal structures of the functional domains of the Ndc80 complex solved (Ciferri et al., 2008), the interactions of the Ndc80 complex with MTs have been well characterised. Cryoelectron microscopy has generated a three-dimensional EM map of the *Caenorhabditis elegans* Ndc80-Nuf2 sub-complex binding to a MT lattice (Wilson-Kubalek et al., 2008). Mapping the crystal structure of the globular heads of Hec1-Nuf2 (Ciferri et al., 2008) along with crystal structures of α and β tubulin (Nogales et al., 1998) into the density map, suggests that the interaction occurs by binding of Ndc80 subunit to the interface between α and β tubulin, with two different weak and strong binding interactions with the MT (Wilson-Kubalek et al., 2008). The MIND/Mis12 complex may facilitate the change from weak to strong binding. Further characterisation of the Ndc80 complex has focused on the loop region within the coiled-coil of Hec1/Ndc80, which was proposed to have a conserved function in the bending of the Ndc80 complex (Ciferri et al., 2008). EM analysis of the loop region of the *Saccharomyces cerevisiae* Ndc80 complexes identifies a kink in the rod of the complex 16 nm away from the Ndc80/Nuf2 head (Wang et al., 2008). The loop is suggested to act like an 'elbow' between the globular Ndc80/Nuf2 and Spc24/Spc25 heads, with a possible role in correct confirmation of MT binding (Wang et al., 2008). These studies highlight that the MIND complex may govern the flexibility of the Ndc80 complex by anchoring the Spc24/Spc25 domain to the kinetochore.

In addition to revealing a C-terminal Spc105p interaction with the MIND complex, further Spc105p peptides could also be seen to bind to the MIND complex. Although initial inspection of these regions did not highlight any significant sequence conservation, further investigation of these regions is required to elucidate their possible role in binding to the MIND complex. The structure of Spc105p/KNL1/Blinkin is still unclear and its role is only just being understood. The N-terminal of blinkin is required for MT binding (Welburn et al., 2010) and the recruitment of Bub1 and BubR1/Mad3p (Kiyomitsu et al., 2007). Blinkin (2342 a.a.) is significantly larger than Spc105p (917 a.a.), which is in contrast to orthologs of both the MIND and Ndc80 complex, where the sizes of each subunit have been relatively conserved (with the exception of Dsn1p). This highlights that although the KMN network is conserved from yeast to human, the Spc105p homologue in higher eukaryotes (KNL1/Blinkin) may have additional roles that are required with the introduction of multiple MTs, necessary for chromosome

segregation of higher eukaryotes. An interaction between the C-terminal of blinkin and Zwint-1 highlights this difference. Zwint-1 is required to associate with the Rod-ZW10-Zwilch (RZZ) complex, which recruits dynein to the kinetochore and is involved in the recruitment of components of the SAC (reviewed in (Karess, 2005)). This complex has only been found in metazoan kinetochores so far, however Kre28p has been suggested to be the ortholog of Zwint-1 (Pagliuca et al., 2009). Zwint-1 has been shown to bind to hKNL-1/blinkin (Kiyomitsu et al., 2007) indicating a conservation in this interaction. The role of Kre28p has been shown to recruit MAPS/+TIPS such as Bim1p and Bik1p and the motor protein Cin8p (Pagliuca et al., 2009) and although these proteins are non-essential their recruitment may help in the generation of a functional kinetochore.

5.3 The role of Mis12/MIND complex in tension sensing

5.3.1 Phosphorylation by Ipl1p/Aurora B

The role of phosphorylation on the whole KMN network has been recently investigated (Welburn et al., 2010). Ipl1/Aurora B activity has been well characterised in its role in phosphorylation of the N-terminal tail domain found on Ndc80/Hec1 (DeLuca et al., 2006, Cheeseman et al., 2006, Wei et al., 2007). In addition to the phosphorylation of the Ndc80 complex, the N-terminal binding region of blinkin and human Dsn1 were also shown to be phosphorylation substrates for Ipl1/Aurora B (Welburn et al., 2010). However the assembly and the recruitment of the KMN network does not appear to be affected by this phosphorylation. Generation of the KMN network with phosphomimetic mutations in the Mis12/MIND complex alone showed comparable affinity to MTs as the wild-type KMN network, yet a significant reduction in MT affinity was seen if either KNL-1 or Ndc80 complex phosphomimetic mutants were added to the wild-type MIND complex. If all 3 phosphomimetic mutants are used to generate the KMN network, MT affinity was completely abolished. Data from this thesis shows that the MIND complex is phosphorylated at a single site by Ipl1p corresponding to Serine 250 of Dsn1p, as previously identified (Westermann et al., 2003). This phosphorylation does not affect the assembly of the MIND complex, neither does it affect the interactions between either the Ndc80 complex or the Spc105p peptide

during ITC experiments, indicating another role for phosphorylation of the MIND complex.

5.3.2 Tension sensing

Increases in phosphorylation due to intrakinetochore tension have been observed (Welburn et al., 2010). Mechanisms in which tension is linked to Ipl1p/Aurora B activity on substrates have been studied (Liu et al., 2009). Models of how Ipl1/Aurora B work in the regulation of kinetochores indicate that this protein is tethered via the other Ipl1 complex subunits to the inner kinetochore generating a finite region in which it can phosphorylate kinetochore substrates (Santaguida and Musacchio, 2009). Movements of these substrates away from the inner kinetochore will decrease the chance of phosphorylation and in the cases of KNL1 and Ndc80 this will lead to an increase in MT affinity. It is more difficult to assign a conclusive role of phosphorylation for the Mis12/MIND complex, therefore mapping the serine 250 of Dsn1p to the structure will be of importance. The serine residue could reside in the head region and phosphorylation may affect the conformation of this domain. Although it does not appear to be essential in that *Saccharomyces cerevisiae* cells with phosphomimetic or phosphonull mutations are still viable (Westermann et al., 2003), phosphorylation may allow ‘fine-tuning’ of the interaction between MT and the kinetochore. Data from this study has found that the head region is flexible and has the potential to sense tension by undergoing structural re-arrangements that have been shown to occur under tension (Joglekar et al., 2009, Wan et al., 2009). Phosphorylation may equally have a role in the recruitment of SAC components (figure 5.3), thereby linking the conformational and phosphorylation state of the MIND complex to the fidelity of chromosome segregation.

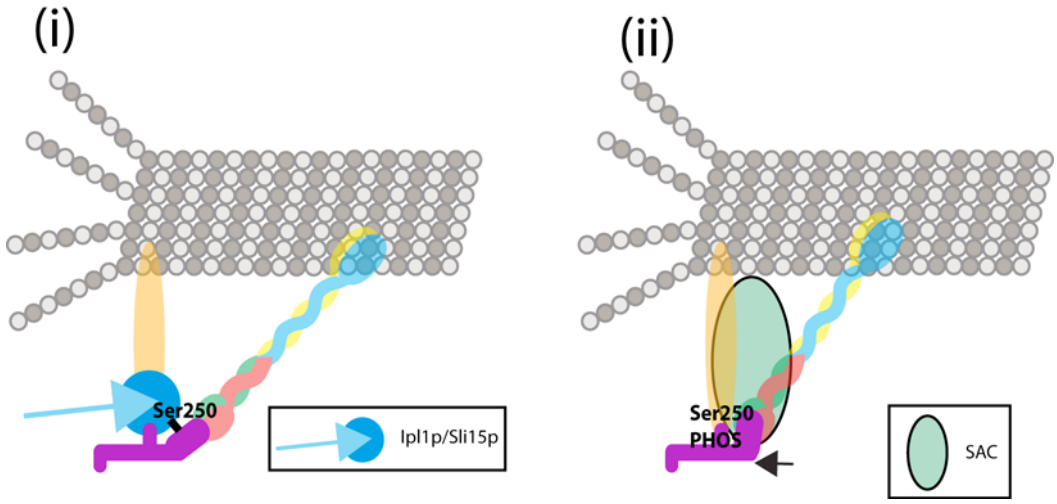

Figure 5.4 Role of Phosphorylation and SAC recruitment

Although all three components of the KMN complex are targets for phosphorylation for simplicity, only phosphorylation of the MIND complex is discussed in this model. Phosphorylation of Dsn1p of MIND was shown to occur at serine 250 and this site (black bar) is proposed to reside in the head region of the MIND complex and phosphorylation may lead to structural re-arrangement of this domain. The model proposes that the head would close bringing the Spc105p and Ndc80 complexes closer, which may lead to the generation of a binding surface that leads to SAC recruitment and possible signalling that is proposed by (Maresca and Salmon, 2010).

5.4 Comparing the MIND complex between budding yeast and humans

In addition to this study of the budding yeast MIND complex, studies by Petrovic *et al* have characterised the structure of the human Mis12 complex (Petrovic et al., 2010). The hMis12 complex has also been identified to be formed by the interactions between sub-complexes of hDsn1/hNsl1 and hMis12/hNnf1. Hydrodynamic analysis and EM studies confirmed the complex was elongated and comprises all subunits in a stoichiometry of 1:1:1:1, similar to that observed for the MIND complex in *Saccharomyces cerevisiae*. The human Mis12 complex is observed to be a 22 nm rod with 4 distinct regions of density seen in class averages, which varies slightly to the comma shape of the *Saccharomyces cerevisiae* MIND complex presented in this thesis (figure 5.5). Sequence comparison of the Mis12/MIND complex components between budding yeast and humans show a low level of overall sequence identity, 16% for Dsn1p, 23% for Mtw1p, 15% for Nsl1p and 14% for Nnf1p. The budding yeast Dsn1p

(66 kDa) and Mtw1p (33 kDa) are larger than their human orthologs, hDsn1 (40 kDa) and Mis12 (24 kDa). Dsn1p is larger due to non-conserved N-terminal insertions (Appendix figure 1) and the C-terminus of Mtw1p shows a non-conserved extension (Appendix figure 2). Both these variations in Dsn1p and Mtw1p may lead to the observed structural differences seen in the EM images (figure 5.5).

Stoichiometric interactions between the hNdc80 and hMis12 complexes were shown to require only the hSpc24/hSpc25 dimer for this interaction, which is conserved between *Saccharomyces cerevisiae* and humans. Petrovic *et al* also observed stoichiometric binding between hMis12 and the C-terminal residues of hKNL-1/blinkin. Cross-linking experiments further identify that the C-terminus of hNsl1 binds hKNL-1/blinkin and is required for an electrostatic interaction between these proteins, this differs from the hydrophobic interaction that this study observes between the budding yeast MIND complex and Spc105p. The C-terminal of hNsl1 also binds to HP1 via a PXVXL motif (Kiyomitsu et al., 2010, Petrovic et al., 2010) and the interaction between MIND and Ndc80 complexes is also found in the C-terminal of hNsl1 which out competes the binding between the Mis12 complex and HP1 (Petrovic et al., 2010). This indicates that Mis12 may be first recruited to the kinetochore by directly binding with HP1 and then would associate with the Ndc80 complex once it is recruited. As the C-terminal of Nsl1p tail is not conserved between humans and budding yeast (Meraldi et al., 2006), this may indicate further differences between the formation of the KMN network in different eukaryotes. The Ndc80 complex is suggested to be recruited to the kinetochore independently of the Mis12 complex in higher eukaryotes, via an interaction with the CENP-H/I/K complex (Okada et al., 2006, Cheeseman et al., 2008). In *Saccharomyces cerevisiae* an interaction between the CENP-H ortholog, Mcm16p has not been seen, suggesting another mechanism in which Ndc80 first associates with the kinetochore of budding yeast.

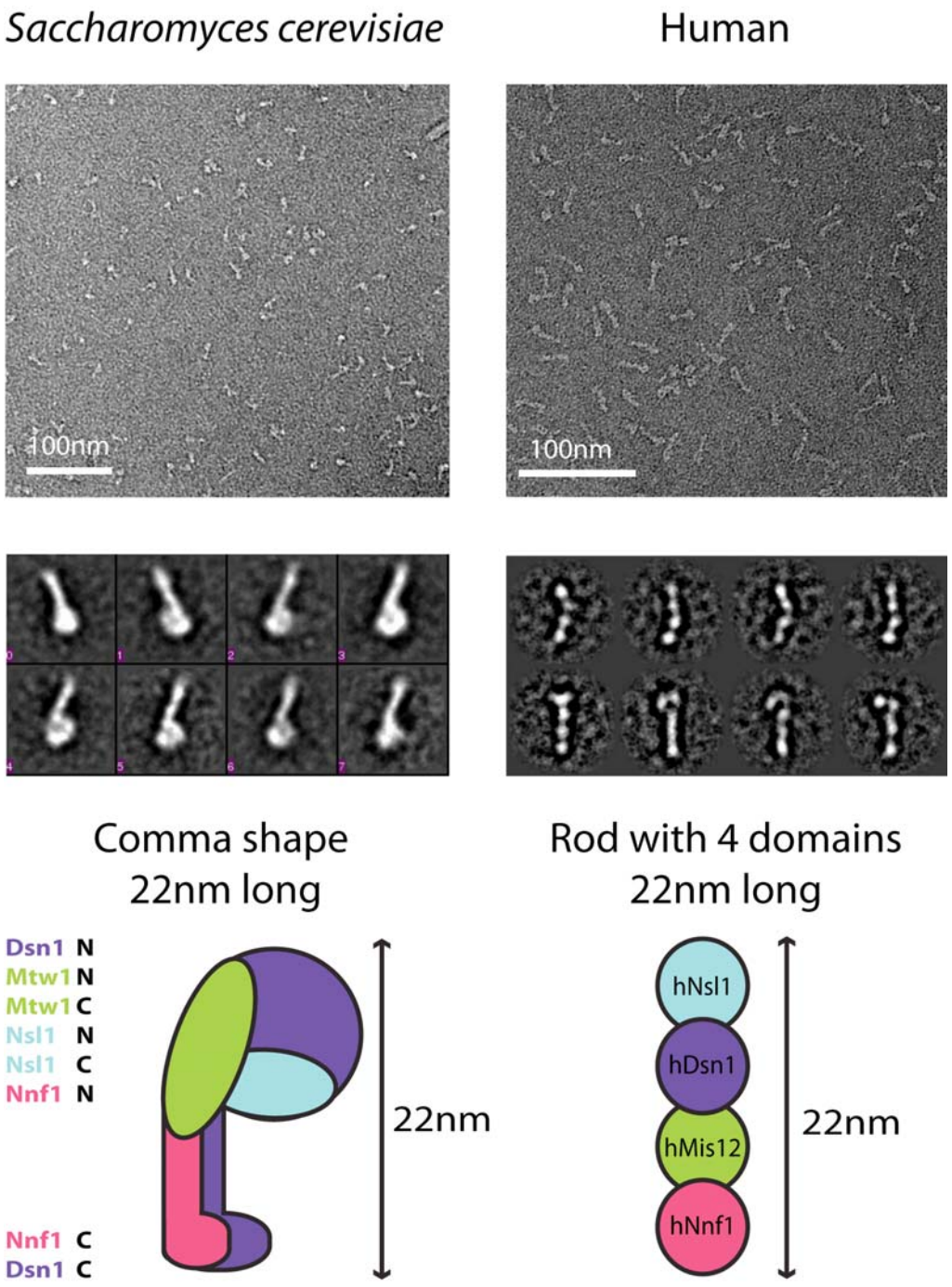

Figure 5.5 Comparison of the *Saccharomyces cerevisiae* MIND and the human Mis12 complexes

Top) EM field view of negatively stained images showing single particles, the scale bars indicate 100 nm. Middle) Two-dimensional class averaging of the complexes. The *Saccharomyces cerevisiae* MIND complex adopts a 22 nm comma shape and the human Mis12 complex is seen to be a long 22 nm rod with four identifiable electron dense domains (Petrovic et al., 2010). Bottom) Schematic representations of each complex, with subunit geometry shown, as discussed in figure 5.2. Both complexes are observed to exist as Dsn1/Nsl1 and Mtw1/Nnf1 sub-complexes ((Petrovic et al., 2010), this study). In the *Saccharomyces cerevisiae* MIND complex, these complexes are proposed to associate side by side generating the extended structure. In the human Mis12 complex the sub-complexes associate on top of each other creating the long rod observed in the EM images (Petrovic et al., 2010).

5.5 Future directions

Cross-linking experiments between the Spc24p/Spc25p hetero-dimer and the full-length MIND complex have been carried out during this study (Appendix figure 3), and are currently being investigated by the Protein Analysis & Proteomics laboratory, Cancer Research UK. The data from these experiments will help to answer two important questions: how are the components of the MIND complex arranged within the complex and which subunits and specific regions generate the interaction between the MIND and Ndc80 complexes? With these data, better knowledge of the domain structure of the MIND complex and its interaction with the Ndc80 complex could create new constructs, which may lead to high-resolution crystal structures. These structures could be mapped into the SAXS and EM data from this thesis, providing a wider study into the MIND complex. Further cross-linking experiments may also be beneficial in defining which region of the MIND complex bind to the Spc105 peptides generated in this study, providing information on how the KMN network forms. This approach may also confirm or disprove the KMN assembly model proposed in this thesis, with respect to separate binding sites within the MIND complex for Spc105p and the Ndc80 complex. The current model is that the Ndc80 complex and KNL-1/Spc105 form different functional arms of the KMN network. Although an interaction has been suggested by pull down studies (Kemmler et al., 2009), it is not conclusive evidence that these complexes can interact directly.

The MIND complex was shown by EM and SAXS data to possess a globular domain at the tip of the tail. Although interactions have been reported between the MIND complex and inner kinetochore proteins (Westermann et al., 2003, De Wulf et al., 2003, Scharfenberger et al., 2003), it is not clear which proteins within the kinetochore are involved in this association. During this thesis, preliminary data have identified three regions of a Mif2p peptide array that the MIND complex associates with (Appendix figure 4). Inspection of these regions has identified that region (i) contains the ‘CENP-C signature box’ which has been shown to be a conserved motif within all CENP-C/Mif2p

homologues (Cohen et al., 2008). Region (ii) corresponds to a predicted coiled-coil region, and region (iii) is found to comprise β-strands B to E of the cupin barrel within Mif2p that has been identified as homo-dimerisation domain (Cohen et al., 2008). Mif2p can be expressed and purified to sufficient levels to undertake ITC experiments and has also shown to be phosphorylated by Ipl1p (Appendix figure 4) as had been previously identified (Westermann et al., 2003). Future experiments will be to characterise binding involving various phosphorylation combinations of Mif2p and the MIND complex. Further investigation of this interaction will be important to relate the interaction of the MIND complex with inner kinetochore proteins, providing further insight into the formation and regulation of the KMN network in the interface between MTs and the centromere. Recently the MIND complex and Mif2p have been found to associate with the monopolin complex that has role in meiosis I in *Saccharomyces cerevisiae*, ensuring that kinetochores on sister chromatids are held together and segregated to the same pole (Corbett et al., 2010). As data from this thesis have shown that MIND complex and Mif2p can be purified, the opportunity to study the roles of these proteins with the monopolin complex in meiosis is a new role that may be investigated.

Chapter 6. Materials and Methods

6.1 Buffers and reagents

Standard chemicals were purchased from Sigma-Aldrich (Dorset UK) unless stated otherwise.

Polymerases were obtained from Roche Applied Science (West Sussex UK)

Restriction enzymes were obtained from New England Biosciences (Hitchin UK).

Buffers were made using deionised water from a Milli-Q purifier (Millipore).

6.2 Constructs

Constructs for recombinant *Escherichia coli* expression that were available in the Macromolecular Structure & Function (MSF) laboratory are listed below.

Table 6-1 Available constructs in the MSF laboratory

Construct	***Derived from***	***Affinity tag and Protease site (in brackets)***	***Antibiotic resistance marker***
pDSN1NTAG	pET28a	N-terminus 6 x His (TEV)	Kanamycin
$pDSN1_{1-290}$	pET28a	N-terminus 6 x His (TEV)	Kanamycin
pMTW1	pET22a	-	Ampicillin
pNNF1.NSL1	pCDFduet	-	Spectinomycin
pNDC80HT.SPC24	pETduet	N-terminus NDC80 6 x His(none)	Ampicillin
pNUF2.SPC25	pRSFduet	-	Kanamycin
pSPC24	pET22a	-	Ampicillin
pSPC25	pET28a	N-terminus 6 x His (Thrombin)	Kanamycin
$pSPC24G_{154-213}$.$SPC25G_{133-221}$	pRSFduet	N-terminus SPC24G 6 x His (TEV)	Kanamycin

Construct	***Derived from***	***Affinity tag and Protease site (in brackets)***	***Antibiotic resistance marker***
pIPL1	pRSFduet	N-terminus IPL1 6 x His (TEV)	Kanamycin
pIPL1/INbox	pRSFduet	N-terminus IPL1 6 x His (TEV)	Kanamycin
pDSN1CTAG	pET28a	C-terminus 6 x His (none)	Kanamycin
pDSN1	pET22a	-	Ampicillin
pDSN1-MTW1	pCDFduet	-	Spectinomycin
pMTW1CTAG	pET28a	C-terminus 6 x His (none)	Kanamycin
pMTW1NTAG	pET28a	N-terminus 6 x His (thrombin)	Kanamycin
pNSL1CTAG	pET28a	C-terminus 6 x His (none)	Kanamycin
pNSL1NTAG	pET28a	N-terminus 6 x His (thrombin)	Kanamycin
pNNF1CTAG	pET28a	C-terminus 6 x His (none)	Kanamycin
pNNF1NTAG	pET28a	N-terminus 6 x His (thrombin)	Kanamycin
pMTW1NMBP	pET28a	N-terminus 6 x His (none) followed by the MBP fusion	Kanamycin
pMTW1CMBP	pET28a	N-terminus 6 x His (thrombin) C-terminus MBP fusion	Kanamycin
pNSL1NMBP	pET28a	N-terminus 6 x His (none) followed by the MBP fusion	Kanamycin
pNSL1CMBP	pET28a	N-terminus 6 x His (thrombin) C-terminus MBP fusion	Kanamycin
pNNF1NMBP	pET28a	N-terminus 6 x His (none) followed by the MBP fusion	Kanamycin
pNNF1CMBP	pET28a	N-terminus 6 x His (thrombin) C-terminus MBP fusion	Kanamycin
pDSN1NMBP	pET28a	N-terminus 6 x His (none) followed by the MBP fusion	Kanamycin
pDSN1CMBP	pET28a	N-terminus 6 x His (thrombin) C-terminus MBP fusion	Kanamycin

6.3 Molecular cloning in *Escherichia coli*

Constructs generated in this thesis are listed below

Table 6-2 Constructs generated in this thesis

Construct	*Derived from*	*Affinity tag and Protease site (in brackets)*	*Antibiotic resistance marker*
pNSL1	pET22a	-	Ampicillin
pNNF1	pET28a	N-terminus 6 x His (Thrombin)	Kanamycin
$pDSN1_{1-490}$	pET28a	N-terminus 6 x His (Thrombin)	Kanamycin
$pDSN1_{103-412}$	pET28a	N-terminus 6 x His (Thrombin)	Kanamycin
$pMTW1_{1-220}$	pET22a	-	Ampicillin
pSPC105	pET28a	N-terminus 6 x His (TEV)	Kanamycin
$pSPC105_{648-917}$	pET28a	N-terminus 6 x His (TEV)	Kanamycin

New constructs were created using the following techniques

6.3.1 Electrocompetent cells

A small aliquot of XL-1 Blue competent cells (Stratagene) was inoculated into 10 ml of LB-Broth and shaken overnight at 37°C. 5 ml of this culture was used to inoculate 1 litre of LB-Broth and the culture was grown at 37°C by a shaking incubator at 200 rpm. Optical density readings at 600nm (OD_{600}), were measured by a BioPhotometer (Eppendorf) with LB-Broth as a blank. When an optical density of 0.6 was reached, the cells were immediately cooled on ice. Cells were then harvested by centrifugation in a Beckman J26 XPI centrifuge at 4,000 × g for 10 minutes at 4°C. The pellet was re-suspended in 200 ml of ice-cold water and was centrifuged as described above. This was repeated two more times and the pellet was finally re-suspended into 1 ml of ice-cold water. 110 µl of glycerol (10% (v/v)) was added and 60 µl aliquots were flash frozen in liquid nitrogen and stored at -80°C.

6.3.2 Transformations

Vectors for cloning were transformed into electrocompetent XL1-Blue cells. Cells, which are stored at -80 °C, were thawed on ice before use. 0.5 μl of plasmid at 50 ng / μl was added to the bacteria and incubated on ice for 20 minutes in a 2mm gap electroporation cuvette. The cells were then electroporated using a micropulser (Biorad) at a voltage of 2.5 kV for 5.8 ms. 750 μl of LB was added immediately and the solution was transferred into an eppendorf tube and incubated by shaking at 37°C, for one hour. The sample was then plated onto a Petri-dish containing LB-agar and appropriate antibiotic. Bacteria containing the plasmid of interest were selected for by the presence of the relevant antibiotic resistance gene.

Table 6-3 Media solutions for bacterial growth

solution	***Composition***
Luria-Bertani (LB) broth media	10 g NaCl, 10 g bacto-tryptone, 5 g bacto-yeast extract for 1000ml of water. Autoclaved
LB – Agar	6g agar added to 400 ml of LB. Autoclaved

Single colonies of bacteria were used to inoculate 5ml of LB containing the relevant antibiotic for selection. Plasmid DNA was purified using the Qiagen mini-prep kit following standard protocol. Purified DNA was finally eluted using EB buffer. Plasmid concentrations were calculated from absorption measurements at both 260nm and 280nm using a NanoDrop ND-100 spectrophotometer.

6.3.3 Agarose gel electrophoresis

For analytical gels, 0.8% agarose in TBE buffer was used. 0.1μl ml^{-1} of ethidium bromide was added to visualise DNA. 2 μl of DNA loading buffer was added to every 5 μl of sample before loading. 10cm × 10cm Horizontal gels (Flowgen biosciences) were run in TBE buffer for 40mins at 80 volts. DNA was visualised by a UV transilluminator

(UVP). Molecular weight of DNA was estimated by comparison to a Hyperladder I DNA marker (Bioline).

Table 6-4 Solutions for agarose gel electrophoresis

solution	*composition*
TBE buffer	5.4 g Tris, 2.75 g Boric acid 1 ml (500mM) EDTA, in 100 ml of water.
DNA loading buffer	0.25 mg/ml (0.25%) bromophenol blue, 30% glycerol.

6.3.4 Restriction Digest

Restrictions digests were carried out overnight (O/N) at 37 °C with appropriate restriction enzymes (1unit μg^{-1} of DNA) in recommended buffers (NEB). Plasmid DNA was purified by excision from an analytical agarose gel and Qiagen gel extraction clean up kit following a standard protocol. The cut plasmid was dephosphorylated by shrimp alkaline phosphatase and purified using the Qiagen PCR cleanup kit.

6.3.5 Primers

Primers were designed with a 5' restriction site followed by 20-45 bp complimentary to the sequence of interest.

Table 6-5 Primers used for generation of constructs in this study

Construct	Primer sequence	Enzymes
pNSL1	(For)gggaattccatatgtcacaaggtcagtccaaaaaa	NdeI
	(Rev)ccgctcgagtcaatcctcctccaggaagtccatta	XhoI
pNNF1	(For)ggccatatggttaactcacatggaatacgg	NdeI
	(Rev)ccactcgagatagttttccttcaattccaagacc	XhoI
$pDSN1_{1-490}$	(For)gggaattccatatgagtctggaacccacacaaacggt	NdeI
	(Rev)tttctcaactcctgcaatgataccatacctaacga	Xho1
$pDSN1_{103-412}$	(For)tttcatatgagactggagaattcaattcttctgc	NdeI
	(Rev)tttctcgagttacctctgtatttccgagtagtcc	Xho1
$pMTW1_{1-220}$	(For)gggaattccatatgtctgcttgctcccactatgagatccac	NdeI
	(Rev)tttctcgagttatctctgcagtagtgcctctacc	Xho1
pSPC105	(For)ataggatccatgaatgtggatgaaagaagccgg	BamHI
	(Rev)ttactcgagttacgtaaactctaaatgtattct	XhoI
$pSPC105_{648-917}$	(For)cccggatccttaatgaatagaat	BamHI
	(Rev)ttactcgagttacgtaaactctaaatgtattct	XhoI

Lyophilised oligo-dexoynucleotides were ordered from Sigma-Aldrich (Dorset UK), were dissolved in TE buffer to a final concentration of 100 μM.

Table 6-6 Composition of TE buffer

solution	*composition*
TE buffer	10mM Tris-HCL pH 8.0, 1mM EDTA.

6.3.6 Polymerase Chain Reaction

Polymerase chain reactions (PCRs) were carried out using Expand High Fidelity PCR system (Roche Applied Science). For each 50μl reaction, 20 ng of *Saccharomyces*

cerevisiae genomic DNA was used as a template with standard concentrations used for other reagents. Thermal cycling using a TC-312 (Techne) was carried out in thin-walled PCR tubes the following thermal profile.

1) **Initial denaturation**: 95°C for 2 minutes;

2) **Loop 1** (10 cycles)
   Denaturing 94°C for 15 seconds

   Annealing 55°C for 30 seconds

   Elongation 72°C for 1 minute 40 seconds

3) **Loop 2** (20 cycles)
   Denaturing 94°C for 15 seconds

   Annealing 55°C for 30 seconds

   Elongation 72°C for 1 minute 40 seconds for first cycle, 3 minutes 20 seconds for last cycle (increase of 5 seconds each cycle)

4) **Final elongation** 72°C for 10 minutes

A 5µl sample of the PCR product was analysed by agarose gel electrophoresis. This was to assess the quality of the DNA by observation of a discrete band with no other contaminants or smears. The remaining reaction was cleaned up using a Qiagen PCR cleanup kit following a standard protocol. The PCR product/insert was subjected to double digest using relevant restriction enzymes and buffers (see section 6.3.4)

6.3.7 Ligation

Purified restricted plasmid and insert were ligated using T4 ligase (NEB). A 1:10 molar ratio of vector to insert was added along with 1 unit of T4 ligase and 1µl and 10× T4 ligase buffer into a total volume of 10µl. The reaction was incubated overnight at room temperature to anneal. 0.5µl of this reaction was then transformed into a 60µl aliquot of

Xl-1 Blue cells (see section 6.3.2). Cells were plated onto LB agar with the relevant antibiotic.

6.3.8 Colony PCR

Colonies were selected using a inoculating loop and first placed into a thin walled PCR tube containing 50µl of PCR master mix with 1.5 units of MangoTaq polymerase (Bioline). The same inoculating loop was then placed into 5ml of LB containing the relevant antibiotic. The following thermal profile was used:

1) **Initial denaturation**: 94°C for 5 minutes;

2) **Loop of 35 cycles**
   Denaturing 94°C for 30 seconds

   Annealing 55°C for 30 seconds

   Elongation 72°C for 1 minute 40 seconds

3) **Final elongation** 72°C for 7 minutes

After the thermal cycle 5µl of the reaction was analysed by agarose gel electrophoresis. Positive reactions will give a band that corresponds to the molecular weight of the insert. The 5ml of inoculated LB was then grown O/N at 37°C and the plasmid of interest was purified using the QIAGEN mini-prep kit.

6.3.9 Sequencing

To check that the insert was correct, DNA was sequenced using the dideoxynucleotide chain terminating inhibitor method and the BigDye Terminator Cycle sequencing kit. Sequencing reactions were cleaned up using ethanol/EDTA precipitation. The samples were analysed by the ABI prism 3730 Capillary sequencing unit (Cancer Research UK equipment park). Sequence data was analyzed using the 4Peaks software and aligned using DNA strider software.

6.4 Molecular cloning for baculovirus expression systems

The gene of interest was cloned into pFastBac^{TM}HT (INVITROGEN) using the same protocol as described in section 6.3. The construct was then transformed by Heat-Shock for 45 seconds at 42°C into the *Escherichia coli* host strain, DH10Bac^{TM}, containing the baculovirus shuttle vector (bacmid). Transformed cells were plated onto LB Agar containing 50 μg/ml kanamycin, 7 μg/ml gentamycin, 10 μg/ml tetracycline, 100 μg/ml Bluo-gal (INVITROGEN) and 40 μg/ml IPTG. After a 48-hour incubation of the plate at 37°C, white colonies with the recombinant bacmid were re-streaked onto fresh LB-agar plates as previously described to confirm the white colony phenotype. Colonies were then inoculated into LB broth, containing 50 μg/ml kanamycin, 7 μg/ml gentamycin, 10 μg/ml tetracycline, and the recombinant bacmid DNA was isolated by a modified Qiagen mini-prep procedure. After addition of N3 buffer, the solution was left on ice for 10 minutes, then span for 10 minutes at 14000 x g. The supernatant was removed and added to 800 μl of isopropanol, mixed and left on ice for 10 minutes. The sample was then moved into a tissue culture hood and the supernatant was removed and 500 μl of ice-cold 70% ethanol was added to the pellet and gently mixed, then centrifuged at 14000 x g for 5 minutes. The supernatant was removed and the pellet left to air dry, and then dissolved into 40 μl of TE. The gene of interest was verified by PCR, using the M13 forward and reverse PCR primers (INVITROGEN). The bacmid was then sent to the Protein production laboratory Cancer Research UK for transfection, creation of a P1 recombinant baculovirus stock, and optimization of insect cell infection and protein expression in Sf9 cells.

6.5 Protein expression, purification and analysis

Proteins were overexpressed in *Escherchia coli* BL21(DE3) RIL cells by recombinant technologies unless otherwise stated.

6.5.1 Transformation into electrocompetent *Escherichia coli*

0.5µl of required plasmid/plasmids were transformed into *Escherichia coli* BL21(DE3) RIL cells using electroporation (see section 6.3.2). Cells were then plated onto LB agar containing the appropriate antibiotic and incubated overnight at 37°C.

6.5.2 Protein expression

A single colony was used to inoculate 100ml of LB-Broth containing relevant antibiotics for plasmid selection and grown overnight by shaking at 37°C. 7ml of this culture was then used to inoculate 2 litre flasks containing 1 litre of LB-broth with relevant antibiotics, with the omission of chloramphenicol that binds to the 30S ribosome, inhibiting protein synthesis. The flasks were grown at 37°C shaking incubator at an rpm of 200 with growth being monitored by recording the optical density at 600nm (OD_{600}). At an OD_{600} of 0.4 the temperature of the incubator was reduced to 18°C and after 20 minutes or at OD_{600} of 0.6, 500µl (0.5mM final concentration) of 1M IPTG was added and the cells were incubated overnight at 18°C.

Cells were harvested by centrifugation in a Beckman J26 XPI centrifuge at 4,000 × g for 20 minutes at 4°C. The cell pellets were resuspended in 50mM Tris pH 7.5, 500mM NaCl, 9% (v/v) glycerol, 0.5% Tween 20, with 1 protease inhibitor cocktail tablet (Roche) per 40 ml of suspended cells.

6.5.3 Protein extraction

Cells were lysed by a Soniprep 150 (MSE) ultrasonic disintegrator on ice by 7 × 30 second pulses at amplitude of 15 microns with 1-minute rest intervals on ice between each pulse. Cell debris, and other insoluble particles were removed by centrifugation at 31,400 × g in a Beckman Allegra 64R centrifuge for 1 hour at 4°C. The supernatant was passed through a 0.22µm filter ready to be used on ÄKTA prime purification system.

6.6 Protein purification

All protein purification using ÄKTA systems were undertaken at 4°C.

6.6.1 Affinity purification

6.6.1.1 Ni-NTA batch method purification

Ni-NTA resin pre-equilibrated with Ni-NTA Buffer A was added to the supernatant in a ratio of 100 μl of resin for every litre of original culture. This was then incubated for 2 hours on a roller mixer at 4°C. The sample and resin was then transferred into a PD-10 column and unbound proteins eluted by gravity. The valve was capped and the protein bound to the Ni-NTA resin was washed with 10ml of ice cold buffer A for 1 hour on a roller mixer at 4°C. Three further 10 ml washes with ice cold buffer A were carried out, without the 1-hour incubation period. 3 ml of ice cold buffer B was then added with the valve capped and left to incubate for 20 minutes on a rotor at 4°C. This fraction was then eluted by gravity. This elution step was repeated six times to ensure complete elution of the protein, in a total volume of 18 ml.

Table 6-7 Composition of buffers used in batch purification

solution	*composition*
Ni-NTA Buffer A	50mM Tris pH 8.5, 200 mM NaCl, 5 mM β- mercaptoethanol, 20mM imidazole, 0.2 mM phenylmethanesulfonylfluoride
Ni-NTA Buffer B	50mM Tris pH 8.5, 500 mM NaCl, 5 mM β- mercaptoethanol, 500mM imidazole

6.6.1.2 HisTrap purification

Immobilized metal ion affinity chromatography (IMAC) was carried out by using a 5 ml HisTrap FF column, connected to a ÄKTA prime system (GE healthcare). The sample was loaded onto a column pre-equilibrated in HisTrap Buffer A at a rate of 1ml/min. With the sample loaded, the column was washed in HisTrap Buffer A at 3 ml/min until the absorbance at 280 nm of the flow through returned to a baseline level. The protein of interest was eluted using a 1-100% gradient of HisTrap buffer B creating a imidazole gradient of 2-500 mM over 10 column volumes (c.v.). 5ml fractions of elutant were collected, with the absorbance at a wavelength of 280nm recorded by the ÄKTA prime systems chromatogram.

Table 6-8 Composition of buffers used in HisTrap affinity purification

solution	*composition*
HisTrap Buffer A	50mM Tris pH 8.5, 500 mM NaCl, 5 mM β- mercaptoethanol, 2mM imidazole, 0.2 mM phenylmethanesulfonylfluoride
HisTrap Buffer B	50mM Tris pH 8.5, 500 mM NaCl, 5 mM β- mercaptoethanol, 500mM imidazole

6.6.1.3 Denatured protein and ATP wash

The denatured proteins were generated by placing 100μl of un-transformed Xl-1 cells into 200 μl of 5 M urea and heating at 100°C for 10 minutes. The cells were spun down and the supernatant used as the denatured protein extract. After sample was loaded onto the HisTrap FF column and washed with buffer A until the baseline absorbance was reached. 10 c.v. of denatured protein and ATP wash was flowed through the column at 1ml/min. The ATP in the solution increased the A_{280} reading, so the column was washed in HisTrap buffer A until the reading returned to the baseline and the imidazole gradient was carried out as described above.

Table 6-9 Composition of denatured protein and ATP wash buffer

solution	*composition*
ATP wash	50mM Tris pH 8.5, 500 mM NaCl, 5 mM β- mercaptoethanol, 2mM imidazole, 5mM ATP, 10 mM $MgCl_2$, 30 μl of denatured protein extract per ml of wash buffer.

6.6.1.4 Amylose affinity chromatography

A 2ml (2 c.v.) slurry of amylose Resin was pre-equilibrated by washing with Amylose buffer A. Protein was added to the resin and left to incubate for 1 hour at 4°C on a rolling platform. The sample was loaded onto a PD-10 column and unbound proteins

were eluted by gravity. The resin wash washed by 20 c.v. of amylose buffer A. MBP constructs were eluted by adding 10 c.v. of amylose buffer B.

Table 6-10 Composition of amylose affinity chromatography buffers

solution	*composition*
Amylose buffer A	50mM Tris pH 7.5, 100 mM NaCl, 5 mM β- mercaptoethanol,
Amylose buffer B	50mM Tris pH 7.5, 100 mM NaCl, 5 mM β- mercaptoethanol, 10 mM maltose

6.6.2 Size exclusion chromatography

Size exclusion chromatography/gel filtration was carried out using Superdex columns on a ÄKTA Fast protein liquid chromatography (FPLC) system (GE Healthcare). Proteins are separated based on their molecular weight and the shape they adopt. The superdex matrix consists of cross-linked agarose and dextran. Larger proteins cannot enter the matrix and therefore elute at a lower volume. Smaller proteins can enter the matrix, increasing residence time, and therefore elute at a later volume. Columns were equilibrated with 1.5 (c.v.) of standard elution buffer. Samples were loaded onto the column in a small volume via an injection loop and washed through the column in standard elution buffer. The ÄKTA FPLC system was set-up to begin fractionation of the isocratic elution with the absorbance at a wavelength of 280nm recorded. Chromatographs were visualised on the UNICORN operating system (GE healthcare). A graph of the K_{av} (determined by the elution volume) on the y-axis against the log of molecular weight of a protein on the x-axis is a linear relationship if the protein adopts a spherical shape. Molecular weight standards were run on the columns, K_{av} was calculated and plotted against the log of the known molecular weight for each standard as shown in figure 6.1.

Table 6-11 Composition of buffer used in size exclusion chromatography

Solution	*composition*
Standard Elution Buffer	50mM Tris pH 8.5, 200 mM NaCl, 5 mM β- mercaptoethanol,

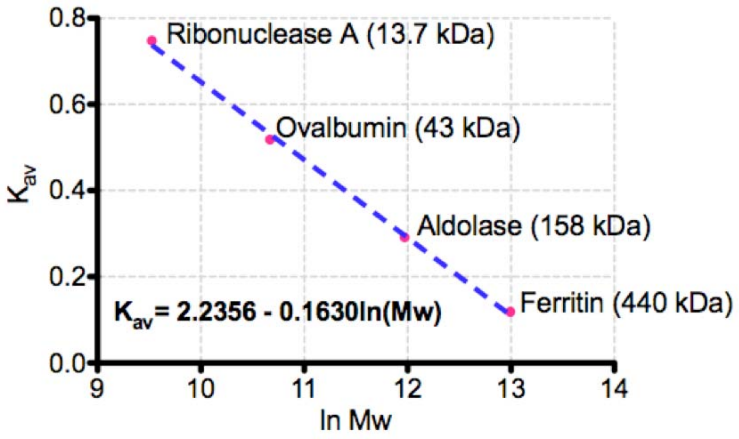

Figure 6.1 Calibration curve for standard proteins on a Superdex 200 16/60 Hiload size exclusion column

6.6.3 Anion exchange chromatography

Anion exchange chromatography was carried out using a MonoQ GL 5/50 on a ÄKTA FPLC system. The column was charged using 5 c.v. of MonoQ buffer A, followed by 5 c.v. of MonoQ buffer B, then another 5 c.v. of MonoQ buffer A. Protein was diluted until the conductivity was less than 15 mS/cm. Protein was loaded onto the column and unbound sample was washed through using buffer A. To elute bound proteins, the column was washed with a gradient of 0-100% Mono Q buffer B over 50 c.v., with 0.5ml fractions collected and the absorbance at a wavelength of 280nm recorded.

Table 6-12 Composition of buffers used in anion exclusion chromatography

solution	***composition***
MonoQ Buffer A	50mM Tris pH 8.5, 100 mM NaCl, 5 mM β- mercaptoethanol,
MonoQ Buffer B	50mM Tris pH 8.5, 1 M NaCl, 5 mM β- mercaptoethanol,

6.6.4 Protein dialysis

Protein samples (1-3 ml) were placed into a D-Tube™ Dialyzer (Novagen) containing semi-permeable membrane windows. The tubes were placed in 1 litre of the dialysis buffer at 4°C. The molecular weight cut off point for the membrane was 8 kDa,

allowing small molecules of the buffer to move freely through the membrane with the protein being retained in the tube. The dialysis buffer was mixed using a magnetic stirrer and after 1 hour the tube was placed into fresh dialysis buffer. In total, five 1-litre buffer changes were carried out, with the last dialysis step occurring overnight.

6.7 SDS-PAGE

To visualise proteins, sodium dodecyl sulphate polyacrylamide gel electrophoresis (SDS-PAGE) (Laemmli, 1970) was carried out to separate denatured proteins based on their size. Separating /resolving gels of various acrylamide percentage were used. The resolving gel solution was placed between two glass plates and covered with 1% SDS and left to polymerise. The 1% SDS solution was removed from the top and the stacking gel solution was placed on top of the resolving layer. A comb was placed into this solution layer to create wells to place protein samples and left to polymerise. Samples were prepared by adding 5 μl of protein loading buffer to every 20 μl of protein solution and heated at 100°C for 5 minutes. Pre-stained protein markers with known molecular weights (NEB) were also heated. The gel was placed into running apparatus (Bio-Rad), with protein samples and the molecular weight marker loaded into the wells. The running tank was filled with 1X SDS running buffer. Voltage between 170 – 200 V was applied across the gel for approximately 1 hour or until the blue dye front had completely run off the bottom of the gel. The gel was then removed from both the gel tank and the glass plates and stained using Coomassie brilliant blue stain. The gel was destained using destain solution.

Table 6-13 Composition of buffer used for SDS-PAGE

solution	*Composition*
Resolving Gel 12%	12% acrylamide:bis-acrylamide (37.5:1), 375 mM Tris-HCl pH8.8, 0.1 % SDS (w/v), 0.05% tetramethylethylenediamine (TEMED), 0.1% ammonium persulphate (APS)
Resolving Gel 15%	15% acrylamide:bis-acrylamide (37.5:1), 375 mM Tris-HCl pH8.8, 0.1 % SDS (w/v), 0.05% tetramethylethylenediamine (TEMED), 0.1% ammonium persulphate (APS)
Stacking Gel	4% acrylamide:bis-acrylamide (37.5:1), 125 mM Tris-HCl pH6.8, 0.1 % SDS (w/v), 0.05% tetramethylethylenediamine (TEMED) 0.1% ammonium persulphate (APS)
10 x SDS running buffer	15.1 g Tris-base 72g glycine, 25ml of 20% SDS (w/v), made up to a volume of 500 ml with water. Diluted to 1 x for use
SDS-PAGE protein loading buffer	0.6 mg/ml (0.6%) bromophenol blue, 250 mM Tris-HCl pH 6.8, 5% SDS (w/v) 30% glycerol (v/v), 15% βMe
Coomassie brilliant blue staining solution	0.2 g Coomassie Brilliant Blue R, 45 ml methanol, 10 ml glacial acetic acid, made up to 100 ml with water.
Destain solution	15 ml methanol, 10 ml glacial acetic acid 75 ml water

6.7.1 Limited proteolysis

Trypsin was added in a 1:150 molar ratio to the MIND complex in a buffer consisting of 50mM Tris pH 7.5, 150 mM NaCl. Aliquots were taken at various time points and proteolysis stopped by adding SDS loading buffer. Identical samples were run on two separate SDS gels, one gel was stained using Coomassie brilliant blue. The second gel was washed, and transferred onto a polyvinylidene fluoride (PVDF) membrane (Amersham Biosciences) in a BioRad transfer chamber at 100 V for 1 hour in transfer

buffer. The membrane was stained for 1 minute, then destained and dried. The bands were analysed by Edman sequencing (The Aberdeen Proteome Facility).

Table 6-14 Solutions used for Limited proteolysis

solution	*Composition*
Wash buffer	50mM Tris, pH8.5, 10% methanol
10 x Transfer buffer	30.3 g Tris-base 144.1 g glycine, made up to a volume of 1 litre with water.
Transfer buffer	100 ml 10 x Transfer buffer, 200ml methanol, 700ml water
membrane staining solution	0.1 g Coomassie Brilliant Blue R, 40 ml methanol, 1 ml glacial acetic acid, made up to 100 ml with water.
destain solution	50% methanol

6.8 Protein concentrations

Protein concentrations were calculated by obtaining the absorption at 280nm with a Nanodrop spectrophotometer ND-1000. Theoretical molar extinction coefficient at 280 nm and molecular weight were derived using the SCRIPPS Protein Calculator server (http://www.scripps.edu/~cdputnam/protcalc.html). Using these values, concentrations in the form of mg protein / ml were calculated.

Table 6-15 Molecular weights and extinction coefficients for proteins

Protein	Molecular weight (kDa)	Extinction coefficient 280nm (M^{-1} cm^{-1})
MIND complex	147.9	99280
Dsn1p/Nsl1p	91.1	68700
Mtw1p/Nnf1p	56.9	30580
$MIND_{1-490}$	138.2	98000
ΔMIND	109.6	82780
$Dsn1_{103-412}$/Nsl1p	60.6	53480
Ndc80 complex	183.2	101130
Spc24/Spc25	49.8	31720
SpcG	16.8	16500
Ipl1p	42.9	47650
Ipl1p/IN box	50.7	54620

6.9 Dynamic light scattering

Dynamic light scattering (DLS) was used to determine the hydrodynamic radius of macromolecules in solution. DLS monitors the fluctuations in the intensity of scattered light from a laser beam. The scattering occurs from Brownian motion of suspended particles in solution in the field of the laser beam. The rate of fluctuations from this scattered light is a consequence of the sizes of molecules. This can be used to determine a hydrodynamic radius, which can be used to calculate a molecular mass. Protein at a concentration of 0.5 mg/ml was measured in a quartz DLS cuvette. Measurements were carried out using a Zetasizer Nano ZS (Malvern Instruments). Data were analysed by the supplied software package.

6.10 Analytical ultracentrifugation

6.10.1 Theory

The process of sedimentation is governed by three factors, the gravitational force, the buoyancy and the hydrodynamic friction.

The gravitational force is $F_{sed} = m\omega^2 r$ **Equation 4**

m = the protein mass

ω^2 = the rotor angular velocity

r = the distance from the centre of rotation

The buoyancy force is $F_b = -m\bar{v}\rho\omega^2$ **Equation 5**

$\bar{v}$ = the partial specific volume of the protein

ρ = the density of the solvent/buffer

The friction force is $F_f = s(kT/D)\omega^2$ **Equation 6**

k = the Boltzmann constant

T = the absolute temperature

D = the diffusion constant

s = the sedimentation coefficient (measured in units of Svedberg, 1 S = 10^{-13} s)

The application of a centrifugal force causes depletion of proteins at the meniscus. Balancing of the gravitational force, the buoyancy and the hydrodynamic friction forces allows the Svedberg equation to be derived

$$s = \frac{MD(1-\bar{v}\rho)}{RT}$$ **Equation 7**

M = the molar mass of the protein

R = the gas constant

6.10.2 Sedimentation velocity

The major parameter derived from sedimentation velocity analysis is the sedimentation coefficient (*s*), which is the velocity per unit centrifugal force.

$$s = \frac{1}{\omega^2 r}\frac{dr}{dt} = \frac{m}{f}$$ **Equation 8**

Analytical ultracentrifugation measures the concentration profiles of the sample cell in the radial direction as a function of time. The application of a centrifugal force causes depletion of proteins at the meniscus. Sedimentation creates a concentration boundary that moves down to the bottom of the sector shaped cell as a function of time.

The Lamm equation describes the evolution of the concentration distribution of proteins as a function of time and radial position under the influence of sedimentation and diffusion in the sector-shaped ultracentrifugal sample cell.

$$\left(\frac{\partial c}{\partial t}\right)_r = -\frac{1}{r}\left\{\frac{\partial}{\partial r}\left[s\omega^2 r^2 c - Dr\left(\frac{\partial c}{\partial r}\right)_t\right]\right\}_t$$ **Equation 9**

Several software packages use the Lamm equation to model the sedimentation boundary and diffusion that occur during SV experiments, which can be used to generate data on the size of the particle and its shape during sedimentation.

6.10.3 Experimental procedure

Protein was analysed at concentrations in the range of 0.1 – 0.5mg/ml in a 50 mM Tris HCl pH 7.5, 100 mM NaCl buffer. Samples were spun at 40,000 rpm for 24 hours at 16 °C in an An-50 Ti rotor in an Optima XL-A ultracentrifuge (Beckman Coulter, Inc.). Optical detection was carried out at 280 nm. Partial specific volume, hydration and Buffer density were derived from the SEDNTERP program and were used. Data were analysed using the Sedfit (Schuck, 2000) program assuming a continuous c(s) distribution with no prior knowledge. The meniscus, the bottom of the cell and the data range used for c(s) analysis were manual assigned for the fitting.

6.11 Crystallisation trials

Samples were concentrated by centrifugation at 5,000 × g in a 20ml Vivaspin 10 kDa concentrator. Protein concentrations were analysed before and after filtering through a 0.22 μM centrifuge filter (Milipore) to check for aggregation. Commercially bought 96 well screens were used to investigate crystallisation conditions (See table below). 90 μl of crystallisation buffer was placed into the reservoir solution and screens were set up using the mosquito crystallisation robot (TTP Labtech). A program was created so that 200 nl of protein and 200 nl of buffer were mixed in the needle and then added to the sitting drop well.

Table 6-16 Commercial screens used for crystallisation trials

Crystal Screen	Catalogue number
Hampton Crystal screen HT	HR2-130
Hampton Index HT	HR2-134
Hampton SaltRx HT	HR2-136
MDL CSS I	MD1-31
MDL CSS II	MD1-32
MDL Memstart & Memsys	MD1-33
MDL Structure Screen I & II	MD1-30
MDL PACT premier	MD1-36
EMERALD BIOSCIENCES WIZARD I + II	EBS-BWZ
JBScreen Classic HTS II S	CS-202L

6.12 Electron microscopy

All proteins used for electron microscopy experiments were in minimal buffer.

Table 6-17 Composition of minimal buffer

solution	*composition*
Minimal Buffer	20mM Tris pH 7.5, 50 mM NaCl,

6.12.1 Negative staining

6 µl of protein was deposited onto a freshly glow discharged, carbon-coated copper grid. After 1 minute the grid was blotted and stained with 2% uranyl acetate for 1 minute and blotted and left to air dry. Grids were examined in a JEOL 1010 electron microscope operated at 80 kV. Images were captured at a magnification of 200,000.

Image J (NIH) was used to measure particle lengths using the scale bar from the images were used to determine pixels per nm. 30 individual particles were used for each value measurement.

6.12.2 Class averaging

Class averaging was carried out using the EMAN suite of programs (Ludtke et al., 1999) The boxer program was used to manually select images from each micrograph with a box size of 80 pixels. 336 images were manually selected and the mean and standard deviation of each image was normalised using the proc2d program. All normalised images were combined into one directory and were centred by the cenalignint program. Two-dimensional averaging of the particles was carried out using the refine2d program, with 8 classes chosen with the minimum number of particles for each class set to 20.

6.12.3 Nanogold staining

Gold labelling was carried out using Ni-NTA-Nanogold (Nanoprobes). This molecule specifically binds to a His-Tag moiety. 0.5 nmol of protein in minimal buffer was incubated with 5 nmol of Ni-NTA-Nanogold solution for 30 minutes at 4°C. This sample was then loaded onto a Superdex 200 10/300 pre-equilibrated with minimal buffer and eluted to remove the unbound gold particles. As the 1.8nm nanogold particle cannot be observed directly under negative stain conditions, Goldenhance™ (Nanoprobes) was used to increase the size of the particle. With the nanogold labelled sample placed onto the carbon-coated grid and blotted, the grid was then placed onto 10 μl of the Goldenhance™ solution for 30 seconds. Grids were rinsed in water, stained with 2% uranyl acetate and visualised as previously described.

6.13 Small-angle X-ray scattering (SAXS)

6.13.1 Experimental procedure

Proteins were concentrated by centrifugation (see section 6.11), filtered and concentrations determined using a Nanodrop spectrophotometer ND-1000 (see section 6.8) Experiments were carried out on beamline X33 of the European Molecular Biology

Laboratory (EMBL) at the DORIS III storage ring, Deutsches Elektronen Synchrotron (DESY) Hamburg.

Samples were loaded into an automated sample chamber. 100 μl of sample was automatically put into a flat in-air cell with mica windows at 16°C. The sample was exposed to monochromated X-rays with a wavelength of 0.15 nm for 30 seconds, with the scattering intensity detected by a Mar345 image plate. Four 30-second exposures for each sample were carried out and the scattering curve generated from the average of these four measurements.

To obtain a scattering curve for the protein alone, scattering curves are measured from the buffer before and after the protein sample is analysed. The two scattering curves from the buffer alone are averaged. This averaged scattering curve is then subtracted from the scattering of the protein, creating a signal that is due to the protein alone.

6.13.2 Theory

The scattering curve is described by intensity (I), and is a function of the momentum transfer *q*.

$$q = \frac{(4\pi \sin\theta)}{\lambda}$$ **Equation 10**

θ is half the angle between the scattering and incident radiation

λ is the wavelength = 0.15nm

As the wavelength is fixed and the scattering angles are small (I) plotted against *q* can be used as a function of the scattering. At low resolution, the scattering can be used to estimate the radius of gyration R_G and the forward / zero angle scattered intensity I(0). R_G is defined as the root-mean squared distance of all the scattering volumes from the centre of the particles mass. I(0) is the intensity of radiation scattered at zero angle (θ = 0°). It is the square of the number of electrons in the scatterer and is used for shape

independent molecular weight determination. Estimations of R_G and I(0) are determined by using the Guinier equation

$$\ln(I) = \ln I(0) - \frac{(q^2 R_G^2)}{3} \qquad \textbf{Equation 11}$$

The Guinier region used for a linear fit is only at a range of $qR_G < 1.3$ for proteins. At low resolution, a plot of ln(I) against q^2 gives the Guinier equation in the form y = mx + c. From the gradient R_G can be derived, and from the y intercept, I(0) can be calculated.

The pair-distribution function *P(r)* is a measurement of the frequency of all inter-atomic vector lengths within a molecule such as a protein. This generates information about the shape of the scattering particle.

$$P(r) = \frac{1}{2\pi^2} \int_0^{D\max} I(q) \bullet qr \bullet \sin(qr) \bullet dq \qquad \textbf{Equation 12}$$

r is the inter-atomic vector distances within the particle

D_{max} is the maximum distance present in the scattering particle

As the integral of equation 12 cannot be directly evaluated, a indirect Fourier transform using programs such as GNOM is used to generate a *P(r)* for proteins. This creates a real space representation of the scattering data, which provides information on both the symmetry of the particle and the domain structure. *P(r)* curves are typically assigned to have values of *r*=0 at zero and D_{max}. The value of D_{max} is determined by creating a range of values between 2-4 x R_G as a rule of thumb, the best value is gives the highest alpha score which is a value of the goodness of fit between the experimental and calculated values. The transformation uses the whole scattering curve and can provide a more accurate calculation of R_G and I(0). Correlating R_G and I(0) values obtained from Guinier plots and *P(r)* curves can provide an evaluation of consistent data.

6.13.3 *Ab initio* methods to generate low-resolution 3D models

Three-dimensional reconstructions of molecular shapes were generated using *ab initio* algorithms used by the program DAMMIN found in the ATSAS 2.1 suite. The algorithm used for this program aims to generate a protein model as closely packed beads inside a sphere. Beads in this sphere are randomly assigned to be either a particle of protein or solvent. Simulated annealing is used to minimize the energy of the system to fit the experimental data. Single beads are moved randomly leading to a new model, the model has energy constraints so that beads assigned as protein must be connected and compacted together. The scattering curve used for the simulations has the maximum data range for q as $\leq 8/R_G$. 10 separate simulations were performed on the same initial data, and models filtered and averaged using DAMAVER. Models were displayed using the program PyMOL (http://www.pymol.org).

6.14 Pull-down experiments

TEV was added at a ratio of 1:50 to the MIND complex to remove the HisTag on the N-terminal of Dsn1p, with the cleavage occurring overnight at 4°C on a rolling platform. Undigested MIND complex, still containing a His-tag and TEV (that has a non-cleavable His-tag) were removed by passing the solution through Ni-NTA resin and were collected. The Ndc80, Spc24/25 and SpcG complexes were bound to Ni-NTA resin pre-equilibrated with interaction buffer A in a PD-10 column. Proteins were left to bind O/N at 4°C on a rolling platform. The resin was then washed with 20 c.v. of interaction buffer A to remove any unbound complexes. The untagged MIND complex was then added to the resin with bound Ndc80, Spc24/25 or SpcG complexes at a molar ratio of 1:1. The solution was then left overnight at 4°C on a rolling platform. The resin was washed with 20 c.v. of interaction buffer A. Proteins were then eluted by 10 c.v. of Interaction buffer B.

Table 6-18 Composition of buffers for pull down assays

Solution	*composition*
Interaction buffer A	50mM Tris pH 7.5, 200 mM NaCl, 5 mM β- mercaptoethanol, 20mM imidazole
Interaction buffer B	50mM Tris pH 7.5, 200 mM NaCl, 5 mM β- mercaptoethanol, 500mM imidazole

6.15 Isothermal titration calorimetry

The ITC microcalorimeter contains a sample cell and reference cell. One component of the binding is injected into the sample cell containing the other component. When these molecules interact, heat is either released or absorbed. This change is heat is detected by the microcalorimeter, and the energy required to return the sample cell to the same temperature as the reference cell is recorded. The binding isotherm is generated by constant injections of the first component and recording the energy required to return the temperature to the reference cell. This curve is used to calculate thermodynamic parameters, association constants and stoichiometry of binding.

ITC experiments were carried using an iTC_{200} (MicroCal, Amherst, MA). Sample concentrations were determined using a Nanodrop spectrophotometer ND-1000 (see section 6.8). 3 μl injections were carried out at 1000 rpm stirring speed with an injection spacing of 3 minutes. Measurements for each protein interaction were repeated three times to test validity, with the thermodynamic data processed using the ORIGIN software (Microcal).

6.16 Peptide array assay

Peptides were synthesised and spotted onto a cellulose membrane. The membrane was activated by washing in activation buffer for 1 hour followed by washes in wash buffer. His-Tagged MIND complex at a concentration of 0.6 μg/ml was added to binding buffer and left to interact with the membrane overnight at 4°C. The membrane was washed,

and transferred into binding buffer containing a 1/1000 dilution of anti-His mouse monoclonal IgG1 antibody for 4 hours at room temperature. The membrane was again washed and transferred into binding buffer containing a 1/1500 dilution of rabbit anti-mouse IgG-HRP conjugated secondary antibodies for 1 hour at room temperature. The membrane was then washed, blotted and coated with enhanced chemiluminescence (ECL) reagents (GE Lifesciences) to promote the luminescence of the HRP conjugate. The membrane was exposed to ECL film (GE healthcare) for 15 seconds and the film developed.

The control experiment was carried out by exactly the same protocol as described but with the omission of the MIND complex binding step.

Table 6-19 Composition of buffers for peptide array assays

solution	***Composition***
Activation buffer	50% ethanol(v/v) , 10% glacial acetic acid (v/v)
Wash buffer	20 mM Tris pH 7.5, 100 mM NaCl, 250 μM TCEP.
Binding buffer	Wash Buffer + 0.1% Tween 20 (v/v), 1% Milk powder (w/v)

6.17 Phosphorylation assay

The MIND complex was dialysed (see section 6.6.4) into phosphorylation buffer. Recombinant *Saccharomyces cerevisiae* Ipl1p/Ipl1p IN box peptide (see section 4.10.1) were added at a molar ratio of 1:100 (Ipl1/MIND complex). The reaction was incubated for 3 hours at room temperature and phosphorylation was analysed by SDS-PAGE (see section 6.7), with the gel composition described below. All bands were excised and phosphorylation sites mapped using MALDI-TOF. Database searches were done using the Mascot server and spectra was analysed using the Scaffold program (http://www.proteomesoftware.com/).

Table 6-20 Composition of phosphorylation buffer

solution	***composition***
phosphorylation buffer	50mM Tris pH 7.5, 150 mM NaCl, 5 mM ATP, 10 mM $MgCl_2$

Table 6-21 Composition of PhosTag™ separating gel

solution	*composition*
10% resolving PhosTag™ gel	10% Acrylamide:Bis-acrylamide (37.5:1), 375 mM Tris-HCl pH8.8, 0.1 % SDS (w/v), 0.05% tetramethylethylenediamine (TEMED), 0.1% ammonium persulphate (APS) 50 μM PhosTag™ ligand 50 μM $MnCl_2$

Appendix

Appendix Figure 1. Dsn1p sequence alignment

Regions between the red arrows indicate the protease resistant domain of Dsn1p identifed by limited proteolysis

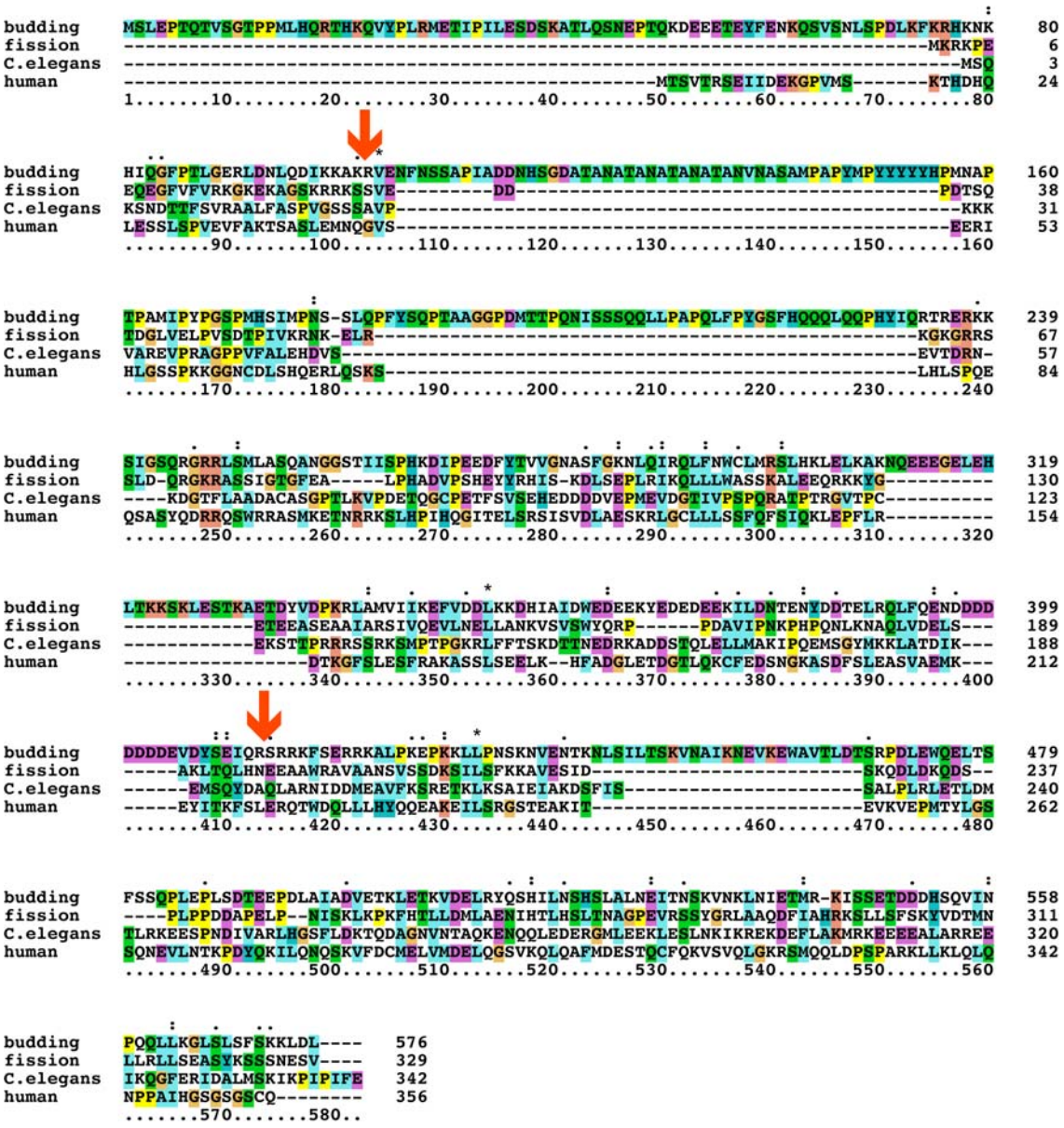

Appendix figure 1 Sequence alignment of Dsn1p

Appendix figure 2. Mtw1p Sequence alignment

Red Arrow indicates where the C-terminal of Mtw1p is cleaved by limited proteolysis

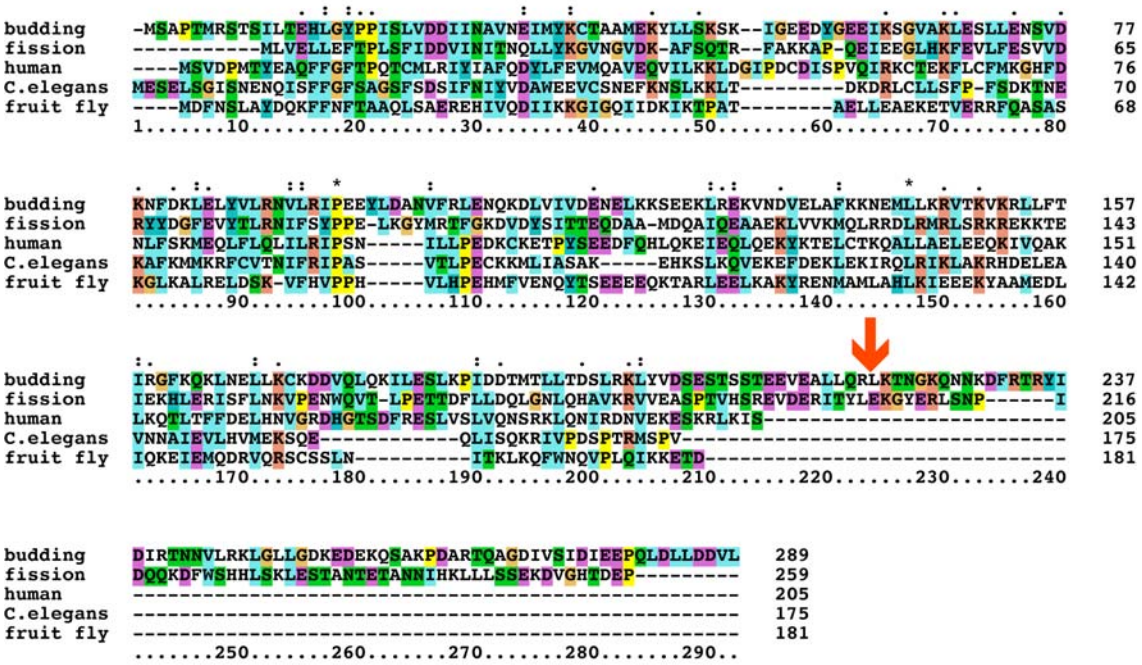

Appendix figure 2 Sequence alignment of Mtw1p

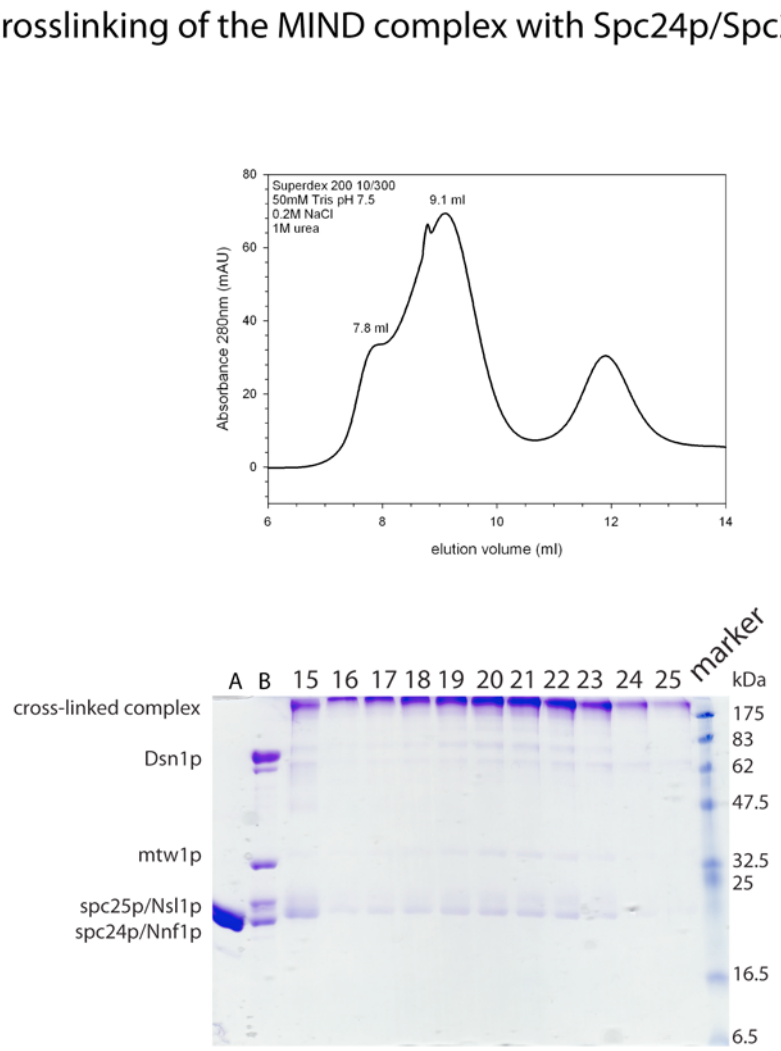

Appendix figure 3 Cross-linking between MIND and Spc24/Spc25

Equimolar amounts of the MIND complex and Spc24/Spc25 were added as well as the cross-linking reagent Bisuccinimidyl-succinamyl-aspartyl-proline SuDP (Soderblom and Goshe, 2006) at a ratio of 500:1 (cross-linker-protein). The interaction was quenched after 30 minutes and the sample was loaded onto a superdex 200 10/300 GL in 1M urea to separate any un-cross-linked complexes. The samples were then ran on a SDS-PAGE gel, with relevant bands excised and sent to the Protein Analysis & Proteomics laboratory, Cancer Research UK for analysis.

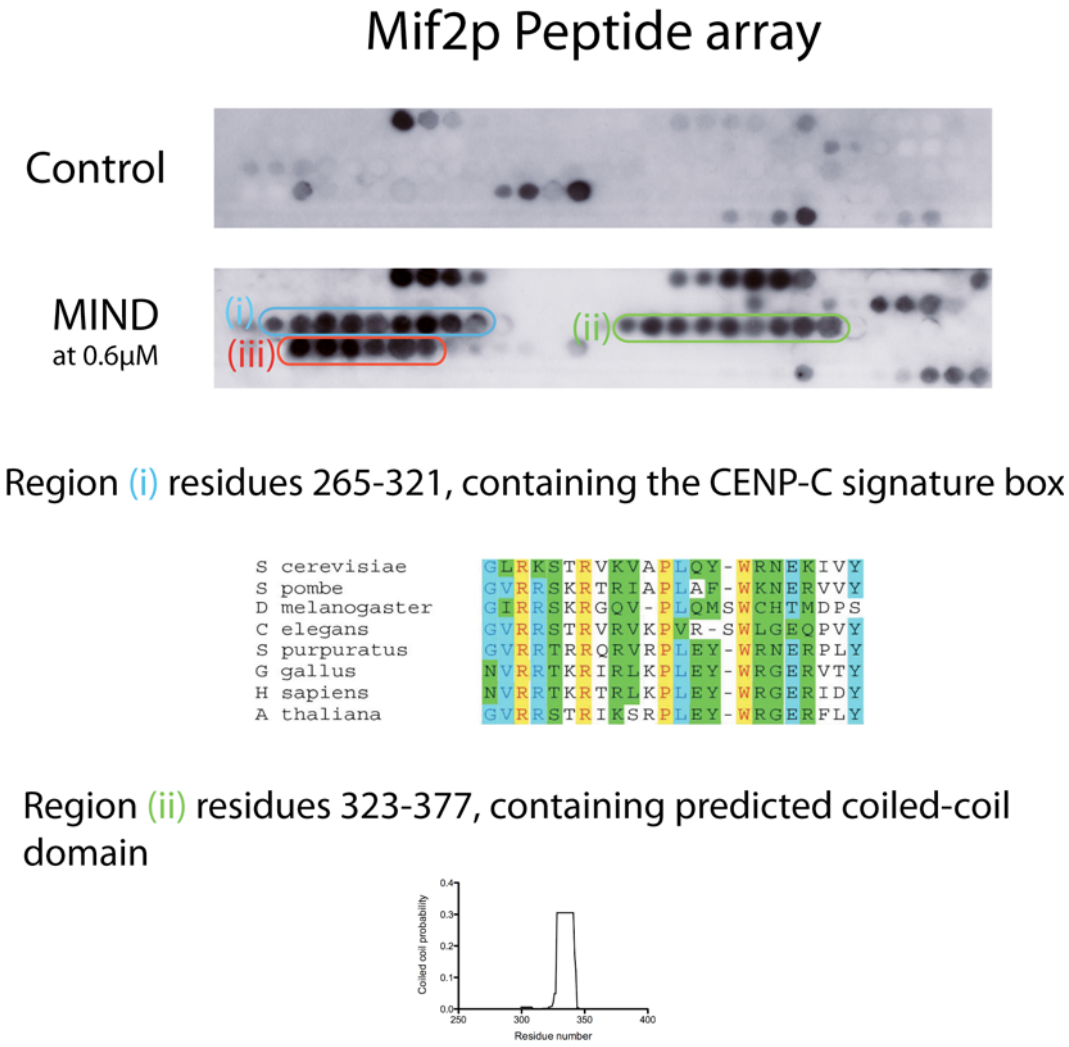

Appendix figure 4. Peptide array of Mif2p interacting with the MIND complex

The MIND complex was found to bind to peptides that correspond to three regions. These region have been found to contain the CENP-C binding motif (Cohen et al., 2008), a predicted coiled-coil motif identified by PCOILS (Lupas et al., 1991) and the dimerisation domain of Mif2p (Cohen et al., 2008). Analysis of the binding to the dimerisation domains indicates that sheets B-E (shown in red in the crystal structure) bind to the MIND complex (with the rest of the cupin barrel shown in green).

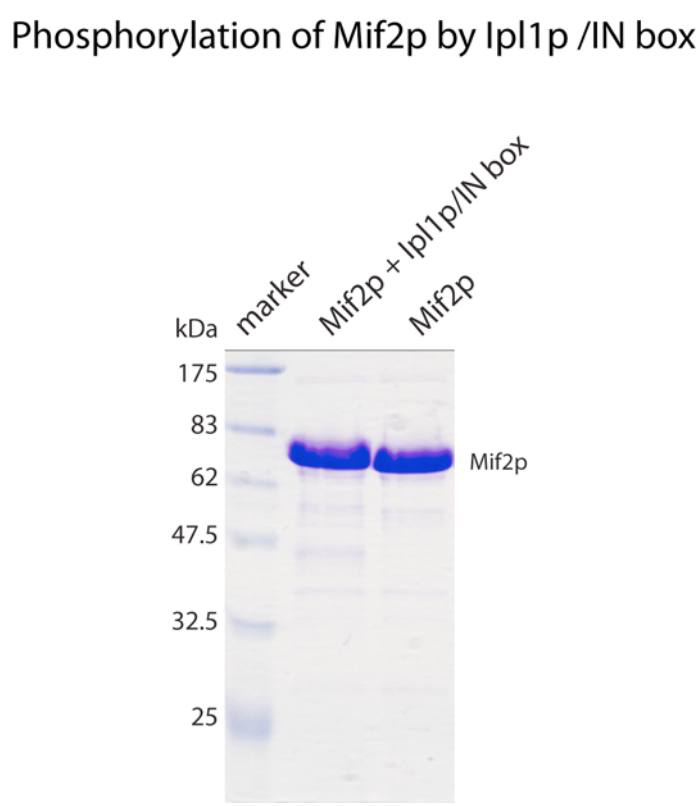

Appendix figure 4 (cont)

Mif2p can be expressed and purified for studies such as ITC. It can also be phosphorylated as seen by a shift in the SDS band after the addition of Ipl1p/IN box and ATP as has been previously observed (Westermann et al., 2003).

Reference List

Adams, R. R., Eckley, D. M., Vagnarelli, P., Wheatley, S. P., Gerloff, D. L., Mackay, A. M., Svingen, P. A., Kaufmann, S. H. & Earnshaw, W. C. (2001) Human INCENP colocalizes with the Aurora-B/AIRK2 kinase on chromosomes and is overexpressed in tumour cells. *Chromosoma,* 110, 65-74.

Adams, R. R., Wheatley, S. P., Gouldsworthy, A. M., Kandels-Lewis, S. E., Carmena, M., Smythe, C., Gerloff, D. L. & Earnshaw, W. C. (2000) INCENP binds the Aurora-related kinase AIRK2 and is required to target it to chromosomes, the central spindle and cleavage furrow. *Curr Biol,* 10, 1075-8.

Al-Bassam, J., Van Breugel, M., Harrison, S. C. & Hyman, A. (2006) Stu2p binds tubulin and undergoes an open-to-closed conformational change. *J Cell Biol,* 172, 1009-22.

Bellizzi, J. J., 3rd, Sorger, P. K. & Harrison, S. C. (2007) Crystal structure of the yeast inner kinetochore subunit Cep3p. *Structure,* 15, 1422-30.

Bharadwaj, R., Qi, W. & Yu, H. (2004) Identification of two novel components of the human NDC80 kinetochore complex. *J Biol Chem,* 279, 13076-85.

Biggins, S. & Murray, A. W. (2001) The budding yeast protein kinase Ipl1/Aurora allows the absence of tension to activate the spindle checkpoint. *Genes Dev,* 15, 3118-29.

Biggins, S., Severin, F. F., Bhalla, N., Sassoon, I., Hyman, A. A. & Murray, A. W. (1999) The conserved protein kinase Ipl1 regulates microtubule binding to kinetochores in budding yeast. *Genes Dev,* 13, 532-44.

Brown, J. H., Volkmann, N., Jun, G., Henschen-Edman, A. H. & Cohen, C. (2000) The crystal structure of modified bovine fibrinogen. *Proc Natl Acad Sci U S A,* 97, 85-90.

Chan, C. S. & Botstein, D. (1993) Isolation and characterization of chromosome-gain and increase-in-ploidy mutants in yeast. *Genetics,* 135, 677-91.

Cheeseman, I. M., Anderson, S., Jwa, M., Green, E. M., Kang, J., Yates, J. R., 3rd, Chan, C. S., Drubin, D. G. & Barnes, G. (2002) Phospho-regulation of kinetochore-microtubule attachments by the Aurora kinase Ipl1p. *Cell,* 111, 163-72.

Cheeseman, I. M., Brew, C., Wolyniak, M., Desai, A., Anderson, S., Muster, N., Yates, J. R., Huffaker, T. C., Drubin, D. G. & Barnes, G. (2001a) Implication of a novel multiprotein Dam1p complex in outer kinetochore function. *J Cell Biol,* 155, 1137-45.

Cheeseman, I. M., Chappie, J. S., Wilson-Kubalek, E. M. & Desai, A. (2006) The conserved KMN network constitutes the core microtubule-binding site of the kinetochore. *Cell,* 127, 983-97.

Cheeseman, I. M., Enquist-Newman, M., Muller-Reichert, T., Drubin, D. G. & Barnes, G. (2001b) Mitotic spindle integrity and kinetochore function linked by the Duo1p/Dam1p complex. *J Cell Biol,* 152, 197-212.

Cheeseman, I. M., Hori, T., Fukagawa, T. & Desai, A. (2008) KNL1 and the CENP-H/I/K complex coordinately direct kinetochore assembly in vertebrates. *Mol Biol Cell,* 19, 587-94.

Cheeseman, I. M., Niessen, S., Anderson, S., Hyndman, F., Yates, J. R., 3rd, Oegema, K. & Desai, A. (2004) A conserved protein network controls assembly of the outer kinetochore and its ability to sustain tension. *Genes Dev,* 18, 2255-68.

Chen, R. H., Waters, J. C., Salmon, E. D. & Murray, A. W. (1996) Association of spindle assembly checkpoint component XMAD2 with unattached kinetochores. *Science,* 274, 242-6.

Chen, Y., Riley, D. J., Chen, P. L. & Lee, W. H. (1997) HEC, a novel nuclear protein rich in leucine heptad repeats specifically involved in mitosis. *Mol Cell Biol,* 17, 6049-56.

Ciferri, C., De Luca, J., Monzani, S., Ferrari, K. J., Ristic, D., Wyman, C., Stark, H., Kilmartin, J., Salmon, E. D. & Musacchio, A. (2005) Architecture of the human ndc80-hec1 complex, a critical constituent of the outer kinetochore. *J Biol Chem,* 280, 29088-95.

Ciferri, C., Pasqualato, S., Screpanti, E., Varetti, G., Santaguida, S., Dos Reis, G., Maiolica, A., Polka, J., De Luca, J. G., De Wulf, P., Salek, M., Rappsilber, J., Moores, C. A., Salmon, E. D. & Musacchio, A. (2008) Implications for kinetochore-microtubule attachment from the structure of an engineered Ndc80 complex. *Cell,* 133, 427-39.

Clarke, L. (1998) Centromeres: proteins, protein complexes, and repeated domains at centromeres of simple eukaryotes. *Curr Opin Genet Dev,* 8, 212-8.

Clarke, L. & Carbon, J. (1980) Isolation of a yeast centromere and construction of functional small circular chromosomes. *Nature,* 287, 504-9.

Cleveland, D. W., Mao, Y. & Sullivan, K. F. (2003) Centromeres and kinetochores: from epigenetics to mitotic checkpoint signaling. *Cell,* 112, 407-21.

Cohen, R. L., Espelin, C. W., De Wulf, P., Sorger, P. K., Harrison, S. C. & Simons, K. T. (2008) Structural and functional dissection of Mif2p, a conserved DNA-binding kinetochore protein. *Mol Biol Cell,* 19, 4480-91.

Cohen-Fix, O., Peters, J. M., Kirschner, M. W. & Koshland, D. (1996) Anaphase initiation in Saccharomyces cerevisiae is controlled by the APC-dependent degradation of the anaphase inhibitor Pds1p. *Genes Dev,* 10, 3081-93.

Connelly, C. & Hieter, P. (1996) Budding yeast SKP1 encodes an evolutionarily conserved kinetochore protein required for cell cycle progression. *Cell,* 86, 275-85.

Corbett, K. D., Yip, C. K., Ee, L. S., Walz, T., Amon, A. & Harrison, S. C. (2010) The monopolin complex crosslinks kinetochore components to regulate chromosome-microtubule attachments. *Cell,* 142, 556-67.

De Antoni, A., Pearson, C. G., Cimini, D., Canman, J. C., Sala, V., Nezi, L., Mapelli, M., Sironi, L., Faretta, M., Salmon, E. D. & Musacchio, A. (2005) The Mad1/Mad2 complex as a template for Mad2 activation in the spindle assembly checkpoint. *Curr Biol,* 15, 214-25.

De Wulf, P., Mcainsh, A. D. & Sorger, P. K. (2003) Hierarchical assembly of the budding yeast kinetochore from multiple subcomplexes. *Genes Dev,* 17, 2902-21.

Deluca, J. G., Dong, Y., Hergert, P., Strauss, J., Hickey, J. M., Salmon, E. D. & Mcewen, B. F. (2005) Hec1 and nuf2 are core components of the kinetochore outer plate essential for organizing microtubule attachment sites. *Mol Biol Cell,* 16, 519-31.

Deluca, J. G., Gall, W. E., Ciferri, C., Cimini, D., Musacchio, A. & Salmon, E. D. (2006) Kinetochore microtubule dynamics and attachment stability are regulated by Hec1. *Cell,* 127, 969-82.

Deluca, J. G., Howell, B. J., Canman, J. C., Hickey, J. M., Fang, G. & Salmon, E. D. (2003) Nuf2 and Hec1 are required for retention of the checkpoint proteins Mad1 and Mad2 to kinetochores. *Curr Biol,* 13, 2103-9.

Deluca, J. G., Moree, B., Hickey, J. M., Kilmartin, J. V. & Salmon, E. D. (2002) hNuf2 inhibition blocks stable kinetochore-microtubule attachment and induces mitotic cell death in HeLa cells. *J Cell Biol,* 159, 549-55.

Desai, A., Rybina, S., Muller-Reichert, T., Shevchenko, A., Hyman, A. & Oegema, K. (2003) KNL-1 directs assembly of the microtubule-binding interface of the kinetochore in C. elegans. *Genes Dev,* 17, 2421-35.

Doheny, K. F., Sorger, P. K., Hyman, A. A., Tugendreich, S., Spencer, F. & Hieter, P. (1993) Identification of essential components of the S. cerevisiae kinetochore. *Cell,* 73, 761-74.

Dong, Y., Vanden Beldt, K. J., Meng, X., Khodjakov, A. & Mcewen, B. F. (2007) The outer plate in vertebrate kinetochores is a flexible network with multiple microtubule interactions. *Nat Cell Biol,* 9, 516-22.

Edman, P. (1960) Phenylthiohydantoins in protein analysis. *Ann N Y Acad Sci,* 88, 602-10.

Espelin, C. W., Kaplan, K. B. & Sorger, P. K. (1997) Probing the architecture of a simple kinetochore using DNA-protein crosslinking. *J Cell Biol,* 139, 1383-96.

Espelin, C. W., Simons, K. T., Harrison, S. C. & Sorger, P. K. (2003) Binding of the essential Saccharomyces cerevisiae kinetochore protein Ndc10p to CDEII. *Mol Biol Cell,* 14, 4557-68.

Euskirchen, G. M. (2002) Nnf1p, Dsn1p, Mtw1p, and Nsl1p: a new group of proteins important for chromosome segregation in Saccharomyces cerevisiae. *Eukaryot Cell,* 1, 229-40.

Fitzgerald-Hayes, M., Clarke, L. & Carbon, J. (1982) Nucleotide sequence comparisons and functional analysis of yeast centromere DNAs. *Cell,* 29, 235-44.

Flemming, W. (1882) *Zellsubstanz, Kern und Zelltheilung,* Leipzig, Vogel.

Fontana, A., Fassina, G., Vita, C., Dalzoppo, D., Zamai, M. & Zambonin, M. (1986) Correlation between sites of limited proteolysis and segmental mobility in thermolysin. *Biochemistry,* 25, 1847-51.

Gillett, E. S., Espelin, C. W. & Sorger, P. K. (2004) Spindle checkpoint proteins and chromosome-microtubule attachment in budding yeast. *J Cell Biol,* 164, 535-46.

Goh, P. Y. & Kilmartin, J. V. (1993) NDC10: a gene involved in chromosome segregation in Saccharomyces cerevisiae. *J Cell Biol,* 121, 503-12.
Goshima, G., Kiyomitsu, T., Yoda, K. & Yanagida, M. (2003) Human centromere chromatin protein hMis12, essential for equal segregation, is independent of CENP-A loading pathway. *J Cell Biol,* 160, 25-39.
Goshima, G., Saitoh, S. & Yanagida, M. (1999) Proper metaphase spindle length is determined by centromere proteins Mis12 and Mis6 required for faithful chromosome segregation. *Genes Dev,* 13, 1664-77.
Goshima, G. & Yanagida, M. (2000) Establishing biorientation occurs with precocious separation of the sister kinetochores, but not the arms, in the early spindle of budding yeast. *Cell,* 100, 619-33.
Guimaraes, G. J., Dong, Y., Mcewen, B. F. & Deluca, J. G. (2008) Kinetochore-microtubule attachment relies on the disordered N-terminal tail domain of Hec1. *Curr Biol,* 18, 1778-84.
Hainfeld, J. F., Liu, W., Halsey, C. M., Freimuth, P. & Powell, R. D. (1999) Ni-NTA-gold clusters target His-tagged proteins. *J Struct Biol,* 127, 185-98.
Hardwick, K. G., Johnston, R. C., Smith, D. L. & Murray, A. W. (2000) MAD3 encodes a novel component of the spindle checkpoint which interacts with Bub3p, Cdc20p, and Mad2p. *J Cell Biol,* 148, 871-82.
Hardwick, K. G., Weiss, E., Luca, F. C., Winey, M. & Murray, A. W. (1996) Activation of the budding yeast spindle assembly checkpoint without mitotic spindle disruption. *Science,* 273, 953-6.
Hayashi, I. & Ikura, M. (2003) Crystal structure of the amino-terminal microtubule-binding domain of end-binding protein 1 (EB1). *J Biol Chem,* 278, 36430-4.
He, X., Rines, D. R., Espelin, C. W. & Sorger, P. K. (2001) Molecular analysis of kinetochore-microtubule attachment in budding yeast. *Cell,* 106, 195-206.
Hildebrandt, E. R. & Hoyt, M. A. (2000) Mitotic motors in Saccharomyces cerevisiae. *Biochim Biophys Acta,* 1496, 99-116.
Hirel, P. H., Schmitter, M. J., Dessen, P., Fayat, G. & Blanquet, S. (1989) Extent of N-terminal methionine excision from Escherichia coli proteins is governed by the side-chain length of the penultimate amino acid. *Proc Natl Acad Sci U S A,* 86, 8247-51.
Hodges, R. S. (1992) Unzipping the secrets of coiled-coils. *Curr Biol,* 2, 122-4.
Howe, M., Mcdonald, K. L., Albertson, D. G. & Meyer, B. J. (2001) HIM-10 is required for kinetochore structure and function on Caenorhabditis elegans holocentric chromosomes. *J Cell Biol,* 153, 1227-38.
Howell, B. J., Hoffman, D. B., Fang, G., Murray, A. W. & Salmon, E. D. (2000) Visualization of Mad2 dynamics at kinetochores, along spindle fibers, and at spindle poles in living cells. *J Cell Biol,* 150, 1233-50.
Howell, B. J., Moree, B., Farrar, E. M., Stewart, S., Fang, G. & Salmon, E. D. (2004) Spindle checkpoint protein dynamics at kinetochores in living cells. *Curr Biol,* 14, 953-64.
Hoyt, M. A., Totis, L. & Roberts, B. T. (1991) S. cerevisiae genes required for cell cycle arrest in response to loss of microtubule function. *Cell,* 66, 507-17.

Hudson, D. F., Marshall, K. M. & Earnshaw, W. C. (2009) Condensin: Architect of mitotic chromosomes. *Chromosome Res,* 17, 131-44.
Hwang, L. H., Lau, L. F., Smith, D. L., Mistrot, C. A., Hardwick, K. G., Hwang, E. S., Amon, A. & Murray, A. W. (1998) Budding yeast Cdc20: a target of the spindle checkpoint. *Science,* 279, 1041-4.
Hyland, K. M., Kingsbury, J., Koshland, D. & Hieter, P. (1999) Ctf19p: A novel kinetochore protein in Saccharomyces cerevisiae and a potential link between the kinetochore and mitotic spindle. *J Cell Biol,* 145, 15-28.
Janke, C., Ortiz, J., Lechner, J., Shevchenko, A., Magiera, M. M., Schramm, C. & Schiebel, E. (2001) The budding yeast proteins Spc24p and Spc25p interact with Ndc80p and Nuf2p at the kinetochore and are important for kinetochore clustering and checkpoint control. *EMBO J,* 20, 777-91.
Jiang, W., Lechner, J. & Carbon, J. (1993) Isolation and characterization of a gene (CBF2) specifying a protein component of the budding yeast kinetochore. *J Cell Biol,* 121, 513-9.
Joglekar, A. P., Bloom, K. & Salmon, E. D. (2009) In vivo protein architecture of the eukaryotic kinetochore with nanometer scale accuracy. *Curr Biol,* 19, 694-9.
Joglekar, A. P., Bouck, D. C., Molk, J. N., Bloom, K. S. & Salmon, E. D. (2006) Molecular architecture of a kinetochore-microtubule attachment site. *Nat Cell Biol,* 8, 581-5.
Johnston, K., Joglekar, A., Hori, T., Suzuki, A., Fukagawa, T. & Salmon, E. D. (2010) Vertebrate kinetochore protein architecture: protein copy number. *J Cell Biol,* 189, 937-43.
Kaitna, S., Mendoza, M., Jantsch-Plunger, V. & Glotzer, M. (2000) Incenp and an aurora-like kinase form a complex essential for chromosome segregation and efficient completion of cytokinesis. *Curr Biol,* 10, 1172-81.
Kang, J., Cheeseman, I. M., Kallstrom, G., Velmurugan, S., Barnes, G. & Chan, C. S. (2001) Functional cooperation of Dam1, Ipl1, and the inner centromere protein (INCENP)-related protein Sli15 during chromosome segregation. *J Cell Biol,* 155, 763-74.
Karess, R. (2005) Rod-Zw10-Zwilch: a key player in the spindle checkpoint. *Trends Cell Biol,* 15, 386-92.
Kemmler, S., Stach, M., Knapp, M., Ortiz, J., Pfannstiel, J., Ruppert, T. & Lechner, J. (2009) Mimicking Ndc80 phosphorylation triggers spindle assembly checkpoint signalling. *EMBO J,* 28, 1099-110.
Kerres, A., Vietmeier-Decker, C., Ortiz, J., Karig, I., Beuter, C., Hegemann, J., Lechner, J. & Fleig, U. (2004) The fission yeast kinetochore component Spc7 associates with the EB1 family member Mal3 and is required for kinetochore-spindle association. *Mol Biol Cell,* 15, 5255-67.
Kim, J. H., Kang, J. S. & Chan, C. S. (1999) Sli15 associates with the ipl1 protein kinase to promote proper chromosome segregation in Saccharomyces cerevisiae. *J Cell Biol,* 145, 1381-94.
King, R. W., Peters, J. M., Tugendreich, S., Rolfe, M., Hieter, P. & Kirschner, M. W. (1995) A 20S complex containing CDC27 and CDC16 catalyzes the mitosis-specific conjugation of ubiquitin to cyclin B. *Cell,* 81, 279-88.

Kinoshita, E., Takahashi, M., Takeda, H., Shiro, M. & Koike, T. (2004) Recognition of phosphate monoester dianion by an alkoxide-bridged dinuclear zinc(II) complex. *Dalton Trans*, 1189-93.
Kiyomitsu, T., Iwasaki, O., Obuse, C. & Yanagida, M. (2010) Inner centromere formation requires hMis14, a trident kinetochore protein that specifically recruits HP1 to human chromosomes. *J Cell Biol,* 188, 791-807.
Kiyomitsu, T., Obuse, C. & Yanagida, M. (2007) Human Blinkin/AF15q14 is required for chromosome alignment and the mitotic checkpoint through direct interaction with Bub1 and BubR1. *Dev Cell,* 13, 663-76.
Kline, S. L., Cheeseman, I. M., Hori, T., Fukagawa, T. & Desai, A. (2006) The human Mis12 complex is required for kinetochore assembly and proper chromosome segregation. *J Cell Biol,* 173, 9-17.
Koshland, D. & Strunnikov, A. (1996) Mitotic chromosome condensation. *Annu Rev Cell Dev Biol,* 12, 305-33.
Ladbury, J. E. & Doyle, M. L. (2004) *Biocalorimetry 2 : applications of calorimetry in the biological sciences,* Chichester, Wiley.
Laemmli, U. K. (1970) Cleavage of structural proteins during the assembly of the head of bacteriophage T4. *Nature,* 227, 680-5.
Lechner, J. (1994) A zinc finger protein, essential for chromosome segregation, constitutes a putative DNA binding subunit of the Saccharomyces cerevisiae kinetochore complex, Cbf3. *EMBO J,* 13, 5203-11.
Lechner, J. & Carbon, J. (1991) A 240 kd multisubunit protein complex, CBF3, is a major component of the budding yeast centromere. *Cell,* 64, 717-25.
Li, R. & Murray, A. W. (1991) Feedback control of mitosis in budding yeast. *Cell,* 66, 519-31.
Li, Y. & Benezra, R. (1996) Identification of a human mitotic checkpoint gene: hsMAD2. *Science,* 274, 246-8.
Liu, D., Vader, G., Vromans, M. J., Lampson, M. A. & Lens, S. M. (2009) Sensing chromosome bi-orientation by spatial separation of aurora B kinase from kinetochore substrates. *Science,* 323, 1350-3.
Liu, X., Mcleod, I., Anderson, S., Yates, J. R., 3rd & He, X. (2005) Molecular analysis of kinetochore architecture in fission yeast. *EMBO J,* 24, 2919-30.
Ludtke, S. J., Baldwin, P. R. & Chiu, W. (1999) EMAN: semiautomated software for high-resolution single-particle reconstructions. *J Struct Biol,* 128, 82-97.
Luger, K., Mader, A. W., Richmond, R. K., Sargent, D. F. & Richmond, T. J. (1997) Crystal structure of the nucleosome core particle at 2.8 A resolution. *Nature,* 389, 251-60.
Luo, X., Tang, Z., Rizo, J. & Yu, H. (2002) The Mad2 spindle checkpoint protein undergoes similar major conformational changes upon binding to either Mad1 or Cdc20. *Mol Cell,* 9, 59-71.
Lupas, A., Van Dyke, M. & Stock, J. (1991) Predicting coiled coils from protein sequences. *Science,* 252, 1162-4.
Maiolica, A., Cittaro, D., Borsotti, D., Sennels, L., Ciferri, C., Tarricone, C., Musacchio, A. & Rappsilber, J. (2007) Structural analysis of multiprotein complexes by cross-linking, mass spectrometry, and database searching. *Mol Cell Proteomics,* 6, 2200-11.

Mapelli, M., Massimiliano, L., Santaguida, S. & Musacchio, A. (2007) The Mad2 conformational dimer: structure and implications for the spindle assembly checkpoint. *Cell,* 131, 730-43.

Maresca, T. J. & Salmon, E. D. (2010) Welcome to a new kind of tension: translating kinetochore mechanics into a wait-anaphase signal. *J Cell Sci,* 123, 825-35.

Martin-Lluesma, S., Stucke, V. M. & Nigg, E. A. (2002) Role of Hec1 in spindle checkpoint signaling and kinetochore recruitment of Mad1/Mad2. *Science,* 297, 2267-70.

Mcainsh, A. D., Meraldi, P., Draviam, V. M., Toso, A. & Sorger, P. K. (2006) The human kinetochore proteins Nnf1R and Mcm21R are required for accurate chromosome segregation. *EMBO J,* 25, 4033-49.

Mcainsh, A. D., Tytell, J. D. & Sorger, P. K. (2003) Structure, function, and regulation of budding yeast kinetochores. *Annu Rev Cell Dev Biol,* 19, 519-39.

Mccleland, M. L., Gardner, R. D., Kallio, M. J., Daum, J. R., Gorbsky, G. J., Burke, D. J. & Stukenberg, P. T. (2003) The highly conserved Ndc80 complex is required for kinetochore assembly, chromosome congression, and spindle checkpoint activity. *Genes Dev,* 17, 101-14.

Mccleland, M. L., Kallio, M. J., Barrett-Wilt, G. A., Kestner, C. A., Shabanowitz, J., Hunt, D. F., Gorbsky, G. J. & Stukenberg, P. T. (2004) The vertebrate Ndc80 complex contains Spc24 and Spc25 homologs, which are required to establish and maintain kinetochore-microtubule attachment. *Curr Biol,* 14, 131-7.

Mcgrew, J., Diehl, B. & Fitzgerald-Hayes, M. (1986) Single base-pair mutations in centromere element III cause aberrant chromosome segregation in Saccharomyces cerevisiae. *Mol Cell Biol,* 6, 530-8.

Measday, V., Hailey, D. W., Pot, I., Givan, S. A., Hyland, K. M., Cagney, G., Fields, S., Davis, T. N. & Hieter, P. (2002) Ctf3p, the Mis6 budding yeast homolog, interacts with Mcm22p and Mcm16p at the yeast outer kinetochore. *Genes Dev,* 16, 101-13.

Meluh, P. B. & Koshland, D. (1995) Evidence that the MIF2 gene of Saccharomyces cerevisiae encodes a centromere protein with homology to the mammalian centromere protein CENP-C. *Mol Biol Cell,* 6, 793-807.

Meluh, P. B. & Koshland, D. (1997) Budding yeast centromere composition and assembly as revealed by in vivo cross-linking. *Genes Dev,* 11, 3401-12.

Meluh, P. B., Yang, P., Glowczewski, L., Koshland, D. & Smith, M. M. (1998) Cse4p is a component of the core centromere of Saccharomyces cerevisiae. *Cell,* 94, 607-13.

Meraldi, P., Mcainsh, A. D., Rheinbay, E. & Sorger, P. K. (2006) Phylogenetic and structural analysis of centromeric DNA and kinetochore proteins. *Genome Biol,* 7, R23.

Miller, S. A., Johnson, M. L. & Stukenberg, P. T. (2008) Kinetochore attachments require an interaction between unstructured tails on microtubules and Ndc80(Hec1). *Curr Biol,* 18, 1785-91.

Miranda, J. J., De Wulf, P., Sorger, P. K. & Harrison, S. C. (2005) The yeast DASH complex forms closed rings on microtubules. *Nat Struct Mol Biol,* 12, 138-43.

Mitchison, T. & Kirschner, M. (1984) Dynamic instability of microtubule growth. *Nature,* 312, 237-42.

Nabetani, A., Koujin, T., Tsutsumi, C., Haraguchi, T. & Hiraoka, Y. (2001) A conserved protein, Nuf2, is implicated in connecting the centromere to the spindle during chromosome segregation: a link between the kinetochore function and the spindle checkpoint. *Chromosoma,* 110, 322-34.

Nasmyth, K., Peters, J. M. & Uhlmann, F. (2000) Splitting the chromosome: cutting the ties that bind sister chromatids. *Science,* 288, 1379-85.

Nekrasov, V. S., Smith, M. A., Peak-Chew, S. & Kilmartin, J. V. (2003) Interactions between centromere complexes in Saccharomyces cerevisiae. *Mol Biol Cell,* 14, 4931-46.

Niedenthal, R. K., Sen-Gupta, M., Wilmen, A. & Hegemann, J. H. (1993) Cpf1 protein induced bending of yeast centromere DNA element I. *Nucleic Acids Res,* 21, 4726-33.

Nogales, E., Whittaker, M., Milligan, R. A. & Downing, K. H. (1999) High-resolution model of the microtubule. *Cell,* 96, 79-88.

Nogales, E., Wolf, S. G. & Downing, K. H. (1998) Structure of the alpha beta tubulin dimer by electron crystallography. *Nature,* 391, 199-203.

O'shea, E. K., Klemm, J. D., Kim, P. S. & Alber, T. (1991) X-ray structure of the GCN4 leucine zipper, a two-stranded, parallel coiled coil. *Science,* 254, 539-44.

O'toole, E. T., Winey, M. & Mcintosh, J. R. (1999) High-voltage electron tomography of spindle pole bodies and early mitotic spindles in the yeast Saccharomyces cerevisiae. *Mol Biol Cell,* 10, 2017-31.

Obuse, C., Iwasaki, O., Kiyomitsu, T., Goshima, G., Toyoda, Y. & Yanagida, M. (2004) A conserved Mis12 centromere complex is linked to heterochromatic HP1 and outer kinetochore protein Zwint-1. *Nat Cell Biol,* 6, 1135-41.

Okada, M., Cheeseman, I. M., Hori, T., Okawa, K., Mcleod, I. X., Yates, J. R., 3rd, Desai, A. & Fukagawa, T. (2006) The CENP-H-I complex is required for the efficient incorporation of newly synthesized CENP-A into centromeres. *Nat Cell Biol,* 8, 446-57.

Ortiz, J., Stemmann, O., Rank, S. & Lechner, J. (1999) A putative protein complex consisting of Ctf19, Mcm21, and Okp1 represents a missing link in the budding yeast kinetochore. *Genes Dev,* 13, 1140-55.

Osborne, M. A., Schlenstedt, G., Jinks, T. & Silver, P. A. (1994) Nuf2, a spindle pole body-associated protein required for nuclear division in yeast. *J Cell Biol,* 125, 853-66.

Pagliuca, C., Draviam, V. M., Marco, E., Sorger, P. K. & De Wulf, P. (2009) Roles for the conserved spc105p/kre28p complex in kinetochore-microtubule binding and the spindle assembly checkpoint. *PLoS One,* 4, e7640.

Peters, J. M. (2006) The anaphase promoting complex/cyclosome: a machine designed to destroy. *Nat Rev Mol Cell Biol,* 7, 644-56.

Peterson, J. B. & Ris, H. (1976) Electron-microscopic study of the spindle and chromosome movement in the yeast Saccharomyces cerevisiae. *J Cell Sci,* 22, 219-42.
Petrovic, A., Pasqualato, S., Dube, P., Krenn, V., Santaguida, S., Cittaro, D., Monzani, S., Massimiliano, L., Keller, J., Tarricone, A., Maiolica, A., Stark, H. & Musacchio, A. (2010) The MIS12 complex is a protein interaction hub for outer kinetochore assembly. *J Cell Biol,* 190, 835-52.
Pietrasanta, L. I., Thrower, D., Hsieh, W., Rao, S., Stemmann, O., Lechner, J., Carbon, J. & Hansma, H. (1999) Probing the Saccharomyces cerevisiae centromeric DNA (CEN DNA)-binding factor 3 (CBF3) kinetochore complex by using atomic force microscopy. *Proc Natl Acad Sci U S A,* 96, 3757-62.
Pinsky, B. A., Kung, C., Shokat, K. M. & Biggins, S. (2006) The Ipl1-Aurora protein kinase activates the spindle checkpoint by creating unattached kinetochores. *Nat Cell Biol,* 8, 78-83.
Pinsky, B. A., Tatsutani, S. Y., Collins, K. A. & Biggins, S. (2003) An Mtw1 complex promotes kinetochore biorientation that is monitored by the Ipl1/Aurora protein kinase. *Dev Cell,* 5, 735-45.
Porter, A. C. & Farr, C. J. (2004) Topoisomerase II: untangling its contribution at the centromere. *Chromosome Res,* 12, 569-83.
Pot, I., Measday, V., Snydsman, B., Cagney, G., Fields, S., Davis, T. N., Muller, E. G. & Hieter, P. (2003) Chl4p and iml3p are two new members of the budding yeast outer kinetochore. *Mol Biol Cell,* 14, 460-76.
Prilusky, J., Felder, C. E., Zeev-Ben-Mordehai, T., Rydberg, E. H., Man, O., Beckmann, J. S., Silman, I. & Sussman, J. L. (2005) FoldIndex: a simple tool to predict whether a given protein sequence is intrinsically unfolded. *Bioinformatics,* 21, 3435-8.
Przewloka, M. R., Zhang, W., Costa, P., Archambault, V., D'avino, P. P., Lilley, K. S., Laue, E. D., Mcainsh, A. D. & Glover, D. M. (2007) Molecular analysis of core kinetochore composition and assembly in Drosophila melanogaster. *PLoS One,* 2, e478.
Purvis, A. & Singleton, M. R. (2008) Insights into kinetochore-DNA interactions from the structure of Cep3Delta. *EMBO Rep,* 9, 56-62.
Rhodes, G. (2006) *Crystallography made crystal clear : a guide for users of macromolecular models,* Amsterdam ; Boston, Elsevier/Academic Press.
Rial, D. V. & Ceccarelli, E. A. (2002) Removal of DnaK contamination during fusion protein purifications. *Protein Expr Purif,* 25, 503-7.
Rieder, C. L., Cole, R. W., Khodjakov, A. & Sluder, G. (1995) The checkpoint delaying anaphase in response to chromosome monoorientation is mediated by an inhibitory signal produced by unattached kinetochores. *J Cell Biol,* 130, 941-8.
Robinson, P. J. & Rhodes, D. (2006) Structure of the '30 nm' chromatin fibre: a key role for the linker histone. *Curr Opin Struct Biol,* 16, 336-43.
Sandall, S., Severin, F., Mcleod, I. X., Yates, J. R., 3rd, Oegema, K., Hyman, A. & Desai, A. (2006) A Bir1-Sli15 complex connects centromeres to

microtubules and is required to sense kinetochore tension. *Cell,* 127, 1179-91.
Santaguida, S. & Musacchio, A. (2009) The life and miracles of kinetochores. *EMBO J,* 28, 2511-31.
Scharfenberger, M., Ortiz, J., Grau, N., Janke, C., Schiebel, E. & Lechner, J. (2003) Nsl1p is essential for the establishment of bipolarity and the localization of the Dam-Duo complex. *EMBO J,* 22, 6584-97.
Schuck, P. (2000) Size-distribution analysis of macromolecules by sedimentation velocity ultracentrifugation and lamm equation modeling. *Biophys J,* 78, 1606-19.
Shan, X., Xue, Z., Euskirchen, G. & Melese, T. (1997) NNF1 is an essential yeast gene required for proper spindle orientation, nucleolar and nuclear envelope structure and mRNA export. *J Cell Sci,* 110 (Pt 14), 1615-24.
Sironi, L., Mapelli, M., Knapp, S., De Antoni, A., Jeang, K. T. & Musacchio, A. (2002) Crystal structure of the tetrameric Mad1-Mad2 core complex: implications of a 'safety belt' binding mechanism for the spindle checkpoint. *EMBO J,* 21, 2496-506.
Soderblom, E. J. & Goshe, M. B. (2006) Collision-induced dissociative chemical cross-linking reagents and methodology: Applications to protein structural characterization using tandem mass spectrometry analysis. *Anal Chem,* 78, 8059-68.
Soding, J., Biegert, A. & Lupas, A. N. (2005) The HHpred interactive server for protein homology detection and structure prediction. *Nucleic Acids Res,* 33, W244-8.
Sorger, P. K., Severin, F. F. & Hyman, A. A. (1994) Factors required for the binding of reassembled yeast kinetochores to microtubules in vitro. *J Cell Biol,* 127, 995-1008.
Stoler, S., Keith, K. C., Curnick, K. E. & Fitzgerald-Hayes, M. (1995) A mutation in CSE4, an essential gene encoding a novel chromatin-associated protein in yeast, causes chromosome nondisjunction and cell cycle arrest at mitosis. *Genes Dev,* 9, 573-86.
Sudakin, V., Chan, G. K. & Yen, T. J. (2001) Checkpoint inhibition of the APC/C in HeLa cells is mediated by a complex of BUBR1, BUB3, CDC20, and MAD2. *J Cell Biol,* 154, 925-36.
Tanaka, T. U., Rachidi, N., Janke, C., Pereira, G., Galova, M., Schiebel, E., Stark, M. J. & Nasmyth, K. (2002) Evidence that the Ipl1-Sli15 (Aurora kinase-INCENP) complex promotes chromosome bi-orientation by altering kinetochore-spindle pole connections. *Cell,* 108, 317-29.
Terada, Y., Tatsuka, M., Suzuki, F., Yasuda, Y., Fujita, S. & Otsu, M. (1998) AIM-1: a mammalian midbody-associated protein required for cytokinesis. *EMBO J,* 17, 667-76.
Thompson, J. D., Higgins, D. G. & Gibson, T. J. (1994) CLUSTAL W: improving the sensitivity of progressive multiple sequence alignment through sequence weighting, position-specific gap penalties and weight matrix choice. *Nucleic Acids Res,* 22, 4673-80.

Thompson, S. L., Bakhoum, S. F. & Compton, D. A. (2010) Mechanisms of chromosomal instability. *Curr Biol,* 20, R285-95.
Tytell, J. D. & Sorger, P. K. (2006) Analysis of kinesin motor function at budding yeast kinetochores. *J Cell Biol,* 172, 861-74.
Wan, X., O'quinn, R. P., Pierce, H. L., Joglekar, A. P., Gall, W. E., Deluca, J. G., Carroll, C. W., Liu, S. T., Yen, T. J., Mcewen, B. F., Stukenberg, P. T., Desai, A. & Salmon, E. D. (2009) Protein architecture of the human kinetochore microtubule attachment site. *Cell,* 137, 672-84.
Wang, H. W., Long, S., Ciferri, C., Westermann, S., Drubin, D., Barnes, G. & Nogales, E. (2008) Architecture and flexibility of the yeast Ndc80 kinetochore complex. *J Mol Biol,* 383, 894-903.
Wang, H. W. & Nogales, E. (2005) Nucleotide-dependent bending flexibility of tubulin regulates microtubule assembly. *Nature,* 435, 911-5.
Wang, H. W., Ramey, V. H., Westermann, S., Leschziner, A. E., Welburn, J. P., Nakajima, Y., Drubin, D. G., Barnes, G. & Nogales, E. (2007) Architecture of the Dam1 kinetochore ring complex and implications for microtubule-driven assembly and force-coupling mechanisms. *Nat Struct Mol Biol,* 14, 721-6.
Wei, R. R., Al-Bassam, J. & Harrison, S. C. (2007) The Ndc80/HEC1 complex is a contact point for kinetochore-microtubule attachment. *Nat Struct Mol Biol,* 14, 54-9.
Wei, R. R., Schnell, J. R., Larsen, N. A., Sorger, P. K., Chou, J. J. & Harrison, S. C. (2006) Structure of a central component of the yeast kinetochore: the Spc24p/Spc25p globular domain. *Structure,* 14, 1003-9.
Wei, R. R., Sorger, P. K. & Harrison, S. C. (2005) Molecular organization of the Ndc80 complex, an essential kinetochore component. *Proc Natl Acad Sci U S A,* 102, 5363-7.
Welburn, J. P., Vleugel, M., Liu, D., Yates, J. R., 3rd, Lampson, M. A., Fukagawa, T. & Cheeseman, I. M. (2010) Aurora B phosphorylates spatially distinct targets to differentially regulate the kinetochore-microtubule interface. *Mol Cell,* 38, 383-92.
Westermann, S., Avila-Sakar, A., Wang, H. W., Niederstrasser, H., Wong, J., Drubin, D. G., Nogales, E. & Barnes, G. (2005) Formation of a dynamic kinetochore- microtubule interface through assembly of the Dam1 ring complex. *Mol Cell,* 17, 277-90.
Westermann, S., Cheeseman, I. M., Anderson, S., Yates, J. R., 3rd, Drubin, D. G. & Barnes, G. (2003) Architecture of the budding yeast kinetochore reveals a conserved molecular core. *J Cell Biol,* 163, 215-22.
Westermann, S., Drubin, D. G. & Barnes, G. (2007) Structures and functions of yeast kinetochore complexes. *Annu Rev Biochem,* 76, 563-91.
Wigge, P. A., Jensen, O. N., Holmes, S., Soues, S., Mann, M. & Kilmartin, J. V. (1998) Analysis of the Saccharomyces spindle pole by matrix-assisted laser desorption/ionization (MALDI) mass spectrometry. *J Cell Biol,* 141, 967-77.

Wigge, P. A. & Kilmartin, J. V. (2001) The Ndc80p complex from Saccharomyces cerevisiae contains conserved centromere components and has a function in chromosome segregation. *J Cell Biol,* 152, 349-60.

Wilson-Kubalek, E. M., Cheeseman, I. M., Yoshioka, C., Desai, A. & Milligan, R. A. (2008) Orientation and structure of the Ndc80 complex on the microtubule lattice. *J Cell Biol,* 182, 1055-61.

Winey, M. & O'toole, E. T. (2001) The spindle cycle in budding yeast. *Nat Cell Biol,* 3, E23-7.

Wolyniak, M. J., Blake-Hodek, K., Kosco, K., Hwang, E., You, L. & Huffaker, T. C. (2006) The regulation of microtubule dynamics in Saccharomyces cerevisiae by three interacting plus-end tracking proteins. *Mol Biol Cell,* 17, 2789-98.

Yang, M., Li, B., Liu, C. J., Tomchick, D. R., Machius, M., Rizo, J., Yu, H. & Luo, X. (2008) Insights into mad2 regulation in the spindle checkpoint revealed by the crystal structure of the symmetric mad2 dimer. *PLoS Biol,* 6, e50.

Zheng, L., Chen, Y. & Lee, W. H. (1999) Hec1p, an evolutionarily conserved coiled-coil protein, modulates chromosome segregation through interaction with SMC proteins. *Mol Cell Biol,* 19, 5417-28.